DELINEATING EXCITATORY V3 INTERNEURON DIVERSITY IN THE MOUSE SPINAL CORD

by

Dylan Deska-Gauthier

Submitted in partial fulfilment of the requirements
for the degree of Doctor of Philosophy

at

Dalhousie University
Halifax, Nova Scotia
June of 2021

TABLE OF CONTENTS

LIST OF TABLES

LIST OF FIGURES

ABSTRACT

Mammals possess the remarkable ability to manoeuvre the physical world with precise, coordinated, and autonomous control. Interneuron networks in the spinal cord simultaneously integrate and process supraspinal and sensory information while generating basic rhythmic and patterned motor commands. Thus, sensorimotor spinal interneuron circuits ensure the successful execution of goal- and context-specific movement. Utilizing the mouse model system, my Ph.D. work has focused on understanding: 1) the spinal interneuron diversity underlying functionally distinct circuit organizations; and then 2) how that diversity emerges during early embryogenesis. With a focus on excitatory V3 and V2a cardinal interneuron populations in the spinal cord, I first reveal that these two excitatory spinal interneurons topographically cluster into task-specific recruitment modules, which may functionally compensate in the absence of one another. Thus, molecularly and anatomically distinct interneuron subpopulations may be functionally organized based on their behaviour-specific recruitments. Second, I investigate the early embryonic mechanisms guiding the subpopulation diversification of V3 interneurons. I reveal that V3 interneuron subpopulations diversify across hierarchical temporal and spatial developmental pathways. Specifically, differential neurogenesis timing separates V3 INs into either early-born or late-born temporal subclasses leading to distinct transcription factor expression patterns and neuronal migration trajectories. Within each temporal subclass, spatial controls then further delineate V3 INs into molecularly, anatomically, morphologically, and electrophysiologically distinct subpopulations. Taken together, my Ph.D. work has revealed key developmental and functional logic underlying the diversification of excitatory interneurons within the mammalian spinal cord.

LIST OF ABBREVIATIONS USED

5-Ethynyl-2´-deoxyuridine	EdU
Ascending commissural interneurons	aCINs
Ascending ipsilateral interneurons	aINs
Basic Helix-Loop-Helix Domain Containing, Class B, 5	Bhlhb5
Biotin-conjugated dextran amine	BDA
Bone Morphogenetic Protein	BMP
Ceh-10 Homeodomain-Containing Homolog	Chx10
Cellular Fos proto-oncogene	cfos
Central nervous system	CNS
Central pattern generator	CPG
Cerebrospinal fluid-contacting neurons	CSF-cNs
Channelrhodopsin2	ChR2
Cholera-toxin B	CTB
Cholinergic V0	$V0_C$
Cyclic adenosine monophosphate	cAMP
Day postfertilization	dpf
Deoxyribonucleic acid	DNA
Descending commissural interneurons	dCINs
Descending ipsilateral interneurons	dINs
Developing Brain Homeobox 1	Dbx1
Dorsal interneuron class #	dI#

Dorsal interneuron late A/B	dILA/B
Dorsal V3	$V3_d$
Doublesex And Mab-3 Related Transcription Factor 3	DMRT3
Embryonic day #	E#
Embryonic stem cell	ESC
Engrailed 1	En1
Estrogen-related receptor gamma	Nr3b3
Excitatory V0	V0-e
Forkhead Box D3	Foxd3
Forkhead box protein P1	Foxp1
Forkhead box protein P2	Foxp2
Gastrocnemius	GS
Gastrulation Brain Homeobox 1	Gbx1
GATA-binding factor 2/3	Gata2/3
Gluteus maximus	GL
Homeobox HB9	HB9
Ia Inhibitory interneurons	IaI-INs
Iliopsoas	IP
Interneuron	IN
Knockout	KO
Ladybird Homeobox 1	Lbx1
LIM Domain Only 3	Lmo3

LIM Homeobox 3	Lhx3
LIM Homeobox Transcription Factor 1 Beta	Lmx1b
Lumbar segment #	L#
MAF BZIP Transcription Factor A	MafA
Motor neuron	MN
Multipolar commissural descending	MCoD
NK2 Homeobox 2	Nkx2.2
Nuclear Receptor Subfamily 4 Group A Member 2	Nr4a2
Nuclear Receptor Subfamily 5 Group A Member 2	Nr5a2
Oligodendrocyte Transcription Factor 3	Olig3
One Cut Homeobox 1	Onecut1
One Cut Homeobox 2	Onecut2
Orthopedia Homeobox	Otp
Paired box gene 2	Pax2
Paired Like Homeodomain 2	Pitx2
Parvalbumin	PV
Postnatal day #	P#
POU Class 2 Homeobox 2	Pou2f2
PR/SET Domain 8	Prdm8
Principal component #	PC#
Principal component analysis	PCA
Progenitor domain #	p#

Prospero Homeobox 1	Prox1
Renshaw Cells	RC
Retinoic Acid	RA
Retinoid-related orphan receptor alpha	RORα
Retinoid-related orphan receptor alpha	RORβ
Ribonucleic acid	RNA
Roundabout Guidance Receptor 3	Robo3
Short Stature Homeobox 2	Shox2
$Sim1^{Cre}$; $vGluT2^{flox/flox}$	$V3^{OFF}$
Single-minded homolog 1	Sim1
SL LIM Homeobox 1	ISL1
Somatostatin	SST
Sonic hedgehog	Shh
specificity protein 8	Sp8
Streptavidin	Strp
Support vector machine	SVM
Tibialis anterior	TA
Transcription Factor	TF
Unipolar commissural descending	UCoD
V0 dorsal	$V0_d$
V0 ventral	$V0_v$
Ventral interneuron class #	V#

Ventral V3	$V3_v$
Ventrolateral V3	$V3_{VL}$
Ventromedial V3	$V3_{VM}$
Vesicular acetylcholine transporter	VAchT
Vesicular glutamate transporter 1	Vglut1
Vesicular glutamate transporter 2	Vglut2
Wilms Tumor 1	WT1
Zinc finger homeobox	Zfhx

ACKNOWLEDGEMENTS

First and foremost, I would like to deeply thank Dr. Ying Zhang for her unwavering support and mentorship for nearly the last decade. My time in the lab under her supervision has been one of the most enriching and gratifying experiences of my life. Dr. Zhang has always supported and helped me form my scientific curiosities as well as my career and personal goals in life. I am certain my time spent in research up to this point would not have been nearly the same without her as my supervisor.

I would also like to thank all the lab members I have been able to work with over the last several years. First, I would like to thank Dr. Jake Blacklaws who took me under his wing as an undergraduate volunteer when I first started in the lab and Dr. Jeremy Chopek who took me under his wing as a masters student. I would like to thank Laura Bennett and Colin Mackay for their help over the years processing and analysing tissue. I would like to thank Dr. Joanna Borowska for always being willing to collaborate on projects. I would like to thank Dr. Christopher Jones for also always being willing to collaborate and teach Dr. Zhang and I about the world of statistics. I would like to thank Mary Li, Dallas Bennett, Igor Tatarnikov, and all the animal care staff who have helped me maintain and genotype my mouse colonies over the years. I would like to thank Stephen Whitefield and Brianne Lindsay for their imaging support. I would also like to thank Udy MacKenzie for being a colleague and good friend over the last several years in the lab. I would like to specially thank Dr. Han Zhang for continuously inspiring me both inside and outside of the lab. Han has been a true friend, collaborator, and mentor to me both in the lab and on the basketball court.

Lastly, I would like to thank my sister, my mother, my father, and my partner for being my core support system over the years. Thank you, Mary, for putting up with my long hours spent at the lab and always making me laugh.

CHAPTER 1. INTRODUCTION

Spinal interneuron (IN) circuits ensure coordinated spatiotemporal muscle contractions necessary for complex locomotor behaviours. The identification of molecularly distinct spinal IN populations has enabled detailed and effective investigations into the organization of these circuits. Recent revelations of vast spinal IN diversity, particularly within cardinal spinal IN classes, have given rise to enormous challenges, as well as opportunities, in furthering our understanding of the functional circuit architecture underlying motor control.

Distinct spinal IN identities are closely tied to their early developmental origins. Embryonic neurogenesis timing is an essential developmental mechanism for neuronal diversity and organization throughout the central nervous system. In the mouse spinal cord, growing evidence is beginning to reveal that neurogenesis timing acts in tandem with spatial molecular controls to diversify molecularly and functionally distinct post-mitotic interneuron subpopulations. Particularly, in some cases, this temporal ordering of interneuron differentiation has been shown to instruct specific sensorimotor circuit wirings. In zebrafish, *in vivo* preparations have revealed that sequential neurogenesis waves of interneurons and motor neurons form speed-dependent locomotor circuits throughout the spinal cord and brainstem.

In the following introduction sections, I will first focus on recent studies revealing distinct spinal IN subpopulations assembled within rhythm-generating and pattern-forming spinal circuit layers. I will summarize how both general and task-specific spinal IN circuit outputs functionally combine, empowering a wide repertoire of locomotor behaviours. Next, I will discuss temporal

principals of interneuron diversity taken from both mouse and zebrafish systems highlighting how each can lend illuminating insights to the other.

Moving forward, it is important to combine the collective knowledge from different systems to eventually understand how temporally regulated subpopulation fates differentially function across speed- and/or state-dependent sensorimotor movement tasks. I begin to address this challenge through the study of excitatory V3 interneurons presented throughout my result chapters. Taken together, my Ph.D. work has started to narrow the gap between how early temporal and spatial developmental mechanisms give rise to functionally distinct spinal interneuron subpopulations ultimately enabling behavioural flexibility.

1.1 The functional diversity of spinal interneurons and locomotor control

Locomotor movement has enabled vertebrate species to both survive and thrive for millions of years by empowering navigation through dynamic environments across land, sea and air. Spinal interneurons (INs) form the basic motor circuits that ensure coordinated spatiotemporal muscle contractions. Distinct IN populations organize into functionally hierarchical modular circuits producing complex locomotor schemes – such as chewing, scratching, swimming and walking (Goulding, 2009; Grillner, 2003; Kiehn, 2016). In particular, the ventral side of the spinal cord functions as a central pattern generator (CPG) system (Kiehn & Butt, 2003), which can generate basic rhythmic and patterned motor outputs in the absence of descending supraspinal commands and ascending sensory inputs (Brown, 1911; Engberg & Lundberg, 1969; Grillner & Zangger, 1979, 1984; Jankowska et al., 1965, 1967). Furthermore,

both experimental and computational studies indicate that locomotor rhythm and patterns can be generated, manipulated, and deleted independent of one another (Danner et al., 2017; Duysens, 1977; Grillner & Zangger, 1979; Guertin et al., 1995; Kiehn, 2006; Lafreniere-Roula & McCrea, 2005; McCrea & Rybak, 2007, 2008), suggesting a separation of rhythm-generating and pattern-forming spinal IN networks. As such, coordinated, flexible, and purposeful movements are direct products of IN diversity and the corresponding circuit logics within the spinal cord.

Currently, the most common and successful classification of spinal INs is based on their genetic identities. During early embryonic development, molecularly discrete progenitor domains organized along the dorsoventral axis of the folding neural tube give rise to 10 postmitotic cardinal IN populations (ventral: V0-V3, dorsal: dI1-dI6) (Jessell, 2000). Each cardinal group is defined by specific transcription factor (TF) expression profiles, distinctive anatomical properties, and general functional roles in locomotor control (Goulding, 2009). Yet, it has recently become clear that within each cardinal population substantial subpopulation heterogeneity exists, revealing a spinal IN complexity previously unappreciated. Multiple cardinal IN subpopulations have been delineated by their molecular, anatomical, physiological and functional properties. Furthermore, some of these functionally distinct subpopulations display task-specific involvements in motor control. This short review will serve as a snapshot of select recent studies addressing how diverse spinal IN subpopulations functionally integrate within rhythm- generating and pattern-forming spinal circuit layers (Figure 1.1), enabling a vast repertoire of locomotor behaviours.

1.1.1 Locomotor rhythm shared across IN types

Work utilizing fictive locomotor preparations have implicated ipsilateral glutamatergic spinal INs as both sufficient and necessary for rhythmic locomotor output (Grillner, 2003; Hägglund et al., 2010, 2013). But to date, only two molecularly defined spinal IN subpopulations have been suggested as direct contributors to rhythm generation. Firstly, glutamatergic Shox2^{+} non-V2a INs innervate ipsilateral INs but not motor neurons (MNs) and are rhythmically active during fictive locomotion (Dougherty et al., 2013). When their synaptic transmission is blocked, spinal cords display significantly reduced locomotor frequencies without affecting left-right or flexor-extensor patterns (Dougherty et al., 2013). However, spinal cords are still able to produce rhythmic outputs, implying that other IN populations are also important for rhythm generation. Indeed, a second glutamatergic and ipsilaterally projecting HB9^{+} IN population has been shown important, though again not completely necessary, for increasing locomotor frequency (Caldeira et al., 2017).

In addition, we would like to point out that genetic deletion of inhibitory dI6 (Andersson et al., 2012) and V1 INs (Gosgnach et al., 2006) and excitatory commissural V3 INs (Zhang et al., 2008) also affects rhythmicity and frequency of locomotor output. Although it is still not clear if any of these INs are rhythm-generating cells or just regulate rhythm-generating circuits, these results suggest rhythm generation may not be confined to a single IN population but shared across several (Figure 1.1A).

1.1.2 Locomotor Pattern formation

1.1.2.1 Left-right alternation across different speeds

The spinal cord's ability to produce coordinated muscle contractions on either side of the body is paramount for successful locomotion. As an animal transitions between different locomotor speeds, it must accommodate changes in left-right contraction patterns to achieve optimal gaits (in the case of limbed animals) or swimming frequencies (in the case of aquatic non-limbed animals). Indeed, emerging evidence has begun to indicate distinct spinal IN circuit modules comprised of dI6, V0, and V2a IN subpopulations that display speed-dependent left-right coordination (Figure 1.2).

During limbed locomotion, wildtype animals exhibit distinct locomotor gait phenotypes with increasing speeds (Bellardita & Kiehn, 2015; Lemieux et al., 2016). As mice increase in locomotor speed they switch from an initial walking gait to a trotting gait, to finally a galloping/bounding gait. During both walking and trotting mouse hindlimbs alternate, while during galloping/bounding their hindlimbs switch to synchronous outputs. V0 INs are mostly commissural INs originating from the $Dbx1^{+}$ p0 progenitor domain that project to contralateral motor neurons and ventral INs. Before becoming postmitotic, p0 progenitor cells separate into either excitatory V0 ventral (v) or inhibitory V0 dorsal (d) cells (Lanuza et al., 2004; Pierani et al., 2001). Although deletion of V0 INs (V0v & V0d) abolishes left-right alternation at all speeds, when V0v INs are exclusively ablated, left-right alternation is lost at trotting speed, but not at lower speed walking (Bellardita & Kiehn, 2015; Talpalar et al., 2013). Thus, V0v and V0d

subpopulations functionally separate into distinct circuit modules that are differentially recruited across specific locomotor speeds.

In addition to V0v INs, a portion of V2a INs has been implicated in coordinating left-right alternation at exclusively high locomotor speeds in mice. Chx10^{+} V2a INs (Lundfald et al., 2007) form excitatory ipsilateral projections innervating MNs and other ventral IN populations. Interestingly, V2a ablated mice maintain normal left-right alternation at low locomotor speeds but switch to synchrony as locomotor speed increases (Crone et al., 2009). V2a's recruitment is speed dependent, as the percentage of rhythmically bursting V2a INs significantly increases with increased locomotor frequency (Dougherty & Kiehn, 2010; Zhong et al., 2010). As V2a INs project significantly to commissural INs (Crone et al., 2009), some of which are V0v INs (Crone et al., 2008), it is possible for V2a and V0 INs to form a high-speed alternating locomotor circuit module, whereby increased recruitment of ipsilateral V2a INs drives V0v INs enabling transitions from a walking to a trotting gait.

Similar to the case of mice, work in the zebrafish has also revealed that V2a INs exhibit sequential recruitment with increasing locomotor frequencies, whereby the largest subset of recorded V2a INs are recruited at high locomotor frequencies (Ausborn et al., 2012). Furthermore, V2a INs, like MNs, can be categorized into slow, intermediate, and fast subtypes based on their action potential firing properties, corresponding recruitment frequencies, and V2a-MN microcircuit connectivity patterns (Ampatzis et al., 2014; Ausborn et al., 2012; Song et al., 2016). Interestingly, in zebrafish, commissural glutamatergic V0v INs also display slow, intermediate, and fast recruitment subtypes (Björnfors & El Manira, 2016). Thus, incremental frequency-dependent MN recruitment, in addition to an MN's biophysical subtype properties

(Rekling et al., 2000), is likely further determined by upstream V2a and V0v modular microcircuit organizations.

Dorsal emerging dI6 INs have also been implicated in speed-dependent locomotor pattern formation. dI6 INs emerge from $Lbx1^+$ dorsal progenitor cells (Gross et al., 2002) and post-mitotically form distinct subsets that express either WT1 and/or DMRT3 (Andersson et al., 2012) as well as further undefined subset-specific molecular markers (Griener et al., 2017). dI6 INs are mainly inhibitory (Andersson et al., 2012) and are predominately commissural, although they form monosynaptic and disynaptic contacts with both contralateral and ipsilateral MNs (Griener et al., 2017). While dI6 INs are dorsal originating, they settle into ventral and motor-related lamina by the postnatal stages (Andersson et al., 2012; Griener et al., 2017). The majority of dI6 INs are rhythmically active during drug-induced fictive locomotion in the isolated mouse spinal cord (Dyck et al., 2012; Haque et al., 2018). Additionally, electrophysiological recording of dI6 INs during fictive locomotor deletions have implicated dI6 IN subsets in both rhythm- generating and pattern-forming locomotor spinal circuits (Griener et al., 2017). Functional or genetic deletion of either $WT1^+$ (Haque et al., 2018) or $DMRT3^+$ (Andersson et al., 2012) INs in isolated neonatal spinal cords generates irregular fictive locomotor outputs with non-coherent left-right alternation. However, thus far, only $DMRT3^+$ dI6 IN functional outputs have been investigated, in vivo (Andersson et al., 2012). Dmrt3 mutated horses display difficulty transitioning from a trotting gait to a galloping gait with increasing locomotor speed. Instead, DMRT3 mutated horses express a “pace” gait defined by synchronized movement of the legs on one side of the body at higher speeds. Thus, $DMRT3^+$ dI6

INs may play a critical role in proper locomotor pattern formation, particularly during high-speed locomotor tasks.

1.1.2.2 The balance of left-right activities

Currently, most studies of left-right coordination have focused on establishment of left-right alternation, but certain aspects of left-right activities have to be synchronized during locomotion. For example, most animals bounce at high speed, which requires the synchronization of left-right limbs. In addition, to generate stable movement, the strength of the same muscle from left-right limbs or the activation of flexors and extensors on opposite sides of the body all have to be synchronized. Although it is still unclear what neuronal mechanisms underlie these left-right synchronizations, V3 INs have been shown to play some important roles in this function.

$Sim1^{+}$ V3 INs are glutamatergic and derived from the most ventral Nkx2.2-expressing p3 progenitor domain in the neural tube (Zhang et al., 2008). However, understanding V3 INs functional circuit logic has proven a challenge owing to their vast heterogeneity (Blacklaws et al., 2015; Borowska et al., 2013, 2015; Zhang et al., 2008). V3 INs diversify along the dorsoventral axis of the lumbar spinal cord separating into either dorsal (V3d) or ventral (V3v) subsets based on their intrinsic membrane properties, axon projection profiles, and morphologies (Blacklaws et al., 2015; Borowska et al., 2013, 2015). While V3d INs form exclusively commissural ascending propriospinal projections, V3v INs exhibit both commissural and ascending and descending propriospinal axon projections (Blacklaws et al.,

2015). Although majority of V3 INs (~85%) are commissural, there are also ipsilateral V3 projections (Blacklaws et al., 2015; Zhang et al., 2008), and at least some of them are bifurcated from the commissural axons (Chopek et al., 2018). Chopek et al., (2018) utilized single-cell patch-clamp recordings in combination with holographic glutamate uncaging, allowing for the mapping of local cell-cell V3 connectivity in the lumbar spinal cord. Interestingly, Chopek et al. (Chopek et al., 2018) revealed that contralaterally projecting V3v INs could also form bilateral connections with local ipsilateral V3 IN and MN networks. Specifically, commissural V3 INs form a layered ipsilateral microcircuit in which medial V3v INs synapse onto larger lateral V3v INs, which then innervate local ipsilateral MNs. Ipsilateral MNs then also form excitatory glutamatergic synapses back onto both lateral V3v and medial V3v INs. Taken together, this work indicates that commissural V3v INs and local ipsilateral MNs form a positive feedback microcircuit (Figure 1.3A).

Whether the V3-MN layers of connectivity across the mediolateral spinal axis underscore functional layers of motor output is yet to be determined. However, the bilateral projections of V3v INs to both ipsilateral and contralateral spinal networks suggests that V3v INs may play important roles in securing coordinated and balanced excitation between distinct left-right flexor and extensor spinal circuits. Indeed, early work by Zhang et al. (2008) revealed that $V3^{OFF}$ isolated spinal cord preparations displayed significantly uncoordinated and variable left-right and flexor-extensor ventral root bursting during fictive locomotion. Genetic deletion V3 INs also led to unstable and imbalanced gaits. However, whether V3's role in securing stable excitatory coordination between left-right segments is a consequence of V3v's bilateral connectivities is yet to de determined. V3 subpopulation molecular characterization is required

to selectively target V3v INs and study their specific functions. It also remains to determine if V3 INs are required for left-right synchronization during bouncing.

1.1.2.3 Flexor-extensor alternations

The simultaneous activation and paired silencing of antagonist muscle groups around a joint is crucial for intralimb coordination and ultimately for motor execution. Both V1 and V2b INs form inhibitory synapses with ipsilateral INs and MNs, resulting in coordinated flexor-extensor alternations during locomotion and hindlimb reflex withdrawals (Zhang et al., 2014). V1 INs emerge from the p1 progenitor domain marked by the postmitotic expression of Engrailed-1 (En1) (Jessell, 2000; Moran-Rivard et al., 2001) while V2b INs emerge from $Lhx3^{+}$ progenitor cells and postmitotically express $Gata2/3^{+}$ (Al Mosawie et al., 2007). When either V1 or V2b INs are independently silenced, mice maintain the ability to alternate flexor and extensor muscle contractions. However, the combined outputs of V1 and V2b are collectively necessary for flexor-extensor alternation (Zhang et al., 2014), yet, they are differently biased towards flexor or extensor MN pools, respectively (Britz et al., 2015). V1 INs preferentially innervate flexor MNs, whereby select V1 ablation results in hyperflexion during the swing phase. In contrast, V2b INs preferentially innervate extensor MNs, whereby select V2b ablation results in hyperextension during the stance phase (Britz et al., 2015). Thus, while flexor-extensor alternation is functionally shared across V1 and V2b INs, their functional outputs are not redundant, as each IN class is functionally biased towards either flexor or extensor inhibition. Furthermore, it is possible that separate IN subpopulations within V1 and V2b classes

additionally diversify in their joint- and/or MN pool specific functions. Indeed, recent work by Bikoff et al. (2016) revealed multiple V1 IN subpopulations that receive distinct MN pool and muscle afferent inputs. Further work investigating the functional roles of these distinct V1 IN subpopulations in locomotion may help determine the significance of their diverse circuit organizations for flexor-extensor coordination.

1.1.2.4 Gain control of motor outputs and reciprocal connection with motor neurons

MN outputs must be precisely controlled under different contexts to ensure appropriate muscle contraction strengths for a given motor task. Within the spinal cord, several IN subpopulations differentially regulate the strength of MN outputs. In the V0v IN subclass, a subpopulation of V0c INs has been described. V0c INs account for less than 5% of total V0 INs, they are marked by their embryonic and postnatal expression of Pitx2, and are cholinergic (Zagoraiou et al., 2009). V0c INs form large synapses, called C-boutons, onto MNs, serving as a spinal cord intrinsic neuromodulator system where their recruitment increases MN input-output gain through increased action potential firing frequencies (Miles et al., 2007). V0c function was also investigated in vivo. During swimming, mice require increased extensor bursting compared to over ground walking. However, V0c-deleted mice were unable to increase the MN output of ankle extensor gastrocnemius (GS) muscles, resulting in a prohibited swimming phenotype (Zagoraiou et al., 2009). Thus, V0c INs regulate the input-output gains and resulting bursting amplitudes of appropriate MN pools required to achieve high-output motor tasks. Furthermore, V0c inputs may have different post-synaptic effects depending on

the MN type they are innervating. In zebrafish, cholinergic spinal cord INs differentially regulate the excitability of biophysically distinct MN subsets (Bertuzzi & Ampatzis, 2018).

In addition to cholinergic, MNs receive vast excitatory glutamatergic inputs from spinal IN sources. Glutamatergic $Sim1^{+}$ V3 INs are a major class of excitatory spinal INs that directly innervate MNs (Zhang et al., 2008). MN pseudorabies virus injections revealed that a portion of V3v INs form monosynaptic inputs onto mainly commissural and some ipsilateral MNs (Zhang et al., 2008). Particularly, the newly discovered unique V3-MN microcircuits described in section 2a (figure 1.3) (Chopek et al., 2018), further strongly suggests that V3 INs can play important roles in controlling the activity of motor output. Recent *in vivo* studies do suggest that the lack of functional V3 INs, the animals are not able to increase their muscle strength during various locomotor tasks (unpublished data, y.z.).

In addition to gain control of motor output, reciprocal connections between MNs and IN subpopulations can also provide a gateway for MNs to influence upstream spinal IN circuits, instead of merely being a passive executive compartment of the spinal IN circuits. Song et al. (2016) have shown that subpopulations and V2a INs in zebrafish form gap-junctions with MNs, which are recruited under similar swimming frequency ranges. Renshaw cells were among the first spinal interneurons identified using traditional physiological and pharmacological methods. They have a unique reciprocal connection with MNs and form a recurrent inhibitory loop (Figure 1.3, [Bhumbra et al., 2014; Lamotte d'Incamps et al., 2017; Renshaw, 1946]). Genetic studies have revealed that Renshaw cells are a subpopulation of early-born V1 inhibitory INs (Benito-Gonzalez & Alvarez, 2012; Stam et al, 2012). Bikoff et al. (2016) recently revealed that dorsoventrally arranged V1 IN subsets receive joint specific sensory and potentially MN

collateral inputs. Thus, it is possible that distinct V1 IN subsets differentially integrate within joint-specific recurrent motor feedback circuits (Figure 1.3B).

Additional studies are required to investigate the exact functions of these reciprocal connections. Interestingly, Falgairolle et al. (2017) recently showed that optical suppression or activation of MNs can significantly regulate the phase and frequency of drug-induced fictive locomotion of isolated mouse lumbar spinal cords, which provides some confirmation that MNs influence spinal CPG networks in limbed animals.

Taken together, extensive reciprocal connections between MNs and both local inhibitory and excitatory IN populations have recently been unveiled. These connections likely function as respective negative and positive feedback loops for MN activity during movement. Furthermore, the fact that MN outputs back onto spinal IN circuits suggests that MNs do not only integrate upstream spinal circuit activity, but are also active members of the spinal CPG networks.

1.1.3 Concluding remarks on functional diversity of spinal interneurons

In the last two decades, tremendous progress has been made in uncovering the genetic and molecular diversity of spinal INs. These researches have led to enormous advancements in our understanding of the organization and functional logic of the spinal locomotor circuits, some of which were briefly summarized in this review. Such knowledge, however, also puts many challenges before us. It is still a daunting task to connect and connect genetic and molecular identities of individual IN populations to their physiological and functional phenotypes.

Generating novel, or combining available, genetic, electrophysiological and optical tools to trace and manipulate the activities of individual subpopulations should remain a top priority. Furthermore, the potential task-specific recruitments of distinct IN subpopulations demand that functional investigations be undertaken across several motor control paradigms. Lastly, we would like to emphasize that this review has mainly focused on ventral spinal INs that are involved in the 'core' CPG circuits that generate the basic rhythm and patterns of locomotion. Emerging studies have shown that subpopulations of ventral INs, as well as dorsal INs, integrate and mediate specific sensory afferents (Bourane et al., 2015; Bui et al., 2013, 2016; Fink et al., 2014; Hilde et al., 2016; Koch et al., 2017) and descending supraspinal commands (Bouvier et al., 2015; Murray et al., 2018; Ueno et al., 2018) shaping locomotor output. How all these inputs are integrated and ultimately translated into motor actions by spinal INs remains a fascinating question that has begun to be undertaken. Moving forward, we will need to combine all this knowledge to truly understand the mechanisms underlying movement.

1.2 The temporal mechanisms guiding interneuron differentiation in the spinal cord

Interneuron (IN) circuits in the spinal cord are essential for patterned, rhythmic, and flexible motor control. From basic to complex sensorimotor tasks, combinatorial IN recruitments in the spinal cord are required for successful execution of movement. The spinal cord is comprised of vastly heterogeneous IN populations defined by unique molecular identities, intrinsic properties, connectivities, and functional outputs. This IN diversity enables the spinal cord to coordinate varied movement schemes through dynamic environments. Thus, understanding spinal IN diversity, and the developmental mechanisms that give rise to it, is fundamental to understanding movement.

Early work in the mammalian spinal cord revealed a remarkable spatial organization of progenitor domains along the dorsoventral axis during early embryogenesis (Jessell, 2000; Lu et al., 2015). These 11 progenitor domains give rise to distinct post-mitotic interneuron (IN) and motor neuron (MN) cardinal classes (dI1-dI6 INs, dILA-B, V0-V3 INs, MNs) defined by respective transcription factor (TF) expression profiles. Physiological and anatomical studies have revealed general connectivities, electrophysiological properties, and functional outputs of these cardinal IN classes across various model systems (Goulding, 2009; Kiehn, 2016; Deska-Gauthier & Zhang, 2019). However, extensive subpopulation heterogeneity has become evident within each cardinal class (Bikoff, 2019; Gosgnach et al., 2017; Ziskind-Conhaim & Hochman, 2017). Furthermore, the developmental mechanisms underlying such subpopulation diversities are beginning to be understood.

Neurogenesis timing is an essential developmental mechanism for neuronal diversity and organization throughout the central nervous system (Holguera & Desplan, 2018; Oberst et al., 2019). Like wise, it plays an instructive role in the development of IN circuits within the spinal cord. Notably, spinal INs form the final circuits controlling the coordination and rhythmicity of movement. This enables behavioural quantifications of their circuit outputs. Thus, spinal IN circuits are ideal model systems for understanding how differential neurogenesis timing contributes to molecular, cellular and behavioural development in the central nervous system.

To date, neurogenesis timing has been linked to post-mitotic molecular expression profiles, intrinsic membrane properties, circuit connectivities, and behaviour-specific recruitments throughout IN populations in the spinal cord. In the current review, we will focus on mouse and zebrafish model systems to explore how temporal controls of differentiation contribute to spinal IN diversity and corresponding behavioural flexibility.

1.2.1 Lessons from the mouse spinal cord

1.2.1.1 Early temporal mechanisms guide molecular diversity in the mouse spinal cord

One of most revolutionary breakthroughs in understanding the development of spinal neurons was the discovery of spatially organized progenitors during early embryogenesis. Graded morphogens sonic hedgehog (Shh), released from floor plate, and bone morphogenic protein (BMP)/Wnt protein, released from the roof plate, pattern the positions and cross-inhibitory boundaries of 11 discrete progenitor domains along the dorsoventral spinal axis (Jessell, 2000). These progenitor domains in turn give rise to 13 distinct post-mitotic cardinal IN populations

and MNs. However, accumulating evidence suggests vast subpopulation diversity within each cardinal population and differential neurogenesis timing as a potentially key developmental mechanism for such diversity.

Recent work by Delile and colleagues utilized single cell RNA sequencing to systematically profile post-mitotic neurons across early embryonic stages (E9.5-E13.5) in the mouse spinal cord. They revealed a temporal emergence of shared transcription factor networks endowing subpopulation cluster identities across cardinal IN classes. This work was the first to systematically reveal previously under appreciated temporal mechanisms – acting in tandem with spatial controls – delineating IN subpopulation identities in the spinal cord. Indeed, several of these temporally regulated postmitotic TFs have been independently shown necessary for the specification and differentiation of subpopulation identities. Onecut TFs expressed across early-born spinal IN classes (Delile et al., 2019) are necessary for the differentiation of RCs (Stam et al., 2012) and other spinal INs (Harris et al., 2019; Kabayiza et al., 2017); Pou2f2 and Zfhx TFs expressed across intermediate-born spinal IN classes (Delile et al., 2019) are necessary for proper migration (Harris et al., 2019; Masgutova et al., 2019) and molecular specification of laterally positioned V2a INs (Hayashi et al., 2018); and lastly, Nfib TFs expressed across late-born spinal IN classes (Delile et al., 2019) serve as molecular markers for a medial V2a IN subpopulation (Hayashi et al., 2018). Together, this work has illuminated that neurons across the spinal cord may follow shared developmental temporal logic in their molecular diversification from spatially confined progenitor domains. Although, understanding how and whether temporal mechanisms translate into distinct IN phenotypes, circuit integrations and functional outputs remains an ongoing question. Over the last decade, various studies have

begun to investigate how differential neurogenesis timing orders the divergence of IN properties and functions.

1.2.1.2 Interneuron subpopulations emerge from temporally separated progenitors

V1 INs, defined by engrailed-1 TF expression, arise from the p1 progenitor domain between embryonic days (E) 9.5 and E12.5 in the mouse spinal cord (Benito-Gonzalez & Alvarez, 2012; Stam et al., 2012). They project ipsilateral and inhibitory contacts onto both MNs and other IN classes in the ventral spinal cord (Alvarez et al., 2005). In the mouse, V1 INs have been shown necessary for increased locomotor speed (Falgairolle & O'Donovan, 2019; Gosgnach et al., 2006) and flexor-extensor alternation during walking (Britz et al., 2015; Zhang et al., 2014;). Several classically characterized spinal IN types, such as Renshaw Cells (RCs) and Inhibitory Ia-INs were shown to be part of the V1 IN lineage (Alvarez et al., 2005). They were among the first groups of subpopulations recognized within the cardinal populations. Though, the vast heterogeneity of V1 INs was not fully revealed until the combinatorial expression of 19 distinct TFs was shown to delineate approximately 50 distinct V1 subsets throughout the lumbar and thoracic spinal cord (Bikoff et al., 2016; Gabitto et al., 2016; Sweeney et al., 2018).

More interestingly, in addition to revealing RC and Ia-IN V1 lineage, the same research groups showed that RCs and Ia-INs emerge from the p1 progenitor domain at different embryonic timepoints. They revealed that V1 INs could be organized into two general waves of neurogenesis: early (E9.5-E10.5) and late (E11.5-E12.5). The first wave of neurogenesis from the

p1 progenitor domain gives rise to RC cells (Benito-Gonzalez & Alvarez, 2012; Stam et al., 2012), while the second wave gives rise to Inhibitory Ia-Interneurons, FoxP2^{+} V1 INs, and other V1 IN subpopulations (Benito-Gonzalez & Alvarez, 2012). Early-born RCs are marked by the expression of a distinct TF profile (Foxd3, MafB, Onecut1, Onecut2) as well as the calcium binding protein, calbindin (Benito-Gonzalez & Alvarez, 2012; Stam et al., 2012). Upon exiting from the p1 progenitor domain, RCs display a distinct ventrolateral migratory stream settling amongst lateral motor column MNs (Alvarez et al., 2005; Boeri et al., 2018). This early differentiation pathway allows RCs to form unique recurrent inhibitory circuits with MNs (Stam et al., 2012).

The early V1 IN birthdate determines a temporally ordered TF cascade necessary for the specification and maintenance of a RC cell-type specific phenotype (Stam et al., 2012). Transcription factors Onecut1, Onecut2 and Foxd3 are responsible for the immediate postmitotic differentiation of RCs, including their calbindin expression, migration, and circuit formation with MNs. Subsequently, downstream MafB expression is necessary for the maintenance of RC identity during late embryonic stages (Stam et al., 2012). Thus, the specific early neurogenesis timing results in the postmitotic acquirement of a distinct TF expression cascade that facilitates the differentiation, maturation, and circuit integration of RCs separating them from other V1 INs.

While V1 IN subpopulation identity is correlated with neurogenesis time, to what extent their temporal expression profiles are endowed by intrinsic transcription programs or extrinsic signalling pathways remains an ongoing question. To begin to answer this question, Hoang and

colleagues (2018) established an in vitro model system of V1 IN diversification utilizing mouse embryonic stem cell (ESC) cultures. V1 IN subpopulations revealed in vivo (Bikoff et al., 2016; Gabitto et al., 2016) were also revealed in culture (Hoang et al., 2018). ESC V1 IN clades displayed electrophysiological properties and connectivities that recapitulated those observed in the spinal cord. Interestingly, ESC V1 IN subpopulations also displayed distinct neurogenesis birth orders in culture. Calbindin^{+} V1 INs were born first followed by Foxp2^{+} V1 INs. These results, from a system in the absence of many surrounding extrinsic signalling sources, are similar to those observed in vivo (Benito-Gonzalez & Alvarez, 2012; Stam et al., 2012).

Hoang and colleuges (2018) further assessed a potential causative link between neurogenesis timing and subpopulation generation. Through inhibition of Notch signaling, they were able to increase the rate of cell cycle exit and neurogenesis timing. When Notch was inhibited at early stages there was a significant increase in the proportion of early-born Calbindin^{+} V1 INs as well as other TFs belonging to the MafA^{+} V1 clade. This early-born subpopulation increase was accompanied by an almost complete loss of late-born Foxp2^{+} V1 INs. These experiments indicated that when late-born V1 INs were prematurely pushed out of the p1 progenitor domain they switched to an early-born subpopulation fate.

Taken together, both these in vivo and in vitro studies suggest that differential neurogenesis timing enables specific temporal transcription pathways in p1 progenitor cells to be translated into distinct V1 IN subpopulation fates. That is, the transcriptional identity of a V1 IN (or any spinal IN) at the time it becomes post-mitotic may instruct its subpopulation fate choice.

Beyond V1 INs, we have begun to investigate how neurogenesis timing underlies subpopulation divergence within the most ventral-originating V3 IN cardinal class. V3 INs, marked by TF Sim1 expression, exit from the p3 progenitor domain also between E9.5-E12.5 in the mouse spinal cord. V3 INs are mostly commissural and excitatory INs (Blacklaws et al., 2015; Zhang et al., 2008). They are functionally involved in coordinating excitation between left-right extensor centres (Danner et al., 2019) and robust locomotor pattern output (Zhang et al., 2008). As V3 INs become postmitotic, they form distinct dorsolateral and ventrolateral migratory streams. Early-born (E9.5-E10.5) V3 INs follow both dorsolateral and ventrolateral migratory streams and cluster across deep dorsal, intermediate, and ventral laminae by postnatal day (P) 0. In contrast, late-born (E11.5-E12.5) V3 INs almost exclusively follow the ventrolateral migratory stream and cluster mostly within ventral laminae by P0 (Deska-Gauthier et al., 2020). Furthermore, early-born V3 INs display both ascending and descending axonal projections, while late born V3 INs display significantly more descending axonal projections than ascending (Deska-Gauthier et al., 2020). Thus, successive neurogenesis timing fate-restricts late-born V3 INs to anatomically confined subpopulations.

Whether distinct transcriptional pathways are restricted to different temporal waves of V3 neurogenesis, as seen in V1 INs, remains largely unknown. Though, we have shown some evidence that the Sim1 TF, while expressed in all V3 INs, exclusively effects the laminar clustering and electrophysiological properties of early-born dorsal and intermediate V3 IN clusters, but not late-born ventral V3 IN clusters. Much more work is required to reveal the extent temporal mechanisms play in regulating the molecular pathways underlying V3 IN

subpopulation diversity, and how that diversity is then translated into functionally distinct circuit integrations.

1.2.1.3 Select dorsal IN populations emerge from temporally separated progenitors

Select sensory-related dorsal IN populations have also been shown to emerge during specific neurogenesis windows. Dorsal horn progenitors separate along both spatial and temporal axes of control. Two dorsal progenitor lineages, dILA and dILB INs, emerge from $Lbx1^+$ dorsal progenitors during specifically late neurogenesis stages. dILA coexpress Gbx1 with Pax2 and Lbx1 and are inhibitory while dILB coexpress Lmx1b with Lbx1 and are excitatory (Müller et al., 2002; Gross et al., 2002; John et al., 2005; Lai et al., 2016). Of particular note, Gbx1 is exclusively expressed and is necessary for the specification and differentiation of late-born dILA INs (Buckley et al., 2013, 2020; Meziane et al., 2013).

Loss of Gbx1 resulted in abnormal hindlimb gaits during locomotion as well as sensory processing (Buckley et al., 2013; Meziane et al., 2013). Gbx1 knockout (KO) mice displayed a duck-type gait characterized by hyper flexion during the swing phase and a decrease in average locomotor speed in open field tests. They also displayed reduced thermal pain sensitivity and increased slips during beam walking (Meziane et al., 2013). However, whether this was due to Gbx1's early expression in the floor plate, $ISL1^+$ motor neurons, or dILA INs is not clear. Though, Gbx1 KO mice displayed intact motor strength and no changes in the number of $ISL1^+$ MNs nor sensory innervations patterns (Meziane et al., 2013). Taken together, this suggests that

temporally regulated expression of Gbx1 in late-born dorsal INs is necessary for the specification of dILA INs, which are involved in distinct aspects of sensorimotor control.

Sensory mediating cerebrospinal fluid contacting neurons were also shown to have a characteristically late neurogenesis timing in the mouse spinal cord. These neurons are born as late as E14 to E16 from the oligodendrocite and the p2 progenitor domains (Petracca et al., 2016). This neurogenesis window is well beyond the common neurogenesis window observed in the mouse spinal cord. Cerebrospinal fluid contacting neurons settle around the central canal, display a unique morphology with the extension of a dendrite into the central canal, unique mechanosensitive channel expression, and distinct electrophysiological properties (Petracca et al., 2016). While their function has not been shown in mice, they are likely functionally distinct from other p2 originating IN types, V2a and V2b INs. Indeed, in the zebrafish cerebrospinal fluid contacting neurons have been shown responsible for sensing spinal bending and mediating postural control during locomotion (Böhm et al., 2016; Fidelin et al., 2015; Hubbard et al., 2016).

1.2.1.4 Neurogenesis timing can restrict IN specific circuit wirings

Timing of neuronal differential may play a role beyond defining molecular identity of spinal subpopulations to guiding the formation of distinct circuit connectivity. While limited studies have been done to date, there is evidence for IN neurogenesis timing and motor pool specific wiring.

Trans-synaptic viral tracing by Tripodi and colleges (2011) revealed that ipsilateral dI4-6 INs respectively innervating flexor or extensor MNs were spatially, synaptically and temporally separated. Last-order extensor INs were positioned more medially and received high levels of proprioceptive innervation while flexor INs were positioned more laterally and received less proprioceptive innervations. Interestingly, last-order flexor INs were early-born cells (around E10.5) while last-order extensor INs were born later (around E12.5) [Figure1.5A; Tripodi et al., 2011]. The late-born $Lbx1^{+}$ last-order extensor INs were most likely from late dILA,B progenitors (Müller et al., 2002; Gross et al., 2002; John et al., 2005; Lai et al., 2016). Thus, the time that an IN becomes post-mitotic may position it in a specific functional pathway.

Likewise, neurogenetically separated V1 INs display distinct microcircuit connectivity. Early-born V1 RCs (Benito-Gonzalez & Alvarez, 2012; Stam et al., 2012) settled within more ventral clusters and received more proprioceptive innervations from proximal hip muscles (Bikoff et al., 2016). In contrast, presumptive later-born $Sp8^{+}$ V1 INs (Hoang et al., 2018) settled within more dorsal clusters and received more proprioceptive innervations from distal foot muscles (Bikoff et al., 2016) [Figure1.5B]. While the functional relevance of these distinct sensory innervation patterns remains to be determined, it suggests an intriguing link between timing of an INs differentiation and microcircuit specific integration.

1.2.2 Lessons from the zebrafish: Sequential waves of neurogenesis form 'layered' locomotor circuits in the zebrafish spinal cord and brainstem

1.2.2.1 Early maturation of swimming behaviours is underscored by sequential waves of neurogenesis

The zebrafish model has enabled a linking of neuronal lineages to their circuit connectivity and in vivo functional recruitments. Locomotor speed dependent circuits have been extensively studied in the zebrafish spinal cord (Berg et al., 2018). Spinal MN and IN subtypes display unique cellular and subcellular connectivity and biophysical properties enabling their specific recruitment for the regulation of locomotor frequency.

Neurogenesis timing is a key determinant in the formation of speed dependent circuits in the zebrafish spinal cord. Larval zebrafish sequentially develop distinct locomotor behaviours at set postfertilization (pf) timepoints. They first display exclusively large amplitude single tail bends around 1 day (d) pf; followed by high frequency and high amplitude burst swimming around 3 dpf; and finally, slow frequency, low amplitude and continuous swimming around 4-5 dpf (Buss & Drapeau, 2001; Knogler et al., 2014; McLean et al.., 2007; McLean & Fetcho, 2009; Roussel et al., 2020; Saint-Amant, 2010). This developmental timeline of locomotor flexibility is a readout of underlying developmental changes occurring early pf. Several developmental mechanisms occur during this time including a maturation of neuronal intrinsic properties, a refining of synaptic connectivities, including a switch from electrical to chemical synapses, and the staggard neurogenesis of distinct spinal MN and IN types (Buss & Drapeau, 2001; Kimura &

Higashijima, 2019; Kimura et al., 2006; Kishore et al., 2020; McLean et al.., 2007; McLean & Fetcho, 2009; Myers et al., 1986; Roussel et al., 2020; Saint-Amant, 2010; Satou et al., 2012).

It may not be surprising then that McLean and colleagues (2007, 2009) showed that spinal circuits involved in different swimming speeds display a temporal ordering of neurogenesis and differentiation. Spinal INs and MNs involved in high-amplitude and fast swimming speeds emerge first during early larval development (Figure1.6Ai-ii). Subsequently, INs and MNs involved in lower amplitude and slow swimming speeds differentiate (Figure1.6Bi-ii). This temporal ordering of speed-related swimming circuits results in a topographic recruitment map across the dorsovental axis in the larval zebrafish spinal cord (McLean et al., 2007; McLean & Fetcho, 2009). As larval swimming speeds increase so do the recruitments of increasingly ventral INs and MNs. Interesting, while speed-dependent circuits maintain a modular recruitment logic in the adult, they no longer display a clear topographic organization (Ampatzis et al., 2014; Ausborn et al., 2012; Björnfors & El Manira, 2016). Thus, topographic organization in the larvae may be more representative of the sequential differentiation of fast to slow swimming circuits than final neuronal positioning.

1.2.2.2 Spinal neurons separate along neurogenesis time- and speed-matched axes

Spinal MNs can be categorized as either primary or secondary MNs in embryonic and larval zebrafish. Primary MNs are born during an early neurogenesis wave and are recruited during large amplitude and fast frequency escape and swimming movements. Secondary MNs are born during a later neurogenesis wave and are recruited during slow frequency swimming (McLean

& Fetcho, 2009). Furthermore, primary and secondary MNs display unique morphological and electrophysiological properties. Primary MNs have larger soma sizes, smaller input resistances, more extensive dendritic branching, larger axon diameters, more ventromedial axon projection pathways, and settle within relatively more dorsal positions than secondary MNs (Myers et al., 1985, 1986; McLean & Fetch, 2009). Primary and secondary MNs also express distinct calcium channel types resulting in distinct neurotransmitter release properties and downstream muscle fibre control (Wen et al., 2020). Thus, neurogenesis timing appears to serve as an early organizing principle for the anatomical and intrinsic properties of zebrafish MNs resulting in fast and slow swimming control.

Beyond MNs, spinal INs in the zebrafish display strong correlations between their neurogenesis timings and functional recruitment patterns. Distinct excitatory and inhibitory spinal IN lineages integrate within fast and slow-swimming circuits dependent on their neurogenesis timing. Like MNs, and across all studied IN lineages, early-born spinal INs differentiate into fast-swimming circuits while later-born spinal INs differentiate into slow-swimming circuits. Beyond speed matched recruitment patterns, the temporal ordering of IN differentiation also appears to play a key role in the establishment of subtype-specific intrinsic properties and connectivities.

Anatomically and neurochemically distinct V0 INs are produced in a time-dependent manner from heterogeneous p0 progenitor cells in the zebrafish spinal cord (Satou et al., 2012). Commissural and excitatory V0-e INs display a correlation between their neurogenesis timing and axon projection profiles. Ascending commissural V0-e INs are born first; followed by bifurcating commissural V0-e INs; and finally descending commissural V0-e INs. In this case, neurogenesis timing seems to play a direct role in ordering V0 INs axon projection phenotypes.

Accelerated neurogenesis timing by reduced notch signalling resulted in an increased number of early-born ascending V0-e INs (Satou et al., 2012). Thus, neurogenesis timing orders V0e INs down distinct differentiation pathways resulting in temporally ordered axon projection profiles.

Late-born descending V0-e INs can be further subdivided into unipolar (UCoD) and multipolar (MCoD) commissural descending INs. Thus, further subpopulation heterogeneity exists within the late-born neurogenesis window of V0-e INs. Although MCoD INs were specifically recruited during slower swimming speeds in the larvae zebrafish (McLean et al., 2007, 2008), no correlation between morphology and speed-dependent recruitment of V0-e INs was found in the adult spinal cord (Björnfors & El Manira, 2016). It is therefore possible that either early morphological distinctions in the larvae are lost in the adult or that V0-e IN recruitment patterns change with maturation.

In addition to excitatory INs, both commissural and ipsilateral inhibitory INs display neurogenesis matched properties and circuit integrations. Inhibitory and ipsilaterally projecting V1 INs can be generally divided into either early-born or later-born groups. Early-born V1 INs are preferentially recruited during higher swimming frequencies while later-born V1 INs during slower swim frequencies (Kimura et al., 2019). When all V1 INs are ablated, fish display reduced swimming frequencies due to increased cycle periods across both fast and slow speeds. Additionally, during fast swimming bouts, MNs and INs from slow swimming circuits exhibit reduced inhibition (Kimura et al., 2019). Thus, both early-born fast-type and later-born slow-type V1 INs are involved in cycle-burst termination required for swimming frequency (Figure1.6Aiii,Biii). However, fast-type V1 INs are proposed to further inhibit slow V2a IN and

MN circuits during specifically high-speed swimming (Figure1.6Aiii). The neurogenesis timing of V1 INs therefore corresponds to both speed-specific recruitments and functional outputs.

1.2.2.3 Neurogenesis and differentiation timing matches pre- and post-synaptic targets

Recent work from McLean's group have just revealed even further that neurogenesis timing can order the subcellular innervation patterns of last-order inhibitory INs. Inhibitory commissural dI6 INs necessary for left-right alteration form distinct microcircuit connectivities with commissural MNs depending on their neurogenesis times (Kishore et al., 2020). Temporally, morphologically, and synaptically distinct dI6 IN circuits are differentially recruited and function across increasing swimming speeds. Early-born dI6 INs synapse primarily on MN axons and are recruited during highest frequency swimming (Figure1.6Aiii). This axonal innervation is likely functionally necessary for quick MN termination needed for high frequency left-right alteration. Late-born dI6 INs primarily synapse onto MN somas and dendrites and are recruited during slower swimming speeds (Figure1.6Biii) [Kishore et al., 2020]. Interestingly, these temporally regulated synaptic IN-MN innervation patterns appear to be determined by the available post-synaptic targets at the time of dI6 IN neurogenesis (Myers et al., 1986). As late-born dI6 INs exit the cell cycle, MNs begin to extend elaborate dendritic arbors (Kishore and Fetcho, 2013), thus, providing temporally aligned targets (dendrites) for the late-born dI6 INs. Taken together, this works suggests neurogenesis timing may organize neural circuit formation by temporally layering the alignment of pre- and post-synaptic targets.

1.2.2.4 Temporal layering of spinal circuits extends to the brainstem

Moving beyond connections within the spinal cord, the question remains of whether the temporal ordering of spinal circuits extends to peripheral and supraspinal inputs entering the spinal cord. Indeed, recent work by Pujala and colleagues (2019) revealed that temporal neurogenesis ordering of fast to slow locomotor control is extended to circuits in the brain stem. Early-born hindbrain V2a neurons are recruited during fast locomotor bursts, while later-born hindbrain V2a INs are recruited during slower swimming movements (Pujala et al., 2019). Interestingly, descending hindbrain V2a neurons display age- and function-matched connectivity patterns with networks in the spinal cord. Early-born hindbrain V2a neurons form connections to fast locomotor networks in the spinal cord, while later-born hindbrain V2a form connections with slow swimming spinal networks (Pujala et al., 2019). Thus, the temporal layering of spinal circuits involved in fast to slow locomotor control appears to extend beyond the spinal cord to hindbrain motor circuits.

1.2.3 Concluding remarks on temporal developmental mechanisms guiding spinal interneuron diversity

Neurogenesis timing has been shown as a key developmental mechanism in patterning neuronal circuits across the nervous system of varied species (Holguera & Desplan, 2018; Oberst et al., 2019). Indeed, temporal TF networks have been revealed and extensively studied throughout lower invertebrate species, such as Drosophila (Doe, 2017) and C. elegans (Allan &

Thor, 2015). In these cases, a neurons postmitotic identity and fate choice is largely dependent on its dynamic TF state at the time it exits the cell cycle.

While such specific temporal TFs have yet to be revealed within mammalian spinal cord progenitor cells, from the collection of work presented here, they likely exist and play crucial roles in diversifying spinal IN identities emerging from within and between spatially confined progenitors. Indeed, work in the mouse has revealed that some temporally regulated postmitotic TF expressions in specific IN subpopulations instruct distinct circuit connectivity. However, to date, an understanding of how temporally regulated post-mitotic TFs translate into subpopulation specific functional roles has remained largely unexamined in the mouse spinal cord. Yet, in the zebrafish spinal cord, while the molecular logic remains much less understood, several studies have demonstrated how temporally regulated IN types differentially contribute to fast and slow swimming circuits. Thus, moving forward, work done in each model system can lend illuminating insights to the other. Particularly, with the recent discovery of temporally regulated post-mitotic TFs in the mouse spinal cord, it will be interestingly to understand whether differential neurogenesis timing plays a role in determining subpopulation specific expression of these TFs, and then to what extent temporally regulated subpopulation fates differentially function across speed- and/or state-dependent sensorimotor tasks.

1.3 Rationale and Aims

Neuronal networks in the spinal cord are comprised of motoneurons and interneurons, which together are essential for sensorimotor control. Motoneurons serve as the 'final common pathway' by directly controlling muscle contraction in the periphery. Spinal cord interneurons shape this motor control by functioning upstream of motoneurons. Spinal interneurons integrate and process supraspinal and sensory commands as well as generate rhythmic and patterned motor output. As such, spinal interneurons enable successful behavioural flexibility across varied sensorimotor tasks and through dynamic environments.

Observations across invertebrate and vertebrate species have revealed that increasing sensorimotor complexity corresponds to increasing interneuron diversity in the spinal cord. Furthermore, studies from behaving animals, such as zebrafish, lamprey and turtles, have shown that the activation of individual spinal interneurons can be state- and/or speed-dependent. Thus, to understand the circuit logic underlying sensorimotor control it is essential to, first, identify and target interneuron types in the spinal cord, and second, to investigate how those specific interneuron types are utilized across distinct sensorimotor tasks.

For my Ph.D. work, I focused on the V3 class of excitatory interneurons in the mouse spinal cord. V3 INs are defined by their developmental lineage. During early embryogenesis, they express the Sim1 transcription factor as they exit the cell-cycle becoming postmitotic. By postnatal stages, V3 INs display highly heterogenous anatomical and electrophysiological properties. Furthermore, unpublished work from Dr. Zhang's lab has revealed that they function across a diverse range of sensorimotor behaviours. However, whether and how V3

interneuron heterogeneity translate into functional relevance remains unknown. Thus, the driving hypothesis of my thesis is that *the spinal V3 interneuron class in comprised of functionally independent subpopulations, which are differentially recruited across varied sensorimotor behaviours.*

To address this hypothesis, my work aimed to answer two fundamental questions. The first question was to what extent does V3 interneuron diversity underlie behavioural sensorimotor diversity? To answer this question, I utilized task-specific cfos expression and computational analyses presented throughout chapter 2. I uncovered that anatomically distinct V3 interneuron clusters display unique recruitment patterns across speed- and state-dependent behavioural tasks. Thus, V3 interneuron subsets are functionally organized into topographically clustered recruitment modules. The second question I aimed to address was how do V3 interneuron subpopulations within distinct topographical recruitment modules diversify during early embryogenesis? In chapter 3, I show that neurogenesis timing patterns spinal p3-v3 interneurons into divergent subpopulation assemblies. Next, in chapter 4, I further define V3 subpopulations by unique transcription factor expression profiles, morphologies, intrinsic membrane properties, and circuit connectivities. These V3 interneuron subpopulations are diversified across hierarchical temporal and spatial developmental pathways. Taken together, my current work highlights how early embryonic pathways diversify spinal interneurons into heterogeneous subpopulation clusters necessary for behavioural diversity in adulthood.

2. Figures

Figure 1.1 Interneuron (IN) subsets in the ventral spinal cord organize into rhythm-generating and pattern-forming functional layers

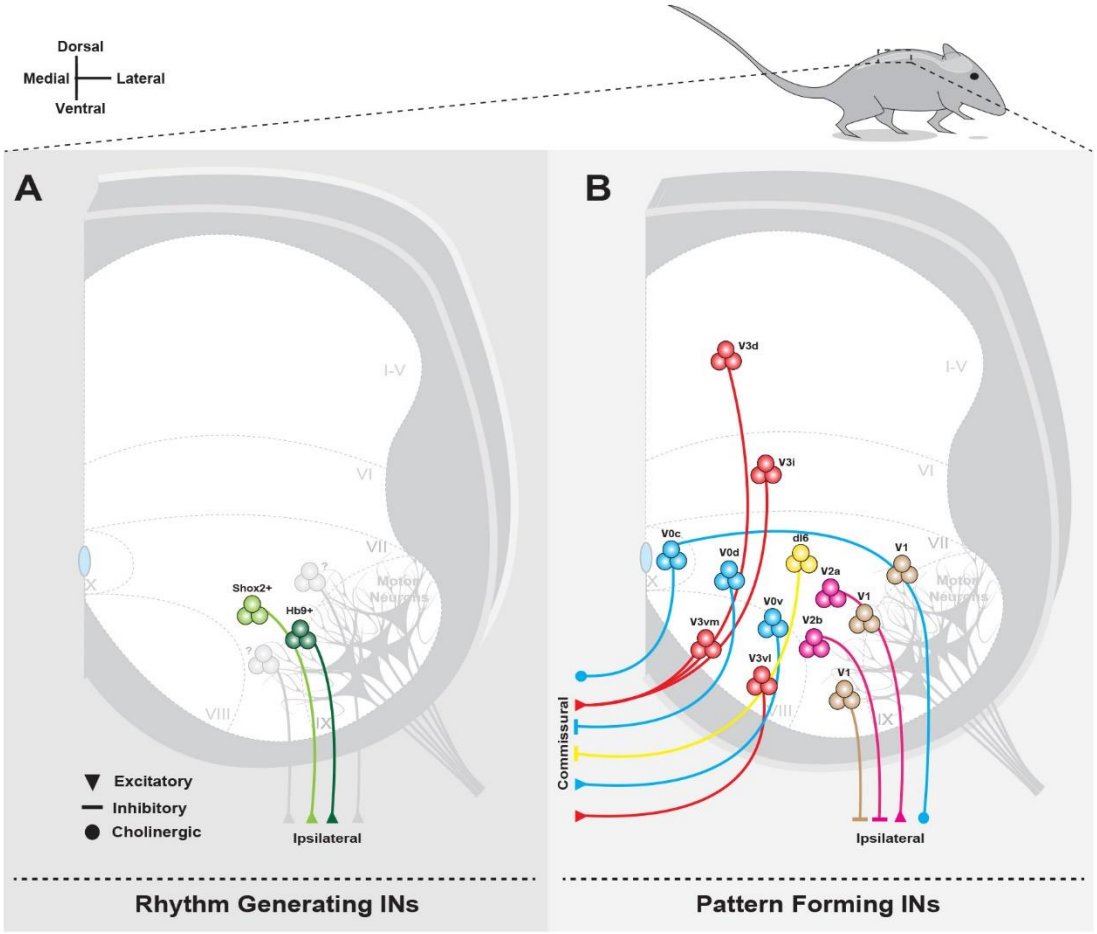

Figure 1.1 Interneuron (IN) subsets in the ventral spinal cord organize into rhythm-generating and pattern-forming functional layers.

Molecularly distinct ventral IN subpopulations possess specific neurochemical (excitatory, inhibitory, or cholinergic) and anatomical (commissural or ipsilateral axon projections) properties. Distinct IN subpopulations then functionally integrate within rhythm-generating (A) or pattern-forming (B) locomotor circuit layers. [V0d (dorsal), V0v (ventral), V3d (dorsal), V3i (intermediate), V3vm (ventromedial), V3vl (ventrolateral)].

Figure 1.2 Distinct pattern-forming IN circuits drive speed-dependent locomotor gait changes in mice

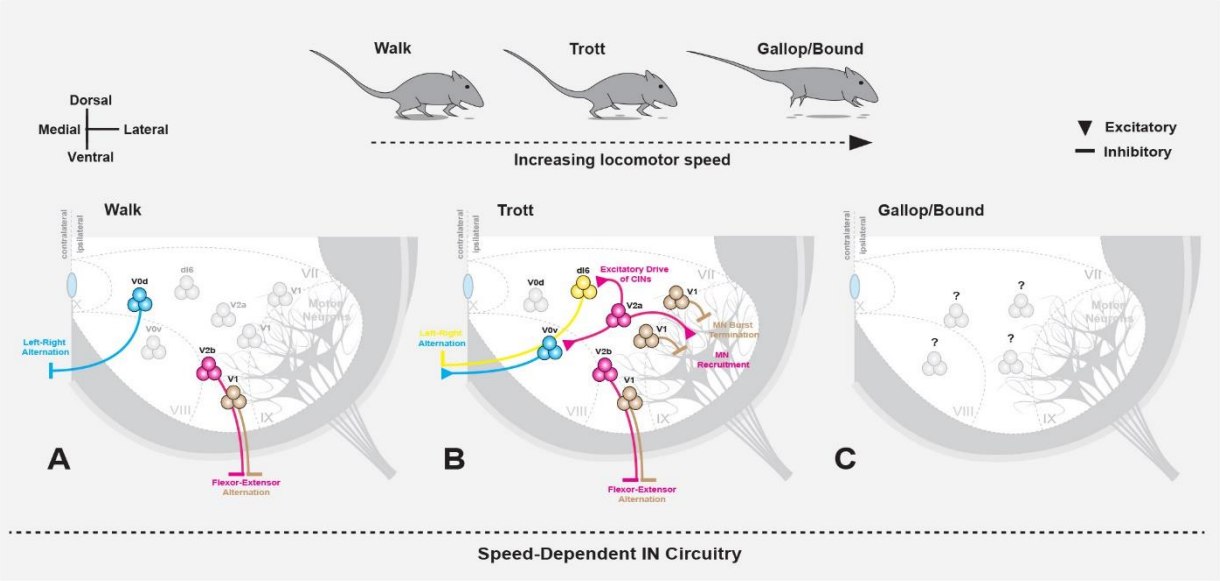

Figure 1.2 Distinct pattern-forming IN circuits drive speed-dependent locomotor gait changes in mice.

At low locomotor speeds V2b and V1 INs collectively secure flexor-extensor alternations while V0d INs secure left-right hindlimb alternations producing a walking gait (A). As locomotion increases to an intermediate speed, V2b and V1 INs continue to secure flexor-extensor alternations, V2a INs drive commissural INs and motor neuron recruitment levels, and dI6 and V0v INs secure left-right alternations, producing a trotting gait (B). At maximum locomotor speeds the spinal IN circuits driving intermittent galloping/bounding gaits are unknown (C).

Figure 1.3 Motor neurons (MNs) form distinct positive and negative feedback loops with ipsilateral and local IN populations

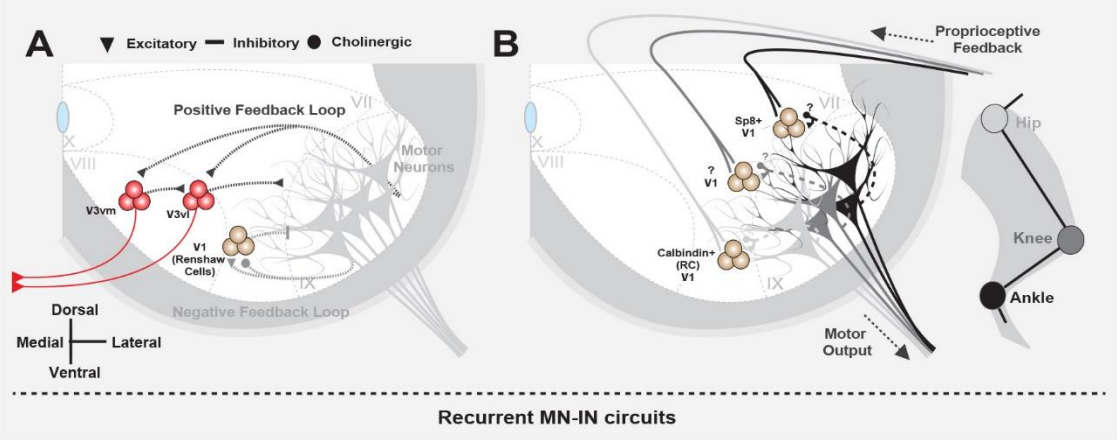

Figure 1.3 Motor neurons (MNs) form distinct positive and negative feedback loops with ipsilateral and local IN populations.

Ventral V3(v) INs diversify into medial (V3vm) and lateral (V3vl) subpopulations and mediate recurrent positive feedback onto local MNs (Chopek et al., 2018). V1 INs, initially described as Renshaw cells (RCs) (Renshaw, 1946), mediate recurrent negative feedback onto local MNs (A). Dorsoventrally arranged V1 IN subsets receive joint specific sensory and potentially motor neuron axon collateral inputs revealing potential joint-specific recurrent motor feedback circuits (B).

Figure 1.4 Snapshot: Spinal IN diversity and locomotor function

Figure 1.5 IN neurogenesis timing and circuit connectivity in the mouse spinal cord

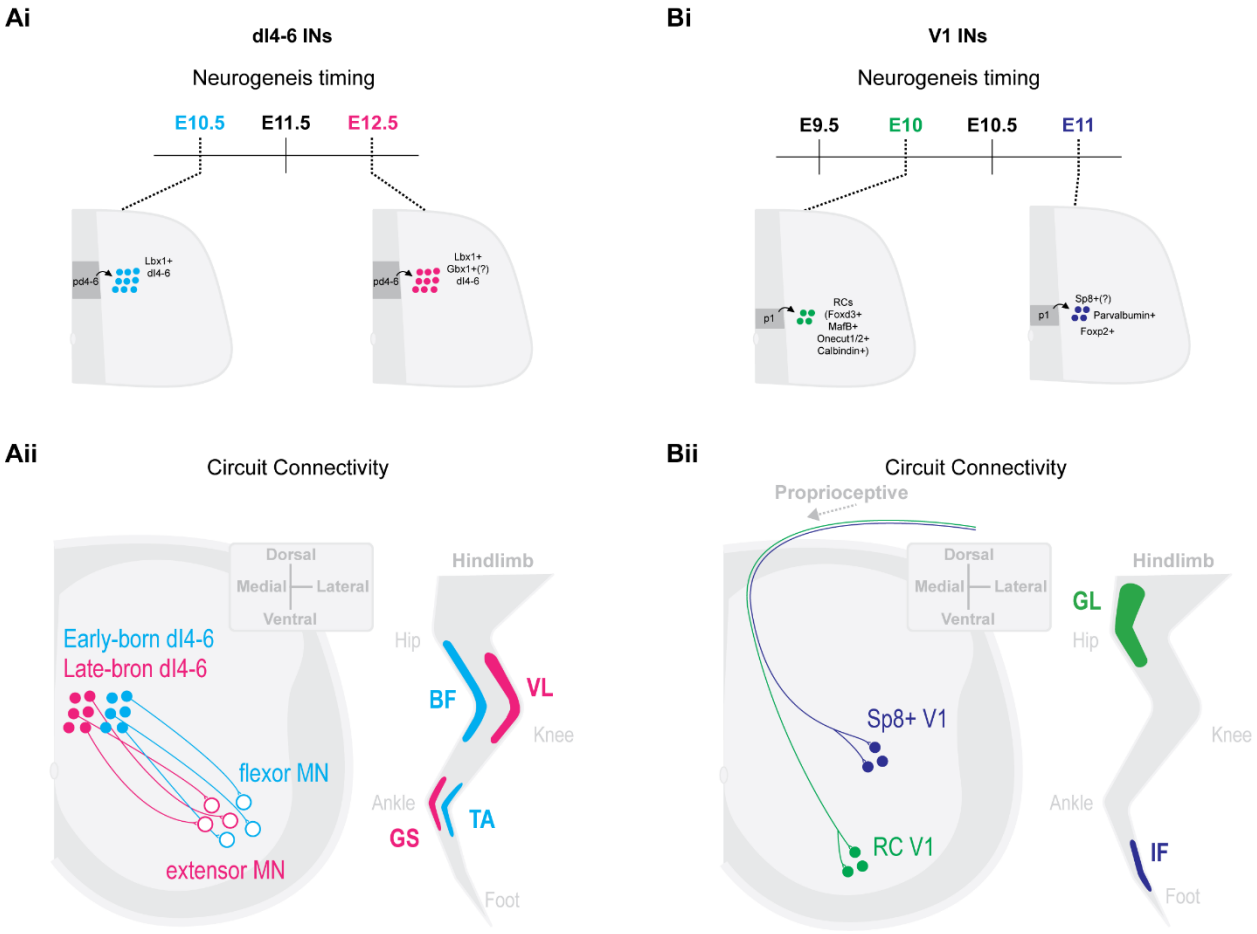

Figure 1.5 IN neurogenesis timing and circuit connectivity in the mouse spinal cord

(Ai) dI4-6 last-order INs emerge during either early-born (E10.5) or late-born (E12.5) neurogenesis waves (Tripodi et al., 2011). Late-born dI4-6 INs are likely dILA/B IN populations and some likely express Gbx1+ (Buckley et al., 2013, 2020; Meziane et al., 2013). (Aii) By postnatal stages early-born dI4-6 INs are positioned laterally preferentially innervate flexor MNs while late-born dI4-6 INs are positioned medially and preferentially innervate extensor MNs (Tripodi et al., 2011) (extensor muscles, vastus lateralis (VL), gastrocnemius (GS); flexor muscles, biceps femoris (BF), Tibialis anterior (TA)). (Bi) Early-born V1 INs (E10) differentiate into Renshaw Cells (RCs) [Benito-Gonzalez & Alvarez, 2012; Stam et al., 2012] while late-born V1 INs (E11) (differentiate into Foxp2+ V1 INs (Benito-Gonzalez & Alvarez, 2012), Parvalbumin+ V1 INs (Benito-Gonzalez & Alvarez, 2012), and likely Sp8+ V1 INs (Hoang et al., 2018). By postnatal stages early-born RC V1 INs settled within more ventral clusters and received more proprioceptive innervations from proximal hip muscles (Bikoff et al., 2016). Presumptive later-born $Sp8^{+}$ V1 INs (Hoang et al., 2018) settle within more dorsal clusters and received more proprioceptive innervations from distal foot muscles (Bikoff et al., 2016) [proximal muscle, Gluteus (GL); distal muscle, intrinsic foot (IF)].

Figure 1.6 Sequential waves of neurogenesis separate zebrafish spinal cord neurons along neurogenesis time- and speed-matched axes

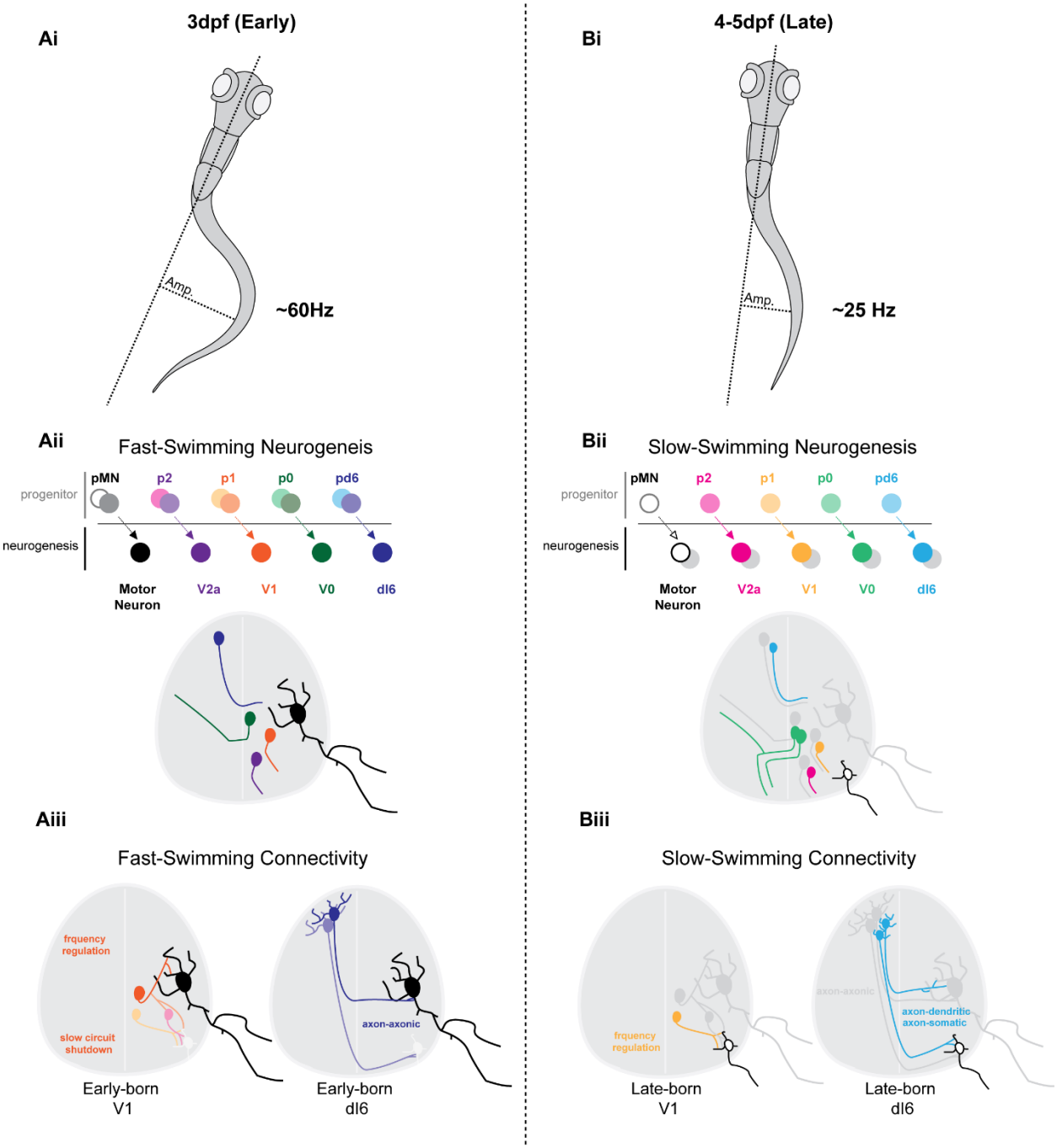

Figure 1.6 Sequential waves of neurogenesis separate zebrafish spinal cord neurons along neurogenesis time- and speed-matched axes

Large amplitude (Amp) and high frequency swimming emerges early at 3 days post feralization (dpf) in the zebrafish larvae (Ai). Small amplitude (Amp) and low frequency swimming emerges later at 4-5 days post feralization (dpf) in the zebrafish larvae (Bi) [McLean et al., 2007; McLean & Fetcho, 2009]. Early maturation of swimming behaviours is underscored by sequential waves of neurogenesis (Aii, early-born and fast swimming recruitment; Bii, late-born and slow swimming recruitment; motor neurons (MNs), McLean & Fetcho, 2009; V0, McLean et al., 2007, 2008, Satou et al., 2012; V2a INs, Kimura et al., 2006; V1 INs, Kimura et al., 2019; dI6 INs, Kishore et al., 2020). Neurogenesis time- and speed-matched spinal IN subclasses display distinct circuit connectivities. Early-born V1 INs regulate MN burst termination of primary MNs during fast-swimming as well as slow-swimming circuit shutdown of slow speed V2a INs and secondary MNs (Kimura et al., 2019). Early-born dI6 INs form axon-axonic synaptic connectivites with MNs and are recruited during fast-swimming (Aiii). Late-born V1 INs regulate MN burst termination of secondary MNs during slow-swimming. Late-born dI6 INs form axon-somatic and axon-dendritic synaptic connectivites with MNs and are recruited during slow-swimming (Biii) [Kishore et al., 2020].

3. References

Akay, T., Tourtellotte, W., Arber, S., & Jessell, T. (2014). Degradation of mouse locomotor pattern in the absence of proprioceptive sensory feedback. Proceedings of the National Academy of Sciences of the United States of America, 111(47), 16877-16882. doi:10.1073/pnas.1419045111

Al Mosawie, A., Wilson, J. M., & Brownstone, R. M. (2007). Heterogeneity of V2-derived interneurons in the adult mouse spinal cord. European Journal of Neuroscience, 26(11), 3003-3015. doi:10.1111/j.1460-9568.2007.05907.x

Allan, D., & Thor, S. (2015). Transcriptional selectors, masters, and combinatorial codes: Regulatory principles of neural subtype specification. Wiley Interdisciplinary Reviews: Developmental Biology, 4(5), 505-528. doi:10.1002/wdev.191

Alvarez, F., Jonas, P., Sapir, T., Hartley, R., Berrocal, M., Geiman, E., . . . Goulding, M. (2005). Postnatal phenotype and localization of spinal cord V1 derived interneurons. Journal of Comparative Neurology, 493(2), 177-192. doi:10.1002/cne.20711

Ampatzis, K., Song, J., Ausborn, J., & El Manira, A. (2014). Separate microcircuit modules of distinct v2a interneurons and motoneurons control the speed of locomotion. Neuron, 83(4), 934-943. doi:10.1016/j.neuron.2014.07.018

Andersson, L., Larhammar, M., Memic, F., Wootz, H., Schwochow, D., Rubin, C., . . . Kullander, K. (2012). Mutations in DMRT3 affect locomotion in horses and spinal circuit function in mice. Nature, 488(7413), 642-646. doi:10.1038/nature11399

Ausborn, J., Mahmood, R., & El Manira, A. (2012). Decoding the rules of recruitment of excitatory interneurons in the adult zebrafish locomotor network. Proceedings of the National Academy of Sciences of the United States of America, 109(52), E3631-E3639. doi:10.1073/pnas.1216256110

Bellardita, C., & Kiehn, O. (2015). Phenotypic characterization of speed-associated gait changes in mice reveals modular organization of locomotor networks. Current Biology, 25(11), 1426-1436. doi:10.1016/j.cub.2015.04.005

Benito Gonzalez, A., & Alvarez, F. (2012). Renshaw cells and ia inhibitory interneurons are generated at different times from p1 progenitors and differentiate shortly after exiting the cell cycle. The Journal of Neuroscience, 32(4), 1156-1170. doi:10.1523/JNEUROSCI.3630-12.2012

Berg, E., Björnfors, E. R., Pallucchi, I., Picton, L., & El Manira, A. (2018). Principles governing locomotion in vertebrates: Lessons from zebrafish. Frontiers in Neural Circuits, 12, 73-73. doi:10.3389/fncir.2018.00073

Bertuzzi, M., & Ampatzis, K. (2018). Spinal cholinergic interneurons differentially control motoneuron excitability and alter the locomotor network operational range. Scientific Reports, 8(1), 1988-1988. doi:10.1038/s41598-018-20493-z

Bhumbra, G., Bannatyne, B. A., Watanabe, M., Todd, A., Maxwell, D., & Beato, M. (2014). The recurrent case for the renshaw cell. The Journal of Neuroscience, 34(38), 12919-12932. doi:10.1523/JNEUROSCI.0199-14.2014

Bikoff, J., Gabitto, M., Rivard, A., Drobac, E., Machado, T., Miri, A., . . . Jessell, T. (2016). Spinal inhibitory interneuron diversity delineates variant motor microcircuits. Cell, 165(1), 207-219. doi:10.1016/j.cell.2016.01.027

Björnfors, E. R., & El Manira, A. (2016). Functional diversity of excitatory commissural interneurons in adult zebrafish. Elife, 5 doi:10.7554/eLife.18579

Blacklaws, J., Deska Gauthier, D., Jones, C., Petracca, Y., Liu, M., Zhang, H., . . . Zhang, Y. (2015). Sim1 is required for the migration and axonal projections of V3 interneurons in the developing mouse spinal cord. Developmental Neurobiology, 75(9), 1003-1017. doi:10.1002/dneu.22266

Boeri, J., Le Corronc, H., Lejeune, F., Le Bras, B., Mouffle, C., Angelim, Monara Kaelle S C, . . . Czarnecki, A. (2018). Persistent sodium current drives excitability of immature renshaw cells in early embryonic spinal networks. The Journal of Neuroscience, 38(35), 7667-7682. doi:10.1523/JNEUROSCI.3203-17.2018

Böhm, U., Prendergast, A., Djenoune, L., Nunes Figueiredo, S., Gomez, J., Stokes, C., . . . Wyart, C. (2016). CSF-contacting neurons regulate locomotion by relaying mechanical stimuli to spinal circuits. Nature Communications, 7, 10866-10866. doi:10.1038/ncomms10866

Borowska, J., Jones, C. T., Deska Gauthier, D., & Zhang, Y. (2015). V3 interneuron subpopulations in the mouse spinal cord undergo distinctive postnatal maturation processes. Neuroscience, 295, 221-228. doi:10.1016/j.neuroscience.2015.03.024

Borowska, J., Jones, C., Zhang, H., Blacklaws, J., Goulding, M., & Zhang, Y. (2013). Functional subpopulations of V3 interneurons in the mature mouse spinal cord. The Journal of Neuroscience, 33(47), 18553-18565. doi:10.1523/JNEUROSCI.2005-13.2013

Bourane, S., Grossmann, K., Britz, O., Dalet, A., Del Barrio, M., Stam, F., . . . Goulding, M. (2015). Identification of a spinal circuit for light touch and fine motor control. Cell, 160(3), 503-515. doi:10.1016/j.cell.2015.01.011

Britz, O., Zhang, J., Grossmann, K., Dyck, J., Kim, J., Dymecki, S., . . . Goulding, M. (2015). A genetically defined asymmetry underlies the inhibitory control of flexor-extensor locomotor movements. Elife, 4 doi:10.7554/eLife.04718

Buckley, D., Burroughs Garcia, J., Kriks, S., Lewandoski, M., & Waters, S. (2020). Gbx1 and Gbx2 are essential for normal patterning and development of interneurons and motor neurons in the embryonic spinal cord. Journal of Developmental Biology, 8(2) doi:10.3390/jdb8020009

Buckley, D., Burroughs Garcia, J., Lewandoski, M., & Waters, S. (2013). Characterization of the Gbx1-/- mouse mutant: A requirement for Gbx1 in normal locomotion and sensorimotor circuit development. Plos One, 8(2), e56214-e56214. doi:10.1371/journal.pone.0056214

Bui, T., Akay, T., Loubani, O., Hnasko, T., Jessell, T., & Brownstone, R. (2013). Circuits for grasping: Spinal dI3 interneurons mediate cutaneous control of motor behavior. Neuron, 78(1), 191-204. doi:10.1016/j.neuron.2013.02.007

Bui, T., Stifani, N., Akay, T., & Brownstone, R. (2016). Spinal microcircuits comprising dI3 interneurons are necessary for motor functional recovery following spinal cord transection. Elife, 5 doi:10.7554/eLife.21715

Buss, R. R., & Drapeau, P. (2001). Synaptic drive to motoneurons during fictive swimming in the developing zebrafish. Journal of Neurophysiology, 86(1), 197-210. doi:10.1152/jn.2001.86.1.197

Caldeira, V., Dougherty, K., Borgius, L., & Kiehn, O. (2017). Spinal Hb9::Cre-derived excitatory interneurons contribute to rhythm generation in the mouse. Scientific Reports, 7, 41369-41369. doi:10.1038/srep41369

Chopek, J., Nascimento, F., Beato, M., Brownstone, R., & Zhang, Y. (2018). Sub-populations of spinal V3 interneurons form focal modules of layered pre-motor microcircuits. Cell Reports, 25(1), 146-156.e3. doi:10.1016/j.celrep.2018.08.095

Crone, S., Quinlan, K., Zagoraiou, L., Droho, S., Restrepo, C., Lundfald, L., . . . Sharma, K. (2008). Genetic ablation of V2a ipsilateral interneurons disrupts left-right locomotor coordination in mammalian spinal cord. Neuron, 60(1), 70-83. doi:10.1016/j.neuron.2008.08.009

Crone, S., Zhong, G., Harris Warrick, R., & Sharma, K. (2009). In mice lacking V2a interneurons, gait depends on speed of locomotion. The Journal of Neuroscience, 29(21), 7098-7109. doi:10.1523/JNEUROSCI.1206-09.2009

Danner, S., Shevtsova, N., Frigon, A., & Rybak, I. (2017). Computational modeling of spinal circuits controlling limb coordination and gaits in quadrupeds. Elife, 6 doi:10.7554/eLife.31050

Danner, S., Zhang, H., Shevtsova, N., Borowska Fielding, J., Deska Gauthier, D., Rybak, I., & Zhang, Y. (2019). Spinal V3 interneurons and left-right coordination in mammalian locomotion. Frontiers in Cellular Neuroscience, 13, 516-516. doi:10.3389/fncel.2019.00516

Delile, J., Rayon, T., Melchionda, M., Edwards, A., Briscoe, J., & Sagner, A. (2019). Single cell transcriptomics reveals spatial and temporal dynamics of gene expression in the developing mouse spinal cord. Development, 146(12) doi:10.1242/dev.173807

Deska Gauthier, D., Borowska Fielding, J., Jones, C., & Zhang, Y. (2020). The temporal neurogenesis patterning of spinal p3-V3 interneurons into divergent subpopulation assemblies. The Journal of Neuroscience, 40(7), 1440-1452. doi:10.1523/JNEUROSCI.1518-19.2019

Deska-Gauthier, D., & Zhang, Y. (2019). The functional diversity of spinal interneurons and locomotor control. Current Opinion in Physiology, 8, 99-108. doi:https://doi.org/10.1016/j.cophys.2019.01.005

Doe, C. (2017). Temporal patterning in the drosophila CNS. Annual Review of Cell and Developmental Biology, 33, 219-240. doi:10.1146/annurev-cellbio-111315-125210

Donelan, J. M., & Pearson, K. (2004). Contribution of sensory feedback to ongoing ankle extensor activity during the stance phase of walking. Canadian Journal of Physiology and Pharmacology, 82(8-9), 589-598. doi:10.1139/y04-043

Dougherty, K., Zagoraiou, L., Satoh, D., Rozani, I., Doobar, S., Arber, S., . . . Kiehn, O. (2013). Locomotor rhythm generation linked to the output of spinal shox2 excitatory interneurons. Neuron, 80(4), 920-933. doi:10.1016/j.neuron.2013.08.015

Dougherty, K., & Kiehn, O. (2010). Functional organization of V2a-related locomotor circuits in the rodent spinal cord. Annals of the New York Academy of Sciences, 1198, 85-93. doi:10.1111/j.1749-6632.2010.05502.x

Duysens, J. (1977). Fluctuations in sensitivity to rhythm resetting effects during the cat's step cycle. Brain Research, 133(1), 190-195. doi:10.1016/0006-8993(77)90063-4

Dyck, J., Lanuza, G., & Gosgnach, S. (2012). Functional characterization of dI6 interneurons in the neonatal mouse spinal cord. Journal of Neurophysiology, 107(12), 3256-3266. doi:10.1152/jn.01132.2011

Ellaway, P., Taylor, A., & Durbaba, R. (2015). Muscle spindle and fusimotor activity in locomotion. Journal of Anatomy, 227(2), 157-166. doi:10.1111/joa.12299

Engberg, I., & Lundberg, A. (1969). An electromyographic analysis of muscular activity in the hindlimb of the cat during unrestrained locomotion. Acta Physiologica Scandinavica, 75(4), 614-630. doi:10.1111/j.1748-1716.1969.tb04415.x

Falgairolle, M., Puhl, J., Pujala, A., Liu, W., & O'Donovan, M. (2017). Motoneurons regulate the central pattern generator during drug-induced locomotor-like activity in the neonatal mouse. Elife, 6 doi:10.7554/eLife.26622

Fidelin, K., Djenoune, L., Stokes, C., Prendergast, A., Gomez, J., Baradel, A., . . . Wyart, C. (2015). State-dependent modulation of locomotion by GABAergic spinal sensory neurons. Current Biology, 25(23), 3035-3047. doi:10.1016/j.cub.2015.09.070

Fink, A. J. P., Croce, K., Huang, Z. J., Abbott, L. F., Jessell, T., & Azim, E. (2014). Presynaptic inhibition of spinal sensory feedback ensures smooth movement. Nature, 509(7498), 43-48. doi:10.1038/nature13276

Gabitto, M., Pakman, A., Bikoff, J., Abbott, L. F., Jessell, T., & Paninski, L. (2016). Bayesian sparse regression analysis documents the diversity of spinal inhibitory interneurons. Cell, 165(1), 220-233. doi:10.1016/j.cell.2016.01.026

Gosgnach, S., Bikoff, J., Dougherty, K., El Manira, A., Lanuza, G., & Zhang, Y. (2017). Delineating the diversity of spinal interneurons in locomotor circuits. The Journal of Neuroscience, 37(45), 10835-10841. doi:10.1523/JNEUROSCI.1829-17.2017

Gosgnach, S., Lanuza, G., Butt, S. J. B., Saueressig, H., Zhang, Y., Velasquez, T., . . . Goulding, M. (2006). V1 spinal neurons regulate the speed of vertebrate locomotor outputs. Nature, 440(7081), 215-219. doi:10.1038/nature04545

Goulding, M. (2009). Circuits controlling vertebrate locomotion: Moving in a new direction. Nature Reviews.Neuroscience, 10(7), 507-518. doi:10.1038/nrn2608

Griener, A., Zhang, W., Kao, H., Haque, F., & Gosgnach, S. (2017). Anatomical and electrophysiological characterization of a population of dI6 interneurons in the neonatal mouse spinal cord. Neuroscience, 362, 47-59. doi:10.1016/j.neuroscience.2017.08.031

Grillner, S., & Zangger, P. (1979). On the central generation of locomotion in the low spinal cat. Experimental Brain Research, 34(2), 241-261. doi:10.1007/BF00235671

Grillner, S., & Zangger, P. (1984). The effect of dorsal root transection on the efferent motor pattern in the cat's hindlimb during locomotion. Acta Physiologica Scandinavica, 120(3), 393-405. doi:10.1111/j.1748-1716.1984.tb07400.x

Grillner, S. (2003). The motor infrastructure: From ion channels to neuronal networks. Nature Reviews Neuroscience, 4(7), 573-586. doi:10.1038/nrn1137

Gross, M., Dottori, M., & Goulding, M. (2002). Lbx1 specifies somatosensory association interneurons in the dorsal spinal cord. Neuron, 34(4), 535-549. doi:10.1016/S0896-6273(02)00690-6

Guertin, P., Angel, M. J., Perreault, M. C., & McCrea, D. A. (1995). Ankle extensor group I afferents excite extensors throughout the hindlimb during fictive locomotion in the cat. The Journal of Physiology, 487(1), 197-209. doi:10.1113/jphysiol.1995.sp020871

Hägglund, M., Borgius, L., Dougherty, K., & Kiehn, O. (2010). Activation of groups of excitatory neurons in the mammalian spinal cord or hindbrain evokes locomotion. Nature Neuroscience, 13(2), 246-252. doi:10.1038/nn.2482

Hägglund, M., Dougherty, K., Borgius, L., Itohara, S., Iwasato, T., & Kiehn, O. (2013). Optogenetic dissection reveals multiple rhythmogenic modules underlying locomotion. Proceedings of the National Academy of Sciences of the United States of America, 110(28), 11589-11594. doi:10.1073/pnas.130436511

Haque, F., Rancic, V., Zhang, W., Clugston, R., Ballanyi, K., & Gosgnach, S. (2018). wt1. The Journal of Neuroscience, 38(25), 5666-5676. doi:10.1523/JNEUROSCI.0328-18.2018

Harris, A., Masgutova, G., Collin, A., Toch, M., Hidalgo Figueroa, M., Jacob, B., . . . Clotman, F. (2019). Onecut factors and Pou2f2 regulate the distribution of V2 interneurons in the mouse developing spinal cord. Frontiers in Cellular Neuroscience, 13, 184-184. doi:10.3389/fncel.2019.00184

Hayashi, M., Hinckley, C., Driscoll, S., Moore, N., Levine, A., Hilde, K., . . . Pfaff, S. (2018). Graded arrays of spinal and supraspinal V2a interneuron subtypes underlie forelimb and hindlimb motor control. Neuron, 97(4), 869-884.e5. doi:10.1016/j.neuron.2018.01.023

Hilde, K., Levine, A., Hinckley, C., Hayashi, M., Montgomery, J., Gullo, M., . . . Pfaff, S. (2016). Satb2 is required for the development of a spinal exteroceptive microcircuit that modulates limb position. Neuron, 91(4), 763-776. doi:10.1016/j.neuron.2016.07.014

Hoang, P., Chalif, J., Bikoff, J., Jessell, T., Mentis, G., & Wichterle, H. (2018). Subtype diversification and synaptic specificity of stem cell-derived spinal interneurons. Neuron, 100(1), 135-149.e7. doi:10.1016/j.neuron.2018.09.016

Holguera, I., & Desplan, C. (2018). Neuronal specification in space and time. Science, 362(6411), 176-180. doi:10.1126/science.aas9435

Hubbard, J., Böhm, U., Prendergast, A., Tseng, P., Newman, M., Stokes, C., & Wyart, C. (2016). Intraspinal sensory neurons provide powerful inhibition to motor circuits ensuring postural control during locomotion. Current Biology, 26(21), 2841-2853. doi:10.1016/j.cub.2016.08.026

Jessell, T. M. (2000). Neuronal specification in the spinal cord: Inductive signals and transcriptional codes. Nature Reviews Genetics, 1(1), 20-29. doi:10.1038/35049541

John, A., Wildner, H., & Britsch, S. (2005). The homeodomain transcription factor Gbx1 identifies a subpopulation of late-born GABAergic interneurons in the developing dorsal spinal cord. Developmental Dynamics, 234(3), 767-771. doi:10.1002/dvdy.20568

Kabayiza, K., Masgutova, G., Harris, A., Rucchin, V., Jacob, B., & Clotman, F. (2017). The onecut transcription factors regulate differentiation and distribution of dorsal interneurons during

spinal cord development. Frontiers in Molecular Neuroscience, 10, 157-157. doi:10.3389/fnmol.2017.00157

Kiehn, O., & Butt, S. J. B. (2003). Physiological, anatomical and genetic identification of CPG neurons in the developing mammalian spinal cord. Progress in Neurobiology, 70(4), 347-361. doi:10.1016/S0301-0082(03)00091-1

Kiehn, O. (2006). Locomotor circuits in the mammalian spinal cord. Annual Review of Neuroscience, 29, 279-306. doi:10.1146/annurev.neuro.29.051605.112910

Kiehn, O. (2016). Decoding the organization of spinal circuits that control locomotion. Nature Reviews.Neuroscience, 17(4), 224-238. doi:10.1038/nrn.2016.9

Kimura, Y., Okamura, Y., & Higashijima, S. (2006). Alx, a zebrafish homolog of Chx10, marks ipsilateral descending excitatory interneurons that participate in the regulation of spinal locomotor circuits. The Journal of Neuroscience, 26(21), 5684-5697. doi:10.1523/JNEUROSCI.4993-05.2006

Kimura, Y., & Higashijima, S. (2019). Regulation of locomotor speed and selection of active sets of neurons by V1 neurons. Nature Communications, 10(1), 2268-2268. doi:10.1038/s41467-019-09871-x

Kishore, S., Cadoff, E., Agha, M., & McLean, D. (2020). Orderly compartmental mapping of premotor inhibition in the developing zebrafish spinal cord. Science, 370(6515), 431-436. doi:10.1126/science.abb4608

Kishore, S., & Fetcho, J. (2013). Homeostatic regulation of dendritic dynamics in a motor map in vivo. Nature Communications, 4, 2086-2086. doi:10.1038/ncomms3086

Knogler, L., Ryan, J., Saint Amant, L., & Drapeau, P. (2014). A hybrid electrical/chemical circuit in the spinal cord generates a transient embryonic motor behavior. The Journal of Neuroscience, 34(29), 9644-9655. doi:10.1523/JNEUROSCI.1225-14.2014

Koch, S., Del Barrio, M., Dalet, A., Gatto, G., Günther, T., Zhang, J., . . . Goulding, M. (2017). RORß spinal interneurons gate sensory transmission during locomotion to secure a fluid walking gait. Neuron, 96(6), 1419-1431.e5. doi:10.1016/j.neuron.2017.11.011

Lafreniere Roula, M., & McCrea, D. (2005). Deletions of rhythmic motoneuron activity during fictive locomotion and scratch provide clues to the organization of the mammalian central pattern generator. Journal of Neurophysiology, 94(2), 1120-1132. doi:10.1152/jn.00216.2005

Lai, H., Seal, R., & Johnson, J. (2016). Making sense out of spinal cord somatosensory development. Development, 143(19), 3434-3448. doi:10.1242/dev.139592

Lamotte d'Incamps, B., Bhumbra, G., Foster, J., Beato, M., & Ascher, P. (2017). Segregation of glutamatergic and cholinergic transmission at the mixed motoneuron renshaw cell synapse. Scientific Reports, 7(1), 4037-4037. doi:10.1038/s41598-017-04266-8

Lanuza, G., Gosgnach, S., Pierani, A., Jessell, T., & Goulding, M. (2004). Genetic identification of spinal interneurons that coordinate left-right locomotor activity necessary for walking movements. Neuron, 42(3), 375-386. doi:10.1016/S0896-6273(04)00249-1

Lemieux, M., Josset, N., Roussel, M., Couraud, S., & Bretzner, F. (2016). Speed-dependent modulation of the locomotor behavior in adult mice reveals attractor and transitional gaits. Frontiers in Neuroscience, 10, 42-42. doi:10.3389/fnins.2016.00042

Lu, D., Niu, T., & Alaynick, W. (2015). Molecular and cellular development of spinal cord locomotor circuitry. Frontiers in Molecular Neuroscience, 8, 25-25. doi:10.3389/fnmol.2015.00025

Lundfald, L., Restrepo, C. E., Butt, S. J. B., Peng, C., Droho, S., Endo, T., . . . Kiehn, O. (2007). Phenotype of V2-derived interneurons and their relationship to the axon guidance molecule EphA4 in the developing mouse spinal cord. European Journal of Neuroscience, 26(11), 2989-3002. doi:10.1111/j.1460-9568.2007.05906.x

Masgutova, G., Harris, A., Jacob, B., Corcoran, L., & Clotman, F. (2019). Pou2f2 regulates the distribution of dorsal interneurons in the mouse developing spinal cord. Frontiers in Molecular Neuroscience, 12, 263-263. doi:10.3389/fnmol.2019.00263

Mayer, W., Murray, A., Brenner Morton, S., Jessell, T., Tourtellotte, W., & Akay, T. (2018). Role of muscle spindle feedback in regulating muscle activity strength during walking at different speed in mice. Journal of Neurophysiology, doi:10.1152/jn.00250.2018

McCrea, D., & Rybak, I. (2007). Modeling the mammalian locomotor CPG: Insights from mistakes and perturbations. Prog Brain Res, 165, 235-253. doi:10.1016/S0079-6123(06)65015-2

McCrea, D., & Rybak, I. (2008). Organization of mammalian locomotor rhythm and pattern generation. Brain Research Reviews, 57(1), 134-146. doi:10.1016/j.brainresrev.2007.08.006

McLean, D., Fan, J., Higashijima, S., Hale, M., & Fetcho, J. (2007). A topographic map of recruitment in spinal cord. Nature, 446(7131), 71-75. doi:10.1038/nature05588

McLean, D., Masino, M., Koh, I. Y. Y., Lindquist, W. B., & Fetcho, J. (2008). Continuous shifts in the active set of spinal interneurons during changes in locomotor speed. Nature Neuroscience, 11(12), 1419-1429. doi:10.1038/nn.2225

McLean, D., & Fetcho, J. (2009). Spinal interneurons differentiate sequentially from those driving the fastest swimming movements in larval zebrafish to those driving the slowest ones. The Journal of Neuroscience, 29(43), 13566-13577. doi:10.1523/JNEUROSCI.3277-09.2009

Meziane, H., Fraulob, V., Riet, F., Krezel, W., Selloum, M., Geffarth, M., . . . Rhinn, M. (2013). The homeodomain factor Gbx1 is required for locomotion and cell specification in the dorsal spinal cord. Peerj, 1, e142-e142. doi:10.7717/peerj.142

Miles, G., Hartley, R., Todd, A., & Brownstone, R. (2007). Spinal cholinergic interneurons regulate the excitability of motoneurons during locomotion. Proceedings of the National

Academy of Sciences of the United States of America, 104(7), 2448-2453. doi:10.1073/pnas.0611134104

Moran Rivard, L., Kagawa, T., Saueressig, H., Gross, M. K., Burrill, J., & Goulding, M. (2001). Evx1 is a postmitotic determinant of v0 interneuron identity in the spinal cord. Neuron, 29(2), 385-399. doi:10.1016/S0896-6273(01)00213-6

Müller, T., Brohmann, H., Pierani, A., Heppenstall, P., Lewin, G., Jessell, T., & Birchmeier, C. (2002). The homeodomain factor lbx1 distinguishes two major programs of neuronal differentiation in the dorsal spinal cord. Neuron, 34(4), 551-562. doi:10.1016/s0896-6273(02)00689-x

Myers, P. Z., Eisen, J. S., & Westerfield, M. (1986). Development and axonal outgrowth of identified motoneurons in the zebrafish. The Journal of Neuroscience, 6(8), 2278-2289. doi:10.1523/JNEUROSCI.06-08-02278.1986

Myers, P. Z. (1985). Spinal motoneurons of the larval zebrafish. Journal of Comparative Neurology, 236(4), 555-561. doi:10.1002/cne.902360411

Oberst, P., Agirman, G., & Jabaudon, D. (2019). Principles of progenitor temporal patterning in the developing invertebrate and vertebrate nervous system. Current Opinion in Neurobiology, 56, 185-193. doi:https://doi.org/10.1016/j.conb.2019.03.004

Petracca, Y., Sartoretti, M., Di Bella, D., Marin Burgin, A., Carcagno, A., Schinder, A., & Lanuza, G. (2016). The late and dual origin of cerebrospinal fluid-contacting neurons in the mouse spinal cord. Development, 143(5), 880-891. doi:10.1242/dev.129254

Pierani, A., Moran Rivard, L., Sunshine, M. J., Littman, D. R., Goulding, M., & Jessell, T. M. (2001). Control of interneuron fate in the developing spinal cord by the progenitor homeodomain protein Dbx1. Neuron, 29(2), 367-384. doi:10.1016/S0896-6273(01)00212-4

Pocratsky, A., Burke, D., Morehouse, J., Beare, J., Riegler, A., Tsoulfas, P., . . . Magnuson, D. S. K. (2017). Reversible silencing of lumbar spinal interneurons unmasks a task-specific network for securing hindlimb alternation. Nature Communications, 8(1), 1963-1963. doi:10.1038/s41467-017-02033-x

Pujala, A., & Koyama, M. (2019). Chronology-based architecture of descending circuits that underlie the development of locomotor repertoire after birth. Elife, 8 doi:10.7554/eLife.42135

Rekling, J. C., Funk, G. D., Bayliss, D. A., Dong, X. W., & Feldman, J. L. (2000). Synaptic control of motoneuronal excitability. Physiological Reviews, 80(2), 767-852. doi:10.1152/physrev.2000.80.2.767

RENSHAW, B. (1946). Central effects of centripetal impulses in axons of spinal ventral roots. Journal of Neurophysiology, 9, 191-204. doi:10.1152/jn.1946.9.3.191

Roussel, Y., Paradis, M., Gaudreau, S., Lindsey, B., & Bui, T. (2020). Spatiotemporal transition in the role of synaptic inhibition to the tail beat rhythm of developing larval zebrafish. Eneuro, 7(1) doi:10.1523/ENEURO.0508-18.2020

Saint Amant, L. (2010). Development of motor rhythms in zebrafish embryos. Progress in Brain Research, 187, 47-61. doi:10.1016/B978-0-444-53613-6.00004-6

Satou, C., Kimura, Y., & Higashijima, S. (2012). Generation of multiple classes of V0 neurons in zebrafish spinal cord: Progenitor heterogeneity and temporal control of neuronal diversity. The Journal of Neuroscience, 32(5), 1771-1783. doi:10.1523/JNEUROSCI.5500-11.2012

Shevtsova, N., Talpalar, A., Markin, S., Harris Warrick, R., Kiehn, O., & Rybak, I. (2015). Organization of left-right coordination of neuronal activity in the mammalian spinal cord: Insights from computational modelling. The Journal of Physiology, 593(11), 2403-2426. doi:10.1113/JP270121

Song, J., Ampatzis, K., Björnfors, E. R., & El Manira, A. (2016). Motor neurons control locomotor circuit function retrogradely via gap junctions. Nature, 529(7586), 399-402. doi:10.1038/nature16497

Stam, F., Hendricks, T., Zhang, J., Geiman, E., Francius, C., Labosky, P., . . . Goulding, M. (2012). Renshaw cell interneuron specialization is controlled by a temporally restricted transcription factor program. Development, 139(1), 179-190. doi:10.1242/dev.071134

Stam, F., Hendricks, T., Zhang, J., Geiman, E., Francius, C., Labosky, P., . . . Goulding, M. (2012). Renshaw cell interneuron specialization is controlled by a temporally restricted transcription factor program. Development, 139(1), 179-190. doi:10.1242/dev.071134

Stepien, A., Tripodi, M., & Arber, S. (2010). Monosynaptic rabies virus reveals premotor network organization and synaptic specificity of cholinergic partition cells. Neuron, 68(3), 456-472. doi:10.1016/j.neuron.2010.10.019

Sweeney, L., Bikoff, J., Gabitto, M., Brenner Morton, S., Baek, M., Yang, J., . . . Jessell, T. (2018). Origin and segmental diversity of spinal inhibitory interneurons. Neuron, 97(2), 341-355.e3. doi:10.1016/j.neuron.2017.12.029

Talpalar, A., Bouvier, J., Borgius, L., Fortin, G., Pierani, A., & Kiehn, O. (2013). Dual-mode operation of neuronal networks involved in left-right alternation. Nature, 500(7460), 85-88. doi:10.1038/nature12286

Tripodi, M., Stepien, A., & Arber, S. (2011). Motor antagonism exposed by spatial segregation and timing of neurogenesis. Nature, 479(7371), 61-66. doi:10.1038/nature10538

Wen, H., Eckenstein, K., Weihrauch, V., Stigloher, C., & Brehm, P. (2020). Primary and secondary motoneurons use different calcium channel types to control escape and swimming behaviors in zebrafish. Proceedings of the National Academy of Sciences of the United States of America, 117(42), 26429-26437. doi:10.1073/pnas.2015866117

Zagoraiou, L., Akay, T., Martin, J., Brownstone, R., Jessell, T., & Miles, G. (2009). A cluster of cholinergic premotor interneurons modulates mouse locomotor activity. Neuron, 64(5), 645-662. doi:10.1016/j.neuron.2009.10.017

Zhang, J., Lanuza, G., Britz, O., Wang, Z., Siembab, V., Zhang, Y., . . . Goulding, M. (2014). V1 and v2b interneurons secure the alternating flexor-extensor motor activity mice require for limbed locomotion. Neuron, 82(1), 138-150. doi:10.1016/j.neuron.2014.02.013

Zhang, Y., Narayan, S., Geiman, E., Lanuza, G., Velasquez, T., Shanks, B., . . . Goulding, M. (2008). V3 spinal neurons establish a robust and balanced locomotor rhythm during walking. Neuron, 60(1), 84-96. doi:10.1016/j.neuron.2008.09.027

Zhong, G., Droho, S., Crone, S., Dietz, S., Kwan, A., Webb, W., . . . Harris Warrick, R. (2010). Electrophysiological characterization of V2a interneurons and their locomotor-related activity in the neonatal mouse spinal cord. The Journal of Neuroscience, 30(1), 170-182. doi:10.1523/JNEUROSCI.4849-09.2010

Ziskind Conhaim, L., & Hochman, S. (2017). Diversity of molecularly defined spinal interneurons engaged in mammalian locomotor pattern generation. Journal of Neurophysiology, 118(6), 2956-2974. doi:10.1152/jn.00322.2017

CHAPTER 2. EXCITATORY SPINAL INTERNEURONS ARE FUNCTIONALLY ORGANIZED INTO TOPOGRAPHICALLY CLUSTERED RECRUITMENT MODULES

Contribution Statement

I would like to acknowledge Dr. Han Zhang and Olivia Laflamme for assisting me in the nerve stimulation experiments. I would like to acknowledge Dr. Han Zhang for performing CTB muscle injection surgeries. I would like to acknowledge Dr. Christopher Jones for consultation on analysis strategies. I would like to acknowledge David Burbidge for writing the MATLAB script for sorting V3 and V2a topographical clusters. I would like to acknowledge Colin Mackay for his assistance in cell counting V3 control and $V3^{OFF}$ $cfos^{+}$ V2a INs. I would like to acknowledge Mingwei Liu for developing a MATLAB cell counter application.

1. Abstract

Animals exhibit a wide range of locomotor behaviors that emerge from the coordinated activity of interneuron circuits in the spinal cord. While spinal interneurons (INs) are known to play essential roles in establishing precise temporal patterns of muscle contraction, the principles governing recruitment of INs across different behaviours remain elusive. Here, we systematically analyze task-specific cfos expression within the excitatory V3 and V2a IN populations in the mouse spinal cord. Our analyses reveal topographical arrangements of V3 and V2a INs into functionally distinct modular domains. V2a IN clusters display distinctly speed-dependent recruitments. In contrast, V3 IN clusters arranged across mediolateral and dorsoventral spinal axes display varied recruitments across speed-, balance-, hindlimb weight load-, and hind paw cutaneous-dependent tasks. These varied V3 cluster recruitments may be in part driven by differential integrations of sensory modality and peripheral nerve-specific inputs. Lastly, we reveal that functional removal of V3 INs results in a task-dependent increase of V2a IN recruitments – presenting the possibility of functional compensation between excitatory spinal IN modules. Taken together, our current work suggests that excitatory spinal INs topographically cluster into task-specific recruitment modules, which may functionally compensate in the absence of one another.

2. Introduction

Coordinated movement emerges through spinal cord interneuron (IN) circuits that engage motor pools and their corresponding muscle groups in precise patterns of activity (Deska-Gauthier & Zhang, 2019; Kiehn, 2016). During basic stereotyped behaviours, such as walking, spinal INs generate the fundamental rhythmic and patterned outputs necessary for robust movement. During more elaborate behavioural demands, such as walking across varied surface inclines or alternating speeds, spinal INs integrate and process dynamic supraspinal and sensory commands shaping task-dependent behavioural outputs (Grillner & El Manira, 2020). As such, the sum of spinal IN circuits enables a vast repertoire of motor behaviours from leisurely walking, to high-speed running, to swimming, and so on (Pierotti et al., 1989; Roy et al., 1991). Yet, the functional architecture and heterogeneity of spinal IN circuits underlying their control of sensorimotor flexibility remains elusive.

Spinal IN diversity emerges during early embryogenesis with the establishment of 10 progenitor domains giving rise to discrete cardinal IN populations (Goulding, 2009; Jessell, 2000). These cardinal IN populations possess distinct neurotransmitter phenotypes, axon projection profiles, laminar distributions, and electrophysiological properties (Goulding, 2009). However, extensive subpopulation heterogeneity has been revealed within each cardinal IN class. Several cardinal IN subpopulations display functionally distinct outputs (Ziskind-Conhaim & Hochman, 2017), and in certain cases, their functional outputs are task-dependent (Crone et al., 2008, 2009; Talpalar et al., 2013; Bellardita & Kiehn, 2015; Zagoraiou et al., 2009). Thus, cardinal IN subpopulation heterogeneity can be hypothesized as the bases of motor diversity. Though, it remains unclear whether genetically and anatomically distinct IN subpopulations are

functionally organized based on their behaviour-specific recruitments. Furthermore, if such functional organization exists, the circuit logic separating IN subpopulations into task-dependent recruitment modules is unknown.

We have approached these issues through a focus on excitatory spinal V3 and V2a IN classes. V3 INs are a major group of excitatory commissural INs important for robust and stable locomotor activity (Zhang et al., 2008). V3 INs arise from the p3 progenitor domain and are defined by post-mitotic expression of the transcription factor Sim1 (Briscoe et al., 1999; Goulding et al., 2002). In the postnatal mouse spinal cord, V3 INs display highly diverse anatomical, electrophysiological and morphological properties (Borowska et al., 2013, 2015; Blacklaws et al., 2015). Similarly, V2a INs are a major group of ipsilateral excitatory INs important for driving stable left-right alternation with increasing locomotor speed (Crone et al., 2008, 2009). V2a INs arise from the p2 progenitor domain marked by post-mitotic Chx10 expression (Ericson et al., 1997). Also similar to V3 INs, V2a INs display diverse anatomical, electrophysiological, morphological, and molecular properties (Al-Mosawie et al., 2007; Crone et al., 2008, 2009; Dougherty & Kiehn, 2010; Zhong et al., 2010; Hayashi et al., 2018).

While spinal V3 and V2a INs have been extensively studied independently, to what extent they are functionally linked to one another has remained largely unexamined. Furthermore, it remains to be understood how anatomical heterogeneity within each class translates to functional heterogeneity. Thus, in the current work, we aimed to uncover the functional relatedness of excitatory IN classes in the spinal cord. First, we examined how V3 and V2a INs are recruited across varied sensorimotor tasks. Utilizing task-specific cfos expression and computational analyses we revealed that topographically clustered V3 and V2a IN subsets have

independent recruitment patterns across speed-, balance-, hindlimb load-, and hind paw cutaneous-dependent locomotor tasks. Interestingly, the unique recruitment patterns of distinct V3 IN clusters may be in part due to the integration of sensory modality and nerve specific innervations. Finally, we explored the possibility of functional compensation between spinal V3 and V2a IN modules. Synaptic removal of V3 INs resulted in a task-dependent increase of V2a IN recruitment. Taken together, our current work suggests that excitatory spinal INs are organized into distinct topographical circuit modules, which differentially combine across varied locomotor tasks and may functionally compensate in the absence of one another.

3. Results

3.1 Topographically clustered V3 and V2a IN subsets display distinct recruitment patterns across varied locomotor tasks.

Animals achieve contextual locomotor behaviours through precise control of muscle activations. For example, running at high speeds, walking on an inclined surface, or swimming all require increased force of hind-limb extensor muscles compared with walking (Hutchison et al., 1989; Leon et al., 1994; Roy et al., 1985, 1991). Yet, context-distinct tasks vary in their precise patterns of activation and the supraspinal and sensory drives mediating their outputs (Akay et al., 2014; Akay & Murray, 2021; Ferreira-Pinto et al., 2018; Mayer et al., 2018). As such, we reasoned that heterogeneous spinal IN populations may be recruited differently across distinct behavioural tasks. The first aim of our current study was therefore to investigate whether excitatory V3 and V2a INs display different activation patterns across different locomotor behaviours.

Work of our group and others have shown that activity dependent expression of the cfos transcription factor is a dependable indicator of spinal interneuron (IN) activity during sensorimotor tasks (Sagar et al., 1988; Borowska et al, 2013; Merkulyeva et al., 2018). To uncover recruitment patterns, we subjected mice to one of nine locomotor tasks (flat surface treadmill running at 15 cm/s, 40 cm/s, or 90 cm/s; incline walking (15 cm/s, +25°); decline walking (15 cm/s, -25°); staggard stepping (forward speed, 15 cm/s, lateral speed, 7cm/s); lateral motion (forward speed, 0 cm/s, lateral speed, 7cm/s); swimming; or sandpaper belt walking) followed by cfos^{+} V3 and V2a IN detection in higher lumbar (L1-L3) spinal cord

segments. To visualize Sim1$^+$ V3 INs, we utilized Sim1Cre;Rosa.lsl.tdTom mice labeling V3 INs with endogenous tdTomato protein fluorescence. To visualize Chx10$^+$ V2a INs, we utilized immunodetection of Chx10, which is expressed into adult stages in lumbar V2a INs (Hayashi et al., 2018). Spinal cord cells labeled by both tdTomato$^+$/cfos$^+$ and Chx10$^+$/cfos$^+$ immunoreactivities following a locomotor task were characterized as recruited V3 INs and recruited V2a INs, respectively (Figure2.1B-D).

V3 and V2a INs were recruited across all locomotor tasks performed (Figure2.1E-M, n=3 animal for each task). Though, their spatial recruitment patterns for each locomotor task were markedly distinct from one another (Figure2.1B,Ci-v). For example, V3 INs display a marked increase in cfos$^+$ INs following decline locomotion (Figure2.1Ii-ii) compared to flat ground locomotion (Figure2.Ei-ii), while V2a INs did not show a noticeable difference in cfos$^+$ INs following these two behaviours (Figure2.1Eiii,Iiii). Additionally, V3 INs, and to a lesser extent V2a INs, displayed unique recruitment patterns across dorsoventral and mediolateral spinal axes depending on the locomotor task being performed. For example, V3 INs displayed a high density of cfos$^+$ dorsal and ventral V3 IN subsets following high surface friction locomotion (Figure2.1Mi-ii), while only ventral cfos$^+$ V3 INs were detected following swimming locomotion (Figure2.1i-ii). Thus, contextually varied locomotor tasks revealed a modular organization of developmentally, molecularly, and topographically distinct excitatory spinal INs.

These spatially distinct recruitment patterns within V3 and V2a IN classes prompted us to further compare the percentages of cfos$^+$ INs between V3 and V2a topographical clusters. To achieve this, we first pooled all cfos$^+$ and cfos$^-$ V3 and V2a INs, respectively, across all analyzed spinal sections (n = 27 animals and 270 sections for each IN class). Density heatmap plots

revealed four V3 IN spatial clusters (cluster 1, dorsomedial; cluster 2, intermediate; cluster 3, ventromedial; cluster 4, ventrolateral; Figure2.2Ai) and two V2a IN spatial clusters (cluster 1, medial; cluster 2, lateral; Figure2.2Bi). To classify individual V3 and V2a INs into corresponding spatial clusters we performed clustering analysis with Gaussian Mixture Models (MATLAB, "fitgmdist", Figure2.2Aii-iv,Bii-iv). Taken together, cluster 1 comprised 14.7 ± 3.9% of total V3, cluster 2 comprised 24.3 ± 5.9% of total V3, cluster 3 comprised 17.7 ± 4.5% of total V3, and cluster 4 comprised 39.6 ± 8.7% of total V3 (Fgure2.2Av). For V2a INs, cluster 1 comprised 78.9 ± 3.3% of total V2a and cluster 2 comprised 21.1 ± 3.3% (Figure2.2Bv).

To better understand the recruitment logic of V3 and V2a IN clusters, we compared locomotor behaviours within four groupings: 1) speed dependent recruitment; 2) balance dependent recruitment 3) hindlimb load dependent recruitment; and 4) hind paw cutaneous dependent recruitment.

3.1.1 V2a IN clusters display uniquely frequency dependent recruitments

We correlated IN recruitments with flat surface locomotor speeds of 15 cm/s, 40 cm/s and 90 cm/s (Figure2.3A). These speeds were chosen as they correspond with distinct locomotor gaits in mice: 15 cm/s, walking; 40 cm/s, trotting; and 90 cm/s, galloping/bounding (Bellardita & Kiehn, 2015; Lemieux et al., 2016). V2a INs displayed marked increases in recruitment with increased locomotor speed (Figure2.3A-C). The percentage of $cfos^{+}$ INs for both V2a cluster 1 and cluster 2 were significantly greater at 40 cm/s and 90 cm/s compared to 15 cm/s

(Figure2.3Biv,Civ). Thus, medial and lateral V2a IN clusters shared increased recruitments with increased locomotor speeds.

Across the other three behavioural groups (balance, Figure2.4; hindlimb load, Figure2.5; hind paw cutaneous, Figure2.6) there were almost no differences in percentage of $cfos^+$ INs in either V2a cluster 1 or cluster 2 compared to flat ground slow speed walking (n=3 animal per task, Figure2.4Biv,Civ; Figure2.5Bv,Cv; Figure2.6Biv,Civ). The one noticeable difference was that medial V2a cluster 2 displayed an increased trend in the percentage of $cfos^+$ INs following swimming compared with overground 15cm/s tasks (Figure2.5&2.7). Interestingly, mice displayed a higher locomotor frequency during swimming (data not shown). Thus, the increased recruitment of medial V2a INs during swimming further validated it's uniquely frequency dependent recruitment pattern.

3.1.2 V3 IN clusters display varied recruitments across speed- and state-dependent tasks

3.1.2.1 Speed dependent recruitment patterns

Both intermediate (V3 cluster 2) and ventral (V3 clusters 3 & 4) V3 IN clusters displayed increased percentages of $cfos^+$ INs with increased locomotor speeds (Figure2.7C,D,E). V3 cluster 2 and cluster 3 had a significantly higher percentage of $cfos^+$ INs at 90 cm/s when compared with 15cm/s (p-value < 0.05, n=3 animals for each speed, Figure2.7Civ,Div). While the percentage of $cfos^+$ INs in V3 cluster 4 was not significant, it also showed an increasing trend from 15 cm/s to 90 cm/s (Figure2.7Eiv).

Interestingly, dorsomedial V3 cluster 1 displayed a unique recruitment pattern with increasing speed (Figure2.7B). While the percentage of cfos$^+$ INs in V3 cluster 1 significantly increased from 15 cm/s to 40 cm/s, it significantly decreased from 40 cm/s to 90 cm/s (Figure2.7Biv). Thus, the majority of V3 IN clusters (cluster 2, 3, 4) displayed increased recruitment with increased speed. However, dorsomedial V3 cluster 1 displayed heightened recruitment at an intermediate speed (40cm/s) compared to both slow (15cm/s) and high (90cm/s) speeds.

3.1.2.2 Balance dependent recruitment patterns

We next assessed potential correlations between balance perturbations and V3 cluster recruitments (Figure2.8). To achieve this, we subjected mice to continuous balance perturbations during either locomotor or non-locomotor tasks. We then compared balance perturbed tasks to nonperturbed flat ground slow speed walking (Figure2.8A).

First, we subjected mice to a staggard stepping tasks (Figure2.8Aii). The staggard stepping task consisted of mice walking on a flat incline at 15 cm/s while the treadmill continuously oscillated side-to-side at a speed of 7 cm/s. This task presumptively increased vestibular and proprioceptive systems with increased lateral loading of the limbs counteracting the opposing lateral shaking force of the treadmill. Interestingly, intermediate (V3 cluster2) and ventral (V3 clusters 3 & 4) V3 IN clusters had significantly higher percentages of cfos$^+$ INs following staggard stepping compared with non-staggard stepping (p-value < 0.05, n=3 animals for each task; Figure2.5C-D). While in contrast, dorsomedial V3 cluster 1 displayed no difference between staggard stepping and non-staggard stepping (Figure2.8B).

We next subjected mice to a purely lateral motion task (Figure2.8Aiii). This task required no locomotion (0cm/s) but required the mice to maintain their balance in response to side-to-side treadmill oscillations (7cm/s). First, intermediate V3 cluster 2 displayed a heightened percentage of cfos$^+$ INs, comparable to staggard stepping (Figure2.8B). Thus, balance maintenance is likely a primary recruiting principal for intermediate V3 INs. Second, both ventromedial V3 cluster 3 and ventrolateral V3 cluster 4 displayed a decreased trend of the percentage of cfos$^+$ INs following lateral motion versus staggard stepping (Figure2.8D,E). Although, they both still had significantly greater percentages of cfos$^+$ INs following lateral motion compared with nonperturbed flat surface walking (p-value < 0.05, n=3 animals for each task, Figure2.8Div,Eiv). Thus, a combination of locomotor drive and balance maintenance likely play roles for heightened ventral V3 IN recruitments during staggard stepping. Lastly, dorsomedial V3 cluster 1 had a lower percentage of cfos$^+$ INs following lateral motion compared to both nonperturbed flat surface walking and staggard stepping (p-value < 0.05, n=3 animals for each task, Figure2.8Biv). Thus, balance maintenance likely plays little to no role in the recruitment of dorsomedial V3 INs.

3.1.2.3 Hindlimb load dependent recruitment patterns

The increased V3 IN recruitments with increased speed and balance disturbance may have been due to an increased loading force of the hindlimb muscles. Thus, we next assessed potential correlations between hindlimb loading and the recruitments of V3 IN clusters. To achieve this,

we subjected mice to a series of locomotor tasks with either heightened or diminished hindlimb loading (Figure2.9A).

We first compared V3 cluster recruitments between flat surface (0°, 15cm/s), incline surface (+25°, 15cm/s), and decline surface (-25°, 15cm/s) walking. Although there were no significant changes of cfos$^+$ V3 INs in all clusters between flat and incline walking (p-value > 0.05, n=3 animals for each task, Figure2.9A-E), all these clusters displayed increasing trends (Figure2.9B-Ev). Interestingly, all four V3 IN clusters displayed a further increased cfos$^+$ trend following decline walking compared to incline and flat surface walking. V3 clusters 2, 3 and 4 had significantly higher percentages of cfos$^+$ INs following decline walking compared with flat surface walking (p-value < 0.05; n=3 animals for each task, Figure5C-Eiv).

Next, we subjected mice to swimming (Figure2.9Aiv), which is the complete unloading of the hindlimbs during a locomotor task. Dorsomedial V3 cluster 1 displayed an almost complete absence of cfos$^+$ INs following swimming (Figure2.9B). Intermediate (cluster2) and ventral (cluster3&4) V3 IN clusters all displayed increased trends of cfos$^+$ INs after swimming compared to flat surface walking (Figure2.9C-D). Thus, hindlimb weight loading is likely not a principal contributor to V3 IN recruitment during locomotion. Interestingly though, the almost complete absence of dorsomedial V3 cluster 1 recruitment during swimming suggested a role of paw-surface contact in its recruitment.

3.1.2.4 Hind paw cutaneous dependent recruitment patterns

V3 IN clusters displayed increased percentages of cfos$^+$ INs following both incline (+25°) and decline (-25°) walking in comparison to flat ground (0°) walking (Figure2.9). While these locomotor tasks had opposite effects on hindlimb load (incline, loading; decline, unloading) they both resulted in a lower friction force acting on the hind paw. We hypothesized this may have resulted in increased stretch and slipping of the paw while in contact with the surface, and therefore, increased mechanoreceptor activation. Thus, we next assessed potential correlations between hind paw mechanoreception and the recruitments of V3 IN clusters.

To test the hypothesis that increased mechanoreception under the paw acts as a recruiting principle for distinct V3 clusters, we subjected mice to flat surface walking (0°, 15cm/s) over a treadmill belt of 60 grade sandpaper. We then compared the percentage of cfos$^+$ INs following sandpaper belt walking, regular treadmill belt walking, and swimming (Figure2.10A).

Both dorsomedial V3 cluster 1 and intermediate V3 cluster 2 had significantly increased percentages of cfos$^+$ INs following sandpaper belt walking versus both regular treadmill belt walking and swimming (p-value < 0.05, n=3 animals for each task, Figure2.10B,C). This suggested mechanoreception may indeed play a role in the recruitment of V3 cluster 1 and 2. On the other hand, while ventral V3 clusters 3 & 4 both displayed increased percentages of cfos$^+$ INs following sandpaper belt walking in comparison to regular belt walking, they both also displayed relatively similar recruitment levels during swimming with sandpaper belt walking (Figure2.10D,E). Thus, mechanoreception likely does not play a direct or exclusive role in the recruitment of ventromedial or ventrolateral V3 clusters.

3.2 V3 IN clusters are differentially recruited by sensory modality and sensory nerve-specific inputs

V3 IN clusters displayed remarkably diverse recruitments across the distinct sensorimotor tasks performed. This was contrasted with V2a IN clusters – which displayed mostly speed-dependent recruitment patterns. These findings led us to speculate whether V3 IN clusters are differentially recruited by distinct sensory inputs from the periphery.

We first aimed to detect potential monosynaptic sensory innervations on V3 INs. We performed dual immunolabeling of parvalbumin and vesicular glutamate transported 1 (Vglut1) in higher lumber spinal cords of P9 Sim1Cre;Rosa.lsl.tdTom mice. We observed parvalbumin^{+}/Vglut1^{+} presynaptic terminals on intermediate V3 INs (Figure2.11A) indicating that some V3 INs might directly receive proprioceptive inputs (Honda, 1995; Arber et al., 2000; Alvarez et al., 2004; Lallemend & Ernfors, 2012).

To better understand the distribution and source of these proprioceptive inputs, we performed anterograde CTB labeling injected into either proximal iliopsoas (IP) and gluteus maximus (GL) hip muscles (Figure2.11Bi), or distal gastrocnemius (GS) and tibialis anterior (TA) ankle muscles (Figure2.11Bii) in P21 Sim1Cre;Rosa.lsl.tdTom mice. Interestingly, we detected both hip and ankle proprioceptive innervations on intermediate V3 INs, but not on neither dorsal nor ventral V3 INs (Figure11Bi), matching our parvalbumin^{+}/Vglut1^{+} results. Though, we did detect Vglut1^{+}/CTB^{-} contacts on dorsal V3 INs (Figure2.11Bi), which could be cutaneous inputs from the periphery (Arber et al., 2000; Alvarez et al., 2004). We did not detect Vglut1^{+} nor CTB^{+} innervations of ventral V3 INs (Figure2.11Bi).

Up to now, ventral V3 INs don't receive direct sensory monosynaptic innervation, nor display any exclusive sensory task-specific recruitments. However, their activation always appeared heightened during any task that required increased motor neuron output. We have previously shown that during early neonatal stages some V3 INs receive recurrent synaptic drive from surrounding motor neurons in the lumbar spinal cord (Chopek et al., 2018). To further investigate the presence of recurrent motor neuron inputs to ventral V3 INs in the adult, we performed immunolabeling for vesicular acetylcholine transporter (VAchT) in the higher lumbar spinal cord of P21 Sim1Cre;Rosa.lsl.tdTom mice. We confirmed VAchT^{+} innervations of ventral V3 INs (Figure2.11C).

We next aimed to better grasp the direct down stream sensory and motor recruitments in the spinal cord. We did this by stimulating specific sensory and motor nerves in the periphery followed by immunolabeling of cfos in the higher lumbar (L1-L3) spinal cord of adult Sim1Cre;Rosa.lsl.tdTom mice (Figure2.11D-Fiv). We focused on three nerves, which each carry unique combinations of sensory and motor information. We first stimulated the femoral nerve (Figure2.11D). The femoral nerve originates from the proximal hindlimb and consists of both cutaneous and proprioceptive sensory as well as motor information (Bailey & Kitchell, 1987; Bailey et al., 1992; Kruspe et al., 2014). Interestingly, following femoral nerve stimulation, we observed a distinct intermediate and ventral density distribution pattern of cfos^{+} V3 INs (Figure2.11Diii-iv). We next stimulated the tibial nerve (Figure2.11E). Similar to the femoral nerve, the tibial nerve consists of cutaneous, proprioceptive and motor information, but originates from the distal hindlimb (Bailey & Kitchell, 1987; Swett & Woolf, 1985; Kambiz et al., 2014). To our surprise, stimulation of the tibial nerve activated different clusters of V3 INs

(Figure2.11Eiv). Compared to femoral nerve stimulation, tibial nerve stimulation recruited less ventral and intermediate cfos^{+} V3 INs but increased dorsal cfos^{+} V3 INs. Last, we stimulated the sural nerve (Figure2.11F), which is a cutaneous sensory branch of the tibial nerve. It transmits mechanosensitive information from the hind paw into the spinal cord (Swett & Woolf, 1985; Kambiz et al., 2014). Sural nerve stimulation almost exclusively activated dorsal V3 INs (Figure2.11Fiv). Thus, hind paw cutaneous sensory afferents most-likely contribute to the specific recruitment of dorsal, and little to intermediate and ventral, V3 IN clusters. Taken together, topographically distinct V3 IN subsets are differentially recruited by peripheral nerves originating from separate proximodistal hindlimb locations.

3.3 Functional removal of V3 INs results in an increased recruitment of V2a INs

One of the most interesting findings from our sensorimotor cfos experiments was that V3 and V2a IN recruitments appeared to be completely distinctive from each other. While V2a IN clusters displayed an almost complete speed-dependent recruitment logic, V3 IN clusters displayed varied recruitment patterns across speed-, balance-, hindlimb load-, and hind paw cutaneous-dependent tasks. These findings suggest a modular organization within the higher lumbar spinal cord. From this, an interesting possibility arose: can distinct excitatory spinal IN modules compensate for the functional loss of other IN modules? To begin to address this question, we repeated task-specific V2a cfos detection experiments in wild type and Sim1^{Cre};Vglut2$^{flox/flox}$ (V3^{OFF}) mice (Figure2.12A-C). This allowed us to address whether the

recruitment levels of V2a INs changed when V3 INs were functionally removed from the spinal cord.

We compared the laminar density distributions and percentages of cfos^{+} V2a INs across control (0cm/s, 0°incline, Figure2.12D), flat ground (15cm/s, 0°incline, Figure2.12E), and incline (15cm/s, +18°incline, Figure12F) walking. There were low levels of cfos^{+} V2a INs in both wildtype and V3^{OFF} mice (Figure2.12D). Intriguingly, following flat surface walking, a trend of an increased percentage of cfos^{+} V2a INs emerged, but not significant (Figure2.12E). However, following incline walking, there was a significantly higher percentage of cfos^{+} V2a INs in V3^{OFF} mice compared to wildtype mice (p-value < 0.05, n=5 animals for each genotype, Figure2.12Fiv). This increase was evident in both medial and lateral V2a IN clusters (Figure2.12Fiii). Thus, our preliminary studies suggest that independent excitatory spinal IN modules may functionally compensate for the loss of one another in a task-specific manner.

4. Discussion

In the current work, we have identified sensorimotor recruitment logic of spatially discrete V3 and V2a spinal IN clusters. Medial and lateral V2a IN clusters displayed specifically speed-dependent recruitment patterns. On the other hand, dorsal, intermediate, ventrolateral and ventromedial V3 IN clusters displayed varying recruitment patterns across speed- and state-dependent tasks. V3 IN clusters differentially integrated sensory modality and nerve-specific signals, which may in part separate them into distinct recruitment modules. Lastly, V2a INs

displayed heightened recruitment levels following incline walking in $V3^{OFF}$ mice suggesting a potential for functional compensation between excitatory INs in the spinal cord.

4.1 V3 and V2a INs organize into spatially distinct modular domains

Distinctive neuronal layers are the basic physical structures for discrete functional circuits in many brain regions – perhaps most evident in the cerebral cortex (Harris & Shepherd, 2015). The spinal cord, especially in the ventral side, lacks such clear laminar structure. Yet, functional studies have indicated that spinal neurons are organized into modular networks allowing for the production of diverse motor behaviours across vertebrate locomotor systems (Matsushima & Grillner, 1992; Bizzi et al., 1995, 2008; Stein et al., 2008; Ausborn et al., 2012; Wiggin et al., 2012; Hägglund et al., 2013; Talpalar et al., 2013; Ampatzis et al., 2014; Bagnall & McLean, 2014; Bellardita & Kiehn, 2015; Björnfors & El Manira, 2016). Recordings from spinal cords of non-mammalian animals demonstrate that the activation of spinal INs can be speed- or/and task-dependent, corresponding to an INs excitatory drive and intrinsic membrane properties (Ampatzis et al., 2014; Björnfors & El Manira, 2016). Our current work further investigated modularity of genetically identified cardinal populations, V3 and V2a INs, in the mouse spinal cord. Although it currently remains not possible to record individual ventral neurons in behaving adult mice, we were able to use the expression of cfos to evaluate activation states of individual V3 INs during specific tasks and map their topographical positions across dorsoventral and mediolateral spinal axes. In doing so, we were able to identify spatially

clustered modular domains, which are recruited separately corresponding to different types of sensorimotor behaviours.

4.1.1 Medial and Lateral V2a IN recruitments

Our clustering analysis separated V2a INs into distinct medial and lateral topographical clusters. These results align with recently published work indicating differential transcription factor expression profiles in medial versus lateral V2a INs in the lumbar spinal cord (Hayashi et al., 2018). Though, both medial and lateral V2a INs displayed an almost exclusive speed-dependent recruitment logic. This suggests medial and lateral V2a INs may be recruited by the same circuit inputs and therefore comprise a shared speed-dependent circuit module. Furthermore, these findings are consistent with previous studies that showed V2a INs important for left-right hindlimb alternation at intermediate, but not slow, locomotor speeds (Crone et al., 2008, 2009). Yet, it was still surprising how unchanged V2a recruitment levels were across all other hindlimb load- and hind paw cutaneous-dependent tasks investigated here. Taken together, V2a INs may exclusively serve as a speed-dependent module in the lumbar spinal cord.

4.1.2 Dorsomedial V3 IN recruitments

Among potential V3 modular domains, the dorsomedial V3 IN cluster displayed the most distinctive recruitment pattern. The activation of dorsomedial V3 INs in the high lumbar segments required hind paw contact on the ground. This was most noticeable by the almost

complete absence of activated dorsomedial V3 INs during swimming. Furthermore, dorsomedial V3 IN recruitment was not hindlimb load-dependent as it displayed equivalent recruitment intensity between incline and decline walking. We then further showed that hind paw cutaneous input could be a potential drive for dorsomedial V3 recruitment by subjecting mice to walking on a sandpaper treadmill belt, which strongly increased dorsomedial V3 IN recruitment. Furthermore, the decreased recruitment of dorsomedial V3 INs at 90 cm/s compared to 40 cm/s is consistent to the observation in decerebrate cats, which showed decreased cutaneous involvement during high speed treadmill walking compared to intermediate speeds (Hurteau et al., 2017). The most direct evidence, however, is when we stimulated the hind paw cutaneous sural nerve revealing its almost exclusive recruitment of dorsomedial V3 INs. Thus, dorsomedial V3 INs likely mediate hind paw cutaneous inputs during over ground activities.

4.1.3 Intermediate V3 IN recruitments

The intermediate V3 IN cluster displayed heightened recruitments during both locomotor and non-locomotor tasks. Interestingly, it showed heightened recruitments during decline walking and staggard stepping that were equivalent to the non-locomotor lateral motion task. This suggests that the intermediate V3 IN population may not be directly involved in hindlimb weight-supporting/loading tasks, but instead for initiation changes during locomotion. Indeed, we detected both hip and ankle proprioceptive innervations onto intermediate V3 INs, as well as marked femoral nerve stimulation recruitment. Unlike dorsal V3 INs, intermediate V3 INs

were also recruited during swimming at levels equivalent to slow speed walking. Proprioception is required during swimming (Akay et al., 2014) and might explain why intermediate, but not dorsal, V3 INs were recruited.

Lastly, it needs to be mentioned that intermediate V3 INs also displayed heightened recruitment following sandpaper walking. While this may be due to intermediate V3 INs also processing hind paw cutaneous inputs, we reasoned this unlikely as intermediate V3 INs displayed minimum recruitment following sural nerve stimulation. Another possibility is that the heightened intermediate V3 IN recruitment could be in response to gait changes inducing increased proprioception (for example, increased limb flexion) during sandpaper walking. We are currently in the process of exploring this hypothesis by conducting hindlimb kinematic analyses during regular versus sandpaper walking.

4.1.4 Ventromedial and ventrolateral V3 IN recruitments

Previous work from our lab revealed that ventromedial and ventrolateral V3 INs form distinct microcircuit connectivities with both one another and local ipsilateral motor neurons (Chopek et al., 2018). Our topographical clustering analysis further revealed distinct V3 IN density centres at both ventromedial and ventrolateral positions. This enabled us to independently quantify the recruitment patterns of ventromedial and ventrolateral V3 IN clusters. Interestingly, ventromedial and ventrolateral V3 IN clusters displayed similar recruitment patterns, although, there was one notable difference when comparing lateral motion with swimming. Ventrolateral V3 INs displayed equivalent recruitment levels between lateral motion

and swimming, while ventromedial V3 INs displayed a slightly diminished trend in recruitment during swimming compared with lateral motion.

While we are only able to speculate on the potential recruitment drives differentiating lateral motion and swimming, one possibility is different axial motor neuron activity. While swimming elicited a rostrocaudal wave propagation of axial muscle contraction in the mice, our lateral motion task elicited strong and rigid axial muscle contractions to maintain body posture (data not shown). As ventral V3 INs receive recurrent excitatory drive from local motor neurons (Chopek et al., 2018), it is possible that ventromedial V3 INs receive stronger medial motor column (axial muscle) feedback while ventrolateral V3 INs receive stronger lateral motor column (limb muscle) feedback. Indeed, V1 IN subsets receive topographically matched motor neuron pool specific feedback along the dorsoventral spinal axis (Bikoff et al., 2016). That is, dorsal-positioned $Sp8^{+}$ V1 INs are more innervated by dorsal-position ankle motor neuron pools than ventral-positioned hip motor neuron pools. This topographical circuit logic could extend across the mediolateral axis to V3 INs, such that, medial-positioned motor neurons (axial) feedback onto ventromedial V3 more than lateral-positioned motor neurons (limb), and visa versa. We are currently in the process of exploring this hypothesis further via muscle specific retrograde labeling experiments.

4.2 Recruitment independence of V3 and V2a INs

Our cfos experiments suggest that V3 and V2a INs are independently recruited from one another. While select V3 IN clusters and V2a IN clusters displayed heightened recruitments with

increasing speed, V3 INs further displayed heightened recruitments across other state-dependent tasks, while V2a INs did not. Thus, while independent V3 and V2a IN modules may be functionally coupled during increased speed, they are uncoupled across other tasks such as decline walking.

While we began to investigate the sensory circuit logic underlying the independent recruitments of spatially clustered V3 IN subsets, we did not investigate differences between V2a and V3 INs. Going forward, it will be interesting to investigate how distinct sensory, supraspinal, and local microcircuit connectivities contributed to respective V3 and V2a cluster specific recruitment patterns.

4.3 Potential functional compensation by excitatory spinal IN modules

Lastly, we provide preliminary evidence for functional compensation between independent excitatory IN modules in the spinal cord. We functionally removed V3 INs by conditionally knocking out vesicular glutamate transporter 2 within exclusively $Sim1^{+}$ V3 INs. This resulted in an inability of V3 INs to load glutamate into their presynaptic vesicles rendering them functionally inert.

It is important to note that our $V3^{OFF}$ mouse model is a chronic knockout of Vglut2 that starts upon Sim1 expression during early embryonic stages. Thus, it is possible that the increased V2a recruitment we observed in $V3^{OFF}$ mice was in response to a developmental compensation. Indeed, other neurotransmitter phenotypes have been shown necessary for the proper

embryonic assembly of neural circuits in the spinal cord (Myers et al., 2005) and throughout the brain (Blackenship & Feller, 2010; Huang & Scheiffele, 2008)

To address this issue, we plan to utilize an intersectional transgenic approach to express inhibitory Designer Receptors Exclusively Activated by Designer Drugs (Ray et al., 2011) channels within Vglut2^{+} and Sim1^{+} V3 INs. This approach will allow us to conditionally inhibit V3 IN activity during the experimental time alone.

Taken together, our current work provides new insights into the functional circuit logic of excitatory spinal INs required for sensorimotor flexibility. In particular, the potential functional compensation we observed of distinct excitatory IN modules may provide new perspectives when attempting to understand spinal circuit changes following spinal cord injury and disease.

5. Materials and Methods

Mouse strains

$Sim1^{Cre}$ mice (Zhang et al, 2008) were crossed with TdTomato (TdTom) Ai14 conditional reporter mice (Jackson Laboratory) to generate $Sim1^{Cre}$;Rosa.lsl.tdTom mice (Zhang et al., 2008; Blacklaws et al., 2015). These mice were used for fate mapping $Sim1^{+}$ V3 interneurons during postnatal stages. $V3^{OFF}$ mice were created by crossing $Sim1^{Cre}$ mice with $Vglut2^{flox}$ mice (Jackson Laboratory) to produce $Sim1^{Cre}$;$Vglut2^{flox/+}$ mice, which were then crossed again with $Vglut2^{flox}$ to produce second generation $Sim1^{Cre}$;$Vglut2^{flox/flox}$. V3OFF mice were compared with wt;$Vglut2^{flox/flox}$ (wildtype controls). All procedures were performed in accordance with the Canadian Council on Animal Care and approved by the University Committee on Laboratory Animals at Dalhousie University.

Spinal cord tissue dissection, processing and sectioning

Spinal cords were obtained at postnatal stages (P9, P21-35). Prior to perfusion mice were anaesthetized via intraperitoneal injections of a ketamine (60mg/kg) and xylazine (12mg/kg) cocktail. Once a mouse no longer responded to the pedal reflex they were transcardially perfused with phosphate-buffered saline (PBS) and then 4% paraformaldehyde (Electron Microscopy Sciences) [PFA] in PBS. Following perfusion, spinal cords were dissected and incubated in 4% PFA for 1h (P9) or 4h (P21-P35) on ice. Spinal cords were then washed in PBS three times for 20mins each on ice followed by overnight in PBS at 4°C. Subsequently spinal cords were cryoprotected in 30% sucrose in PBS at 4°C for 2-3 nights. Cryoprotected spinal cords were then embedded in O.C.T compound (Fisher Healthcare) and flash frozen at -55

degrees in a mixture of dry ice and ethanol. Frozen higher lumbar (L1-L3) spinal cord segments were sectioned transversely using a cryostat (Leica CM1950) at 30 micrometers onto Superfrost Plus Microscope Slides (Fisherbrand).

Task-specific recruitment behaviours and nerve stimulations

For V3 and V2a recruitments, P21-P35 $Sim1^{Cre}$;Rosa.lsl.tdTom mice were subjected to nine distinct behavioural tasks, respectively. Upon competition of all behavioural tasks mice were given 1h of recovery before spinal cord dissection. Slow speed locomotion was achieved by subjecting mice to constant treadmill locomotion at a speed of 15 cm/s – at this speed mice perform predominately a walking gait (Bellardita & Kiehn, 2015; Lemieux et al., 2016). Intermediate speed locomotion was achieved by subjecting mice to three treadmill locomotor bouts of 15 minutes at 40 cm/s with 5 minutes rest between each bout – at this speed mice perform predominately a trotting gait (Bellardita & Kiehn, 2015; Lemieux et al., 2016). High speed locomotion was achieved by subjecting mice to 30-45 second treadmill locomotor bouts at 90 cm/s every five minutes for 1 hour total – at this speed mice perform predominately galloping or bounding gaits (Bellardita & Kiehn, 2015; Lemieux et al., 2016). Treadmill speeds were slowly ramped up to 90 cm/s from rest over a time period of 30-40 seconds for each bout. For incline and decline locomotion, mice were subjected to treadmill locomotion at 15 cm/s for 1h with a treadmill inclined at an angle of +25 degrees, or a declined at an angle of -25 degrees. For “staggard stepping” locomotion, mice were subjected to treadmill locomotion at 15 cm/s for 1h on a treadmill continuously oscillating side-to-side at a speed of 7cm/s. For “lateral motion”, mice stood stationary on a treadmill as it continuously oscillated side-to-side at a speed of 7cm/s, with no forward movement, for 1h. For swimming locomotion, mice were place

in pool containing distilled water maintained at a temperature ranging from 30-35 degrees Celsius for 1 hour.

For V2a recruitments in $Sim1^{Cre}$;$Vglut2^{flox/flox}$ and wt;$Vglut2^{flox/flox}$ mice, animals were subjected to either control (left in cage), flat surface walking (15cm/s , 0 degree incline), or incline walking (15cm/s, +18 degrees incline). Flat surface and incline walking consisted of 2 minute locomotor bout with 2 minutes of rest in between for 1 hour. Control mice were left undisturbed in their cages for 1 hour. Upon competition of task mice were given 1h of recovery before spinal cord dissection.

Femoral, tibial, and sural nerve stimulations were performed on P35 mice, respectively. The stimulation was 5 - 7 times threshold, 50 Hz single pulse with 5s intervals, lasting for 60 minutes and followed by 1h recovery before spinal cord dissection.

Anterograde tract tracing

Chloera Toxin Subunit B (CTB) conjugated with Alexa Fluor 488 (0.5mg/1ml PBS) [Molecular Probes] was injected into either proximal iliopsoas (IP) and gluteus maximus (GL) hip muscles or distal gastrocnemius (GS) and tibialis anterior (TA) ankle muscles in P14 Sim1Cre;Rosa.lsl.tdTom mice. 7 days after CTB injections, animals were euthanized and spinal cords dissected at P21.

Immunohistochemistry

Mounted spinal cord sections were first incubated in PBS containing 0.1% Triton X (PBS-T) for 3 consecutive washes of 5 minutes each. Subsequently, spinal cord sections were incubated in

0.1% PBS-T solution containing primary antibodies and 10% heat-inactivated horse serum (Invitrogen). Sheep anti-Chx10 primary antibody (1:1000) [abcam, ab16141] was used to identify V2a INs. rabbit anti-DsRed (1:2000) [Clontech, 632496] or goat anti-TdTomato (1:1000) [Sicgenantibodies, AB8181-200] were used to magnify endogenous TdTomato fluoresce in V3 INs. Rabbit anti-cfos (1:2000) [sysy, 226003] or mouse anti-cfos (1:1000) [abcam, ab208942] were used to identify $cfos^{+}$ interneurons. With rabbit anti-cfos sections were incubated in primary antibody solution for 2 nights at 4°C. With mouse anti-cfos sections were incubated in primary antibody solution for 2 nights at 4°C. To confirm reliability between cfos antibodies, we performed dual immunolabeling of spinal cord sections with rabbit anti-cfos and mouse anti-cfos (Supplemental1). For immunoreactivity of presynaptic terminals, chicken anti-parvalbumin (1:500) [sysy, 195006], guinea pig anti-vglut1 (1:1000) [Millipore, AB5905], goat anti-VAchT (1:1000) [Millipore, ABN100], and goat anti-CTB (1:10 000) [List Biological Laboratories, 703] were used. Following primary antibody incubation, spinal cord sections were washed with PBS for 15 mins (3x5min fresh solution). Sections were then incubated in PBS solution containing secondary antibodies for 1 hour at 4°C. Secondary antibodies used were donkey anti rabbit (1:500, Alexa Fluor 594, Jackson ImmunoResearch, 711-585-152); donkey anti goat (1:500, Alexa Fluor 594, Jackson ImmunoResearch, 705-585-147); donkey anti sheep (1:500, Alexa Fluor 488, Jackson ImmunoResearch, 713-545-147); donkey anti mouse (1:500, Alexa Fluor 647, Jackson ImmunoResearch, 715-605-151); donkey anti rabbit (1:500, Alexa Fluor 647, Jackson ImmunoResearch, 711-605-152); donkey anti goat (1:500, Alexa Fluor 488, Invitrogen, A11055); donkey anti guinea pig (1:500, Alexa Fluor 647, Jackson ImmunoResearch, 706-175-148); and donkey anti chicken (1:500, Alexa Fluor 488, Jackson ImmunoResearch, 703-545-155). Lastly,

sections were washed with PBS for 15 mins (3x5min fresh solution) and cover-slipped with fluorescent mounting medium (Dako).

Image capture, cell position, and cell cluster analysis

Fluorescent micrographs of spinal cord sections were captured using a Zeiss LSM 710 upright confocal microscope with ZEN 2009 Microscope and Imaging Software. Cfos images were taken with a 20x objective and stitched together to capture entire spinal cord section. Cell laminar positions were quantified using ImageJ and MATLAB. Using the ImageJ Cell Counter Plugin, x,y coordinates of individual cell bodies as well as the maximum and minimum x,y coordinates of corresponding spinal cord outlines were denoted. A total of 10 randomly chosen 30 µm transverse sections were analyzed between L1 to L3 spinal segments per animal. Cell body laminar distribution and cell body density contour plots were subsequently constructed utilizing *grid-data* and *contour* functions in MATLAB. Briefly, within each section cell body x,y positions were normalized against the maximum and minimum hemicord x,y coordinates. Heat maps were then constructed to display cell body densities across the mediolateral and dorsoventral axes.

For cell cluster analysis, spatial clusters were identified by fitting the mapping of all TdTomato$^+$ cells (both cfos$^+$ and cfos$^-$ V3 INs from all mice sampled, n=27 mice) and all Chx10+ cells (both cfos$^+$ and cfos$^-$ V2a INs from all mice sampled, n=27 mice) to a mixture of 2-dimensional Gaussian distributions with shared covariance structures. The fit was determined using "fitgmdist" in MATLAB. V3 INs were fit into four clusters and V2a INs were fit into two clusters. The total percentages of V3 and V2a INs that were cfos$^+$ were compared for each cluster across

distinct locomotor tasks. cfos^{+} IN clusters were statistically compared via one-way ANOVA and post hoc Tukey's test on Prism Graphpad.

6. Figures

Figure 2.1 Excitatory V3 and V2a INs display distinct recruitment patterns across varied sensorimotor tasks

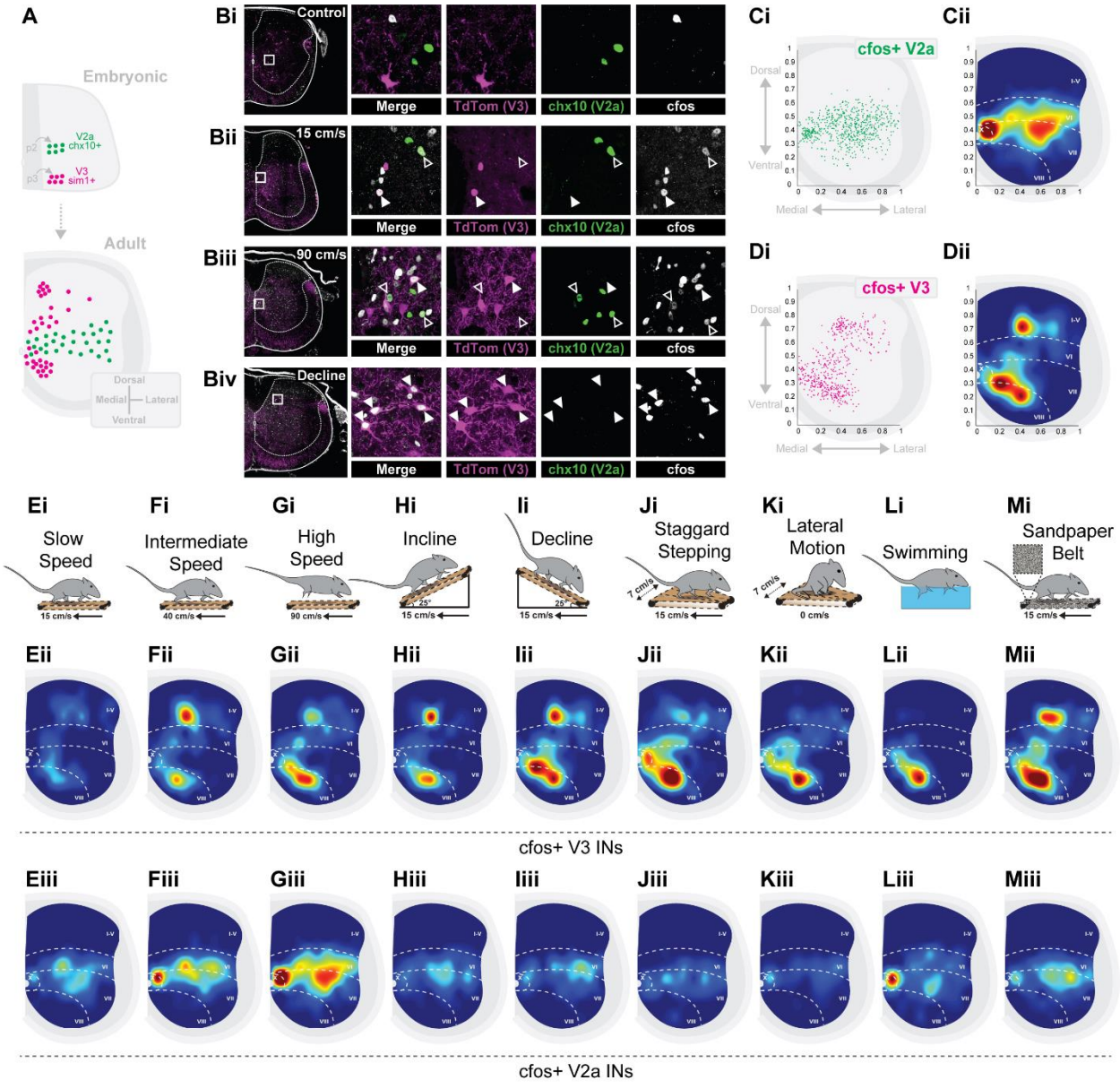

Figure 2.1 Excitatory V3 and V2a INs display distinct recruitment patterns across varied sensorimotor tasks

(A) Summary schematic of V3 and V2a embryonic lineages and adult laminar distributions in higher lumbar (L1-L3) spinal cords. (B) Representative images of cfos immunoreactivities in TdTom$^+$ V3 INs and Chx10$^+$ V2a INs in higher lumbar (L1-L3) spinal cord sections from adult Sim1Cre;Rosa.lsl.tdTom mice (Bi, control; Bii, slow speed walking (15cm/s); Biii, high speed running (90cm/s); Biv, decline walking (15cm/s, -25 degrees)). Filled arrows, cfos$^+$ V2a INs; unfilled arrows, cfos$^+$ V3 INs. (C,D) Example laminar cell distribution plots (i) and heat map density plots (ii) of cfos$^+$ V2a INs following high speed running (C, n=3 animals) and cfos$^+$ V3 INs following decline walking (D, n=3 animals) from higher lumbar (L1-L3) spinal cord segments. (E-M) Task-specific illustrations (i) and corresponding heat map density plots of cfos$^+$ V3 INs (ii, n=3 animals for each task) and cfos$^+$ V2a INs INs (iii, n=3 animals for each task) from higher lumbar (L1-L3) spinal cord segments.

Figure 2.2 V3 and V2a INs can be separated into discrete topographical clusters

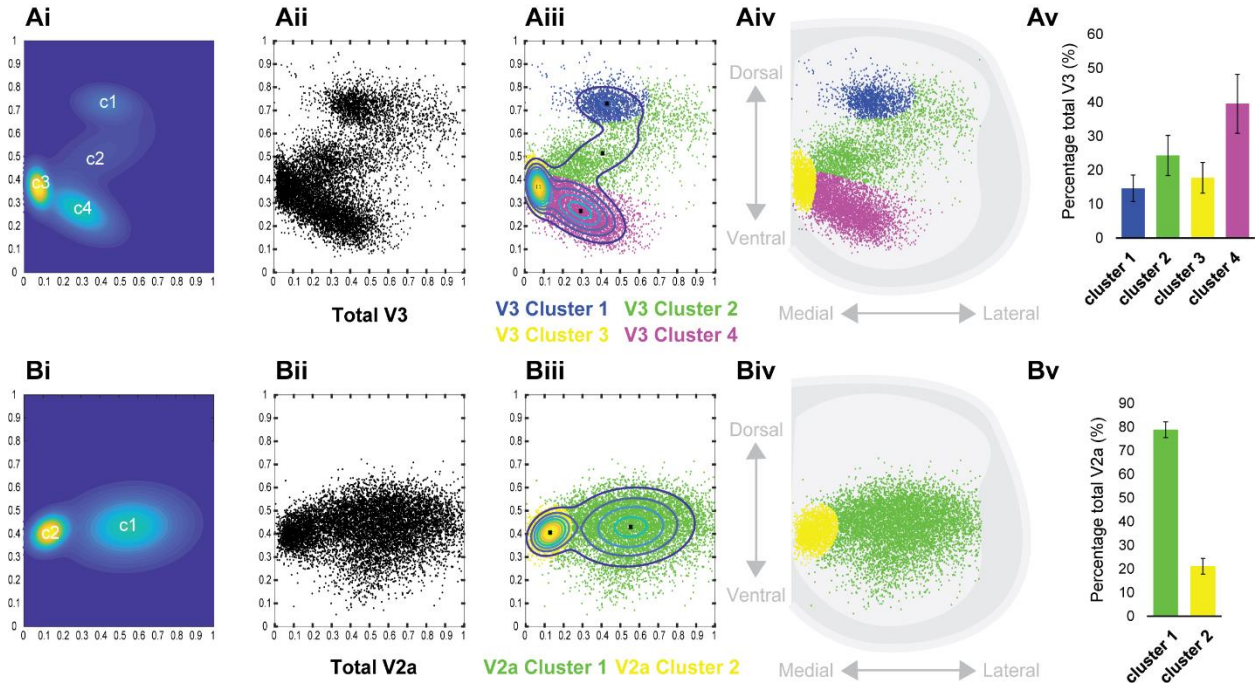

Figure 2.2 V3 and V2a INs can be separated into discrete topographical clusters

(Ai,Bi) Heat map density plots of total V3 INs (Ai, n=27 animals, 270 sections) and total V2a INs (Bi, n=27 animals, 270 sections) from higher lumbar (L1-L3) spinal cord segments. V3 INs display four distinct laminar clusters (c1, c2, c3, c4) and V2a INs display two distinct laminar clusters (c1, c2). (Aii,Bii) Laminar cell distribution plots of total V3 INs (Aii, n=27 animals, 270 sections) and total V2a INs (Bii, n=27 animals, 270 sections) from higher lumbar (L1-L3) spinal cord segments. (Aiii-iv,Biii-iv) Laminar cell distribution plots of total V3 INs separated into four clusters (Aiii-iv) and total V2a INs separated into two clusters (Biii-iv) using Gaussian Mixture Models (MATLAB, “fitgmdist”). (Av,Bv) Percentages of the total V3 INs with each of four clusters (Av) and V2a INs with each of two clusters (Bv).

Figure 2.3 V2a IN cluster recruitments across speed-dependent locomotor tasks

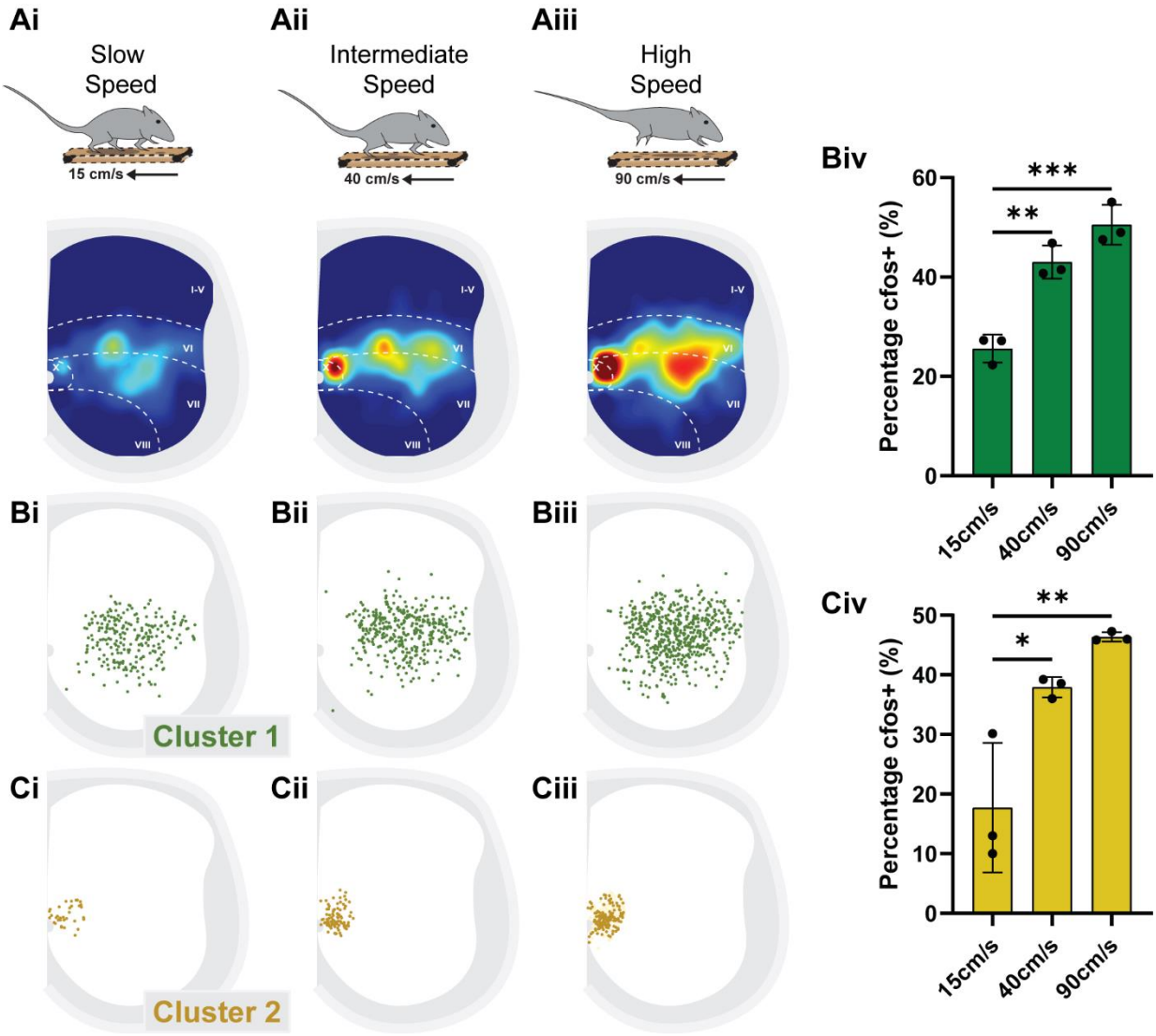

Figure 2.3 V2a IN cluster recruitments across speed-dependent locomotor tasks

(A) Task-specific illustrations and corresponding heat map density plots of $cfos^+$ V2a INs (n=3 animals for each task). (B-C) Laminar cell distribution plots (i-iii) and percentages of total $cfos^+$ INs (iv) within V2a cluster 1 (B) and cluster 2 (C) [n=3 animals for each task; B-Eiv, * p-value < 0.05, ** p-value < 0.01, *** p-value < 0.001, one-way ANOVA and post hoc Tukey's test).

Figure 2.4 V2a IN cluster recruitments across balance-dependent locomotor tasks

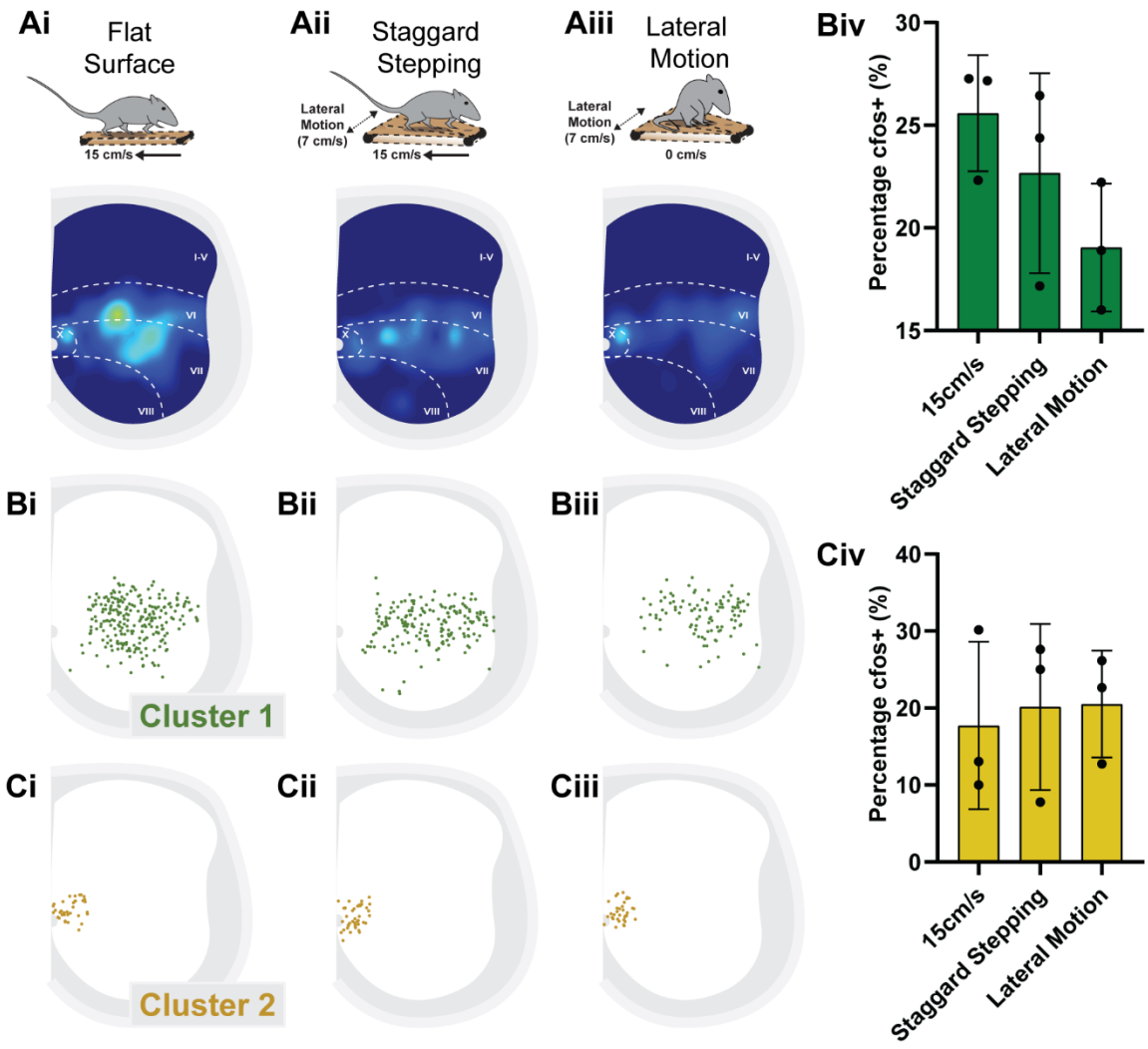

Figure 2.4 V2a IN cluster recruitments across balance-dependent locomotor tasks

(A) Task-specific illustrations and corresponding heat map density plots of cfos$^+$ V2a INs (n=3 animals for each task). (B-C) Laminar cell distribution plots (i-iii) and percentages of total cfos$^+$ INs (iv) within V2a cluster 1 (B) and cluster 2 (C) [n=3 animals for each task; B-Eiv, * p-value < 0.05, ** p-value < 0.01, *** p-value < 0.001, one-way ANOVA and post hoc Tukey's test).

Figure 2.5 V2a IN cluster recruitments across hindlimb load-dependent locomotor tasks

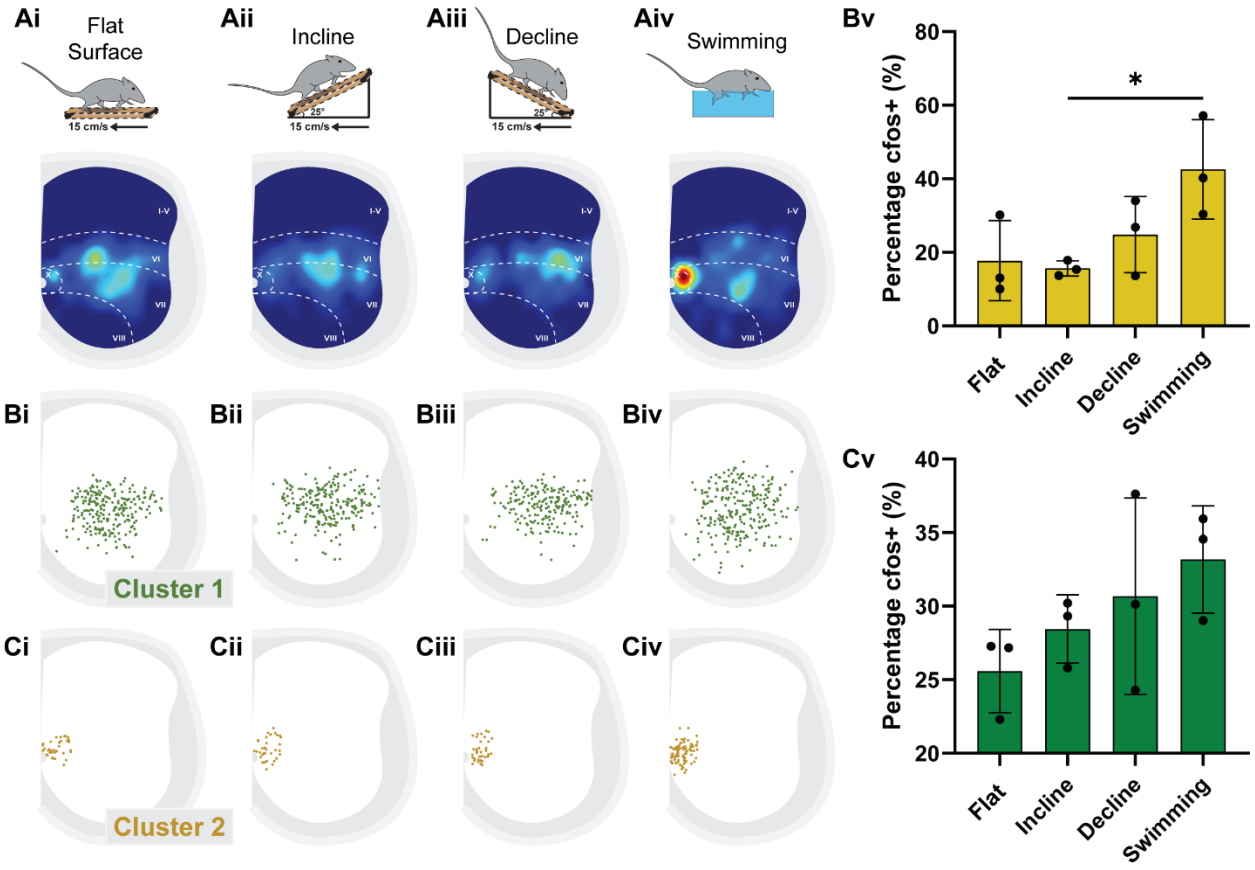

Figure 2.5 V2a IN cluster recruitments across hindlimb load-dependent locomotor tasks

(A) Task-specific illustrations and corresponding heat map density plots of $cfos^+$ V2a INs (n=3 animals for each task). (B-C) Laminar cell distribution plots (i-iv) and percentages of total $cfos^+$ INs (v) within V2a cluster 1 (B) and cluster 2 (C) [n=3 animals for each task; B-Ev, * p-value < 0.05, ** p-value < 0.01, *** p-value < 0.001, one-way ANOVA and post hoc Tukey's test).

Figure 2.6 V2a IN cluster recruitments across hind paw cutaneous-dependent locomotor tasks

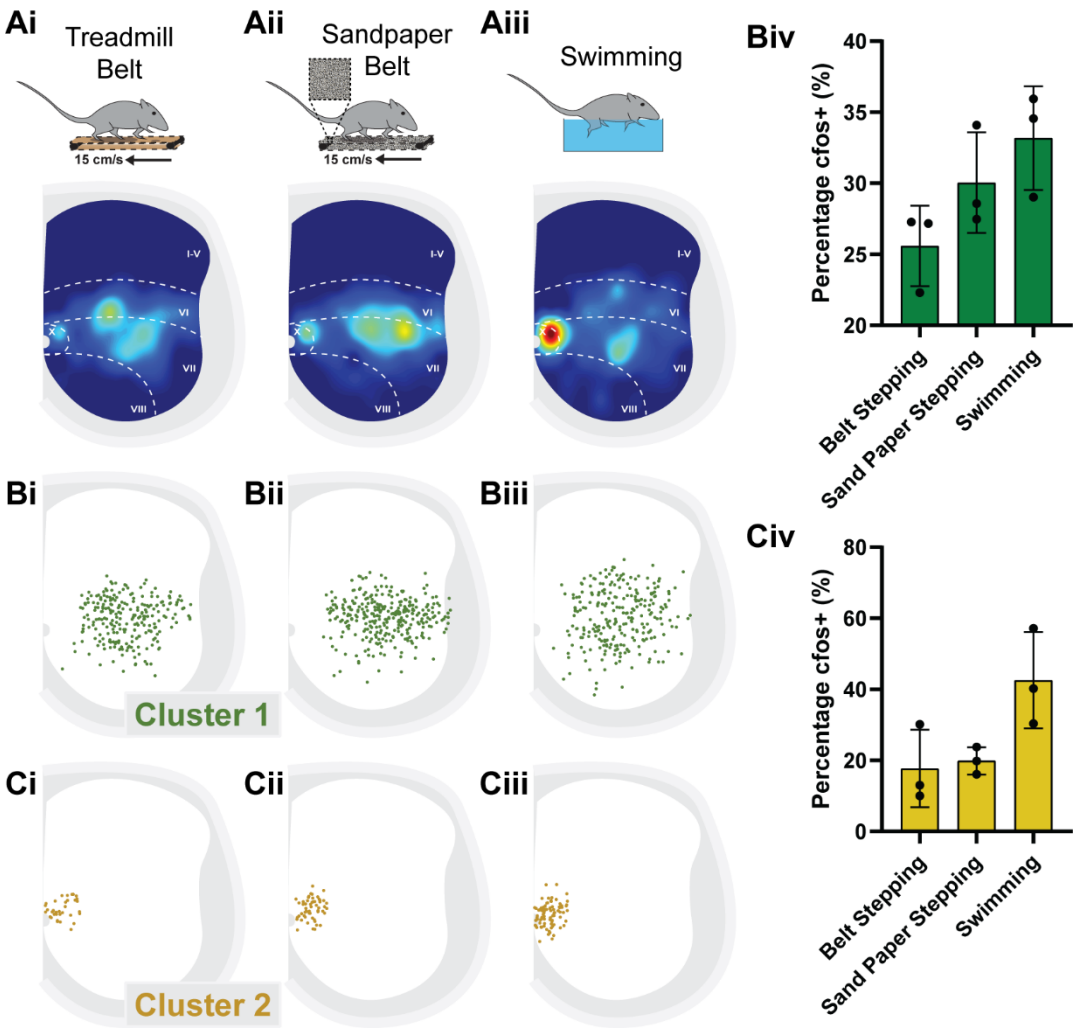

Figure 2.6 V2a IN cluster recruitments across hind paw cutaneous-dependent locomotor tasks

(A) Task-specific illustrations and corresponding heat map density plots of $cfos^+$ V2a INs (n=3 animals for each task). (B-C) Laminar cell distribution plots (i-iii) and percentages of total $cfos^+$ INs (iv) within V2a cluster 1 (B) and cluster 2 (C) [n=3 animals for each task; B-Eiv, * p-value < 0.05, ** p-value < 0.01, *** p-value < 0.001, one-way ANOVA and post hoc Tukey's test).

Figure 2.7 V3 IN cluster recruitments across speed-dependent locomotor tasks

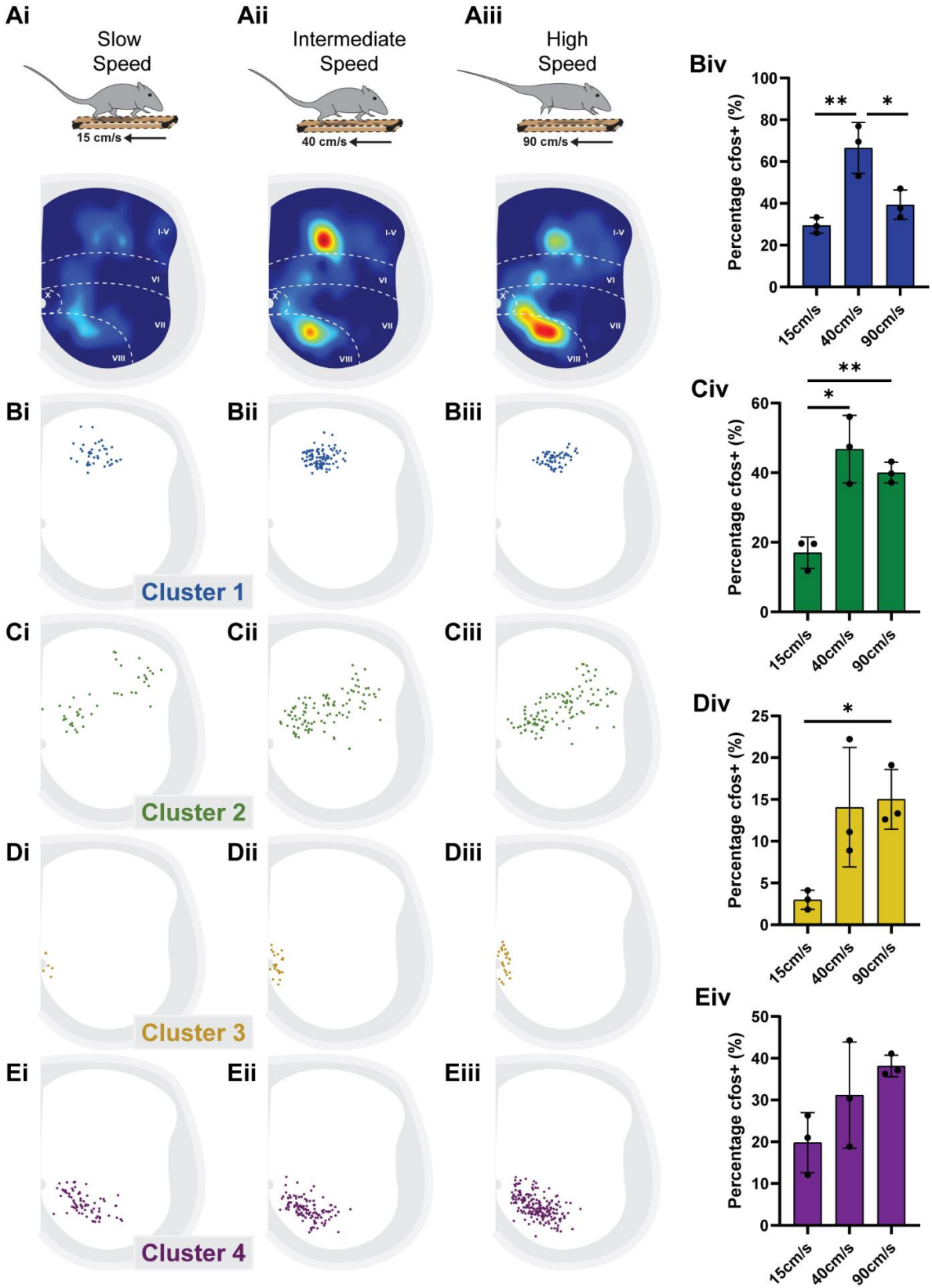

Figure 2.7 V3 IN cluster recruitments across speed-dependent locomotor tasks

(A) Task-specific illustrations and corresponding heat map density plots of $cfos^+$ V3 INs (n=3 animals for each task). (B-E) Laminar cell distribution plots (i-iii) and percentages of total $cfos^+$ INs (iv) within V3 cluster 1 (B), cluster 2 (C), cluster 3 (D) and cluster 4 (E) [n=3 animals for each task; B-Eiv, * p-value < 0.05, ** p-value < 0.01, *** p-value < 0.001, one-way ANOVA and post hoc Tukey's test).

Figure 2.8 V3 IN cluster recruitments across balance-dependent locomotor tasks

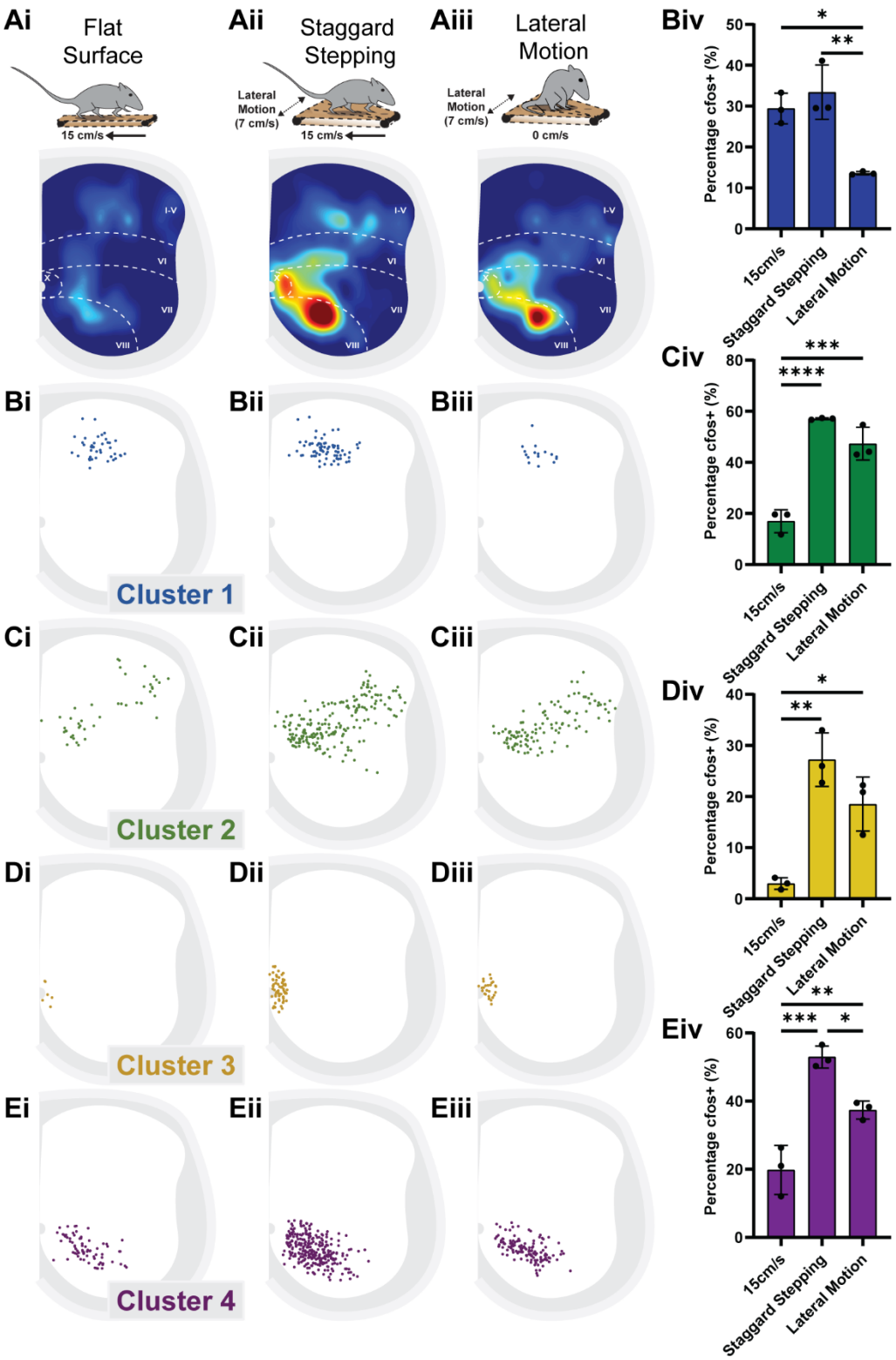

Figure 2.8 V3 IN cluster recruitments across balance-dependent locomotor tasks

(A) Task-specific illustrations and corresponding heat map density plots of $cfos^+$ V3 INs (n=3 animals for each task). (B-E) Laminar cell distribution plots (i-iii) and percentages of total $cfos^+$ INs (iv) within V3 cluster 1 (B), cluster 2 (C), cluster 3 (D) and cluster 4 (E) [n=3 animals for each task; B-Eiv, * p-value < 0.05, ** p-value < 0.01, *** p-value < 0.001, one-way ANOVA and post hoc Tukey's test).

Figure 2.9 V3 IN cluster recruitments across hindlimb load-dependent locomotor tasks

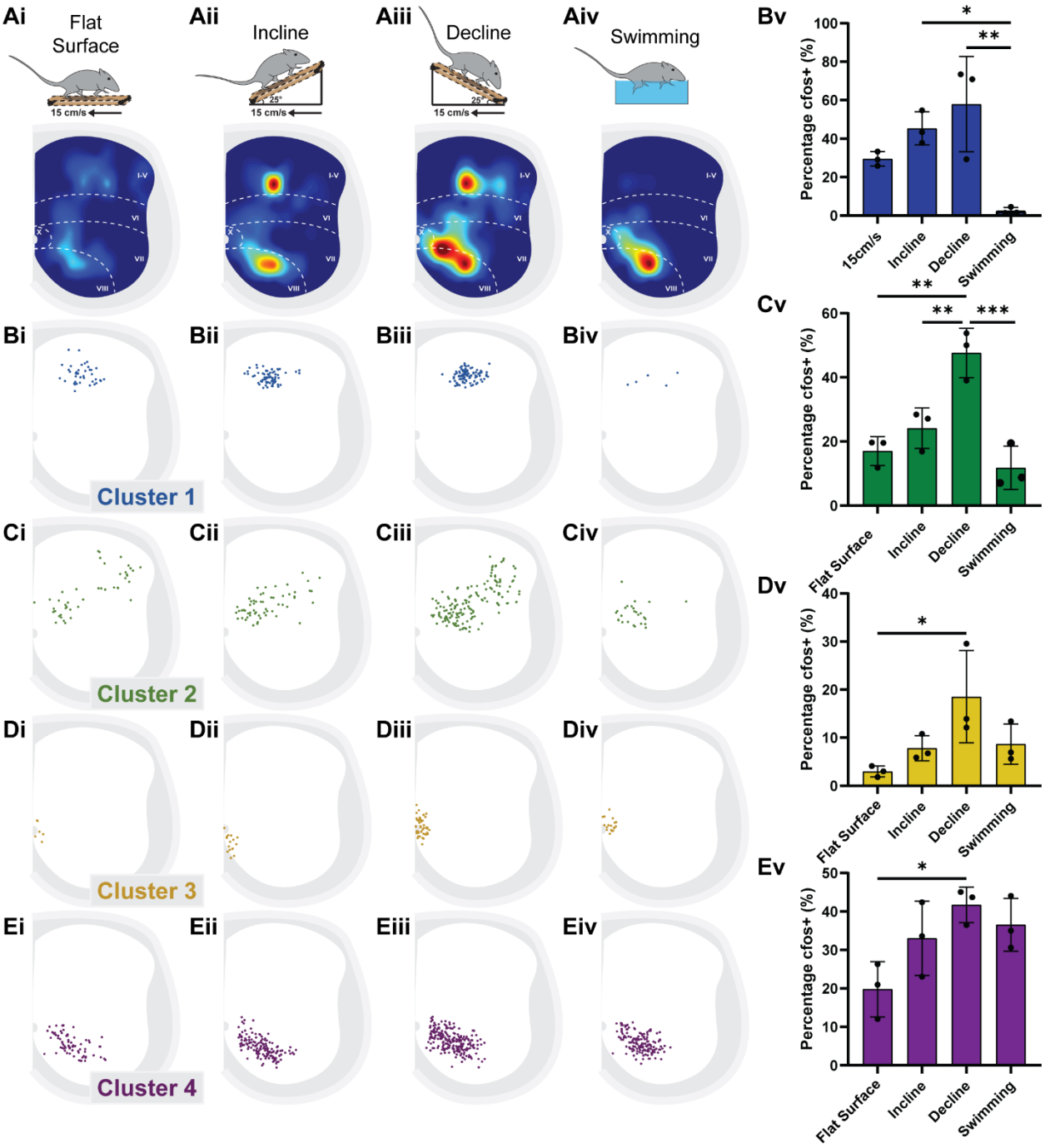

Figure 2.9 V3 IN cluster recruitments across hindlimb load-dependent locomotor tasks

(A) Task-specific illustrations and corresponding heat map density plots of $cfos^+$ V3 INs (n=3 animals for each task). (B-E) Laminar cell distribution plots (i-iv) and percentages of total $cfos^+$ INs (v) within V3 cluster 1 (B), cluster 2 (C), cluster 3 (D) and cluster 4 (E) [n=3 animals for each task; B-Ev, * p-value < 0.05, ** p-value < 0.01, *** p-value < 0.001, one-way ANOVA and post hoc Tukey's test).

Figure 2.10 V3 IN cluster recruitments across hind paw cutaneous-dependent locomotor tasks

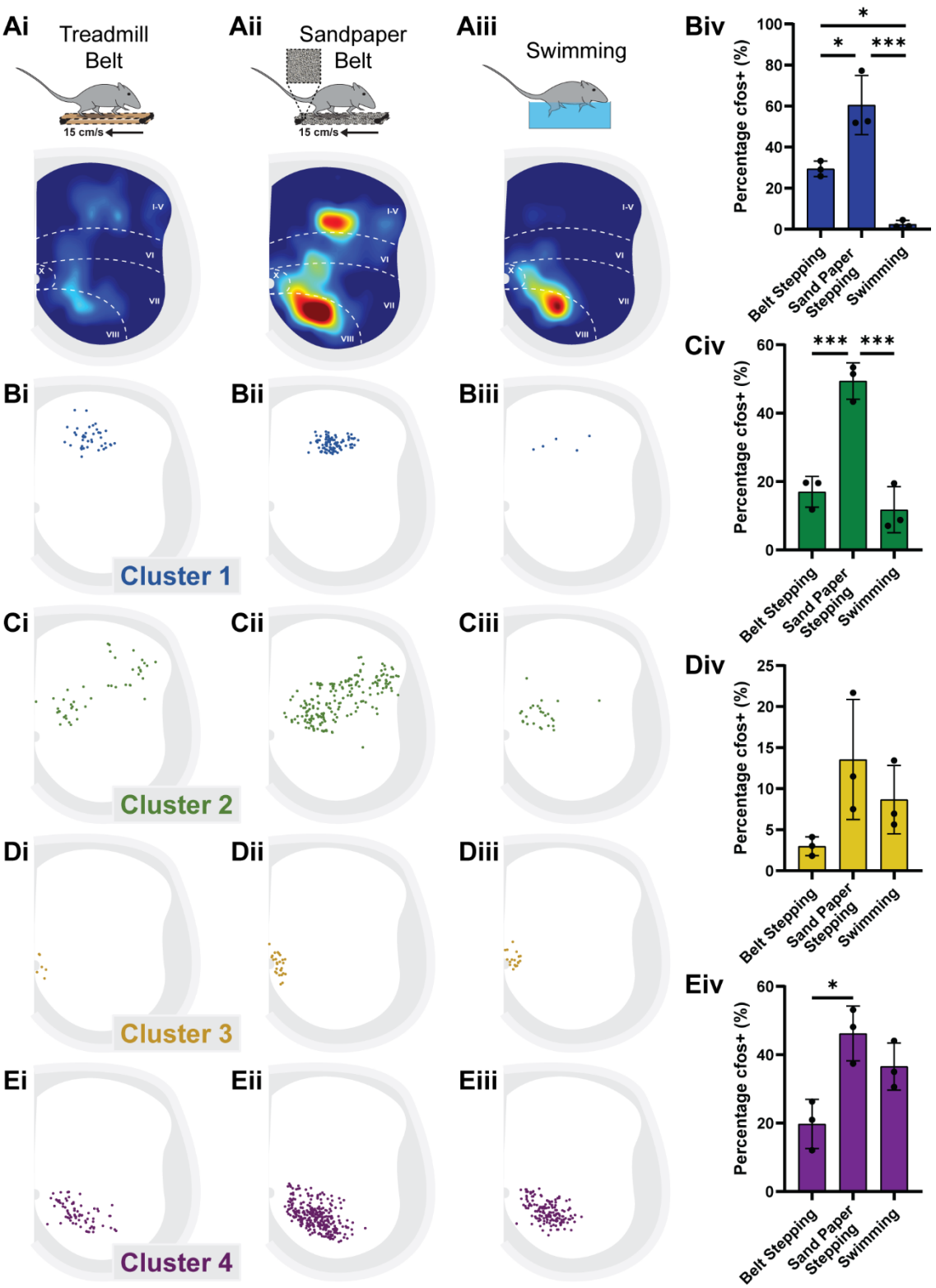

Figure 2.10 V3 IN cluster recruitments across hind paw cutaneous-dependent locomotor tasks

(A) Task-specific illustrations and corresponding heat map density plots of $cfos^+$ V3 INs (n=3 animals for each task). (B-E) Laminar cell distribution plots (i-iii) and percentages of total $cfos^+$ INs (iv) within V3 cluster 1 (B), cluster 2 (C), cluster 3 (D) and cluster 4 (E) [n=3 animals for each task; B-Eiv, * p-value < 0.05, ** p-value < 0.01, *** p-value < 0.001, one-way ANOVA and post hoc Tukey's test).

Figure 2.11 V3 IN clusters are differentially recruited by sensory modality and sensory nerve-specific inputs

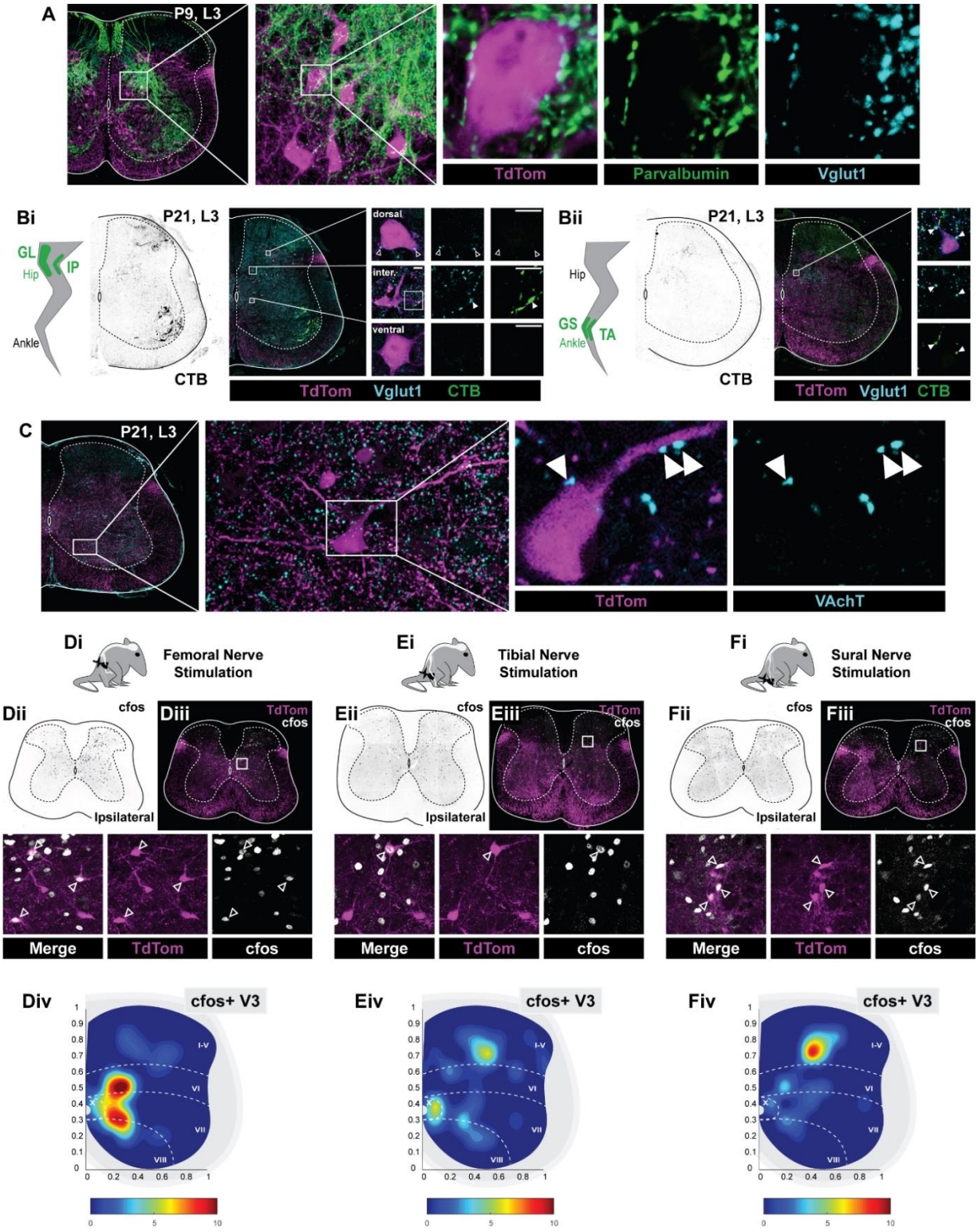

Figure 2.11 V3 IN clusters are differentially recruited by sensory modality and sensory nerve-specific inputs

(A) Representative image of parvalbumin$^+$/Vglut1$^+$ presynaptic proprioceptive terminals innervating TdTom$^+$ V3 INs in an L3 spinal segment of a P9 Sim1Cre;Rosa.lsl.tdTom mouse spinal cord. (B) Representative image of CTB$^+$ and Vglut1$^+$ presynaptic terminals innervating TdTom$^+$ V3 INs in an L3 spinal segment of a P21 Sim1Cre;Rosa.lsl.tdTom mouse spinal cord. (Bi) CTB injected into proximal iliopsoas (IP) and gluteus maximus (GL) hip muscles. (Bii) CTB injected into distal gastrocnemius (GS) and tibialis anterior (TA) ankle muscles. Filled arrows, CTB$^+$/Vglut1$^+$ inputs onto V3 INs; unfilled arrows, CTB$^-$/Vglut1$^+$ inputs onto V3 INs. (C) Representative image of VAchT$^+$ presynaptic terminals innervating TdTom$^+$ V3 INs in an L3 spinal segment of a P21 Sim1Cre;Rosa.lsl.tdTom mouse spinal cord. (D-F) Nerve specific stimulation illustrations of femoral (Di), tibial (Ei), and sural (Fi) nerves. Representative images of cfos immunoreactivities following nerve specific stimulations from higher lumbar (L1-L3) spinal cord segments of adult (>P35) Sim1Cre;Rosa.lsl.tdTom mice (D-Fii). Representative images of cfos$^+$ V3 INs following nerve specific stimulation (D-Fiii). Heat map density plots of cfos$^+$ V3 INs from higher lumbar (L1-L3) spinal cord segments of adult (>P35) Sim1Cre;Rosa.lsl.tdTom mice (D-Fiv, n=2 animals for each nerve stimulation).

Figure 2.12 Functional removal of V3 INs results in a task-specific increase of V2a IN recruitment

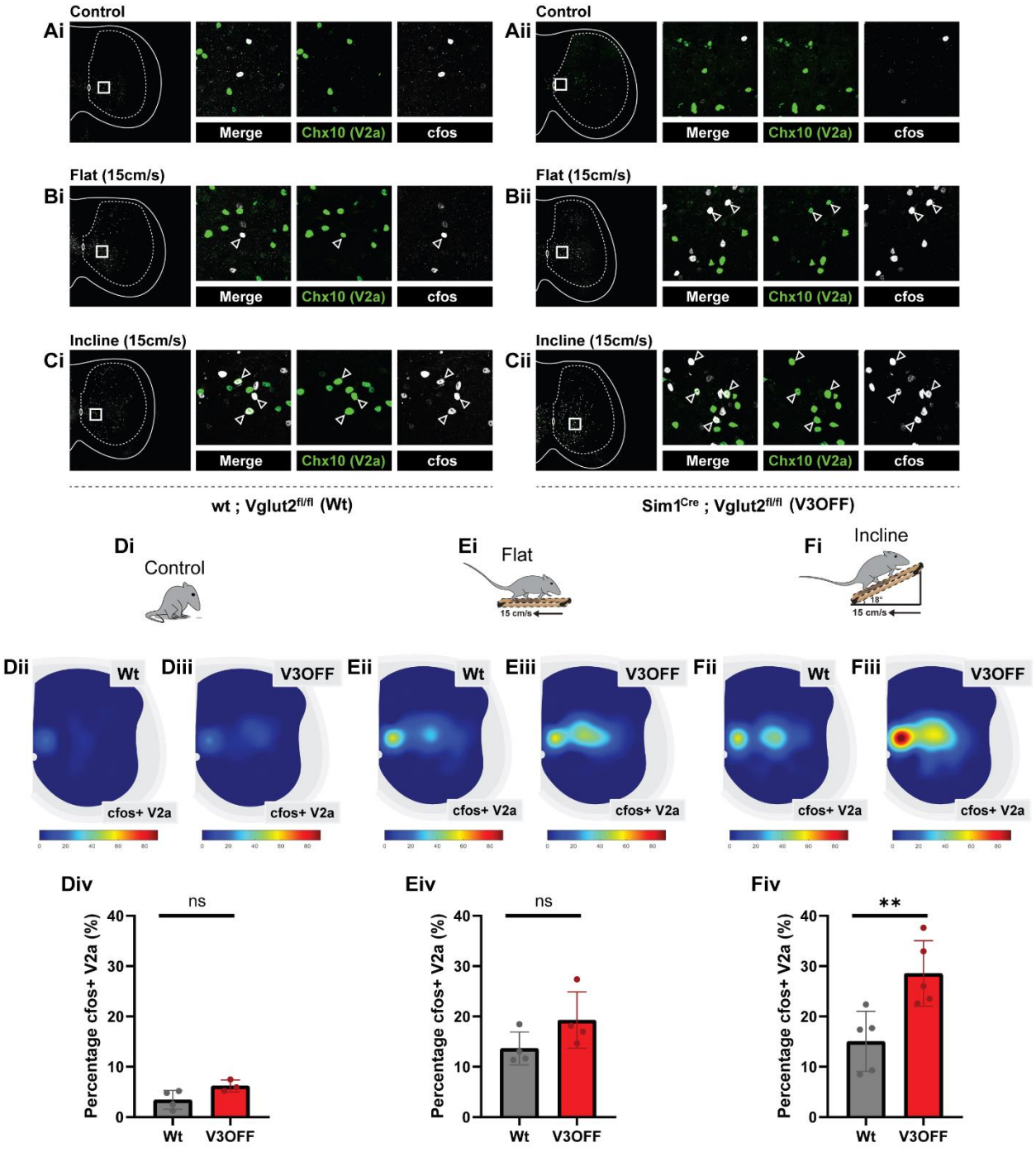

Figure 2.12 Functional removal of V3 INs results in a task-specific increase of V2a IN recruitment

(A-C) Representative images of cfos^{+} V2a INs in higher lumbar (L1-L3) spinal cords following control (A), flat surface walking (B), and incline walking (C) tasks in adult (>P21) Vglut2$^{flox/flox}$ (A-Ci, Wt) and Sim1^{Cre};Vglut2$^{flox/flox}$ (A-Cii, V3^{OFF}) mice. (D-F) Task-specific illustrations (D-Fi) and corresponding heat map density plots of cfos^{+} V2a INs (D-Fii, n=4 animals for each task and genotype) following control (D), flat surface walking (E) and incline walking (F) tasks in adult (>P21) Vglut2$^{flox/flox}$ (D-Fii, Wt) and Sim1^{Cre};Vglut2$^{flox/flox}$ (D-Fii, V3^{OFF}) mice. (E-Fiv) Percentages of cfos^{+} V2a INs following control (Wt, n=4; V3^{OFF}, n=3; Div), flat surface walking (Wt, n=4; V3^{OFF}, n=4; Eiv) and incline walking (Wt, n=5; V3^{OFF}, n=5; Fiv) tasks (ns p-value > 0.05, * p-value < 0.05, ** p-value < 0.01, unpaired t-test).

7. Supplemental Figures

Supplemental Figure 2.1 Dual cfos immunolabeling of an L3 spinal cord section following high speed running (90cm/s)

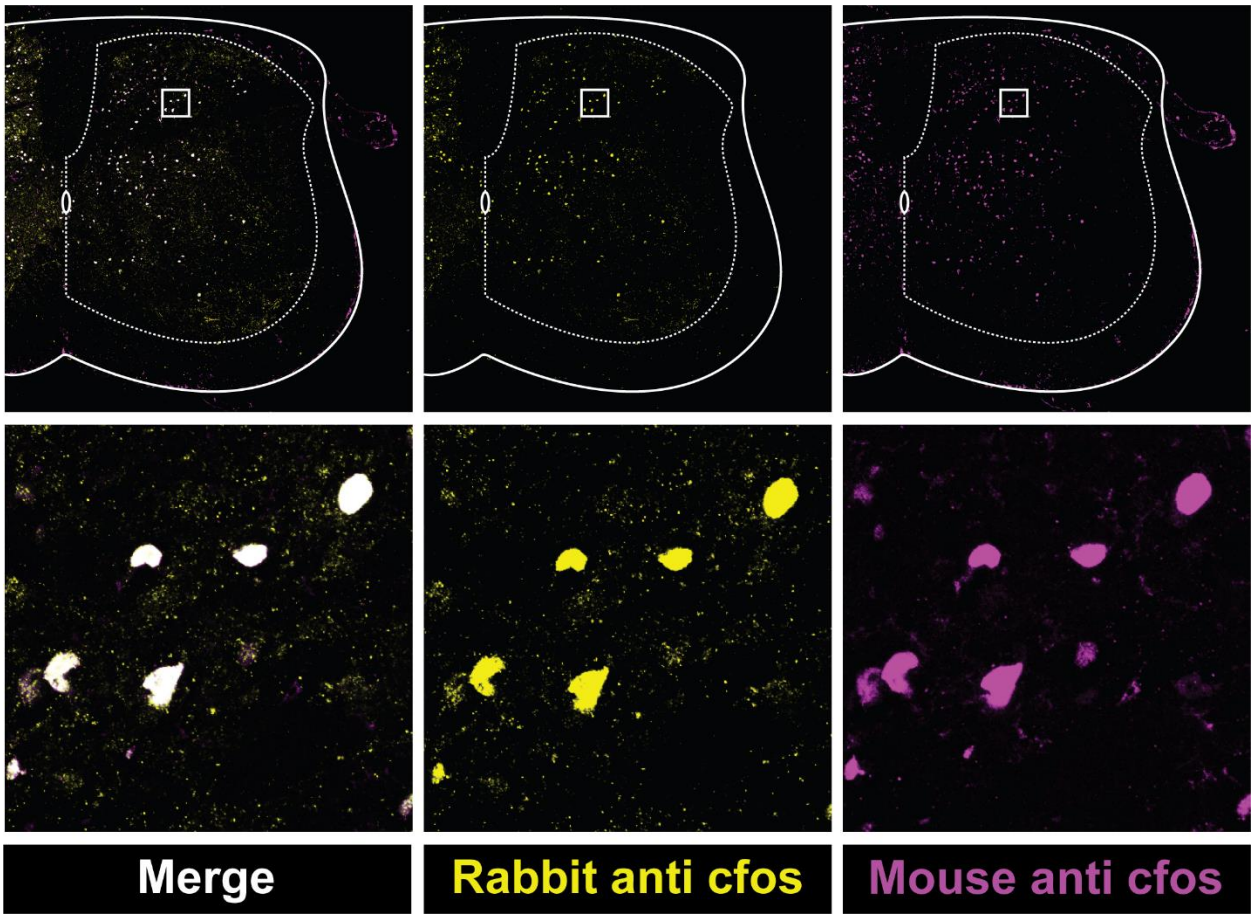

8. References

Akay, T., Tourtellotte, W., Arber, S., & Jessell, T. (2014). Degradation of mouse locomotor pattern in the absence of proprioceptive sensory feedback. *Proceedings of the National Academy of Sciences of the United States of America, 111*(47), 16877-16882. doi:10.1073/pnas.1419045111

Akay, T., & Murray, A. (2021). Relative contribution of proprioceptive and vestibular sensory systems to locomotion: Opportunities for discovery in the age of molecular science. *International Journal of Molecular Sciences, 22*(3) doi:10.3390/ijms22031467

Al Mosawie, A., Wilson, J. M., & Brownstone, R. M. (2007). Heterogeneity of V2-derived interneurons in the adult mouse spinal cord. *European Journal of Neuroscience, 26*(11), 3003-3015. doi:10.1111/j.1460-9568.2007.05907.x

Alvarez, F., Villalba, R., Zerda, R., & Schneider, S. (2004). Vesicular glutamate transporters in the spinal cord, with special reference to sensory primary afferent synapses. *Journal of Comparative Neurology, 472*(3), 257-280. doi:10.1002/cne.20012

Ampatzis, K., Song, J., Ausborn, J., & El Manira, A. (2014). Separate microcircuit modules of distinct v2a interneurons and motoneurons control the speed of locomotion. *Neuron, 83*(4), 934-943. doi:10.1016/j.neuron.2014.07.018

Arber, S., Ladle, D. R., Lin, J. H., Frank, E., & Jessell, T. M. (2000). ETS gene Er81 controls the formation of functional connections between group ia sensory afferents and motor neurons. *Cell, 101*(5), 485-498. doi:10.1016/S0092-8674(00)80859-4

Ausborn, J., Mahmood, R., & El Manira, A. (2012). Decoding the rules of recruitment of excitatory interneurons in the adult zebrafish locomotor network. *Proceedings of the National Academy of Sciences of the United States of America, 109*(52), E3631-E3639. doi:10.1073/pnas.1216256110

Bagnall, M., & McLean, D. (2014). Modular organization of axial microcircuits in zebrafish. *Science, 343*(6167), 197-200. doi:10.1126/science.1245629

Bailey, C. S., Kitchell, R. L., Guinan, M. J., & Sharp, J. W. (1992). Dorsal nerve root origins of the cutaneous nerves of the feline pelvic limb. *Anatomia, Histologia, Embryologia, 21*(1), 23-31. doi:10.1111/j.1439-0264.1992.tb00315.x

Bailey, C. S., & Kitchell, R. L. (1987). Cutaneous sensory testing in the dog. *Journal of Veterinary Internal Medicine, 1*(3), 128-135. doi:10.1111/j.1939-1676.1987.tb02000.x

Bellardita, C., & Kiehn, O. (2015). Phenotypic characterization of speed-associated gait changes in mice reveals modular organization of locomotor networks. *Current Biology, 25*(11), 1426-1436. doi:10.1016/j.cub.2015.04.005

Bikoff, J. B. (2019). Interneuron diversity and function in the spinal motor system. *Current Opinion in Physiology, 8*, 36-43. doi:https://doi.org/10.1016/j.cophys.2018.12.013

Bizzi, E., Cheung, V. C. K., d'Avella, A., Saltiel, P., & Tresch, M. (2008). Combining modules for movement. *Brain Research Reviews, 57*(1), 125-133. doi:10.1016/j.brainresrev.2007.08.004

Bizzi, E., Giszter, S. F., Loeb, E., Mussa Ivaldi, F. A., & Saltiel, P. (1995). Modular organization of motor behavior in the frog's spinal cord. *Trends in Neurosciences (Regular Ed.), 18*(10), 442-446. doi:10.1016/0166-2236(95)94494-P

Björnfors, E. R., & El Manira, A. (2016). Functional diversity of excitatory commissural interneurons in adult zebrafish. *Elife, 5* doi:10.7554/eLife.18579

Blacklaws, J., Deska Gauthier, D., Jones, C., Petracca, Y., Liu, M., Zhang, H., . . . Zhang, Y. (2015). Sim1 is required for the migration and axonal projections of V3 interneurons in the developing mouse spinal cord. *Developmental Neurobiology, 75*(9), 1003-1017. doi:10.1002/dneu.22266

Blankenship, A., & Feller, M. (2010). Mechanisms underlying spontaneous patterned activity in developing neural circuits. *Nature Reviews Neuroscience, 11*(1), 18-29. doi:10.1038/nrn2759

Borowska, J., Jones, C. T., Deska Gauthier, D., & Zhang, Y. (2015). V3 interneuron subpopulations in the mouse spinal cord undergo distinctive postnatal maturation processes. *Neuroscience, 295*, 221-228. doi:10.1016/j.neuroscience.2015.03.024

Borowska, J., Jones, C., Zhang, H., Blacklaws, J., Goulding, M., & Zhang, Y. (2013). Functional subpopulations of V3 interneurons in the mature mouse spinal cord. *The Journal of Neuroscience, 33*(47), 18553-18565. doi:10.1523/JNEUROSCI.2005-13.2013

Briscoe, J., Sussel, L., Serup, P., Hartigan O'Connor, D., Jessell, T. M., Rubenstein, J. L., & Ericson, J. (1999). Homeobox gene Nkx2.2 and specification of neuronal identity by graded sonic hedgehog signalling. *Nature, 398*(6728), 622-627. doi:10.1038/19315

Chopek, J., Nascimento, F., Beato, M., Brownstone, R., & Zhang, Y. (2018). Sub-populations of spinal V3 interneurons form focal modules of layered pre-motor microcircuits. *Cell Reports, 25*(1), 146-156.e3. doi:10.1016/j.celrep.2018.08.095

Crone, S., Quinlan, K., Zagoraiou, L., Droho, S., Restrepo, C., Lundfald, L., . . . Sharma, K. (2008). Genetic ablation of V2a ipsilateral interneurons disrupts left-right locomotor coordination in mammalian spinal cord. *Neuron, 60*(1), 70-83. doi:10.1016/j.neuron.2008.08.009

Crone, S., Zhong, G., Harris Warrick, R., & Sharma, K. (2009). In mice lacking V2a interneurons, gait depends on speed of locomotion. *The Journal of Neuroscience, 29*(21), 7098-7109. doi:10.1523/JNEUROSCI.1206-09.2009

de Leon, R., Hodgson, J. A., Roy, R. R., & Edgerton, V. R. (1994). Extensor- and flexor-like modulation within motor pools of the rat hindlimb during treadmill locomotion and swimming. *Brain Research, 654*(2), 241-250. doi:10.1016/0006-8993(94)90485-5

Deska-Gauthier, D., & Zhang, Y. (2019). The functional diversity of spinal interneurons and locomotor control. *Current Opinion in Physiology, 8*, 99-108. doi:https://doi.org/10.1016/j.cophys.2019.01.005

Dougherty, K., & Kiehn, O. (2010). Functional organization of V2a-related locomotor circuits in the rodent spinal cord. *Annals of the New York Academy of Sciences, 1198*, 85-93. doi:10.1111/j.1749-6632.2010.05502.x

Ericson, J., Rashbass, P., Schedl, A., Brenner Morton, S., Kawakami, A., van Heyningen, V., . . . Briscoe, J. (1997). Pax6 controls progenitor cell identity and neuronal fate in response to graded shh signaling. *Cell, 90*(1), 169-180. doi:10.1016/s0092-8674(00)80323-2

Ferreira Pinto, M., Ruder, L., Capelli, P., & Arber, S. (2018). Connecting circuits for supraspinal control of locomotion. *Neuron, 100*(2), 361-374. doi:10.1016/j.neuron.2018.09.015

Goulding, M., Lanuza, G., Sapir, T., & Narayan, S. (2002). The formation of sensorimotor circuits. *Current Opinion in Neurobiology, 12*(5), 508-515. doi:10.1016/s0959-4388(02)00371-9

Goulding, M. (2009). Circuits controlling vertebrate locomotion: Moving in a new direction. *Nature Reviews.Neuroscience, 10*(7), 507-518. doi:10.1038/nrn2608

Grillner, S., & El Manira, A. (2020). Current principles of motor control, with special reference to vertebrate locomotion. *Physiological Reviews, 100*(1), 271-320. doi:10.1152/physrev.00015.2019

Hägglund, M., Dougherty, K., Borgius, L., Itohara, S., Iwasato, T., & Kiehn, O. (2013). Optogenetic dissection reveals multiple rhythmogenic modules underlying locomotion. *Proceedings of the National Academy of Sciences of the United States of America, 110*(28), 11589-11594. doi:10.1073/pnas.1304365110

Harris, K., & Shepherd, G. M. G. (2015). The neocortical circuit: Themes and variations. *Nature Neuroscience, 18*(2), 170-181. doi:10.1038/nn.3917

Hayashi, M., Hinckley, C., Driscoll, S., Moore, N., Levine, A., Hilde, K., . . . Pfaff, S. (2018). Graded arrays of spinal and supraspinal V2a interneuron subtypes underlie forelimb and hindlimb motor control. *Neuron, 97*(4), 869-884.e5. doi:10.1016/j.neuron.2018.01.023

Honda, C. N. (1995). Differential distribution of calbindin-D28k and parvalbumin in somatic and visceral sensory neurons. *Neuroscience, 68*(3), 883-892. doi:10.1016/0306-4522(95)00180-Q

Huang, Z. J., & Scheiffele, P. (2008). GABA and neuroligin signaling: Linking synaptic activity and adhesion in inhibitory synapse development. *Current Opinion in Neurobiology, 18*(1), 77-83. doi:10.1016/j.conb.2008.05.008

Hurteau, M., Thibaudier, Y., Dambreville, C., Chraibi, A., Desrochers, E., Telonio, A., & Frigon, A. (2017). Nonlinear modulation of cutaneous reflexes with increasing speed of locomotion in spinal cats. *The Journal of Neuroscience, 37*(14), 3896-3912. doi:10.1523/JNEUROSCI.3042-16.2017

Hutchison, D. L., Roy, R. R., Hodgson, J. A., & Edgerton, V. R. (1989). EMG amplitude relationships between the rat soleus and medial gastrocnemius during various motor tasks. *Brain Research, 502*(2), 233-244. doi:10.1016/0006-8993(89)90618-5

Jessell, T. M. (2000). Neuronal specification in the spinal cord: Inductive signals and transcriptional codes. *Nature Reviews Genetics, 1*(1), 20-29. doi:10.1038/35049541

Kambiz, S., Baas, M., Duraku, L. S., Kerver, A. L., Koning, A. H. J., Walbeehm, E. T., & Ruigrok, T. J. H. (2014). Innervation mapping of the hind paw of the rat using evans blue extravasation, optical surface mapping and CASAM. *Journal of Neuroscience Methods, 229*, 15-27. doi:10.1016/j.jneumeth.2014.03.015

Kiehn, O. (2016). Decoding the organization of spinal circuits that control locomotion. *Nature Reviews.Neuroscience, 17*(4), 224-238. doi:10.1038/nrn.2016.9

Kruspe, M., Thieme, H., Guntinas Lichius, O., & Irintchev, A. (2014). Motoneuron regeneration accuracy and recovery of gait after femoral nerve injuries in rats. *Neuroscience, 280*, 73-87. doi:10.1016/j.neuroscience.2014.08.051

Lallemend, F., & Ernfors, P. (2012). Molecular interactions underlying the specification of sensory neurons. *Trends in Neurosciences, 35*(6), 373-381. doi:10.1016/j.tins.2012.03.006

Lemieux, M., Josset, N., Roussel, M., Couraud, S., & Bretzner, F. (2016). Speed-dependent modulation of the locomotor behavior in adult mice reveals attractor and transitional gaits. *Frontiers in Neuroscience, 10*, 42-42. doi:10.3389/fnins.2016.00042

Matsushima, T., & Grillner, S. (1992). Neural mechanisms of intersegmental coordination in lamprey: Local excitability changes modify the phase coupling along the spinal cord. *Journal of Neurophysiology, 67*(2), 373-388. doi:10.1152/jn.1992.67.2.373

Mayer, W., Murray, A., Brenner Morton, S., Jessell, T., Tourtellotte, W., & Akay, T. (2018). Role of muscle spindle feedback in regulating muscle activity strength during walking at different speed in mice. *Journal of Neurophysiology,* doi:10.1152/jn.00250.2018

Merkulyeva, N., Veshchitskii, A., Gorsky, O., Pavlova, N., Zelenin, P., Gerasimenko, Y., . . . Musienko, P. (2018). Distribution of spinal neuronal networks controlling forward and backward locomotion. *The Journal of Neuroscience, 38*(20), 4695-4707. doi:10.1523/JNEUROSCI.2951-17.2018

Myers, C., Lewcock, J., Hanson, M. G., Gosgnach, S., Aimone, J., Gage, F., . . . Pfaff, S. (2005). Cholinergic input is required during embryonic development to mediate proper assembly of spinal locomotor circuits. *Neuron, 46*(1), 37-49. doi:10.1016/j.neuron.2005.02.022

Pierotti, D. J., Roy, R. R., Gregor, R. J., & Edgerton, V. R. (1989). Electromyographic activity of cat hindlimb flexors and extensors during locomotion at varying speeds and inclines. *Brain Research, 481*(1), 57-66. doi:10.1016/0006-8993(89)90485-X

Ray, R., Corcoran, A., Brust, R., Kim, J., Richerson, G., Nattie, E., & Dymecki, S. (2011). Impaired respiratory and body temperature control upon acute serotonergic neuron inhibition. *Science, 333*(6042), 637-642. doi:10.1126/science.1205295

Roy, R. R., Hutchison, D. L., Pierotti, D. J., Hodgson, J. A., & Edgerton, V. R. (1991). EMG patterns of rat ankle extensors and flexors during treadmill locomotion and swimming. *Journal of Applied Physiology, 70*(6), 2522-2529. doi:10.1152/jappl.1991.70.6.2522

Roy, R. R., Hutchison, D. L., Pierotti, D. J., Hodgson, J. A., & Edgerton, V. R. (1991). EMG patterns of rat ankle extensors and flexors during treadmill locomotion and swimming. *Journal of Applied Physiology, 70*(6), 2522-2529. doi:10.1152/jappl.1991.70.6.2522

Sagar, S. M., Sharp, F. R., & Curran, T. (1988). Expression of c-fos protein in brain: Metabolic mapping at the cellular level. *Science, 240*(4857), 1328-1331. doi:10.1126/science.3131879

Stein, P. S. G. (2008). Motor pattern deletions and modular organization of turtle spinal cord. *Brain Research Reviews, 57*(1), 118-124. doi:10.1016/j.brainresrev.2007.07.008

Swett, J. E., & Woolf, C. J. (1985). The somatotopic organization of primary afferent terminals in the superficial laminae of the dorsal horn of the rat spinal cord. *Journal of Comparative Neurology, 231*(1), 66-77. doi:10.1002/cne.902310106

Talpalar, A., Bouvier, J., Borgius, L., Fortin, G., Pierani, A., & Kiehn, O. (2013). Dual-mode operation of neuronal networks involved in left-right alternation. *Nature, 500*(7460), 85-88. doi:10.1038/nature12286

Wiggin, T., Anderson, T., Eian, J., Peck, J., & Masino, M. (2012). Episodic swimming in the larval zebrafish is generated by a spatially distributed spinal network with modular functional organization. *Journal of Neurophysiology, 108*(3), 925-934. doi:10.1152/jn.00233.2012

Zagoraiou, L., Akay, T., Martin, J., Brownstone, R., Jessell, T., & Miles, G. (2009). A cluster of cholinergic premotor interneurons modulates mouse locomotor activity. *Neuron, 64*(5), 645-662. doi:10.1016/j.neuron.2009.10.017

Zhang, Y., Narayan, S., Geiman, E., Lanuza, G., Velasquez, T., Shanks, B., . . . Goulding, M. (2008). V3 spinal neurons establish a robust and balanced locomotor rhythm during walking. *Neuron, 60*(1), 84-96. doi:10.1016/j.neuron.2008.09.027

Zhong, G., Droho, S., Crone, S., Dietz, S., Kwan, A., Webb, W., . . . Harris Warrick, R. (2010). Electrophysiological characterization of V2a interneurons and their locomotor-related activity in the neonatal mouse spinal cord. *The Journal of Neuroscience, 30*(1), 170-182. doi:10.1523/JNEUROSCI.4849-09.2010

Ziskind Conhaim, L., & Hochman, S. (2017). Diversity of molecularly defined spinal interneurons engaged in mammalian locomotor pattern generation. *Journal of Neurophysiology, 118*(6), 2956-2974. doi:10.1152/jn.00322.2017

CHAPTER 3. THE TEMPORAL NEUROGENESIS PATTERNING OF SPINAL P3-V3 INTERNEURONS INTO DIVERGENT SUBPOPULATION ASSEMBLIES

Contribution Statement

I would like to acknowledge Dr. Joanna Borowska for performing the patch-clamp recordings and electrophysiological analyses. I would like to acknowledge Dr. Christopher Jones for assisting in the statistical analysis. I would like to acknowledge Mingwei Liu for developing a MATLAB cell counter application.

1. Abstract

Neuronal diversity provides the spinal cord with the functional flexibility required to perform complex motor tasks. Spinal neurons arise during early embryonic development with the establishment of spatially and molecularly discrete progenitor domains that give rise to distinct, but highly heterogeneous, post-mitotic interneuron (IN) populations. Our previous studies have shown that Sim1-expressing V3 INs, originating from the p3 progenitor domain, are anatomically and physiologically divergent. However, the developmental logic guiding V3 subpopulation diversity remains elusive. In specific cases of other IN classes, neurogenesis timing can play a role in determining the ultimate fates and unique characteristics of distinctive subpopulations. To examine whether neurogenesis timing contributes to V3 diversity, we systematically investigated the temporal neurogenesis profiles of V3 INs in the mouse spinal cord. Our work uncovered that V3 INs were organized into either early-born (E9.5-E10.5) or late-born (E11.5-E12.5) neurogenic waves. Early-born V3 INs displayed both ascending and descending commissural projections and clustered into subgroups across dorsoventral spinal laminae. In contrast, late-born V3 INs became fate-restricted to ventral laminae, displayed mostly descending and local commissural projections, and uniform membrane properties. Furthermore, we found that the post-mitotic transcription factor, Sim1, although expressed in all V3 INs, exclusively regulated the dorsal clustering and electrophysiological diversification of early-born, but not late-born, V3 INs, which indicates that neurogenesis timing may enable new born V3 INs to interact with different post-mitotic differentiation pathways. Thus, our work demonstrates neurogenesis timing as a developmental mechanism underlying the post-mitotic differentiation of V3 INs into distinct subpopulation assemblies.

2. Introduction

As mitotic progenitor cells undergo their final division phase, they exit the cell-cycle becoming postmitotic neurons. The timing of a neuron's cell-cycle exit, marking its genesis, plays a vital role in determining its terminal fate specification via the dynamic exposure of intrinsic and extrinsic factors (Holguera & Desplan, 2018; Syed et al., 2017). Within layered neural tissues, such as the neocortex and retina, distinct neuronal populations differentiate into anatomically organized rows stacked across a single spatial axis. Neurogenesis timing plays an essential role in ordering postmitotic neurons into distinct layers from common progenitor domains (Sultan & Shi, 2018; Kawaguchi, 2019; Bassett & Wallace, 2012). Within other neural tissues, such as the ventral spinal cord and brainstem, postmitotic neurons do not form distinctive anatomically layered structures, but instead are organized into clustered and/or mosaic arrangements across multiple anatomical axes. The role of neurogenesis timing in ordering such complex neuronal diversity from common progenitor domains remains largely unknown.

Interneurons (INs) within the spinal cord form highly heterogeneous circuits, which are crucial for varied sensorimotor functions (Deska-Gauthier & Zhang, 2019; Kiehn, 2016; Goulding, 2009). Spinal IN diversity emerges during early embryonic development with the establishment of spatially and molecularly discrete progenitor domains along the dorsoventral axis (Jessell, 2000). As progenitor cells become post-mitotic, they express distinct transcription factors, display unique axon projection profiles, and migrate to final mediolateral and dorsoventral locations within specific spinal lamina. Recent work, however, has revealed vast IN subpopulation diversity within cardinal classes born from the same progenitor domains (Bikoff et al., 2016; Hayashi et al., 2018; Gosgnach et al., 2017). Interestingly, it was suggested that

some of these IN subpopulations are generated at specific embryonic timepoints. For example, Renshaw cells are the earliest born neurons among all V1 INs (Benito-Gonzalez & Alvarez, 2012; Stam et al., 2012). Yet, the full extent that temporal factors play in ordering IN diversity between lineage-related subpopulations remains obscure. In addition, to what extent neurogenesis timing can influence early postmitotic transcription factor functions, and thus, subpopulation fate specifications, remains unclear.

V3 INs are a major cardinal class of spinal INs. V3 INs are glutamatergic, display predominately commissural axon projections, and are necessary for robust locomotor output (Zhang et al., 2008). V3 INs emerge from the most-ventral, Nkx2.2^{+} p3 progenitor domain, as marked by postmitotic expression of the Sim1 transcription factor. During early embryonic stages, post-mitotic V3 INs form divergent migratory streams and begin to express diverse transcription factor combinations (Francius et al., 2013). By postnatal stages, clusters of V3 INs assemble from ventral to deep dorsal horn laminae. These spatially separate V3 IN subpopulations are also morphologically, and electrophysiologically heterogeneous (Borowska et al., 2013, 2015). Interestingly, the Sim1 transcription factor – although expressed in all V3 INs – exclusively regulates the laminar clustering of dorsal and intermediate V3 IN subpopulations (Blacklaws et al., 2015). However, the factors influencing Sim1's subpopulation specific functions until now have remained unknown.

In the current study, we have begun to address the developmental logic guiding divergent V3 IN differentiation through investigating the role of p3-V3 neurogenesis timing. First, we investigated the neurogenesis timing of anatomically distinct V3 IN subsets. Second, we investigated the functional capacity of the Sim1 transcription factor in promoting V3 IN

diversity across distinct neurogenesis times. Anatomically discrete V3 INs were temporally organized into either early- or late-neurogenesis waves. Early-born (E9.5-E10.5) V3 INs were a mixture of ascending and descending commissural INs, which formed discrete clusters distributed in specific laminae of both ventral and deep dorsal horns. Late-born (E11.5-E12.5) V3 INs were mostly descending commissural INs, which predominately clustered within ventral laminae. Further, the Sim1 transcription factor exclusively regulated the dorsal clustering and electrophysiological diversification of early-born, but not late-born V3 INs. Thus, our work indicates that the temporal control of V3 neurogenesis may have a dynamic interaction with Sim1's postmitotic function. As a result, Sim1 promotes the physiological and anatomical diversification of distinctly early-born V3 INs.

3. Results

3.1 Anatomically distinct V3 IN subpopulations display distinct temporal neurogenesis patterns

3.1.1 Neurogenesis timing orders postmitotic V3 INs into spatially and temporally distinct migratory streams

As Nkx2.2^{+} p3 progenitor cells exit their final division cycle, they express the Sim1 transcription factor defining them as postmitotic V3 INs (Zhang et al., 2008, Figure3.1A). Sim1^{+} V3 INs, indicated by the expression of tdTomato in the lumbar spinal cord of Sim1^{Cre};Rosa.lsl.tdTom mice, continue to express Nkx2.2 at E10.5 (~ 100%, n=1 animal, Figure3.1Ai), E11.5 (99% V3, n=4 animals, data not shown, Figure3.1Aii) and E12.5 (95% V3, n=4 animals), Figure3.1Aiii). During E10.5 and E11.5, V3 INs move laterally from the midline; however, by E12.5, V3 INs begin to form distinct dorsolateral and ventrolateral migratory streams moving V3 IN subsets away from ventromedial spinal laminae (Figure3.1B).

To determine whether neurogenesis timing orders postmitotic V3 INs into early embryonic migratory streams, we pulsed pregnant mice with EdU at E9.5, E10.5, E11.5, or E12.5, respectively. We then mapped the neurogenesis timing of V3 INs by combining EdU detection with Nkx2.2 immunolabeling in E12.5 lumbar spinal segments (Figure3.1Ci-iv). Interestingly, at E12.5, both dorsolateral and ventrolateral V3 IN migratory streams were exclusively composed of early-born V3 INs (those pulsed at E9.5 [Figure3.1D, n=3 animals] and E10.5 [Figure3.1E, n=3 animals]). Neither V3 INs pulsed at E11.5 (Figure3.1F, n=3 animals) nor E12.5 (Figure3.1G, n=3 animals) entered the migratory streams at E12.5.

While early-born V3 INs exclusively formed embryonic migratory streams at E12.5, it remained possible for late-born V3 INs to also form postmitotic migratory streams, but at later embryonic timepoints. To examine this possibility, we repeated EdU pulsing at E9.5, E10.5, E11.5, or E12.5, and quantified EdU^+ V3 INs in E14.5 $Sim1^{Cre}$;Rosa.lsl.tdTom spinal cords (Figure3.1I). By E14.5, early-born (E9.5&E10.5, n=3 animals for each EdU pulse time) V3 INs distributed away from the p3 progenitor domain in both dorsal and lateral directions (Figure3.1Iii,iv). Interestingly, late-born E11.5 EdU^+ V3 INs also displayed assemblies away from the p3 rogenitor domain (n=3 animals), dominantly restricted in a lateral direction (Figure3.1Iiii,iv). Late-born E12.5 EdU^+ V3 (n=3 animals), however, displayed almost no sign of migration and predominately clustered in the ventromedial spinal cord (Figure3.1Iiii,iv).

Taken together, neurogenesis timing ordered V3 INs into temporally and spatially distinct postmitotic migratory streams. Between E11.5-E12.5, early-born (E9.5&E10.5) V3 INs formed dorsolateral and ventrolateral migratory streams. Subsequently, between E13.5-E14.5, late-born (E11.5) V3 INs formed predominately a ventrolateral migratory stream, while E12.5 EdU^+ V3 INs did not display substantial migration away from the p3 progenitor.

3.1.2 Dorsoventral V3 IN clusters display distinct neurogenesis windows in the postnatal high lumbar spinal cord

Our previous studies (Blacklaws et al., 2015), and current work, have shown that subsets of V3 INs cluster across dorsoventral and mediolateral axes in low thoracic and high lumbar (L1-3) spinal cords, postnatally (Figure3.2A). These laminarly discrete dorsal and ventral V3 IN clusters

display distinct axon projection profiles, intrinsic membrane properties, and dendritic morphologies (Blacklaws et al., 2015; Borowska et al., 2013, 2015). Thus, we next asked whether neurogenesis timing underlies V3 postnatal heterogeneity. To begin, we assayed the neurogenetic timing of V3 laminar clusters in P0 high lumbar (L1-L3) spinal cords via pre-emptive EdU pulsing (Figure3.2Bi-iv). We then plotted EdU^+ V3 INs across spinal laminae (Figure3.2Ci-Gi) and quantified their distributions across dorsoventral and mediolateral spinal axes (Figure3.2Cii-Gii, n=4 animals for each EdU pulse time).

Dorsal and intermediate V3 INs displayed a restricted neurogenesis window consisting mostly of early-born (E9.5-E10.5) neurogenesis times (Figure3.2C,D). These results are in accordance with early embryonic V3 dorsolateral and ventrolateral migratory streams being comprised of early-born V3 INs (Figure3.1). In contrast to dorsal and intermediate V3 IN clusters, ventral V3 INs displayed a wide neurogenesis window spanning E9.5 to E12.5 (Figure3.2C-G). However, while E9.5 to E11.5 EdU^+ V3 INs spanned mediolateral locations within the ventral V3 IN cluster (Figure3.2Ciii-Eiii), E12.5 EdU^+ V3 INs localized almost exclusively within ventromedial locations (Figure3.2Fiii). Thus, while dorsal and intermediate high lumbar V3 INs displayed a narrow neurogenesis window, mostly between E9.5-E10.5, ventral V3 INs display a wide neurogenesis window ranging between E9.5 to E12.5.

3.1.3 Commissural descending and ascending V3 INs display distinct neurogenesis windows

Previously, we showed that dorsal and intermediate V3 INs project almost exclusively ascending axons while ventral V3 INs display a mixture of both ascending and descending axon projections

(Blacklaws et al., 2015). To identify the axon projection profiles and neurogenesis times of V3 INs, we used retrograde biotin-conjugated dextran amine (BDA) tracing of $Sim1^{Cre}$;Rosa.lsl.tdTom P0 spinal cords that were pre-emptively pulsed with EdU at respective E9.5, E10.5, E11.5, or E12.5 timepoints (Figure3.3Ai,ii). BDA^+ V3 INs were then grouped as either V3 ascending or descending commissural INs (CINs) depending if they were labeled caudal or rostral to the BDA injection site, respectively.

Both ascending and descending V3 CINs spanning dorsoventral spinal laminae were labeled with E9.5 and E10.5 EdU pulsing (Figure3.3Bi,ii). However, at these early neurogenesis time points, ascending V3 INs had a higher portion of their total cell numbers labeled relative to the descending V3 INs (Figure3.3Biv, n=3 animals for each EdU time point). In contrast, E11.5 EdU^+ V3 INs were almost exclusively descending CINs (Figure3.3Biii,iv, n=3 animals for each EdU time point). Interestingly, E12.5 EdU^+ V3 INs displayed a complete absence of both ascending and descending axon projections at P0 (data not shown). We reasoned that E12.5 EdU^+ V3 INs may not project to adjacent segments, but rather project within restricted local segments. To test this, we inserted BDA just lateral to the ventral commissure on one half of the spinal cord and analyzed cells directly contralateral to the injection site. Indeed, the E12.5 EdU^+ V3 INs/BDA^+ remained restricted to the local segment, thus identifying these late dividing V3 INs as locally-projecting V3 CINs (Figure3.3C).

Taken together, in the higher lumbar spinal cord a major wave of V3 neurogenesis occurs between E9.5-E10.5. These early-born V3 INs diversify into heterogeneous clusters across dorsoventral and mediolateral spinal axes, comprised mostly of V3 ascending and some V3 descending CINs. Subsequently, two other distinct V3 IN subsets born at E11.5 and E12.5, are

generated. Those V3 INs born at E11.5, define a group of ventral localized V3 descending CINs, while those V3 INs born at E12.5 define a ventromedial population, that contain local segmental projections (Figure3.3E). Thus, V3 neurogenesis timing correlates with V3's postnatal anatomical heterogeneity. Furthermore, this temporal neurogenesis order of V3 IN diversity appears to be p3 lineage specific, as the total number of ascending and descending CINs were equivalent across E9.5-E12.5 neurogenesis times (Figure3.3Di-v, n=3 animals for each EdU pulse time).

3.2 Post-mitotic Sim1 expression specifically promotes the anatomical and physiological diversification of early-born V3 INs.

3.2.1 Sim1 expression is essential for the laminar clustering of early-born, but not late-born, V3 INs

We have previously shown that Sim1 is necessary for V3 dorsal and intermediate, but not ventral, clustering, exclusively within low thoracic and high lumbar spinal segments (Blacklaws et al., 2015). As such, the differential neurogenesis timing of V3 IN subsets along dorsoventral spinal axes prompted us to further investigate whether Sim1 differentially regulates the formation of temporally ordered V3 IN subsets.

We first examined whether Sim1 regulates V3 cell cycle exit as distinct V3 INs are undergoing neurogenesis. We compared V3 IN neurogenesis profiles in Sim1 control and knockout (KO) mice via embryonic EdU pulsing. We then analyzed their distributions at E12.5, similar to previously described. Sim1 KO V3 INs displayed uniform cell cycle exit relative to wild-type cells

across all stages examined (E9.5-E12.5) (Figure3.4A,B, n=4 animals for each EdU pulse time). Next, we analyzed their laminar distributions at P0 (n=4 animals for each EdU pulse time). In Sim1 KOs, early-born V3 INs (E9.5-E10.5) displayed disorganized laminar distributions across the dorsoventral axis (Figure3.4Ci,ii,Dii), while late-born V3 INs (E11.5-E12.5) maintained organized laminar distributions (Figure3.4Ciii,iv,Diii). Taken together, Sim1 did not affect V3 IN cell cycle exit. However, Sim1's postmitotic expression drives the dorsoventral migration and laminar clustering of exclusively early-born (E9.5-E10.5) but not late-born (E11.5-E12.5) V3 INs by P0. These results indicate Sim1 may promote dorsal and intermediate laminar clustering within a confined pool of early-born V3 INs.

3.2.2 Sim1 expression is essential for the electrophysiological diversification of V3 IN subpopulations across the dorsoventral axis

In addition to their spatial partition, by P0, dorsal and ventral V3 IN clusters display distinct electrophysiological properties in the high lumbar (L1-L3) spinal cord (Borowska et al., 2013, 2015). As early-born V3 dorsoventral clustering is perturbed in Sim1 KO animals, we examined whether Sim1 is also necessary for the physiological separation of dorsoventral V3 INs at P0.

To assess electrophysiological properties, we conducted whole-cell patch clamp recordings of V3 INs in slices from Sim1 wild-type and Sim1 KO spinal cords at P0 (Figure3.5A). In our previous study, we generated a computational model that used 4 electrophysiological properties (the slope of frequency-current plot (F-I slope), membrane capacitance (Cm), sag voltage amplitude, and first-spike frequency) to calculate the principle component 1 (PC1) score

for each V3 IN. We demonstratethat respective PC1 scores could be used to separate V3 INs into dorsal or ventral subpopulations at different ages (Borowska et al., 2015, 2013), which was also observed in the P0 wildtype V3 INs in our current study (Figure3.5D). However, in Sim1 KO V3 INs, PC1 scores were no longer significantly difference between $V3_v$, (1.12±0.82, n=23) and $V3_d$, (1.00±0.69, n=17; ns, P-value > 0.05, Figure3.5E). Further assessment of the individual attributes used in the model revealed that all four attributes (F-I slope, Cm, sag voltage amplitude, first-spike frequency) were significantly different between $V3_d$ and $V3_v$ INs in Sim1 wild-type cords (Figure3.6Bi-iv), while in Sim1 KO mice, neither 1st spike frequency (Figure3.6Ci) nor sag amplitude (Figure3.5Cii) were statistically significant between ventral and dorsal V3 INs. Thus, Sim1 is required for both the correct laminar clustering and electrophysiological diversification of early-born dorsal V3 INs in the high lumbar (L1-L3) spinal cord.

4. Discussion

In the current study, we have systematically investigated the neurogenesis patterns of spinal V3 INs uncovering significant temporal components contributing to the spatial, anatomical and physiological diversification of V3 INs. Our data have revealed that early-born V3 INs (E9.5-E10.5) cluster across dorsoventral spinal laminae displaying both ascending and descending commissural axon projections within low thoracic and high lumbar segments (Figure3.6Ai). In contrast, late-born V3 INs (E11.5-E12.5) cluster almost exclusively within ventral spinal laminae displaying descending and local commissural axon projections (Figure3.6Aii). Furthermore, we uncovered that the V3-defining Sim1 transcription factor, although expressed in all V3 INs, exclusively regulated the anatomical and electrophysiological clustering of early-born dorsal V3 INs (Figure3.6B). This latter result indicates that sequentially generated V3 INs may regulate their terminal subpopulation characteristics through temporally-restricted post-mitotic differentiation pathways. Thus, we propose that the timing of neurogenesis serves as a crucial developmental strategy in ordering V3 subpopulation fates across the dorsoventral spinal axis.

4.1 V3 Neurogenesis timing and postnatal subpopulation diversification

During early embryonic development, gradient morphogen expression profiles along the neural tube determine the spatial motif of progenitor domains that generate diverse populations of spinal interneurons (Jessell, 2000; Goulding, 2009). However, this spatial arrangement is not able to account for the extensive subpopulations that have recently been discovered within respective cardinal spinal interneuron classes. Temporal regulation of spinal IN neurogenesis

has been shown to play crucial roles in the formation of dorsal Lbx1^{+} INs (John et al., 2005), V0 INs (Satou et al., 2012), V1 Renshaw cells (Benito-Gonzalez & Alvarez, 2012; Stam et al., 2012) and most recently Gata2/3^{+} cerebrospinal fluid-contacting neurons (CSF-cNs) (Petracca et al., 2016) and V2a INs (Hayashi et al., 2018). In our current work, by systematically tracing V3 IN neurogenesis, we further demonstrate the contribution of temporal factors in the formation of highly diversified spinal IN subpopulations.

In mice, V3 INs are generated from the most ventral progenitor domain, p3, between E9.5 and E12.5. Although, currently no molecular factors have been fully characterized to define V3 subpopulations, previous studies from us and others have demonstrated high heterogeneity of V3 INs. Here, we further revealed that anatomically and physiologically distinct V3 IN subpopulations displayed distinct temporal neurogenesis patterns. By mapping all the V3 INs generated between E9.5-12.5, we found that early-born V3 INs (E9.5-E10.5) formed early embryonic (E12.5) migratory streams and, by P0, clustered across separate laminar locations. Late-born V3 INs (E11.5-E12.5) remained close to their originated position, the ventral and medioventral region of the spinal cord (particularly those born at E12.5). Early-born V3 INs travel further away from their progenitor region, a trait shared by other spinal INs. Renshaw cells, which are one of the earliest born V1 IN subpopulations, migrate to the furthest edge of the ventral horn, while most other V1 INs distribute across Lamina VII (Gonzalez & Alvarez, 2012). In the case of a late-born population (>E14.5), Gata2/3^{+} CSF-cNs neurons were only found around the central canal (Petracca et al., 2016). Such a migration trend may be different from what was found for motor neurons, which is more similar to cortical differentiation, where late-born motor neurons migrate through early-born motor neurons in an inside-out order (Dewitz et al., 2018). The

mechanisms that direct the migrations of spinal INs are not well known. Nonetheless, our results indicate that the timing of neurogenesis is crucial for the spatial distribution of spinal INs to reach the correct positions in forming diverse neural circuits.

Another interesting finding from our study is that in addition to their diverse laminar locations, early-born V3 INs (E9.5-E10.5) display mixed commissural ascending or descending axon projections. Though, our current results cannot rule out that small amount of early-born V3 INs are bifurcating (Nissen et al., 2005). In contrast, late-born V3 INs have much more restricted projection profiles. V3 INs born at E11.5 almost exclusively projected descending commissural axons and those born at E12.5 projected exclusively local commissural axons. Few studies have systematically investigated differential projection profiles within individual spinal INs populations. In our study, it appears such time-dependent acquisition of projection profiles might be V3 IN specific, since the total spinal INs did not share this trend. This suggests a possible V3 lineage specific temporal development strategy.

The results described above also indicate that, in comparison to late-born V3 INs, early-born V3 INs displayed more diverse topological distributions, anatomical characteristics and electrophysiological properties, leading to more potential subpopulations (Figure3.6Bi, Ci). Such progressive restriction of post-mitotic IN fates from a common progenitor domain has recently been demonstrated in the cerebral cortex. Sultan et al. (2018) revealed that successive divisions of radial glial progenitors generates distinct groups of inhibitory INs. Interestingly, they also showed that post-mitotic INs could be generally categorized into either early- or late-born IN groups, where the physiologically and morphologically distinct, chandelier cells, were exclusively born at later time points. The unique neurogenesis timing of the small and distinct

chandelier cell population raises the possibility that neurogenesis timing could be playing even more of a role in ordering the differentiation of distinct subpopulations within the spinal V3 cardinal class. In addition to the anatomical and physiological criteria we have used to separate V3 subpopulations here, it is possible that further molecularly and/or activity-dependent V3 subpopulations emerge during distinct neurogenesis times. Thus, in order to further uncover the full extent of neurogenesis timing and V3 diversity it will be necessary to more precisely uncover molecularly and functionally distinct V3 IN subpopulations in the future. Taken together, our results support the idea that differential waves of neurogenesis serve as a developmental strategy to guide diversification of unique IN subpopulations across anatomical spinal axes.

4.2 Sim1 differentially promotes the diversification of early-born V3 INs

As progenitor cells exit from the cell cycle, they are exposed to various intrinsic and extrinsic factors promoting their terminal fate specifications. For example, Stam et al. (2012) showed that the expression of Onecut1 and Onecut2 transcription factors during the first wave of V1 IN neurogenesis is a key step in the Renshaw Cell differentiation program. In addition, the development of Renshaw Cells is also dependent on the presence of the forkhead transcription factor Foxd3. The molecular mechanisms that regulate the temporal differentiation of V3 IN subpopulations are still not clear. However, we found that Sim1 differentially promotes the specification of certain characteristics of V3 IN subpopulations confined within distinct windows of neurogenesis.

Our previous work showed that the loss of Sim1 expression did not change the identity of V3 INs, but was crucial for proper V3 IN migration and axon projections (Blacklaws et al., 2015). Interestingly, here we further demonstrated that Sim1 regulates the anatomical and physiological specification of early-born (E9.5-E10.5) but not late-born (E11.5-E12.5) V3 INs. This result strongly indicates that the timing of the neurogenesis enables V3 INs to engage in different and specific post-mitotic molecular programs. At least one of these molecular programs may involve Sim1, which plays different functional roles across distinct neurogenesis times**.** We would also like to emphasize that even though Sim1 may not regulate the clustering and electrophysiological diversification of late-born V3 INs, it may play potentially other functional roles in those subpopulations. Nevertheless, our current data indicate that V3 INs inherit unique transcription factor expression profiles depending on their neurogenesis time, as has been shown in the retina (Clark et al., 2019) and cerebral cortex (Mayer et al., 2018; Zhong et al., 2018). Indeed, Delile et al. (2019) recently took advantage of single cell mRNA sequencing across early embryonic spinal stages revealing temporally distinct gene expression dynamics across p3-V3 neurogenesis. This may modulate the differential regulatory control of Sim1 between sequentially generated V3 IN subpopulations. Furthermore, studies from supraspinal regions have revealed that Sim1 forms distinct heterodimer complexes and plays unique developmental roles in different CNS tissues (Michaud et al., 1998; Caqueret et al., 2005; Marion et al., 2005; Xu & Fan, 2007; Osterberg et al., 2011; Schweitzer et al., 2013; Blacklaws et al., 2015). Sim1 expression levels may also differ amongst distinct subpopulations, as has recently been demonstrated for Chx10 expression in anatomically distinct V2a IN subpopulations (Hayashi et al., 2018). Lastly, variations in Sim1/DNA binding in V3 IN

subpopulations could modulate Sim1 transcriptional activity (Deplancke et al., 2016). It will be important going forward to uncover how the temporal components of V3 neurogenesis interact with post-miotic Sim1 expression to diversify V3 IN subpopulations across the anatomical axes of the spinal cord.

Taken together, through investigation of the p3-V3 spinal IN lineage, we have uncovered a significant temporal component to V3's post-mitotic anatomical and physiological diversification. With progressive divisions of p3 progenitor cells, post-mitotic V3 INs become increasingly fate-restricted to ventral laminae, descending and local commissural axon projections, and uniform membrane properties. Furthermore, we suggest this could in part be due to the temporal restriction of Sim1's post-mitotic function to early-born V3 INs. Thus, in addition to layered supraspinal tissues, our current work indicates neurogenesis timing as a developmental mechanism underlying the post-mitotic assembly of non-layered neural circuits in the spinal cord.

5. Materials and Methods

Mouse strains

$Sim1^{Cre}$ mice (Zhang et al, 2008; Goulding Lab, Salk Institute) were crossed with TdTomato (TdTom) Ai14 conditional reporter mice (Jackson Laboratory) to generate $Sim1^{Cre}$;Rosa.lsl.tdTom mice (Zhang et al., 2008; Blacklaws et al., 2015). These mice were used for fate mapping $Sim1^{+}$ V3 interneurons through embryonic and postnatal stages. Sim1 knock-out (KO) mice were generated by crossing $Sim1^{Cre}$;Rosa.lsl.tdTom mice with $Sim1^{taulacz}$ mice (Goulding Lab, Salk Institute) to produce $Sim1^{Cre/taulacz}$;Rosa.lsl.tdTom mice (Blacklaws et al., 2015). All procedures were performed in accordance with the Canadian Council on Animal Care and approved by the University Committee on Laboratory Animals at Dalhousie University.

Spinal cord tissue dissection, processing and sectioning

Spinal cords were obtained at embryonic (E11.5, E12.5, E14.5) and postnatal (P0) stages. For embryonic ages the date of fertilization were identified by the presence of a vaginal plug. The morning of vaginal plug discovery was defined as embryonic day 0.5 (E0.5). Prior to embryonic dissection, pregnant mothers were anaesthetized via intraperitoneal injections of a ketamine (60mg/kg) and xylazine (12mg/kg) cocktail. Once a mouse no longer responded to the pedal reflex it was decapitated and its embryos removed via cesarean section. Embryonic and postnatal mice were euthanized via decapitation and spinal cords were subsequently dissected in oxygenated Ringer's Solution (111mM NaCl, 3.08 mM KCl, 11mM glucose, 25 mM NaHCO3, 1.25 mM MgSO4, 2.52 mM CaCl2, 1.18 mM KH2PO4, pH 7.4). Spinal cords were fixed with 4% paraformaldehyde (Electron Microscopy Sciences) [PFA] in phosphate-buffered saline (PBS) at 4

degrees Celsius for varying times (E11.5 for 20mins; E12.5 for 25mins; E14.5 for 35mins; P0 for 1h). Following fixation, spinal cords were washed in PBS at 4 degrees Celsius overnight and subsequently cryoprotected in 30% sucrose in PBS at 4 degrees Celsius overnight. Cryoprotected spinal cords were embedded in O.C.T compound (Fisher Healthcare) and flash frozen at -55 degrees in a mixture of dry ice and ethanol. Frozen Lower thoracic and higher lumbar (T12-L3) spinal cord segments were sectioned transversely using a cryostat (Leica CM1950). Embryonic spinal cords were sectioned at 14 micrometers and postnatal spinal cords were sectioned at 30 micrometers onto Superfrost Plus Microscope Slides (Fisherbrand).

5-Ethynyl-2´-deoxyuridine (EdU) pulse labeling of V3 IN neurogenesis profiles

EdU (Thermo Fisher Scientific) was dissolved in saline solution to make 6mg EdU/1ml saline solution. Pregnant $Sim1^{Cre}$;Rosa.lsl.tdTom mice were injected with EdU solution (6mg/ml) according to their body weight (50µl/10g) at gestational stages E10.5, E11.5, and E12.5, respectively. Pregnant $Sim1^{Cre}$;Rosa.lsl.tdTom mice injected at E9.5 were pulsed with 12mg/ml EdU solution. EdU pulsed spinal cords were collected at E12.5, E14.5 or P0. Mice pulsed and analyzed at E12.5 were first pulsed with EdU followed by a 2h window before spinal cord dissection. Fluorescent labeling of DNA incorporated EdU was achieved using a Click-iT® EdU Alexa Fluor® 647 Imaging Kit (Thermofisher). To determine the neurogenesis profiles of anatomically distinct V3 IN subsets, fluorescent labeling of EdU was performed following immunohistochemistry and retrograde tract tracing protocols.

Retrograde tract tracing with biotin-conjugated dextran amine (BDA)

Axonal projection patterns of P0 V3 INs were determined via retrograde BDA tracing of isolated $Sim1^{Cre}$;Rosa.lsl.tdTom spinal cords. Immediately following spinal cord dissection, 3000 MW, lysine fixable, BDA (Molecular Probes) was inserted into one half of the high lumbar spinal cord roughly between L1 and L2 segments. Injected spinal cords were incubated overnight in Ringer's Solution (111mM NaCl, 3.08 mM KCl, 11mM glucose, 25 mM NaHCO3, 1.25 mM MgSO4, 2.52 mM CaCl2, 1.18 mM KH2PO4, pH 7.4) bubbled with 95%O2/5%CO2 at 20 degrees Celsius. Following incubation, spinal cords underwent aforementioned processing and sectioning protocols. These tract tracing procedures were previously described in greater detail (Glover, 1995; Nissen et al., 2005; Blacklaws et al., 2015). Fluorescent labeling of BDA was performed in concert with immunohistochemistry and Click-iT® EdU labeling of spinal cord sections. Either Alexa Fluor 405-conjugated streptavidin (Thermofisher), Alexa Fluor 488-conjugated streptavidin (Thermofisher), or Alexa Fluor 647-conjugated streptavidin (Thermofisher) was diluted at 1:500 and added to secondary antibody solutions.

Immunohistochemistry

Mounted spinal cord sections were first incubated in PBS containing 0.1% Triton X (PBS-T) for 3 consecutive washes of 5 mins each. Subsequently, spinal cord sections were incubated in 0.1% PBS solution containing primary antibodies and 10% heat-inactivated horse serum (Invitrogen) overnight at 4 degrees Celsius. Primary antibodies used were mouse anti-nkx2.2 (DSHB, cat#74.5A5, 1:100) and rabbit anti-DsRed (Clontech, cat#632496, 1:2000). Following primary AB incubation, spinal cord sections were washed with 0.1% PBST for 15 mins (3x5min fresh

solution) and subsequently incubated in 0.1% PBS solution containing secondary anti-bodies (Alexa Fluor conjugated streptavidin when relevant) and 10% heat-inactivated horse serum (Invitrogen) for 2h at 4 degrees Celsius. Secondary antibodies used were Alexa Fluor 488 donkey anti-mouse IgG (Jackson ImmunoResearch, cat#715-545-150, 1:500) and Alexa Fluor 594 donkey anti-rabbit IgG (Jackson ImmunoResearch, cat#711-585-152, 1:500). When applicable, secondary antibody incubation was followed by Click-iT® EdU Alexa Fluor® 647 fluorescent labeling (Thermofisher) and Hoechst 33342 Solution (ThermoFisher) staining. Lastly, spinal cord sections were washed in PBS for 15 mins (3x5min fresh solution) and cover-slipped with fluorescent mounting medium (Dako).

Image capture and cell position analysis

Fluorescent micrographs of spinal cord sections were captured using a Zeiss LSM 710 upright confocal microscope with ZEN 2009 Microscope and Imaging Software. Cell numbers and laminar positions were quantified using ImageJ and MATLAB. Using the ImageJ Cell Counter Plugin, x,y coordinates of individual cell bodies as well as the maximum and minimum x,y coordinates of corresponding spinal cord outlines were denoted. At E12.5, a total of three spinal cords were processed and analyzed for each EdU pulse time and genotype (E9.5, n=3 animals; E10.5, n=3 animals; E11.5, n=3 animals; E12.5, n=3 animals) for both Sim1 control and KO. At E14.5, a total of three spinal cords were processed and analyzed for each EdU pulse time (E9.5, n=3; E10.5, n=3; E11.5, n=3; E12.5, n=3). For each animal, 10 randomly chosen 14 µm transverse sections were analyzed within approximate lower thoracic and higher lumbar segments per animal. At P0, four spinal cords were processed and analyzed for each EdU pulse time (E9.5, n=4; E10.5, n=4; E11.5, n=4; E12.5, n=4) for both Sim1 control and KO. For each

animal, a total of 9 randomly chosen 30 µm transverse sections were analyzed for high lumbar (L1-L3) segments per animal. Cell body laminar distribution and cell body density contour plots were subsequently constructed utilizing *grid-data* and *contour* functions in MATLAB. Briefly, within each section cell body x,y positions were normalized against the maximum and minimum hemicord x,y coordinates. Heat maps were then constructed to display cell body density across the mediolateral and dorsoventral axes at P0.

Patch-clamp recording and intrinsic properties analysis

P0 Sim1 control and Sim1 KO mice were decapitated and their higher lumbar spinal cords (T13-L3) dissected in ice-cold oxygenated modified sucrose Ringer's solution (3.5 mM KCL, 25 mM NaHCO3, 1.2 mM KH2PO4, 1.3 mM MgSO4, 1.2 mM CaCl2, 10 mM glucose, 212.5 mM sucrose, 2 mM MgCl2, pH 7.4). Dissected cords were then sectioned into 300–350µm transverse slices using a vibratome (Leica VT1200 S). Following a >30 minute recovery period slices were transferred into a recording chamber mounted on an Olympus BX51WI microscope and perfused with Ringer's Solution (111mM NaCl, 3.08 mM KCl, 11mM glucose, 25 mM NaHCO3, 1.25 mM MgSO4, 2.52 mM CaCl2, 1.18 mM KH2PO4, pH 7.4) bubbled with 95%O2/5%CO2 at room temperature. V3 INs were identified and visualized through the expression of tdTomato fluorescent protein using a 40× water-immersion objective (numerical aperture, 0.8), with the aid of a DAGE-MTI IR-1000 CCD camera. Conventional whole-cell voltage- and current-clamp recordings were made using a MultiClamp 700B amplifier (Molecular Devices Inc., Sunnyvale, California, USA). Patch-clamp recording pipettes were filled with a recording buffer containing 128 mM K-gluconate, 4 mM NaCl, 0.0001 mM CaCl2, 10 mM HEPES, 1 mM glucose, 5 mM Mg-ATP, 0.3 mM GTP-Li. In order to facilitate mapping of recorded neurons 0.4 mg/ml lucifer yellow

dilithium salt (LY; Sigma-Aldrich) and 1 mg/ml neurobiotin (Vector Laboratories) were added to the pipette solution before recording. All electrophysiological data were obtained by Clampex 10.3 (Molecular Devices Inc.) and analyzed with Clampfit 10.3 and Spike2 5.0 (Cambridge Electronic Design) software.

Experimental Design and Statistical Analysis

To compare the temporal pattern of V3 subpopulations with different projection profiles, a total of three spinal cords were processed and analyzed for each EdU pulse time (E9.5, n=3; E10.5, n=3; E11.5, n=3). For each individual spinal cord, sections were analyzed two segments rostral (t13-L1) and two segments caudal (L2-L3) to the injection site. A total of 12 sections (20% of entire cord) were analyzed both rostral to (descending) and caudal to (ascending) the BDA injection site. The percentage of EdU^+ descending and ascending V3 INs displayed unequal variances. Thus, statistical significance between descending versus ascending V3 at each EdU pulse time were measured via Unpaired t-test with Welch's unequal variances correction on Prism Graphpad.

The comparative analysis of the laminar distribution patterns between Sim1 control and Sim1 KO mice were adopted from Laumonnerie and colleges (2015). Briefly, normalized hemicord distributions were divided into five rows and five columns producing 25 discrete bins along the dorsoventral and mediolateral axes. The total number of V3 INs within each bin were compared between Sim1 control and Sim1 KO cords. Statistical significance was measured via the non-parametric two-tailed Mann-Whitney Test on Prism Graphpad.

A model used to partition V3 INs into distinct electrophysiological categories was previously described (Borowska et al., 2013, 2015). Briefly, 4 electrophysiological attributes (x1, x2, x3, x4) = (F/I slope, membrane capacitance, sag amplitude, and 1st spike frequency), obtained from 122 P21 V3 INs, were selected from a set of 21 parameters based on their utility to categorize cells using a method based on principle component analysis (Borowska et al., 2013). It was found that the sign of the first principal component (PC1) of the 4 attributes could be used to partition INs into two categories that happened to correspond to cells in either the dorsal or ventral lobes of the spinal cross-section (corresponding to the regions above and below the central canal, respectively). The same model was used to compute PC1 for the cells analyzed in this article as follows:

PC1=0.56 ((x_1-0.48))/0.39-0.55 ((x_2-49))/23-0.39 ((x_3-37))/32-0.49 ((x_4-20))/8.8

where the vector of model coefficients (0.56, 0.55, 0.39, 0.49) is the first empirical orthogonal function of the four attributes, (0.48, 49, 37, 20) and (0.39, 23, 32, 8.8) are the means and standard deviations of the four attributes, all computed from the data used in Borowska et al., 2013. Statistical significance differences between dorsal and ventral V3 INs in Sim1 control and Sim1 KO mice were measured using the non-parametric Kruskal-Wallis Test.

6. Figures

Figure 3.1 Neurogenesis timing orders postmitotic V3 INs into spatially and temporally distinct migratory streams

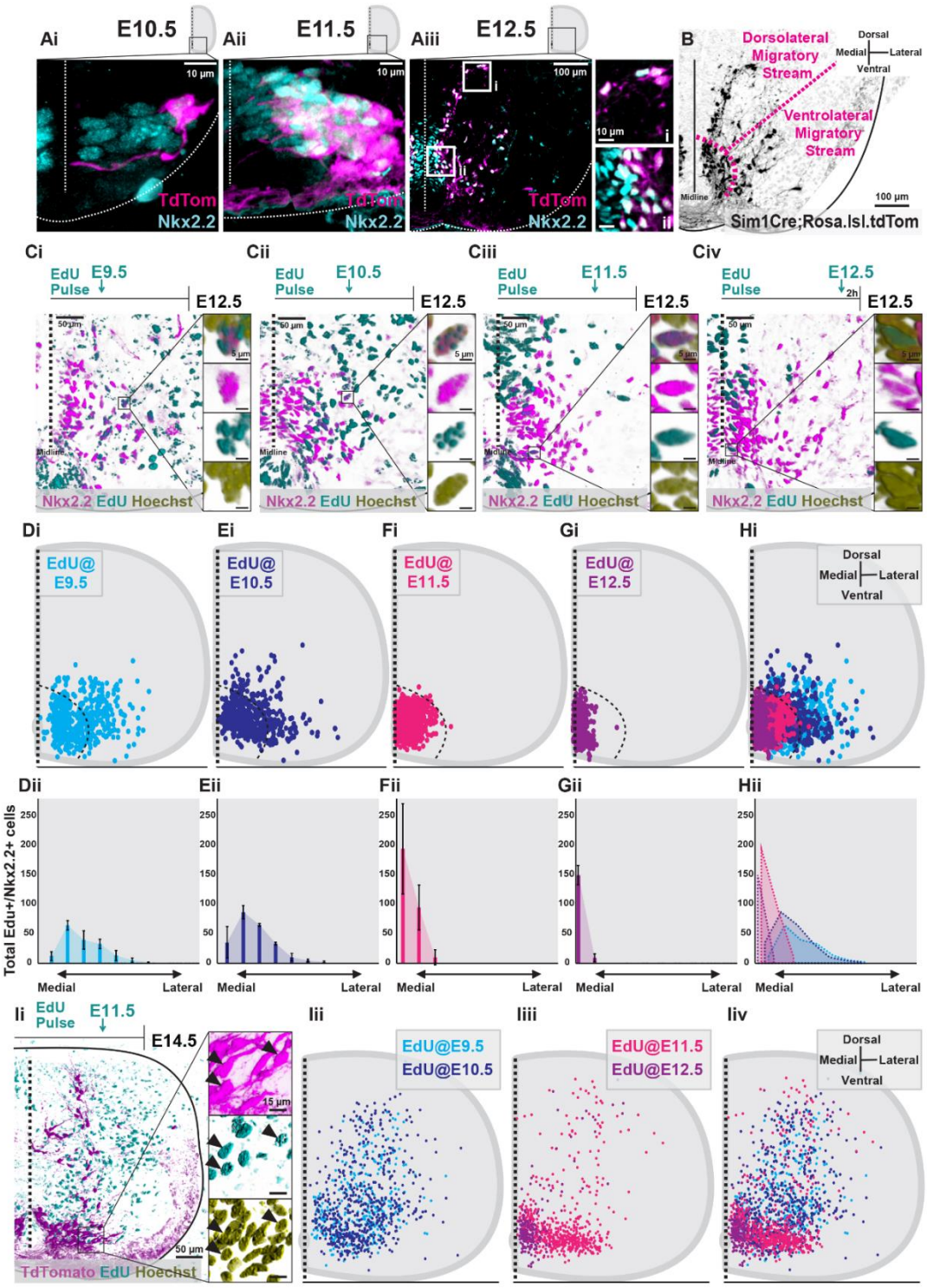

Figure 3.1 Neurogenesis timing orders postmitotic V3 INs into spatially and temporally distinct migratory streams

(A) Representative images of Nkx2.2 immunoreactivity and TdTomato+ V3 INs from $Sim1^{Cre}$;Rosa.lsl.tdTom mice at E10.5 (Ai), E11.5 (Aii) and E12.5 (Aiii) (scale bars = 100µm and 10µm). (B) Representative image of $TdTomato^{+}$ V3 INs clustered within presumed dorsolateral and ventrolateral migratory streams at E12.5 (scale bar = 100µm). (C) Representative images of EdU pulses at E9.5 (Ci), E10.5 (Cii), E11.5 (Ciii), and E12.5 (Civ) and subsequent detection EdU^{+}, $Nkx2.2^{+}$, and $Hoechst^{+}$ labeling at E12.5 (scale bars = 50µm and 5µm). (D-H) Hemicord $EdU^{+}/Nkx2.2^{+}/Hoechst^{+}$ cell position plots (i) and mediolateral cell count quantifications (ii) at E12.5 from respective E9.5 (Di,ii, n=3 animals), E10.5 (Ei,ii, n=3 animals), E11.5 (Fi,ii, n=3 animals), E12.5 (Gi,ii, n=3 animals) EdU pulse times. Combined EdU pulse times at E12.5 (Hi,ii, n=3 animals for each EdU pulse time). (I) Representative image of $EdU^{+}/TdTomato^{+}/Hoechst^{+}$ V3 INs at E14.5 pulsed with EdU at E11.5 (scale bars = 50µm and 15µm) (Ii). E14.5 hemicord $EdU^{+}/TdTomato^{+}$ cell position plots of E9.5 and E10.5 early-born V3 (Iii,iv, n=3 animals for each EdU pulse time), and E11.5 and E12.5 late-born V3 (Iiii,iv, n=3 animals for each EdU pulse time).

Figure 3.2 Dorsoventral V3 IN clusters display distinct neurogenesis windows in the postnatal high lumbar spinal cord

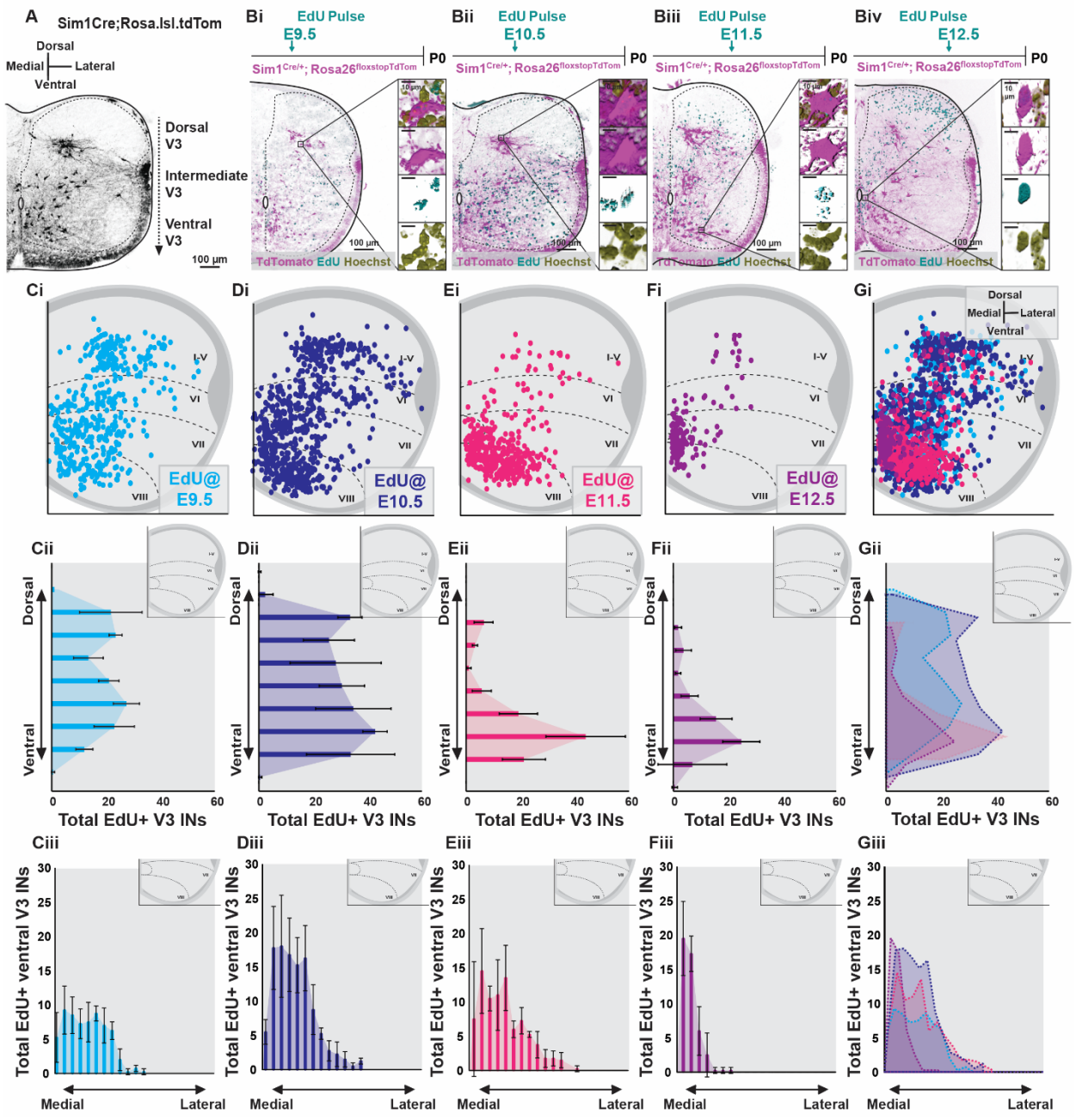

Figure 3.2 Dorsoventral V3 IN clusters display distinct neurogenesis windows in the postnatal high lumbar spinal cord

(A) Representative image of TdTomato^{+} V3 INs separated within distinct dorsal, intermediate and ventral laminar clusters in the high lumbar (L3) spinal cord of P0 Sim1^{Cre};Rosa.lsl.tdTom mice (scale bar = 100µm). (B) Representative images of EdU^{+}/TdTomato^{+}/Hoechst^{+} V3 INs at P0 pulsed at respective E9.5 (Bi), E10.5 (Bii), E11.5 (Biii) and E12.5 (Biv) times points (scale bars = 100µm and 10µm). (C-G) Hemicord EdU^{+}/TdTomato^{+} cell position plots (i), dorsoventral cell count quantifications (ii), and ventral V3 mediolateral cell count quantifications (iii) at P0 from respective E9.5 (Ci-iii, n=4 animals), E10.5 (Di-iii, n=4 animals), E11.5 (Ei-iii, n=4 animals), E12.5 (Fi-iii, n=4 animals) EdU pulse times. Combined EdU pulse times (Gi-iii, n=4 animals for each EdU pulse time)**.**

Figure 3.3 Commissural descending and ascending V3 INs display distinct neurogenesis times

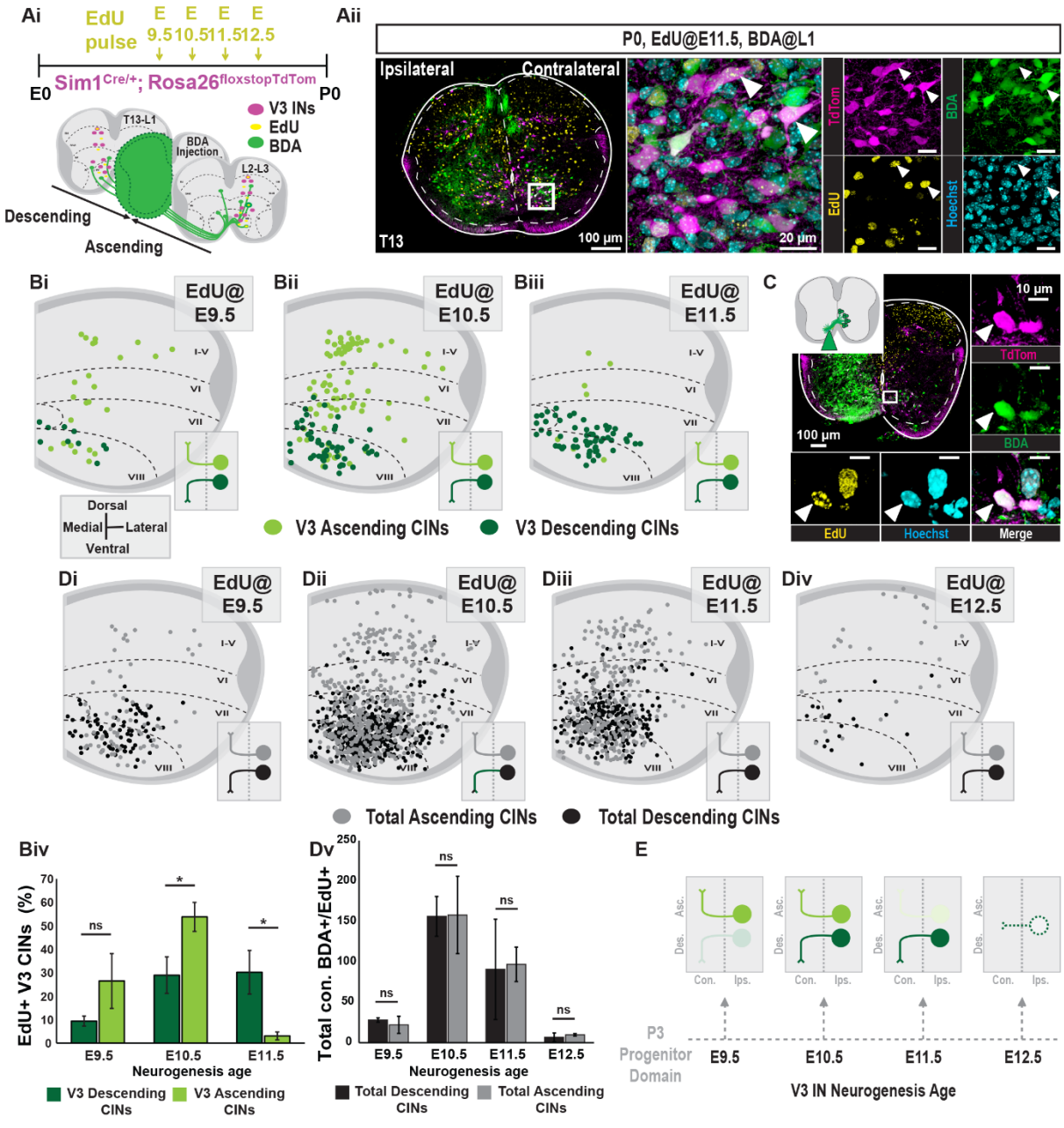

Figure 3.3 Commissural descending and ascending V3 INs display distinct neurogenesis times

(A) V3 neurogenesis profiles were determined by injecting EdU into pregnant $Sim1^{Cre}$;Rosa.lsl.tdTom mice at E9.5, E10.5, E11.5, or E12.5. To classify V3 INs as ascending or descending, hemicord BDA injections were inserted between L1-L2 spinal cord segments P0 (Ai). Representative image of EdU pulsed at E11.5 and subsequent hemicord L1 BDA injection and EdU detection of descending V3 INs in the t13 spinal cord segment at P0 (scale bars = 100µm, 20µm, 20µm) (Aii). (B) Hemicord cell position plots of BDA^+ and EdU^+ V3 INs contralateral to the BDA injection (Bi, E9.5 [n=3 animals]; Bii, E10.5 [n=3 animals]; Biii, E11.5 [n=3 animals]). Edu^+/BDA^+ V3 INs located rostral to the BDA injection site are classified as descending (dark green), and cells caudal to the site are classified as ascending (light green). Quantification of the percentage of total descending and ascending V3 CINs born at E9.5, E10.5 and E11.5 (Biv, n=3 animals for each EdU pulse time, error bars = standard deviation, *, p-value < 0.05, Unpaired t-test with Welch's correction). (C) EdU^+ V3 INs pulsed at E12.5 displayed no descending nor ascending projections. To capture locally projecting V3 CINs we adapted our tract tracing procedure by inserting BDA just lateral to the ventral commissure. Under these conditions, E12.5 EdU^+ V3 INs were labeled as local CIN V3 at P0 (scale bar = 100µm & 10µm). (D) Hemicord cell position plots of total BDA^+ and EdU^+ commissural INs (Di, E9.5 [n=3 animals]; Dii, E10.5 [n=3 animals]; Diii, E11.5 [n=3 animals]; Div, E12.5 [n=3 animals]). Edu^+/BDA^+ V3 INs located rostral to the BDA injection site are classified as descending (black), and cells caudal to the site are classified as ascending (gray). Quantification of the total number of descending and ascending CINs born at E9.5, E10.5, E11.5, and E12.5 (Dv, n=3 animals for each EdU pulse time,

error bars = standard deviation, *, p-value < 0.05, Unpaired t-test with Welch's correction). (E) Summary neurogenesis timeline of V3 IN projection profiles.

Figure 3.4 Sim1 expression is essential for the laminar clustering of early-born V3 INs

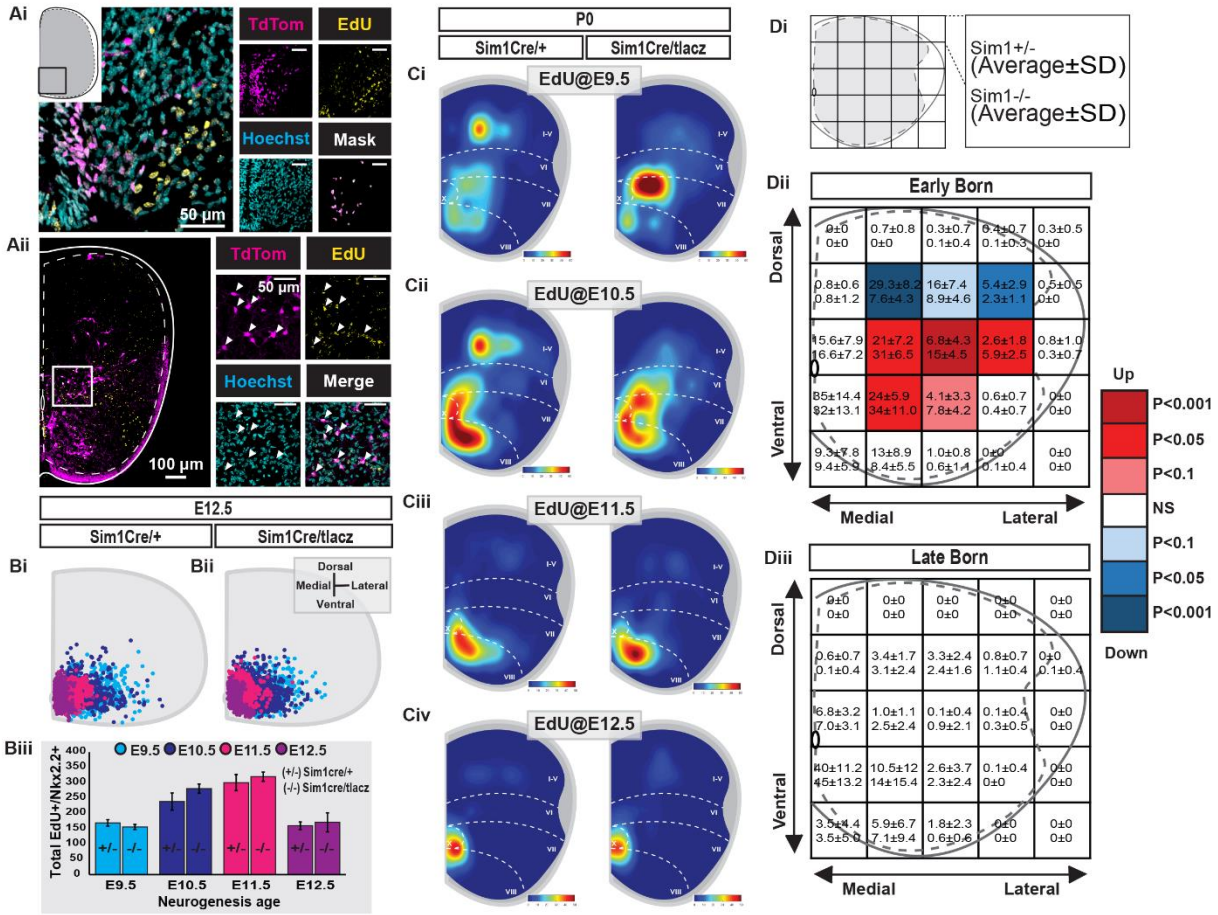

Figure 3.4 Sim1 expression is essential for the laminar clustering of early-born V3 INs

(Ai) Representative image of E9.5 pulsed EdU detection (confirmed by Hoechst staining) and Nkx2.2 immunoreactivity in E12.5 lumbar spinal section of a $Sim1^{Cre/tualacz}$ mouse (Scale bars = 50µm & 50µm). Merged image (Mask) shows colocalization masks of EdU^{+}/$Hoechst^{+}$/$nkx2.2^{+}$ cells using Imaris software. (Aii) Representative image of EdU detection (confirmed with by Hoechst staining) in V3 INs (TdTom) in a P0 high lumbar spinal section of a $Sim1^{Cre/taulacz}$;Rosa.lsl.tdTom mouse (Scale bars = 50µm & 50µm). (B) Hemicord cell position plots of EdU^{+}/$Hoechst^{+}$/$Nkx2.2^{+}$ cells in E12.5 lumbar segments of $Sim1^{Cre}$ (Bi) and $Sim1^{Cre/taulacz}$ (Bii) (n=3 animals for each pulse age and genotype). The total number of $Nkx2.2^{+}$/EdU^{+} cells from respective pulse times (E9.5, E10.5, E11.5, E12.5) from E12.5 lumbar spinal segments compared between Sim1 control ($Sim1^{Cre}$) and knockout ($Sim1^{Cre/taulacz}$) mice (Biii, n=3 animals for each pulse age and genotype, error bars = standard deviation, p-value > 0.05, Unpaired t-test with Welch's correction). (C) Hemicord cell position plots of EdU^{+}/$Hoechst^{+}$/$TdTom^{+}$ cells in P0 Higher lumbar (L1-L3) segments of $Sim1^{Cre}$;Rosa.lsl.tdTom and $Sim1^{Cre/taulacz}$;Rosa.lsl.tdTom mice pulsed at E9.5 (Ci), E10.5 (Cii), E11.5 (Ciii), and E12.5 (Civ) [n=4 animals for each EdU pulse age and genotype]. (D) EdU^{+} V3 hemicord cell position plots of P0 higher lumbar (L1-L3) spinal cord sections were pooled together as either early-born (EdU^{+}: E9.5, E10.5, n=8 animals total for each genotype) or late-born (EdU^{+}: E11.5, E12.5, n=8 animals total for each genotype) groups. 5x5 grids were superimposed over hemicord cell position plots producing 25 discrete bins with specific medial-lateral and dorsal-ventral positions. EdU^{+} V3 IN counts within corresponding bins were then compared between $Sim1^{Cre}$;Rosa.lsl.tdTom (Sim1 control) and $Sim1^{Cre/taulacz}$;Rosa.lsl.tdTom (Sim1 knockout) cords for early-born and late-born groups: (early-

born, Sim1 control (n=8 animals) vs. knockout (n=8 animals); late-born, Sim1 control (n=8 animals) vs. knockout (n=8 animals). The average count and standard deviation for Sim1 control [top of bin, average ± standard deviation)] and Sim1 knockout [bottom of bin, average ± standard deviation] cords are indicated (Di-iii). Statistical significance between Sim1 control and knockout counts of the same bin were measured with a two-tailed Mann-Whitney Test. Bins with average counts less than 1 in both control and knockout were considered non-significant. P-values are presented as a heat map with white bins indicating no change, blue bins indicating gradations of reduced numbers in Sim1 knockout, and red bins indicating gradations of increased numbers in Sim1 knockout (Dii,iii).

Figure 3.5 Sim1 expression is essential for the electrophysiological diversification of dorsal V3 IN subsets in the higher lumbar spinal cord

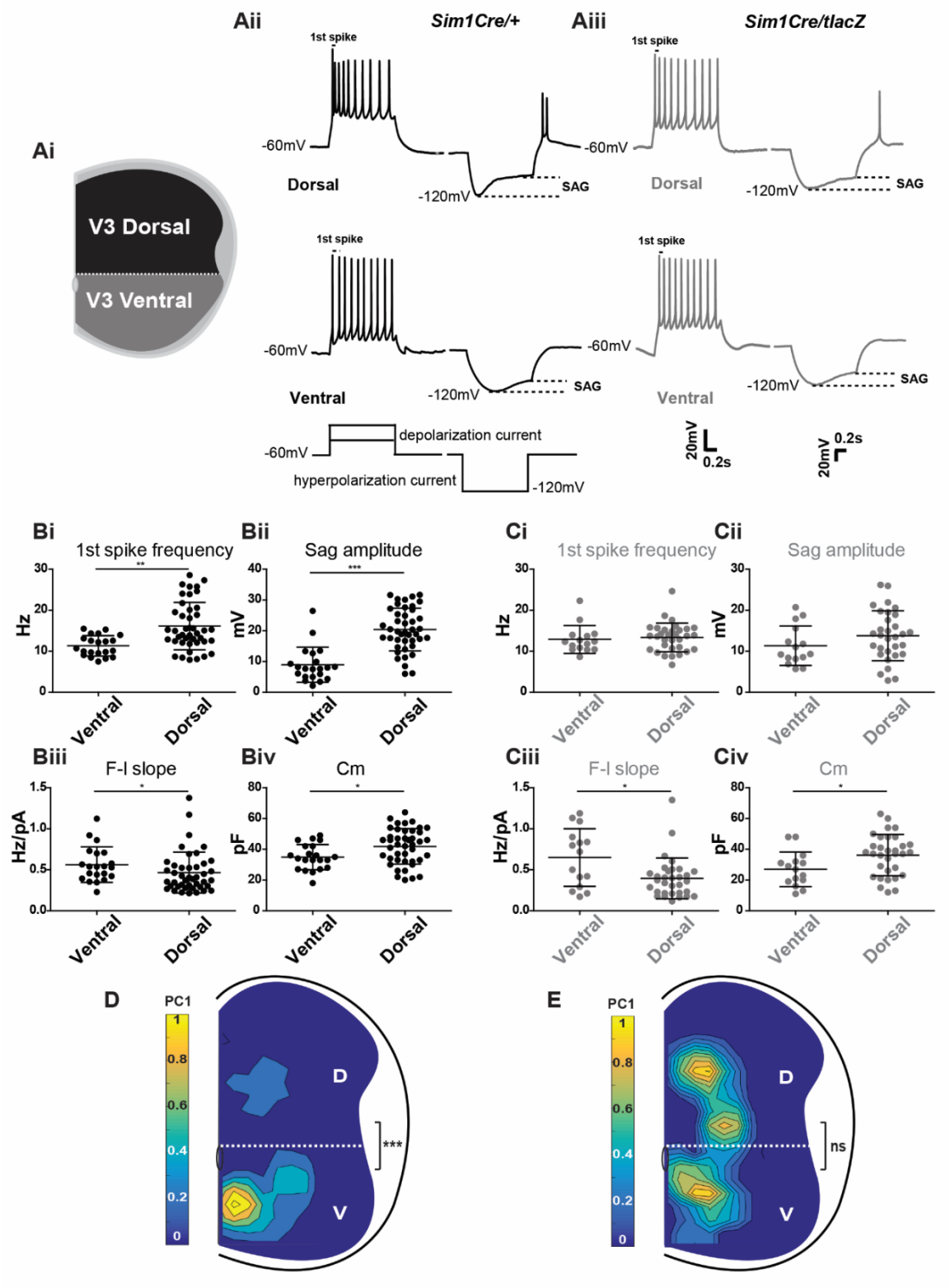

Figure 3.5 Sim1 expression is essential for the electrophysiological diversification of dorsal V3 IN subsets in the higher lumbar spinal cord.

(A) Spatial criteria for recorded V3 INs as either dorsal or ventral (Ai). Representative current-clamp traces from Sim1 control (Aii) and Sim1 Knockout (Aiii) dorsal V3 ($V3_d$) and ventral V3 ($V3_v$) INs responding to 1 s suprathreshold (left) and sub-threshold (right) 40 pA current injections. First spike frequencies and sag voltages are indicated on traces. (B,C) 1^{st} spike frequency (Bi,Ci), Sag amplitude (Bii,Cii), F-I slope (Biii,Ciii), and membrane capacitance (Cm) [Biv,Civ] comparisons between ventral ($V3_v$) and dorsal ($V3_d$) V3 INs in Sim1 control (B) and knockout mice (C) [each point represents an individual cell, error bars = standard deviation, *, p-value < 0.05, **, p-value < 0.01, ***, p-value < 0.001, two-tailed Mann-Whitney Test]. (D,E) Contour plots of V3 IN PC1 scores across the mediolateral and dorsoventral axis of higher lumbar (L1-L3) P0 Sim1 control (D) and Sim1 knockout (E) spinal cords. Colour bars indicate PC1 score from high (yellow) to low (blue). Dashed line indicates separation of $V3_d$ and $V3_v$ INs above and below the central canal, respectively. Statistical significance between PC1 scores of dorsal and ventral V3 INs in Sim1 control and KO mice was determined using the Kruskal-Wallis Test (D, Sim1 control $V3_d$, n=25, $V3_v$, n=33, ***, p-value < 0.001; E, Sim1 Knockout $V3_d$, n=23, $V3_v$, n=17; ns, p-value > 0.05).

Figure 3.6 The temporal neurogenesis ordering of post-mitotic V3 IN diversity

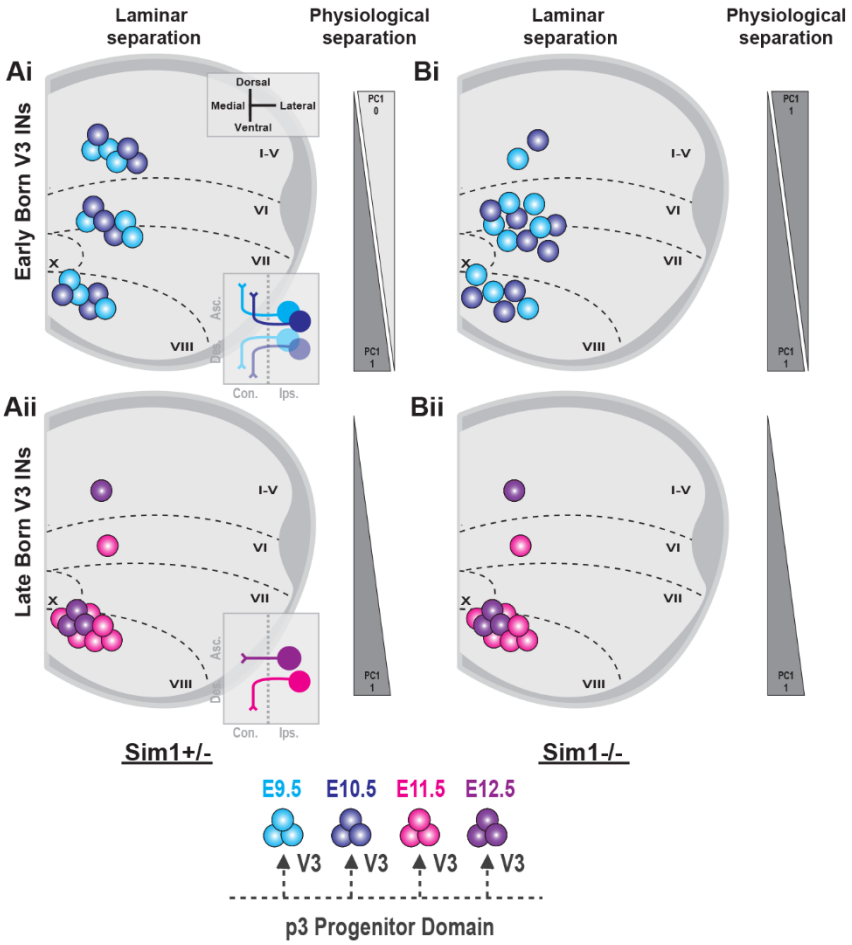

Figure 3.6 The temporal neurogenesis ordering of post-mitotic V3 IN diversity

Postnatal V3 INs display distinct temporal neurogenesis patterns across dorsoventral and mediolateral low thoracic (t12-t13) and high lumbar (L1-L3) spinal segments. Early-born (E9.5-E10.5) V3 INs assemble within ventral, intermediate, and dorsal V3 IN laminar clusters and display both ascending and descending commissural axon projections (Ai). In contrast, late-born V3 INs (E11.5-E12.5) are fate restricted to ventral laminar clusters and descending or local commissural axon projections profiles (Aii). In Sim1 knockout spinal cords, early-born V3 INs no longer form significant dorsoventral laminar clustering nor electrophysiological diversification (Bi), while late-born V3 INs display unchanged ventral clustering and electrophysiological properties (Bii).

7. References

Bassett, E., & Wallace, V. (2012). Cell fate determination in the vertebrate retina. *Trends in Neurosciences (Regular Ed.), 35*(9), 565-573. doi:10.1016/j.tins.2012.05.004

Benito-Gonzalez, A., & Alvarez, F. (2012). Renshaw cells and ia inhibitory interneurons are generated at different times from p1 progenitors and differentiate shortly after exiting the cell cycle. *The Journal of Neuroscience, 32*(4), 1156-1170. doi:10.1523/JNEUROSCI.3630-12.2012

Bikoff, J., Gabitto, M., Rivard, A., Drobac, E., Machado, T., Miri, A., . . . Jessell, T. (2016). Spinal inhibitory interneuron diversity delineates variant motor microcircuits. *Cell, 165*(1), 207-219. doi:10.1016/j.cell.2016.01.027

Blacklaws, J., Deska Gauthier, D., Jones, C., Petracca, Y., Liu, M., Zhang, H., . . . Zhang, Y. (2015). Sim1 is required for the migration and axonal projections of V3 interneurons in the developing mouse spinal cord. Developmental Neurobiology, 75(9), 1003-1017. doi:10.1002/dneu.22266

Borowska, J., Jones, C. T., Deska Gauthier, D., & Zhang, Y. (2015). V3 interneuron subpopulations in the mouse spinal cord undergo distinctive postnatal maturation processes. Neuroscience, 295, 221-228. doi:10.1016/j.neuroscience.2015.03.024

Borowska, J., Jones, C., Zhang, H., Blacklaws, J., Goulding, M., & Zhang, Y. (2013). Functional subpopulations of V3 interneurons in the mature mouse spinal cord. The Journal of Neuroscience, 33(47), 18553-18565. doi:10.1523/JNEUROSCI.2005-13.2013

Caqueret, A., Coumailleau, P., & Michaud, J. (2005). Regionalization of the anterior hypothalamus in the chick embryo. *Developmental Dynamics, 233*(2), 652-658. doi:10.1002/dvdy.20372

Clark, B., Stein O'Brien, G., Shiau, F., Cannon, G., Davis Marcisak, E., Sherman, T., . . . Blackshaw, S. (2019). Single-cell RNA-seq analysis of retinal development identifies NFI factors as regulating mitotic exit and late-born cell specification. *Neuron,* doi:10.1016/j.neuron.2019.04.010

Delile, J., Rayon, T., Melchionda, M., Edwards, A., Briscoe, J., & Sagner, A. (2019). Single cell transcriptomics reveals spatial and temporal dynamics of gene expression in the developing mouse spinal cord. *Development, 146*(12) doi:10.1242/dev.173807

Deplancke, B., Alpern, D., & Gardeux, V. (2016). The genetics of transcription factor DNA binding variation. Cell, 166(3), 538-554. 10.1016/j.cell.2016.07.012

Deska-Gauthier, D., Zhang, Y. (2019). The functional diversity of spinal interneurons and locomotor control. *Current Opinion in Physiology*, 8, 99-108. doi: 10.1016/j.cophys.2019.01.005

Dewitz, C., Pimpinella, S., Hackel, P., Akalin, A., Jessell, T., & Zampieri, N. (2018). Nuclear organization in the spinal cord depends on motor neuron lamination orchestrated by

catenin and afadin function. *Cell Reports, 22*(7), 1681-1694. doi:10.1016/j.celrep.2018.01.059

Francius, C., Harris, A., Rucchin, V., Hendricks, T., Stam, F., Barber, M., . . . Clotman, F. (2013). Identification of multiple subsets of ventral interneurons and differential distribution along the rostrocaudal axis of the developing spinal cord. *Plos One, 8*(8), e70325-e70325. doi:10.1371/journal.pone.0070325

Gosgnach, S., Bikoff, J., Dougherty, K., El Manira, A., Lanuza, G., & Zhang, Y. (2017). Delineating the diversity of spinal interneurons in locomotor circuits. *The Journal of Neuroscience, 37*(45), 10835-10841. doi:10.1523/JNEUROSCI.1829-17.2017

Goulding, M. (2009). Circuits controlling vertebrate locomotion: Moving in a new direction. *Nature Reviews.Neuroscience, 10*(7), 507-518. doi:10.1038/nrn2608

Hayashi, M., Hinckley, C., Driscoll, S., Moore, N., Levine, A., Hilde, K., . . . Pfaff, S. (2018). Graded arrays of spinal and supraspinal V2a interneuron subtypes underlie forelimb and hindlimb motor control. *Neuron, 97*(4), 869-884.e5. doi:10.1016/j.neuron.2018.01.023

Holguera, I., & Desplan, C. (2018). Neuronal specification in space and time. *Science, 362*(6411), 176-180. doi:10.1126/science.aas9435

Jessell, T. M. (2000). Neuronal specification in the spinal cord: Inductive signals and transcriptional codes. *Nature Reviews Genetics, 1*(1), 20-29. doi:10.1038/35049541

John, A., Wildner, H., & Britsch, S. (2005). The homeodomain transcription factor Gbx1 identifies a subpopulation of late-born GABAergic interneurons in the developing dorsal spinal cord. *Developmental Dynamics, 234*(3), 767-771. doi:10.1002/dvdy.20568

Kawaguchi, A. (2019). Temporal patterning of neocortical progenitor cells: How do they know the right time? *Neuroscience Research, 138*, 3-11. doi:10.1016/j.neures.2018.09.004

Kiehn, O. (2016). Decoding the organization of spinal circuits that control locomotion. *Nature Reviews Neuroscience, 17*(4), 224-238. doi:10.1038/nrn.2016.9

Laumonnerie, C., Tong, Y., Alstermark, H., & Wilson, S. (2015). Commissural axonal corridors instruct neuronal migration in the mouse spinal cord. Nature Communications, 6, 7028-7028. 10.1038/ncomms8028

Marion, J., Yang, C., Caqueret, A., Boucher, F., & Michaud, J. (2005). Sim1 and Sim2 are required for the correct targeting of mammillary body axons. Development, 132(24), 5527-5537. 10.1242/dev.02142

Mayer, C., Hafemeister, C., Bandler, R., Machold, R., Batista Brito, R., Jaglin, X., . . . Satija, R. (2018). Developmental diversification of cortical inhibitory interneurons. *Nature, 555*(7697), 457-462. doi:10.1038/nature25999

McHanwell, S., & Biscoe, T. J. (1981). The localization of motoneurons supplying the hindlimb muscles of the mouse. *Philosophical Transactions - Royal Society.Biological Sciences, 293*(1069), 477-508. doi:10.1098/rstb.1981.0082

Michaud, J. L., Rosenquist, T., May, N. R., & Fan, C. M. (1998). Development of neuroendocrine lineages requires the bHLH-PAS transcription factor SIM1. Genes & Development, 12(20), 3264-3275. 10.1101/gad.12.20.3264

Nissen, U., Mochida, H., & Glover, J. (2005). Development of projection-specific interneurons and projection neurons in the embryonic mouse and rat spinal cord. *Journal of Comparative Neurology, 483*(1), 30-47.

Osterberg, N., Wiehle, M., Oehlke, O., Heidrich, S., Xu, C., Fan, C., . . . Roussa, E. (2011). Sim1 is a novel regulator in the differentiation of mouse dorsal raphe serotonergic neurons. PLoS One, 6(4), e19239-e19239. 10.1371/journal.pone.0019239

Petracca, Y., Sartoretti, M., Di Bella, D., Marin Burgin, A., Carcagno, A., Schinder, A., & Lanuza, G. (2016). The late and dual origin of cerebrospinal fluid-contacting neurons in the mouse spinal cord. *Development, 143*(5), 880-891. doi:10.1242/dev.129254

Satou, C., Kimura, Y., & Higashijima, S. (2012). Generation of multiple classes of V0 neurons in zebrafish spinal cord: Progenitor heterogeneity and temporal control of neuronal diversity. *The Journal of Neuroscience, 32*(5), 1771-1783. doi:10.1523/JNEUROSCI.5500-11.2012

Schweitzer, J., Löhr, H., Bonkowsky, J., Hübscher, K., & Driever, W. (2013). Sim1a and Arnt2 contribute to hypothalamo-spinal axon guidance by regulating Robo2 activity via a Robo3-dependent mechanism. Development, 140(1), 93-106. 10.1242/dev.087825

Stam, F., Hendricks, T., Zhang, J., Geiman, E., Francius, C., Labosky, P., . . . Goulding, M. (2012). Renshaw cell interneuron specialization is controlled by a temporally restricted transcription factor program. *Development, 139*(1), 179-190. doi:10.1242/dev.071134

Sultan, K., & Shi, S. (2018). Generation of diverse cortical inhibitory interneurons. *Wiley Interdisciplinary Reviews: Developmental Biology, 7*(2) doi:10.1002/wdev.306

Sürmeli, G., Akay, T., Ippolito, G., Tucker, P., & Jessell, T. (2011). Patterns of spinal sensory-motor connectivity prescribed by a dorsoventral positional template. *Cell, 147*(3), 653-665. doi:10.1016/j.cell.2011.10.012

Sweeney, L., Bikoff, J., Gabitto, M., Brenner Morton, S., Baek, M., Yang, J., . . . Jessell, T. (2018). Origin and segmental diversity of spinal inhibitory interneurons. *Neuron, 97*(2), 341-355.e3. doi:10.1016/j.neuron.2017.12.029

Syed, M., Mark, B., & Doe, C. (2017). Playing well with others: Extrinsic cues regulate neural progenitor temporal identity to generate neuronal diversity. *Trends in Genetics (Regular Ed.), 33*(12), 933-942. doi:10.1016/j.tig.2017.08.005

Vanderhorst, V. G., & Holstege, G. (1997). Organization of lumbosacral motoneuronal cell groups innervating hindlimb, pelvic floor, and axial muscles in the cat. *Journal of Comparative Neurology, 382*(1), 46-76. doi:10.1002/(SICI)1096-9861(19970526)382:1<46::AID-CNE4>3.0.CO;2-K

Xu, C., & Fan, C. (2007). Allocation of paraventricular and supraoptic neurons requires Sim1 function: A role for a Sim1 downstream gene PlexinC1. Molecular Endocrinology, 21(5), 1234-1245. 10.1210/me.2007-0034

Yakovenko, S., Mushahwar, V., VanderHorst, V., Holstege, G., & Prochazka, A. (2002). Spatiotemporal activation of lumbosacral motoneurons in the locomotor step cycle. *Journal of Neurophysiology, 87*(3), 1542-1553. doi:10.1152/jn.00479.2001

Zhang, Y., Narayan, S., Geiman, E., Lanuza, G., Velasquez, T., Shanks, B., . . . Goulding, M. (2008). V3 spinal neurons establish a robust and balanced locomotor rhythm during walking. *Neuron, 60*(1), 84-96. doi:10.1016/j.neuron.2008.09.027

Zhong, S., Zhang, S., Fan, X., Wu, Q., Yan, L., Dong, J., . . . Wang, X. (2018). A single-cell RNA-seq survey of the developmental landscape of the human prefrontal cortex. *Nature, 555*(7697), 524-528. doi:10.1038/nature25980

CHAPTER 4. EXCITATORY SPINAL V3 INTERNEURON SUBPOPULATIONS DIVERSIFY ACROSS HIERARCHICAL TEMPORL AND SPATIAL DEVELOPMENTAL PATHWAYS

Contribution Statement

I would like to acknowledge Dr. Joanna Borowska for performing the patch-clamp recordings and electrophysiological analyses. I would like to acknowledge Dr. Christopher Jones for his contributions to devising analysis strategies and statistical testing. I would like to acknowledge Colin Mackay and Laura Bennett for assisting in spinal cord tissue sectioning. I would like to acknowledge Mingwei Liu for developing a MATLAB cell counter application.

1. Abstract

Neural circuits in the spinal cord are comprised of vastly heterogeneous interneurons required for appropriate execution of movement. Discrete spinal interneuron classes emerge during early embryogenesis, although by postnatal stages extensive subpopulation diversity exists within each class. While combinatorial transcription factor profiles reveal distinct molecular IN clusters, how this molecular logic is acquired and to what extent it translates into functional distinctions between spinal IN subpopulations remains largely unknown. In the current work, through a focus on the cardinal V3 interneuron class, we reveal hierarchical early embryonic temporal-spatial mechanisms underlying molecular subpopulation diversification in the mouse spinal cord. First, neurogenesis timing separates V3 interneurons into either early-born or late-born temporal subclasses upon cell-cycle exit. Second, post-mitotic spatial mechanisms further diversify V3 INs within each temporal subclass into molecularly, anatomically, morphologically, and electrophysiologically distinct subpopulations. Thus, our work reveals early embryonic temporal and spatial mechanisms as key developmental logic for the diversification of spinal interneurons into functionally distinct subpopulations.

2. Introduction

Neuronal circuits in the spinal cord directly control the coordination, precision, and adaptability of movement. This extensive feat of sensorimotor control is achieved through the vast diversity of molecularly, anatomically, morphologically, and physiologically distinct spinal interneurons (INs) [Deska-Gauthier & Zhang, 2019; Gosgnach et al., 2017; Goulding, 2009]. Thus, understanding the IN logic of the spinal cord is essential for understanding the central control of movement.

Spinal IN diversification begins during early embryogenesis. Counteracting morphogen gradients establish 11 progenitor domains that give rise to discrete post-mitotic cardinal IN classes and motor neurons (MNs) (Jessell, 2000). While these cardinal IN classes possess general anatomical and functional properties, each further displays extensive subpopulation heterogeneity by postnatal stages (Arber, 2012; Goulding, 2009; Kiehn, 2016, Lu et al., 2015). The best example is the delineation of up to 50 distinct subpopulations within the V1 IN class alone by the combinatorial expression of 19 transcription factors (Bikoff et al., 2016; Gabitto et al., 2016). Functional separation of molecularly distinct IN subpopulations has also been revealed across several cardinal IN classes postnatally (Deska-Gauthier & Zhang, 2019).

It has been shown that some spinal IN subpopulations are born within specific time windows during neurogenesis. For example, Renshaw cells, which are a physiologically and molecularly defined subpopulation of V1 INs, appear to diversify from their cardinal class as soon as they exit the cell cycle during an early neurogenesis wave. On the other hand, another V1

subpopulation, Ia-INs, are born during a later neurogenesis wave (Benito-Gonzalez & Alvarez, 2012; Stam et al., 2012).

Recent systematic single cell sequencing work revealed a network of early embryonic transcription factors that separate spinal IN classes into molecularly distinct post-mitotic clades. Interestingly, each of these clades display a distinct temporal identity (Delile et al., 2019). For example, transcription factors denoting RC identity appear within the first emerging V1 IN clade. For most spinal INs, however, molecular clusters revealed through single cell sequencing work have not been linked to distinct neurogenesis trajectories nor functionally meaningful subpopulations.

The p3-originating V3 IN class is defined by post-mitotic Sim1 transcription factor expression. Upon cell exit, V3 INs separate into four distinct clades defined by temporally ordered transcription factor expression profiles between embryonic ages (E) 9.5-E13.5 (Delile et al., 2019). Our previous work indicated that, by E14.5, V3 INs organize into neurogenically and spatially distinct clusters (Deska-Gauthier et al., 2020) and display diverse axon projection profiles (Blacklaws et al., 2015). By postnatal stages, spatially clustered V3 INs display distinct electrophysiological properties (Borowska et al., 2013, 2015), local microcircuit connectivities (Chopek et al., 2018), and excitatory motor outputs (Danner et al., 2019) necessary for robust locomotor control (Zhang et al., 2008). Yet, how early embryonic V3 molecular diversity translates into subpopulation specific circuit integrations, and ultimately postnatal functional recruitments, remains unknown.

In the current work, we uncovered five spatially and molecularly discrete V3 IN subpopulations. We then demonstrated that these subpopulations emerge during temporally separate neurogenesis windows and diversify across spatiotemporally divergent differentiation streams between E10.5 to E14.5. These spatially and temporally distinct V3 IN subpopulations display unique molecular identities, axon projection profiles, morphologies, and electrophysiological properties. Thus, our work reveals the combination of early embryonic spatiotemporal mechanisms as key developmental logic for the diversification of spinal INs into functionally distinct subpopulations.

3. Results

3.1 Topographically clustered V3 IN subsets display distinct transcription factor expression profiles

V3 interneurons (INs) are heterogeneous. At early embryonic stages, V3 IN subtypes express various transcription factor (TF) combinations (Delile et al., 2019; Francius et al., 2013). Our previous studies demonstrated that by post natal day (P) 0, spatially clustered V3 INs displayed distinctive morphological, electrophysiological, and anatomical properties throughout the lower thoracic and higher lumbar spinal cord (Blacklaws et al., 2015; Borowska et al., 2013, 2015) [Figure4.1A-B]. Yet, it is unclear whether early embryonic TF express profiles can be correlated to functionally distinct V3 IN subpopulations. Thus, we first aimed to characterize postnatal V3 IN molecular profiles assembled across higher lumbar spinal laminae.

To address V3 IN molecular diversity we focused on a cohort of TFs that define distinct subsets of INs in the embryonic and neonatal mouse spinal cord (Bikoff et al. 2016; Delile et al., 2019; Francius et al., 2013; Hayashi et al., 2018). We assessed the immunoreactivity of 17 candidate TFs in V3 INs throughout higher lumbar (L1-L3) spinal cord segments of postnatal day (P) 0 Sim1Cre;Rosa.lsl.tdTom mice (Figure4.1A,B; Supplemental4.1A).

Nine TFs were differentially expressed in V3 IN subsets: Olig3, Pou2f2, Lmo3, Bhlhb5, Nr3b3, Onecut2, Prox1, Nr4a2, and Onecut1 (Supplemental4.1B,C). Of those, Olig3, Pou2f2, Nr3b3, Onecut2 and Prox1 displayed distinct expression patterns within spatially clustered V3 IN subsets and were analysed further. Olig3^{+} and Prox1^{+} V3 INs clustered within the ventral spinal cord. Olig3^{+} V3 INs distributed throughout laminae XIII (Figure4.1Ci,Di,Ei), while Prox1^{+}

V3 INs displayed a more refined ventromedial clustering within laminae XIII and X (Figure4.1Civ,Div,Eiv). Pou2f2^{+} and Onecut2^{+} V3 INs clustered more intermediately within laminae VI and VII. Pou2f2^{+} V3 INs displayed a slightly more dorsomedial cluster (Figure4.1Ciii,Diii,Eiii), while Onecut2^{+} V3 INs clustered more laterally (Figure4.1Cv,Dv,Ev). Lastly, Nr3b3^{+} V3 INs displayed a predominantly dorsomedial cluster within laminae V (Figure4.1Cii,Dii,Eii).

Although these molecularly identified V3 IN subsets displayed separate laminar clustering patterns, in several cases, some of them displayed overlapping distribution borders. Therefore, we next examined the potential combinatorial expressions of Olig3, Pou2f2, Nr3b3, Onecut2 and Prox1 within single V3 INs. To achieve this, we performed dual TF immunoreactivities across all possible combinations in Sim1Cre;Rosa.lsl.tdTom higher lumbar spinal cords (Supplemental4.2). Interestingly, of all TF combinations, only two pairs displayed overlap. The first was between Pou2f2 and Onecut2 (Supplemental4.2H) TFs. 10 ± 2% (n=4) of Pou2f2^{+} V3 INs co-expressed Onecut2 while 30 ± 6% (n=4) of Onecut2^{+} V3 INs co-expressed Pou2f2. The second was between Olig3 and Prox1 (Supplemental4.2D). While only 7 ± 1% (n=4) of Olig3^{+} V3 INs co-expressed Prox1, 46 ± 9% (n=4) of Prox1^{+} V3 INs co-expressed Olig3 due to the smaller number of total Prox1^{+} V3 INs.

Taken together, Olig3^{+}, Pou2f2^{+}, Nr3b3^{+}, Onecut2^{+} and Prox1^{+} V3 INs form spatially distinct, and mostly molecularly discrete V3 IN subsets (Figure4.1Fi-ii). In total, they account for approximately 70% of all V3 INs (35 ± 2 % Olig3^{+}; 19 ± 1% Nr3b3^{+}; 11 ± 2% Pou2f2^{+}; 5 ± 1 % Prox1^{+}; 4 ± 1 % Onecut2^{+}; n=4) within the neonatal higher lumbar spinal [Figure4.1Fiii].

3.2 Molecularly distinct V3 IN subsets emerge during early- or late-born neurogenesis windows

Mouse V3 INs arise from the p3 progenitor domain between E9.5 to E12.5 (Deska-Gauthier et al., 2020). Recent work by Delile and colleagues (2019) indicated temporal TF expression profiles of post-mitotic spinal neurons that varied across successive neurogenesis stages. Thus, we next investigated the generation time course of molecularly distinct V3 IN subsets across the p3-V3 neurogenesis window.

To assess the neurogenesis timing of V3 IN subsets, pregnant Sim1Cre;Rosa.lsl.tdTom mice were pulsed with thymidine analog, 5-Ethynyl-2´-deoxyuridine (EdU), at E9.5, E10.5, E11.5, or E12.5 and subsequently analyzed for EdU detection in Olig3$^+$, Pou2f2$^+$, Nr3b3$^+$, Onecut2$^+$ or Prox1$^+$ V3 INs at E14.5 (Figure4.2A). By E14.5, V3 INs have settled into their final laminar positions and display comparable neurogenesis patterns to P0 (Blacklaws et al., 2015; Deska-Gauthier et al., 2020).

A major wave of p3-V3 neurogenesis first occurred between E9.5-E10.5. Onecut2$^+$, Pou2f2$^+$ and Nr3b3$^+$ V3 INs all emerged during this time, though by E14.5, they separated into distinct spatial clusters (Figure4.2B-D). At E11.5, Onecut2$^+$ and Pou2f2$^+$ V3 INs were no longer generated (Figure4.2Biii,Diii). Few Nr3b3$^+$ V3 INs were also generated at this time (Figure4.2Ciii). However, at E11.5, a substantial increase in the neurogenesis of Olig3$^+$ and Prox1$^+$ V3 INs was observed (Figure4.2Eiii,Fiii). By E12.5, a substantial proportion of Prox1$^+$ V3 INs were still born as well as a smaller subset of ventromedially clustered Olig3$^+$ V3 INs (Figure4.2Eiv,Fiv).

Taken together, molecularly distinct V3 IN subsets emerged in two major neurogenesis waves: early-born (E9.5-E10.5); and late-born (E11.5-E12.5) waves, respectively. Interestingly, early-born born V3 INs (Onecut2^{+}, Pou2f2^{+}, Nr3b3^{+}) displayed both divergent molecular and spatial distributions across ventromedial and dorsoventral spinal axes by E14.5. Late-born V3 INs (Olig3^{+} and Prox1^{+}) displayed less pronounced molecular and spatial divergence as they were spatially restricted to ventral (EdU@E11.5), and then ventromedial (EdU@E12.5), laminae. Furthermore, the co-expression overlaps between Pou2f2-Onecut2 (Supplemental4.2H) and Olig3-Prox1 (Supplemental4.2D) were confined to TFs within the same neurogenesis windows. In contrast, TFs expressed in spatially overlapping but temporally separated V3 INs (for example Pou2f2-Prox1, Supplemental4.2I) displayed almost zero co-expression. Thus, Olig3, Pou2f2, Nr3b3, Onecut2 and Prox1 each uniquely define the spatiotemporal identities of the distinct V3 IN subsets they are expressed in.

3.3 V3 INs molecularly diversify along hierarchical neurogenic and post-mitotic pathways

Although at 14.5 V3 INs formed molecularly and spatially distinct subsets, several of these subsets emerged from the p3 progenitor domain during the same neurogenesis wave. We, and other researchers, observed that upon cell-cycle exit, post-mitotic V3 INs organize into divergent migratory streams along commissural pre-crossing dorsal horn neuronal processes (Laumonnerie et al., 2015; Supplemental4.3]. This successive spatial divergence raised the question of whether V3 INs of the same neurogenesis wave are molecularly discrete from birth

or post-mitotically acquire molecular specificity as they spatially separate. Thus, we first investigated the early molecular expression profiles of early-born V3 INs.

We performed triple immunoreactivity of Onecut2, Pou2f2 and Nr3b3 in Sim1Cre;Rosa.lsl.tdTom lumbar spinal cords between E10.5 and E14.5 (Figure4.3A,C,G). Interestingly, at E10.5, the majority of V3 INs were molecularly unspecified. 93.5 ± 0.7% (n=3) of V3 INs co-expressed Onecut2, Pou2f2 and Onecut2 together (Figure4.3A,Gi). At E11.5, however, there was a dramatic reduction in the number of V3 INs co-expressing all three early-born transcription factors (4.4 ± 1.5% total V3, n=3), with the emergence of V3 INs expressing either dual early-born TF combinations (23.2 ± 1.5% total V3), or single early-born TFs (33.1 ± 0.8% total V3) [Figure4.3Gii]. Early-born V3 INs then continued to molecularly and spatially diverge between E12.5 to E14.5 (Figure4.3Giii-v). Thus, early-born V3 INs first exited the p3 progenitor domain into a molecularly unspecified intermediate state. They then molecularly separated post-mitotically.

Next, we aimed to uncover whether V3 INs from separate neurogenesis waves shared overlapping intermediate states before choosing either early- or late-born molecular fates. At E10.5, Olig3 and Prox1 immunoreactivities were almost completely absent in V3 INs (Figure4.3B). However, at E11.5, we first observed the emergence of Olig3^{+} V3 INs. To investigate potential intermediate state overlap between early- and late-born V3 INs, we performed dual TF immunoreactivity of Olig3-Onecut2 (Figure4.3E) and Olig3-Pou2f2 (Figure4.3F) TF combinations. Remarkably, we detected no co-expression of Olig3 with either Onecut2 or Pou2f2 at Ell.5, even though cells were spatially overlapping (Figure4.3E,F). Thus,

temporally segregated neurogenesis waves likely serve as the first organizing principle of V3 INs to early- or late-born molecular identities.

Next, we investigated the early molecular expression profiles of late-born V3 INs between E12.5 and E14.5 (Figure4.3D,H). At both E12.5 and E13.5, the majority of Prox1$^+$ V3 INs co-expressed Olig3 (81 ± 10% at E12.5; 90 ± 2% at E13.5). By E14.5, about half of Prox1$^+$ V3 INs (54 ± 8%) co-expressed Olig3 (the same ratio observed at P0 [Supplemental4.2D]). Across all three stages, Prox1$^+$/Olig3$^+$ V3 INs represented only a small proportion of total Olig3$^+$ V3 INs. Thus, Prox1$^+$ V3 INs represent a small and overlapping subpopulation of Olig3$^+$ V3 INs, which molecularly specify by E14.5.

Taken together, V3 INs were molecularly diversified along a temporal hierarchy during early embryonic development. Neurogenesis timing first segregated Onecut2, Pou2f2, and Nr3b3 TFs to early-born V3 INs and then Olig3 and Prox1 to late-born V3 INs. Subsequently, post-mitotic early- and late-born V3 INs specified into molecularly and spatially distinct subsets by E14.5, respectively (Figure4.3I).

3.4 V3 axon projection diversity emerges across successive embryonic time points

V3 INs acquired molecular specificity during early post-mitotic timepoints. Yet, it remained unclear whether this molecular divergence translates into functional divergence. To begin to answer this question, we first investigated the axon projection profiles of V3 IN subsets across early embryonic stages (E11.5-E14.5).

First, we investigated the general emergence of V3 axon projections between E11.5 to E13.5. We performed retrograde biotin-dextran-amine (BDA) tract tracing in Sim1Cre;Rosa.lsl.tdTom mice followed by tissue clearing with Cubic-1 solution. This enabled us to image fully intact spinal cords and analyze complete V3 projection volumes with 3D Imaris software (Figure4.4A-C, Supplemental4.4, 4.5, 4.6). Interestingly, at E11.5, V3 INs displayed almost exclusively descending projections with the majority being descending ipsilateral (~85% dINs, Figure4.4A, Supplemental4.4). At E12.5, we first observed the emergence of ascending commissural V3 axon projections (Figure4.4B, Supplemental4.5), and finally by E13.5, we observed a further increase in the proportion of descending commissural V3 axon projections (Figure4.4C, Supplemental4.6). Thus, V3 INs displayed an early embryonic temporal ordering of their axon projections with predominately descending ipsilateral projections emerging first at E11.5 (Figure4.4Aiii), followed by ascending commissural projections at E12.5 (Figure4.4Biii), and lastly, a continued increase of descending commissural projections at E13.5 (Figure4.4Ciii).

The temporally ordered emergence of V3 axon projections raised the possibility of divergent axon projections profiles between early-born and late-born V3 IN subsets. Indeed, we have previously shown that V3 INs born after E11.5 become fate restricted to more descending commissural and local axon projection profiles (Deska-Gauthier et al., 2020). To investigate the axon projection emergences of molecularly distinct V3 IN subsets, we performed retrograde BDA tract tracing with post-hoc immunolabeling in Sim1Cre;Rosa.lsl.tdTom mice between E11.5-E13.5.

At E11.5, we first detected exclusively Onecut2^{+}, and to a much lesser extent, Pou2f2^{+} V3 projecting INs (Figure4.4D,Gi). 98 ± 1.5% (n=3) of all descending ipsilateral projecting V3 INs

were Onecut2$^+$ (Figure4.4Gi,Hi). 90 ± 13% (n=3) of all commissural projecting V3 INs were Pou2f2$^+$ (n=3), although they were a much smaller proportion of total projecting V3 INs compared to descending ipsilateral Onecut2$^+$ V3 INs (Figure4.4Gi,Hii-iii).

At E12.5, emerging ascending commissural projecting V3 INs were a mixture of Pou2f2$^+$ (15 ± 7.5%, n=3), Nr3b3$^+$ (9 ± 2.5%, n=3), and Olig3$^+$ V3 IN subsets (21 ± 6%, n=3; Figure4.4E,Gii,Hii). Descending ipsilateral projecting V3 INs remained almost exclusively Onecut2$^+$ (99 ± 2%, n=3; Figure4.4E,Gii,Hi). Interestingly, at E13.5, we observed a notable increase in the proportion of Olig3$^+$ descending commissural projecting V3 INs (E12.5, 34.5 ± 18%, n=3; E13.5, 66 ± 18%, n=3; Figure4.4F,Giii,Hii-iii). In contrast, the number of Onecut2$^+$, Pou2f2$^+$ and Nr3b3$^+$ projecting V3 INs remained relatively unchanged at E13.5 (Figure4.4Hi-iii). Of note, we did not detect any Prox1$^+$ V3 axon projections ascending nor descending the spinal cord at these early embryonic stages (data not shown).

Taken together, the temporal ordering of V3 molecular diversity coincided with the emergence of subset specific axon projection profiles. Early-born Onecut2$^+$ and Pou2f2$^+$ V3 INs projected their axons first at E11.5, followed by Nr3b3$^+$ and Olig3$^+$ V3 projections at E12.5, and then finally a continued emergence of Olig3$^+$ V3 projections at E13.5.

3.5 V3 IN subsets display molecular, spatial, and axon projection specificities by E14.5

We furthered our tract-tracing experiments to E14.5 (at which point V3 INs are fully molecularly and spatially separated) to integrate the molecular, spatial, and axon projection organizations of V3 IN subsets. First, we investigated how V3 INs are organized based on their spatial and

projection identities across rostrocaudal, dorsoventral, and mediolateral axes. We performed dual retrograde tract tracing in Sim1Cre;Rosa.lsl.tdTom mice followed by tissue clearing with Cubic-1 solution (Figure4.5A-C, Supplemental4.7-9). This allowed us to investigate how V3 INs of distinct projection types are spatially arranged amongst one another within intact three dimensional space.

Descending ipsilateral and descending commissural V3 INs each displayed distinct columnar arrangements across the rostrocaudal axis at E14.5 (Figure4.5A-C, Supplemental4.7-9). Descending commissural V3 INs clustered within laminae VIII while descending ipsilateral clustered just dorsal and lateral in laminae VII. In contract, ascending commissural V3 distributed throughout dorsal, intermediate and ventral laminae across the rostrocaudal spinal cord (Figure4.5A-C, Supplemental4.7-9).

We further confirmed these laminar distributions by superimposing cross-section distributions from retrograde labelling experiments with single dextran tracing at E14.5 (Figure4.5D-F). Taken together, by E14.5, descending commissural and ipsilateral projecting V3 INs formed distinct columnar arrangements throughout the higher lumbar spinal cord. In contrast, ascending commissural V3 INs distributed across spinal axes and did not display any single columnar organization. In total, descending commissural V3 INs comprised 48 ± 7.5% (n=3, Figure4.5E,Fi,iv) of total projecting V3, ascending commissural V3 INs comprised 34.5 ± 3% (n=3, Figure4.5E,Fii,iv) of total projecting V3, and descending ipsilateral V3 INs comprised 17 ± 10% (n=3, Figure4.5E,Fiii,iv) of total projecting V3.

Next, we aimed to further characterize the projection profiles of molecularly and spatially separate V3 IN subsets. We employed single retrograde tracing with post-hoc immunolabeling at E14.5. Onecut2$^+$ V3 INs clustered within laminae VII were almost exclusively descending ipsilateral making up 99 ± 1% (n=3) of all descending ipsilateral V3 INs (Figure4.6A). In contrast, Nr3b3$^+$ V3 INs clustered within dorsomedial laminae V were almost exclusively ascending commissural, and made up 30 ± 2.5% (n=3) of all ascending commissural V3 INs (Figure4.6B). Olig3$^+$ V3 INs clustered within ventral laminae VIII were exclusively commissural. While they predominantly displayed descending commissural projections (71 ± 1% total projecting Olig3$^+$ V3, n=3; Figure4.6C) they also displayed a notable subset of ascending commissural projections (28 ± 1% total projecting Olig3$^+$ V3, n=3; Figure4.6C). Lastly, Pou2f2$^+$ V3 INs clustered within intermediate laminae VII displayed a mixture of descending ipsilateral (21 ± 5% total projecting Pou2f2$^+$ V3, n=2; Figure4.6D), descending commissural (45 ± 4.5% total projecting Pou2f2$^+$ V3, n=2; Figure4.6D), and ascending commissural axon projections (34 ± 1% total projecting Pou2f2$^+$ V3, n=2; Figure4.6D).

The mixed projections of Olig3$^+$ and Pou2f2$^+$ raised the possibility of bifurcating axons. Indeed, we observed a small proportion of bifurcating V3 INs from our dual retrograde tracing experiments. We detected a small number of ascending commissural and descending ipsilateral bifurcating V3 INs (Supplemental4.7) as well as descending commissural and descending ipsilateral bifurcating V3 INs (Supplemental4.9). Though, we did not detect any ascending commissural and descending commissural bifurcating V3 INs (Supplemental4.8).

To investigate the molecular identity of bifurcating V3 INs, we further performed different combinations of dual retrograde tracing followed by longitudinal sectioning and

immunolabeling at E14.5 (Figure4.6E). Again, we did not observe any ascending commissural and descending commissural bifurcating V3 INs (Figure4.6Ei). Although, we did detect both ascending and descending commissural V3 with bifurcating descending ipsilateral axons. Interestingly, both of these bifurcating axon projection patterns were from Pou2f2^{+} V3 INs (Figure4.6Eii-iii). Thus, Pou2f2^{+} V3 INs appeared as the sole source of bifurcating V3 INs.

Taken together, by E14.5, V3 INs displayed a remarkable anatomical and molecular organization within the higher lumbar spinal cord. Distinct V3 IN subsets displayed unique spatial clustering, axons projection profiles, and TF expression identities (Figure4.6I).

3.6 Combined electrophysiological and morphological properties separate V3 IN subpopulations into discrete clusters

We next aimed to investigate the potential functional divergences of neurogenetically distinct V3 IN subsets. Previously, using unsupervised clustering analysis, we showed that V3 INs can be generally separated into either dorsal or ventral identities based on four electrophysiological membrane attributes from P0 to P21 (Borowska et al., 2013, 2015). However, here we have revealed molecularly distinct V3 IN subsets that display refined laminar clustering patterns beyond just their dorsoventral positions (Figure4.1). Further, while these molecularly identified V3 INs form generally separate laminar clusters, in several cases, neurogenetically distinct V3 INs display overlapping spatial distributions (Supplemental4.2). Thus, to uncover how V3 developmental separation translates to postnatal functional separation, we performed a

combinatorial parameter investigation of V3 spatial, molecular, morphological and electrophysiological properties.

We performed whole-cell patch clamp recordings of P7-P12 TdTomato$^+$ V3 INs in higher lumbar (L1-L3) spinal cord slices of Sim1CreTdTomato mice. V3 IN molecular identities and spatial positions were determined via post hoc neurobiotin and immunohistochemical staining (Figure4.7Ai,Bi,Ci,Di). Due to diminished Onecut2 immunoreactivity after P5, we were unable to reliably identify Onecut2$^+$ V3 INs post hoc (data not shown), and so, Onecut2$^+$ V3 INs were not included in our analysis. We analyzed both electrophysiological and morphological properties to capture a full spectrum of V3 intrinsic properties (Figure4.7Aii-iii,Bii-iii,Cii-iii,Dii-iii). For electrophysiological properties, we performed both suprathreshold and subthreshold current injections to obtain both active and passive membrane properties. For morphological properties, we reconstructed recorded V3 dendritic tress and quantified dendritic complexities and laminar distributions via Sholl Analysis (Supplemental4.10).

To identify significant predictors of potential V3 IN subset separation, we performed single-factor ANOVAs of all electrophysiological and morphological variables between Nr3b3$^+$, Pou2f2$^+$, Olig3$^+$ and Prox1$^+$ V3 IN groups. Of the 40 total electrophysiological factors, 13 were statistically different between at least two or more of the four V3 IN groups (p-values < 0.01/13, n = 46 total cells, Supplemental4.11A). Of the 7 total morphological factors, all 7 were statistically different between at least two or more of the four V3 IN groups (p-values < 0.01/7, n = 33 total cells, Supplemental4.11B).

While the above analysis revealed that molecularly distinct V3 INs displayed highly varied intrinsic properties, no single electrophysiological nor morphological predictor fully separated the four groups. Thus, we next aimed to determine whether some combination of predictors could provide better separation. To achieve this, we performed supervised clustering analysis.

First, we employed a principal component analysis (PCA) of the top eight most significant electrophysiological predictors (capacitance, input resistance, sage slope, sage amplitude (120mV), rheobase, rheobase spike latency, first spike latency, AP threshold) [Supplemental4.12A] and the top six most significant morphological predictors (total Intercepts (0-100µm), max intercepts, total Intercepts (100-200µm), mean intercepts, cell body volume, sum intercepts) [Supplemental4.12B], respectively. Although both electrophysiological and morphological PCAs accounted for variation between V3 IN subsets (electrophysiological, PC1 [42.59%] & PC2 [17.15%], Supplemental12Ai; morphological, PC1 [72.97%] & PC2 [15.46%], Supplemental4.12Bi), several of the predictors were highly correlated with one another (Supplemental4.11C).

For the electrophysiological data, four of the top eight predictors were highly correlated (input resistance/capacitance; rheobase spike latency/first spike latency) [Supplemental4.11Ci]. To reduce the number of predictors, one of each pair was removed from the analysis leaving six predictors total (capacitance, sage slope, sage amplitude (120mV), rheobase, first spike latency, AP threshold (first spike)). For the morphological data, several of the top six predictors were highly correlated (Supplemental4.11Cii), thus, we also removed two predictors, leaving four predictors total (total Intercepts (0-100µm), max intercepts, mean intercepts, cell body

volume). We continued our analysis with these six electrophysiological and four morphological predictors.

To visualize potential clustering, scatter plots of the first two principal components were constructed for the six electrophysiological predictors (PC1 [43.06%] & PC2 [19.89%], Figure4.7Ei, Supplemental4.12C) and the four morphological predictors (PC1 [81.78%] & PC2 [13.26%], Figure4.7Eii, Supplemental4.12D). Similar to our previous work (Borowska et al., 2013, 2015), the electrophysiological principal components revealed two general clusters: 1) more dorsal Nr3b3$^+$ and Pou2f2$^+$ V3 INs; and 2) more ventral Olig3$^+$ and Prox1$^+$ V3 INs (Figure4.7Ei). Intriguingly, the morphological principal components displayed a somewhat less clear, yet unique, separation pattern (Figure4.7Eii). Pou2f2$^+$ V3 INs appeared the most divergent of the four subpopulations along the PC1 axis. This is not surprising as Pou2f2$^+$ V3 INs displayed uniquely large and complex dendritic trees (Supplemental4.13Bii). Olig3$^+$ V3 INs separated from both Prox1$^+$ and Nr3b3$^+$ V3 INs along the PC2 axis (Figure4.7Eii).

Interestingly, the electrophysiological and morphological PCA clusters revealed distinct separation patterns between V3 IN subsets. While electrophysiological properties appeared to separate V3 INs along the dorsoventral spinal axis, morphological properties did not display a clear spatial correlation. This prompted us to investigate a combination of these predictors. As such, we performed a principal component analysis (PCA) of the six electrophysiological and the four morphological properties combined (PC1 [48.53%] & PC2 [16.08%], Figure4.7Eiii, Supplemental4.13). With the combined analysis, V3 IN subsets displayed more distinct clusters across PC1 and PC2 axes (Figure4.7E). Thus, combined electrophysiological and morphological parameters are required to most accurately separate molecularly distinct V3 INs.

Next, to achieve a more quantitative analysis of V3 subset separation, the electrophysiological and morphological predictors were standardized and subjected to supervised classification analysis using a support vector machine (SVM) learner. V3 molecular prediction accuracies were obtained based on: 1) only electrophysiological predictors (Figure4.7Fi); 2) only morphological predictors (Figure4.7Fii); and 3) a combination of both electrophysiological and morphological predictors (Figure4.7Fiii).

All three predictor groups produced accuracies significantly greater than chance, which would produce a prediction accuracy of approximately 25% (1 in 4). The combined predictors produced the highest total prediction accuracy (85%, Figure4.7Fiii), followed by the electrophysiological predictors (76%, Figure4.7Fi), and then finally the morphological predictors (70%, Figure4.7Fii).

Each of the three prediction models displayed distinct accuracy and error trends. First, the electrophysiological prediction model was able to predict Nr3b3$^+$ V3 INs with 100% accuracy. Furthermore, electrophysiological prediction errors were mostly confined within either a more dorsal Nr3b3$^+$ and Pou2f2$^+$ V3 IN group, or a more ventral Olig3$^+$ and Prox1$^+$ V3 IN group (Figure4.7Fi). These results align with our previous findings of dorsal V3 INs displaying highly distinctive electrophysiological properties compared to ventral V3 INs (Borowska et al., 2013, 2015). Next, the morphological prediction model most accurately predicted Pou2f2$^+$ V3 INs at 83%. Morphological prediction errors did not display any clear patterns (Figure4.7Fii). Lastly, and somewhat remarkably, the combined prediction model was able to predict both Olig3$^+$ V3 INs and Pou2f2$^+$ V3 INs with 100% accuracy (Figure4.7Fiii). This was somewhat surprising to us as both Olig3$^+$ and Pou2f2$^+$ V3 INs share overlapping spatial distribution patterns with one another and surrounding V3 IN subsets (Supplemental4.2).

The 100% predictions accuracies of Olig3+ and Pou2f2^{+} V3 INs prompted us to further investigate how V3 IN subset intrinsic properties correlate with their spatial positions. To that end, we plotted V3 combined PC1 and PC2 scores against their dorsoventral cell body positions, respectively (Figure4.7Gi-iii). Interestingly, V3 INs displayed a clear inverse correlation between their PC2 scores and dorsoventral positions (Figure4.7Gii). In contrast, V3 INs did not display any clear correlation between their PC1 scores and dorsoventral positions (Figure4.5Giii). However, when V3 dorsoventral positions were plotted against their PC1 scores they formed four distinct clusters almost completely separated by their molecular identities (Figure4.5Giii). We previously revealed that V3 molecular identities uniquely define V3 IN spatiotemporal identities (Figure4.2). Furthermore, when we plotted the PC1 distributions of each molecularly distinct V3 IN subset they appeared strikingly similar to the inverses of their neurogenesis timing profiles (Figure4.7Giv). This raised the exciting possibility that both the molecular and intrinsic identities of V3 INs are explained by a combination of their final laminar settling positions and early embryonic neurogenesis timings.

3.7 Neurogenesis timing separates V3 IN intrinsic properties into early-born or late-born identities

To investigate the potential role V3 neurogenesis timing and intrinsic property separation, we pulsed pregnant Sim1Cre;Rosa.lsl.tdTom mice with EdU at either E10.5, E11.5, or E12.5 followed by patch-clamp recordings between P6-P12 in higher lumbar (L1-L3) spinal cord slices. We then identified V3 neurogenesis timings via biotin and EdU detection post-hoc (Figure4.8A,B,C). To

eliminate potential confounding spatial separation we target V3 INs within ventral laminae across all three neurogenesis ages (Supplemental4.14Ai,Bi,Ci).

We next investigated the six electrophysiological (capacitance, sage slope, sage amplitude (120mV), rheobase, first spike latency, AP threshold (first spike)) and four morphological (total Intercepts (0-100µm), max intercepts, mean intercepts, cell body volume) properties that separated molecular V3 IN subsets (Supplemental4.14D). Several of these properties were distinct between neurogenesis times. Furthermore, E11.5 and E12.5 EdU^+ V3 INs displayed similarly distinct properties from E10.5 EdU^+ V3 INs across several comparisons (Supplemental4.14Di,Dii,Div,Dv,Dviii,Dix). This division line between E10.5 and E11.5-E12.5 matched our previous molecular findings of distinct early-born (E9.5-E10.5) and late-born (E11.5-E12.5) V3 IN groups (Figure4.2).

We next divided EdU^+ V3 INs into either early-born (EdU@E10.5) or late-born (EdU@E11.5 E12.5) identities and focused on three distinct properties (total dendritic intercepts (0-100µm), sage amplitude (120mV), AP threshold (first spike); Figure4.8Di-iv, Supplemental4.14E). Principal component analysis of these three distinct properties revealed clear separation between early-born and late-born V3 INs across the PC1 axis (Figure4.8E). Furthermore, classification analysis using support vector machine (SVM) learner had a total prediction accuracy of 83.3% (Figure4.8F). Thus, neurogenesis timing separated ventrally clustered V3 INs into early-born or late-born intrinsic property identities.

Lastly, to investigate this neurogenesis organization principal beyond ventral V3 INs to all V3 subsets we repeated our temporal three factor analysis with $Pou2f2^+$, $Nr3b3^+$, $Olig3^+$ and $Prox1^+$

V3 IN subsets (Figure4.8G). As before, principal component analysis revealed clear separation between early-born Pou2f2^{+} and Nr3b3^{+} V3 INs and late-born Olig3^{+} and Prox1^{+} V3 INs across the PC1 axis (Figure4.8H). Classification analysis using support vector machine (SVM) learner also had a total prediction accuracy of 90.9% for grouped early-born (Pou2f2^{+} & Nr3b3^{+} V3) and late-born (Olig3^{+} & Prox1^{+} V3) molecular V3 subsets (Figure4.8I). Thus, combined spatial laminar positioning and neurogenesis timing separate molecularly distinct V3 IN subsets into electrophysiologically and morphologically distinct identities.

4. Discussion

Taken together, we have uncovered hierarchical early embryonic temporal-spatial logic underlying V3 IN subpopulation diversity. First, temporal mechanisms separated V3 INs into either early-born or late-born subclasses (Figue4.9A). Early-born V3 INs exited the p3 progenitor domain between E9.5-E10.5 and shared early post-mitotic expressions of Nr3b3, Onecut2 and Pou2f2 transcription factors. Late-born V3 INs exited the p3 progenitor domain between E11.5-E12.5 and expressed Olig3 and Prox1 transcription factors. By postnatal stages, early-born V3 INs displayed extensive dendritic complexities, large Sag amplitudes, higher action potential firing thresholds and varied laminar distributions. Late-born V3 INs displayed moderate dendritic complexities, small sag amplitudes, lower action potential firing thresholds and ventral laminar distributions (Figure4.9C). Following temporal separation, post-mitotic V3 IN subpopulations migrated along ventrodorsal and mediolateral spinal axes. Spatially separate V3 INs within each temporal subclass further differentiated into molecularly, physiologically and anatomically discrete topographical clusters (Figure4.9B). Thus, V3 IN subpopulations are delineated by a combination of their early embryonic spatial and temporal identities.

4.1 Molecular diversity in the spinal cord and transcription factors as interneuron subpopulation markers.

In the past several years, it has become clear that spinal INs diversify well beyond their early identified developmental lineages. Recent single-cell sequencing and combinatorial transcription factor assays have enabled unbiased investigations of the key principles

underlying the molecular diversity of interneurons in the postnatal spinal cord. For example, while anatomical and physiological studies revealed inhibitory RoRβ$^+$ (Abraira et al. 2017) and excitatory SST$^+$ (Duan et al., 2014; Christensen et al., 2016) dorsal IN types, single cell RNA sequencing further revealed combinatorial expression profiles within each population. RoRβ$^+$ INs can be further divided into 15 inhibitory subtypes and SST$^+$ INs into at least 10 subtypes (Häring et al., 2018).

Similarly, Sathyamurthy and colleges (2018) used massively parallel single nucleus RNA-sequencing revealing 43 molecularly characterized neuronal populations in the postnatal spinal cord. They first revealed highly divergent gene expression profiles between excitatory and inhibitory IN types. Differential gene expression between inhibitory and excitatory spinal INs has also been demonstrated during embryonic stages (Cheng et al., 2004; Glasgow et al., 2005; Mizuguchi et al., 2006). Interestingly, Sathyamurthy and colleges (2018) also found that dorsal INs displayed more discrete and divergent populations than ventral populations. That is, ventral INs shared more molecular markers across populations – indicating a more combinatorial molecular logic – than dorsal IN types. Still, dorsal IN populations display combinatorial molecular expression profiles required for population separation. Across all spinal IN types, while single markers can divide INs into clusters, combinatorial expression profiles are required to define subtype specific identities (Häring et al., 2018; Sathyamurthy et al., 2018). Indeed, the necessity of defining a cell by its combinatorial expression has been long understood in simpler model organisms such as C. elegans and drosophila (Hobert et al., 2010).

This recent single cell sequencing work has also revealed the gene categories that best separate cell types in the adult mammalian spinal cord. Sathyamurthy and colleges (2018) found the

most significant genes for IN type separation were transcription factors, neurotransmitter receptors, ion channels, and cAMP transduction components. Häring and colleges (2018) also utilized a single cell RNA sequencing approach identifying 30 (15 excitatory and 15 inhibitory) molecularly distinct dorsal horn IN subpopulations in the adult spinal cord. Similarly, they found transcription factors, neuropeptides, receptors, and ion channels as the most significant gene categories for spinal cord IN type separation. These gene categories are somewhat expected as they are collectively involved in regulating gene expression networks (transcription factors), cellular signaling (receptors, neuropeptides, cAMP transduction components), and biophysical membrane properties (ion channels). Similar findings have also been revealed for neuronal type separation across other regions of the central nervous system (Zeisel et al., 2018).

Interestingly, Häring and colleges (2018) found that uniquely transcription factors displayed a hierarchical organization across IN subtypes in the dorsal spinal cord. While related neuron subtypes often shared common transcription factor expression profiles, they rarely shared overlapping neuropeptide or receptor expression profiles. Unique combinations of transcription factors, neuropeptides, receptors, and ion channels were displayed within a neuron population, though, only transcription factors revealed relatedness between populations. Thus, transcription factors displayed a hierarchical organization between dorsal IN types, while other gene categories did not. Taken together, this work validates transcription factors as effective molecular markers of post-mitotic spinal IN subpopulations.

4.2 V3 IN molecular diversity

Molecular diversity of V3 INs was analyzed by assessing combinatorial expression of Sim1 with transcription factors previously revealed to mark ventral spinal cord IN subpopulations (Bikoff et al. 2016; Delile et al., 2019; Francius et al., 2013; Hayashi et al., 2018). Among the 17 transcription factors (TFs) tested, 9 were expressed in small subsets of V3 INs at P0.

Interestingly, while only 9 of the 17 TFs we tested were expressed in excitatory V3 INs, 16 of the 17 TFs are expressed in inhibitory V1 INs (Bikoff et al. 2016; Delile et al., 2019). This limited overlap between TF expression in V1 and V3 INs is perhaps predictable, as major differences in anatomical and neurochemical phenotype would coincide with differences in genotype expression. Furthermore, most of the 16 V1 TFs are also expressed in excitatory $V2_a$ and inhibitory $V2_b$ INs (Bikoff et al., 2016; Hayashi et al., 2018). As V1, $V2_a$, and $V2_b$ are ipsilateral projecting INs and V3 are primarily commissural projecting INs, these results suggest that commissural spinal INs may possess molecular signatures distinct from ipsilaterally projecting spinal INs.

Although most Sim1-expressing V3 INs in the lumbar spinal cord are ventral commissural INs, we previously identified 'outlier' V3 IN subsets that diverge from common V3 traits. These include a cluster of V3 INs located in the deep dorsal horn, as well as ventrally located ipsilaterally projecting V3 INs (Zhang et al., 2008; Borowska et al., 2013; Blacklaws et al., 2015). Our electrophysiological recordings also demonstrate diverse intrinsic properties of V3 INs, especially between ventral and dorsal V3 INs (Borowska et al., 2013, 2015). Here we identify specific TFs expressed in these two unique V3 subpopulations. We found that a large

proportion of dorsally clustered V3 INs express Nr3b3 and have ascending commissural axon projections. Onecut2 is exclusively expressed in descending ipsilateral projecting V3 INs located at the lateral edge of the ventral V3 IN cluster. On the other hand, Olig3^{+} V3 INs cluster within ventral laminae VIII, project commissural axons, and make up the largest subpopulation proportion of V3 INs discovered here. Thus, we have revealed molecular signatures for both phenotypically common as well as divergent V3 IN subtypes.

While our current work identified unique V3 IN subpopulations based on co-expression of Sim1 with single TFs, it is increasingly clear that combinatorial expression of two or more TFs is often required to separate discrete spinal IN subpopulations. The necessity for multi-combinatorial transcriptions factor expressions for subpopulation categorization has been demonstrated both within V1 INs (Bikoff et al., 2016; Gabitto et al., 2016; Sweeney et al., 2018) and more recently within $V2_a$ INs (Hayashi et al., 2018). While Prox1 and Onecut2 transcription factors label restricted V3 laminar clusters, Nr3b3^{+} V3 IN labeling is less confined. In addition to dorsal V3 INs, Nr3b3 also denotes a small subset of ventral V3 INs. This observation suggests further molecular specification between Nr3b3^{+} dorsal and ventral V3 IN subsets not currently identified. Furthermore, Pou2f2^{+} and Olig3^{+} V3 INs display varied axon projection profiles. Pou2f2^{+} V3 INs, while spatially clustered, project commissural ascending, commissural descending, and ipsilateral descending axon projections. While a small subset of Pou2f2^{+} V3 INs may be bifurcating, our results suggest it is more likely that the majority of individual Pou2f2^{+} V3 INs possess one of these three axon projection phenotypes. Likewise, Olig3^{+} V3 INs display both commissural ascending and descending axon projections. In this case, we did not detect any bifurcating axon projections. Thus, it is possible that Pou2f2^{+} and Olig3^{+} V3 INs may also be

further subdivided into combinatorial molecular identities that match their specific axon projection subtypes. Indeed, it has been shown embryonically that Olig3$^+$ and Pou2f2$^+$ V3 INs display varied TF expression profiles (Delile et al., 2019). Though, whether and how this translates into anatomical and functional distinctions is not known.

4.3 Mitotic and post-mitotic diversification of spinal INs

In mice, V3 INs are generated from the p3 progenitor domain between E9.5 and E12.5. However, our current work suggests this broad timeline of neurogenesis is organized into two distinct waves: early-born (E9.5-E10.5) and late-born (E11.5-E12.5) V3 INs. Pou2f2$^+$, Nr3b3$^+$ and Onecut2$^+$ V3 INs emerge during the early-born V3 neurogenesis wave while Olig3$^+$ and Prox1$^+$ V3 INs emerge during the late-born V3 neurogenesis wave.

In addition to temporal factors, spinal IN subpopulations have been shown to diversify via heterogeneous progenitor domain origins or local post-mitotic signalling pathways. For example, $V0_d$ and $V0_v$ INs emerge from distinct progenitor domains (Satou et al., 2012), while $V2_a$ and $V2_b$ INs diversify post-mitotically through local Notch signalling (Del Barrio et al., 2007; Kimura et al., 2008; Okigawa et al., 2014). Our current work indicates that early-born V3 INs may share the same progenitor cells. We found that all early-born V3 INs co-express Pou2f2, Onecut2, and Nr3b3 at birth but assume specific molecular and anatomical identities after E10.5 during post-mitotic differentiation. It would be interesting to determine whether local signals, such as Notch or retinoic acid (RA), contribute to the molecular specification of early-born V3 IN subpopulations during post-mitotic stages. Indeed, *in vitro* cell culture work has

shown that RA-dependent Nr3b3 expression results in increased neurite growth during differentiation (Lim et al., 2015). Similar to RA's role in establishing post-mitotic LMC motoneuron subtype diversity (Sockanathan & Jessell, 1998), local RA signaling could contribute to V3 subpopulation specific differentiation as well. While we have revealed the spatiotemporal developmental framework guiding V3 IN diversity, the specific molecular pathways are yet to be discovered.

4.4 Potential functional roles of V3 IN subpopulations

While we have revealed the circuit connectivities and intrinsic membrane properties of V3 IN subpopulations, how these properties translate into functionally distinct recruitments and sensorimotor outputs remains unknown. Yet, our current work has revealed relevant V3 IN subpopulations to target for functional understanding. In particular, we hypothesize that in addition to physiological and morphological separation, early-born and late-born V3 INs may be functionally distinct. To address these issues, we will need to develop intersectional and inducible transgenic mouse approaches for *in vitro* and *in vivo* behavioural analyses.

5. Materials and Methods

Mouse strains

$Sim1^{Cre}$ mice (Zhang et al, 2008) were crossed with TdTomato (TdTom) Ai14 conditional reporter mice (Jackson Laboratory) to generate $Sim1^{Cre}$;Rosa.lsl.tdTom mice (Zhang et al., 2008; Blacklaws et al., 2015) used for fate mapping of $Sim1^{+}$ V3 INs at embryonic and postnatal stages. All procedures were performed in accordance with the Canadian Council on Animal Care and approved by the University Committee on Laboratory Animals at Dalhousie University.

Spinal cord tissue dissection, processing and sectioning

Spinal cords were obtained at embryonic (E9.5-E14.5) and postnatal (P0, P6-P12) stages. For embryonic staging the date of fertilization was identified by the presence of a vaginal plug, and the morning of vaginal plug discovery was defined as E0.5. Prior to dissection of embryos, pregnant mothers were anaesthetized via intraperitoneal injections of a ketamine (60mg/kg) and xylazine (12mg/kg) cocktail. Once a mouse no longer responded to the pedal reflex, it was decapitated and embryos removed via cesarean section. Embryonic and postnatal mice were euthanized via decapitation and spinal cords subsequently dissected in Ringer's Solution (6.49 g/L NaCl; 0.23 g/L KCl; 1.98 g/L D-Glucose;2.1 g/L NaHCO3; 0.31 g/L MgSO4; 0.37 g/L CaCl2;0.15 g/L KH2PO4) bubbled with 95%O2/5%CO2 to maintain a pH of 7.4. Spinal cords were fixed with 4% paraformaldehyde (Electron Microscopy Sciences) [PFA] in phosphate-buffered saline (PBS) at 4°C for varying times (E9.5, 10 mins; E10.5 and E11.5, 15 mins; E12.5, 25 mins; E13.5, 30 mins; E14.5, 35 mins; P0, 1h). Spinal cords were then washed in PBS 3 times for 15 mins each and then overnight at 4°C. The following day, spinal cords were cryoprotected in 20% sucrose in

PBS at 4°C overnight. Tissues were then embedded in O.C.T compound (Fisher Healthcare) and flash-frozen at -55°C in a dry ice/ethanol bath. Frozen lower thoracic and higher lumbar (T12-L3) cord segments were sectioned transversely using a cryostat (Leica CM1950). E9.5-E14.5 cords were sectioned at 14 micrometers and P0 at 30 micrometers onto Superfrost Plus Microscope Slides (Fisherbrand).

Immunohistochemistry

Mounted sections were first incubated in PBS containing 0.1% Triton X (PBS-T) for 3 washes of 5 minutes each. Subsequently, sections were incubated in PBS containing primary antibodies and 10% heat-inactivated horse serum (Invitrogen) overnight at 4°C. Primary antibodies used are listed in Table 1. Following primary antibody incubation, sections were washed three times with PBS for 5 mins each then incubated in PBS containing secondary anti-bodies (and Alexa Fluor conjugated streptavidin when relevant) for 1h at 4°C. Secondary antibodies used are listed in Table 1. When applicable, secondary antibody incubation was followed by Click-iT® EdU Alexa Fluor® 647 fluorescent labeling (Thermofisher). Lastly, sections were washed three times in PBS for 5 mins each and cover-slipped with fluorescent mounting medium (Dako).

Image capture and laminar cell position analysis

Fluorescent micrographs of sections were captured using a Zeiss LSM 710 upright confocal microscope with ZEN 2009 Microscope and Imaging Software. Cell numbers and laminar positions were quantified using ImageJ and MATLAB. Using the ImageJ Cell Counter Plugin, x,y coordinates of individual cell bodies as well as the maximum and minimum x,y coordinates of corresponding spinal cord outlines were denoted. At P0, a total of 10 randomly chosen 30 µm

transverse sections were analyzed between and including T12 to L3 per animal. At embryonic time points (E10.5-E14.5) a total of 10 randomly chosen 14 µm transverse sections were analyzed within approximate lower thoracic and higher lumbar segments per animal. Cell body laminar distribution and cell body density contour plots were subsequently constructed utilizing *grid-data* and *contour* functions in MATLAB. Briefly, within each section, cell body x,y positions were normalized against maximum and minimum hemicord x,y coordinates. Cell density plots and Heat maps were then constructed to display cell body laminar distributions across mediolateral and dorsoventral axes.

5-Ethynyl-2´-deoxyuridine (EdU) pulse labeling of V3 IN neurogenesis profiles

EdU (Thermo Fisher Scientific) was dissolved in saline solution to 6mg EdU/1ml saline. Pregnant $Sim1^{Cre}$;Rosa.lsl.tdTom mice were injected Intraperitoneally with EdU solution based on body weight (50µl/10g) at gestational stages E10.5, E11.5, or E12.5. Comparable mice injected at E9.5 were pulsed with 12mg/ml EdU solution. EdU-pulsed spinal cords were collected at E14.5. Fluorescent labeling of DNA-incorporated EdU was detected using a Click-iT® EdU Alexa Fluor® 647 Imaging Kit (Thermofisher). To determine neurogenesis profiles of molecularly distinct V3 IN subsets, fluorescent labeling of EdU was performed following immunohistochemistry.

Retrograde and anterograde tract tracing

Axonal projection patterns of E11.5-E14.5 V3 INs were determined using retrograde BDA tracing of isolated $Sim1^{Cre}$;Rosa.lsl.tdTom cords. Immediately following spinal cord dissection, 3000 MW, lysine fixable, BDA (Molecular Probes) was inserted into one half of the higher lumbar spinal cord. Insertion sites had a rostrocaudal spread of approximately 700-1000µm in

each direction (data not shown). For dual tracing experiments, E14.5 $Sim1^{Cre}$;Rosa.lsl.tdTom cords were injected with both Dextran, Alexa Fluor™ 488 (3000 MW, Invitrogen, cat# D34682) and Dextran, Biotin (3000 MW, Invitrogen, cat# D7135) at respective rostrocaudal and left-right locations. Injected cords were incubated overnight (16-20h) in Ringer's Solution bubbled with 95%O2/5%CO2 at 20°C.

Following incubation, embryonic postnatal cords were fixed in 4% paraformaldehyde (Electron Microscopy Sciences) [PFA] in PBS at 4°C for varying times (E9.5, 10 mins; E10.5 and E11.5, 15 mins; E12.5, 25 mins; E13.5, 30 mins; E14.5). Spinal cords were then washed in PBS 3 times for 15 mins each and then overnight at 4°C. Following washing spinal cords were either processed for either biotin detection and tissue clearing or tissue sectioning and immunohistochemistry.

For tissue clearing, spinal cords were incubated in 0.1% PBS-T three times of approximately 30 mins. Cords were then incubated in PBS with Alexa Fluor 647-conjugated streptavidin (Thermofisher, cat# S21374) over night at 4°C. Following biotin detection, cords were washed three times in PBS for 30mins at 4°C. They were then incubated 4°C in Cubic-1 solution (Susaki et al., 2014) which contains 25% Urea (crystals) (FisherScientific, cat#U15-500), 15% TritonX-100 (Sigma-Aldrich, cat#T9284), and 25% N,N,N',N'-Tetrakis(2-Hydroxypropyl)ethylenediamine (Sigma-Aldrich, cat# 122262). Cord stayed in solution until cleared (1-2days) and were imaged with a Zeiss LSM 710 upright confocal microscope and ZEN 2009 Microscope and Imaging Software. To fully captured regions of interest extensive z-stack (200-400µm) and stitching (4-8 tiles) functions were utilized with a 10x objective. Images were then analyzed with Imaris using the 'spots' function on Imaris Software.

For tissue sectioning and immunohistochemistry, cords were subjected to aforementioned tissue processing procedures. These procedures are also described in detail elsewhere (Eide & Glover, 1995; Nissen et al., 2005; Blacklaws et al., 2015). Fluorescent labeling of BDA was performed in concert with immunohistochemical labeling of spinal cord sections. Either Alexa Fluor 405-conjugated streptavidin (Thermofisher), Alexa Fluor 488-conjugated streptavidin (Thermofisher), or Alexa Fluor 647-conjugated streptavidin (Thermofisher) was diluted 1:500 and added to secondary antibody solutions.

Patch-clamp recordings and post-hoc immunohistochemistry

P6-P12 $Sim1^{Cre}$;Rosa.lsl.tdTom mice were decapitated and their higher lumbar spinal cords (L1-L3) dissected in ice-cold oxygenated solution (3.5 mM KCL, 25 mM NaHCO3, 1.2 mM KH2PO4, 1.3 mM MgSO4 1.2 mM CaCl2, 10 mM glucose, 212.5 mM sucrose, 2 mM MgCl2, pH 7.4). Dissected cords were then sectioned into 300–350µm transverse slices using a vibratome (Vibratome 300, Vibratome). Following a 30 minute recovery period slices were transferred into Ringer's Solution (111 mM NaCl, 3.08 mM KCl, 11 mM glucose, 25 mM NaHCO3, 1.25 mM MgSO4 2.52 mM CaCl2, 1.18 mM KH2PO4, pH 7.4) bubbled with 95%O2/5%CO2. Whole-cell current-clamp recordings were made using a MultiClamp 700B amplifier (Molecular Devices Inc., Sunnyvale, California, USA). Patch-clamp recording pipettes were filled with a recording buffer containing 128 mM K-gluconate, 4 mM NaCl, 0.0001 mM CaCl2, 10 mM HEPES, 1 mM glucose, 5 mM Mg-ATP, 0.3 mM GTP-Li. For neuron filling, 0.4 mg/ml lucifer yellow dilithium salt (LY; Sigma-Aldrich) and 1 mg/ml neurobiotin (Vector Laboratories) were also added to the pipette solutions. Both active and passive neuronal membrane recordings were obtained with

Clampex 10.3 (Molecular Devices) and analyzed with Clampfit 10.3 and Spike2 5.0 software (Cambridge Electronic Design).

V3 molecular identities were determined via post-hoc immunohistochemistry. Briefly, following recording, spinal cord slices were fixed in 4% PFA for 10mins at room temperature. They were then washed over night in PBS. The following day, they were incubated in 0.1% PBS-T three times for approximately 30 mins each at room temperature on a shaker. They were then incubated in PBS containing primary antibodies and 10% heat-inactivated horse serum (Invitrogen) for two nights at 4°C. Following primary antibody incubation, sections were washed three times with PBS for 15-30 mins at room temperature on a shaker. They were then incubated in PBS containing secondary anti-bodies and Alexa Fluor 488-conjugated streptavidin (Thermofisher) overnight at 4°C. spinal sections finally washed three more times in PBS for 15-30 mins at room temperature and cover-slipped with fluorescent mounting medium (Dako).

Morphology Reconstruction and Analysis

Biotin-filled V3 INs were imaged with a 40x objective using a Zeiss LSM 710 upright confocal microscope and ZEN 2009 Microscope and Imaging Software. Both z-stack (30-60µm) and stitching functions (4-16 tiles) were required to capture the full ranges of neural processes. Three-dimensional neural morphologies were constructed from confocal images with the 'filament tracer' function on Imaris Software. Both automated and semi-automated filament tracing modes were used. Cell body volumes were constructed using the 'surfaces' function.

Following morphology tracing, images were saved as two-dimensional tiff files further subjected to Sholl Analysis (from image) using the Automated Sholl Plugin in Fiji

(Supplemental10). Briefly, concentric circles were constructed at 2µm increments spanning out from the neurons cell body. The total number of dendrites intersecting at each circle of a specific radius was then calculated allowing for a quantitative analysis of V3 dendritic properties. For our purposes, we quantified the total number of dendritic interceptions between set radius distances (total intercepts 0-100µm, total intercepts 100-200µm, total intercepts 200-300µm, total intercepts 300-400µm, total intercepts 400-500µm), the summation of all dendritic interceptions (sum intercepts), the mean number of dendritic interceptions (mean intercepts), the maximum number of dendritic interceptions (max intercepts), the radius at which the maximum number of dendritic interceptions occurred (max intercept radius), and the farthest radius that dendritic interceptions cross (ending radius).

Intrinsic Property Analysis

Recorded V3 INs were categorized as either Nr3b3+, Pou2f2+, Olig3+, or Prox1+ V3 INs via post-hoc immunoreactivity and assigned electrophysiological and morphological properties. We were unable to reliably identify Onecut2+ V3 INs (due to diminished Onecut2 immunoreactivity after P5), and so, Onecut2+ V3 INs were not included in our analysis.

To identify electrophysiological and morphological predictors with significant differences between their mean values we performed single-factor ANOVAs and Tukey's multiple comparisons test. A predictor was deemed significant if at least one group mean was statistically different than the other three. A significant predictor did not necessarily provide a means to separate the four groups. However, it was anticipated that some combination of predictors would provide good separation as assessed by supervised cluster analysis.

Principal component analysis (PCA) was carried out to assess potential separation of the four groups using significant electrophysiological predictors alone, significant morphological predictors alone, and a combination of select electrophysiological and morphological predictors. PC1 and PC2 scores were plotted to visualize potential group separation. PC1 and PC2 score were also respectively plotted against dorsoventral cell body positions. Positions were defined as a ratio between the minimum ventral point (0) of the spinal slice and the maximum dorsal point (1) of the spinal slice.

To provide a more objective quantitative analysis, electrophysiological and morphological predictors were standardized and subjected to supervised classification analysis using the Classification Learner Application in MATLAB. We utilized the support vector machine (SVM) learner as it consistently produced the best classification accuracy.

We used the SVM learner across three different data sets: 1) only electrophysiological predictors (six total: capacitance, sage slope, sage amplitude (120mV), rheobase, rheobase first spike latency, AP threshold (first spike)); 2) only morphological predictors (four total: total Intercepts (0-100µm), max intercepts, mean intercepts, cell body volume); and 3) a combination of both electrophysiological and morphological predictors (capacitance, sage slope, sage amplitude (120mV), rheobase, rheobase first spike latency, AP threshold (first spike), total Intercepts (0-100µm), max intercepts, mean intercepts, cell body volume). Model results were reported as confusion matrices of V3 subset prediction accuracies and error rates.

6. Figures

Figure 4.1 Molecularly distinct V3 INs assemble into distinct topographical clusters

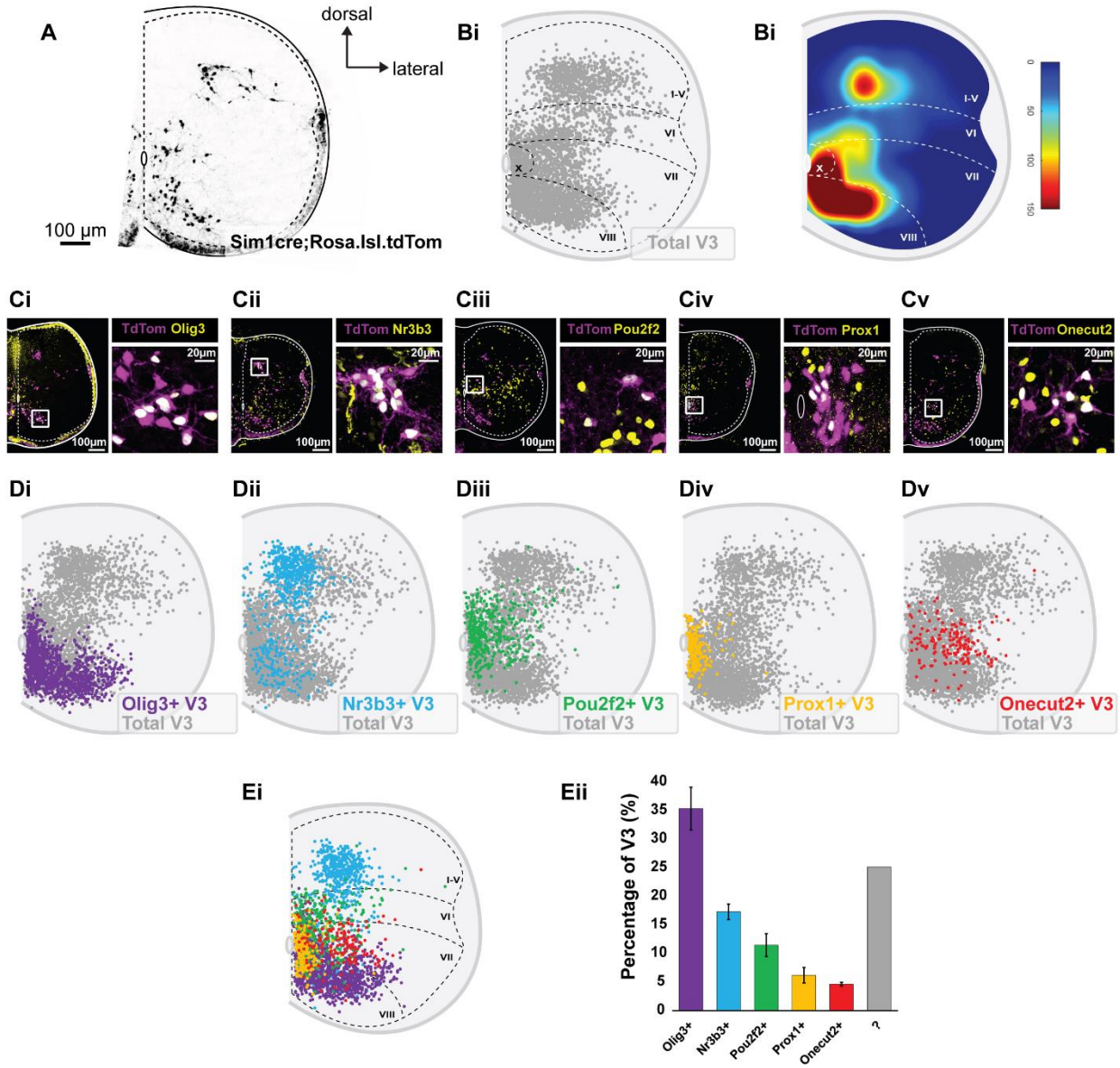

Figure 4.1 Molecularly distinct V3 INs assemble into distinct topographical clusters

(A) Representative image of TdTom^{+} V3 INs in an L2 spinal cord section from a Sim1^{Cre};Rosa.lsl.tdTom P0 mouse. (B) TdTom^{+} V3 laminar distribution plot (Bi) and density heat map plot (Bii) of the higher lumbar spinal cord (L1-L3) at P0 (n=4 animals) (C) Immunohistochemical labeling of Olig3^{+} (Ci), Nr3b3^{+} (Cii), Pou2f2^{+} (Ciii), Prox1^{+} (Civ), and Onecut2^{+} (Cv) V3 IN (TdTom) subsets in higher lumbar (L1-L3) segments at P0. (D) Laminar cell distribution plots of Olig3^{+} (Di), Nr3b3^{+} (Dii), Pou2f2^{+} (Diii), Prox1^{+} (Div), and Onecut2^{+} (Dv) V3 IN subsets in higher lumbar (L1-L3) segments at P0 (n=4 animals for each V3 subset). (E) Combined laminar cell distribution plot of V3 INs subsets in higher lumbar (L1-L3) segments at P0 (n=4 animals for each V3 subset). (Eii) Percentage of total V3 INs that express Olig3, Nr3b3, Pou2f2, Prox1, and Onecut2 in higher lumbar (L1-L3) segments at P0 (n=4 animals).

Figure 4.2 Molecularly distinct V3 INs emerge during early- or late-born neurogenesis windows

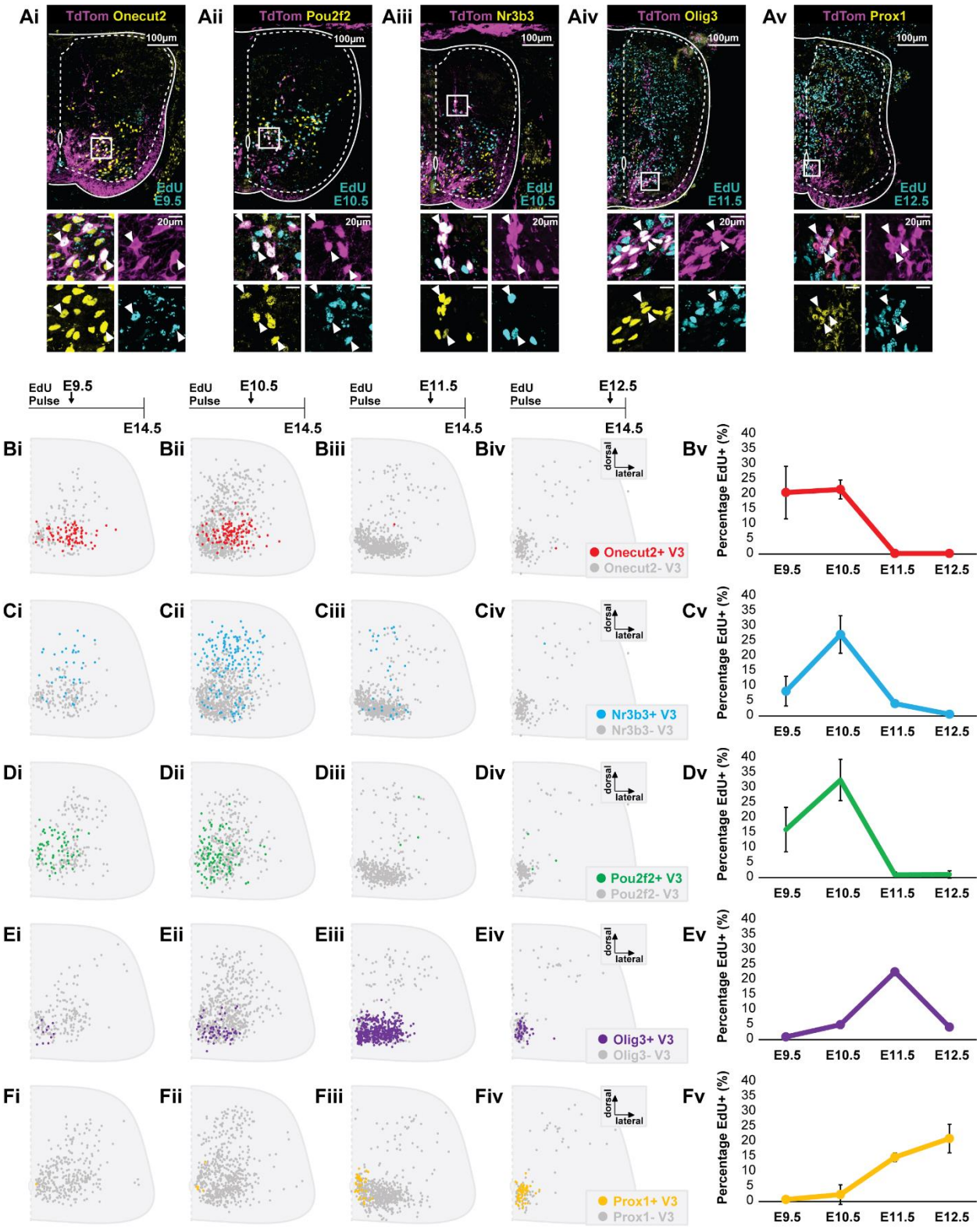

Figure 4.2 Molecularly distinct V3 INs emerge during early- or late-born neurogenesis windows

(A) Representative images of EdU detection in E14.5 higher lumbar (L1-L3) Sim1Cre;Rosa.lsl.tdTom spinal sections of Onecut2$^+$ (Ai, EdU pulsed at E9.5), Pou2f2$^+$ (Aii, EdU pulsed at E10.5), Nr3b3$^+$ (Aiii, EdU pulsed at E10.5), Olig3$^+$ (Aiv, EdU pulsed at E11.5), and Prox1$^+$ (Av, EdU pulsed at E12.5) V3 INs. (B-F) E14.5 laminar distribution plots (i-iv) and EdU$^+$ percentages (v) of Onecut2$^+$ (B), Nr3b3$^+$ (C), Pou2f2$^+$ (D), Olig3$^+$ (E), and Prox1$^+$ (F) V3 INs across E9.5 (i), E10.5 (ii), E11.5 (iii) and E12.5 (iv) EdU pulse times (n=3 animals for each V3 subset and EdU pulse time).

Figure 4.3 Early- and late-born V3 INs continue to molecularly and spatially separate post-mitotically

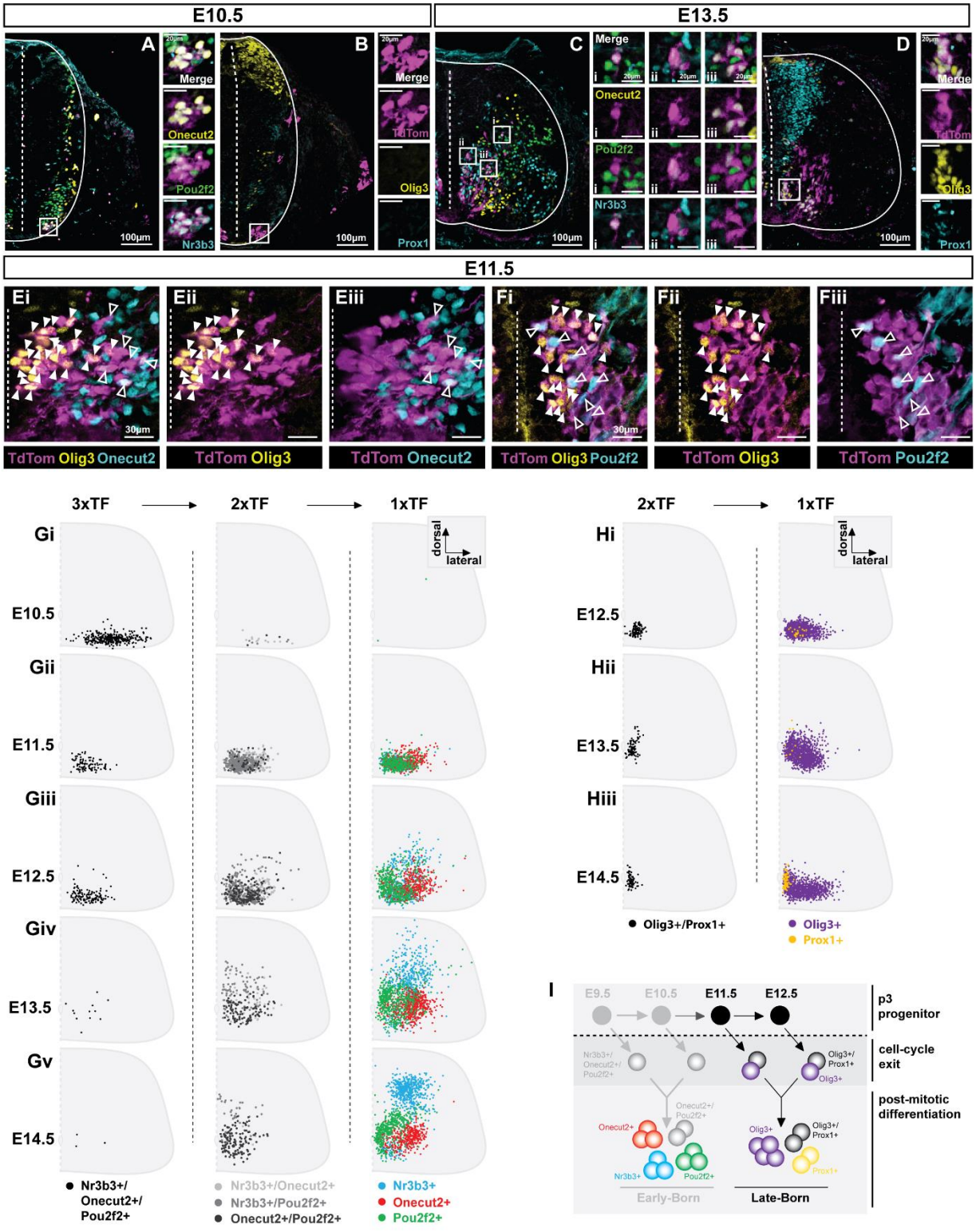

Figure 4.3 Early- and late-born V3 INs continue to molecularly and spatially separate post-mitotically

(A,C) Representative images of Nr3b3, Onecut2 and Pou2f2 immunoreactivity in V3 INs (TdTom) at E10.5 (A) and E13.5 (C) in Sim1Cre;Rosa.lsl.tdTom lumbar sections. (B,D) Representative images of Prox1 and Olig3 immunoreactivity in V3 INs (TdTom) at E10.5 (B) and E13.5 (D) in Sim1Cre;Rosa.lsl.tdTom lumbar sections. (E,F) Representative images of Olig3 with Onecut2 (E) or Pou2f2 (F) immunoreactivity in V3 INs (TdTom) at E11.5 in Sim1Cre;Rosa.lsl.tdTom lumbar sections. (G) Cell distribution plots of V3 INs expressing all three Nr3b3, Onecut2, and Pou2f2 transcription factors (3xTF), two of the three transcription factors (2xTF), or one of the three transcription factors (1xTF) across E10.5 (Gi, n=3), E11.5 (Gii, n=3), E12.5 (Giii, n=3), E13.5 (Giv, n=3), and E14.5 (Gv, n=3). (H) Cell distribution plots of V3 INs expressing both Prox1 and Olig3 (2xTF), or just one of the two transcription factors (1xTF) across E12.5 (Hi, n=2), E13.5 (Hii, n=2), E14.5 (Hiii, n=2). (I) Summary schematic of hierarchal V3 molecular separation. First, differential neurogenesis timing separates V3 INs into either early- and late-born intermediate states. Second, early- and late-born V3 INs further molecularly and spatially specify across post-mitotic stages.

Figure 4.4 V3 axon projection diversity emerges across successive embryonic time points

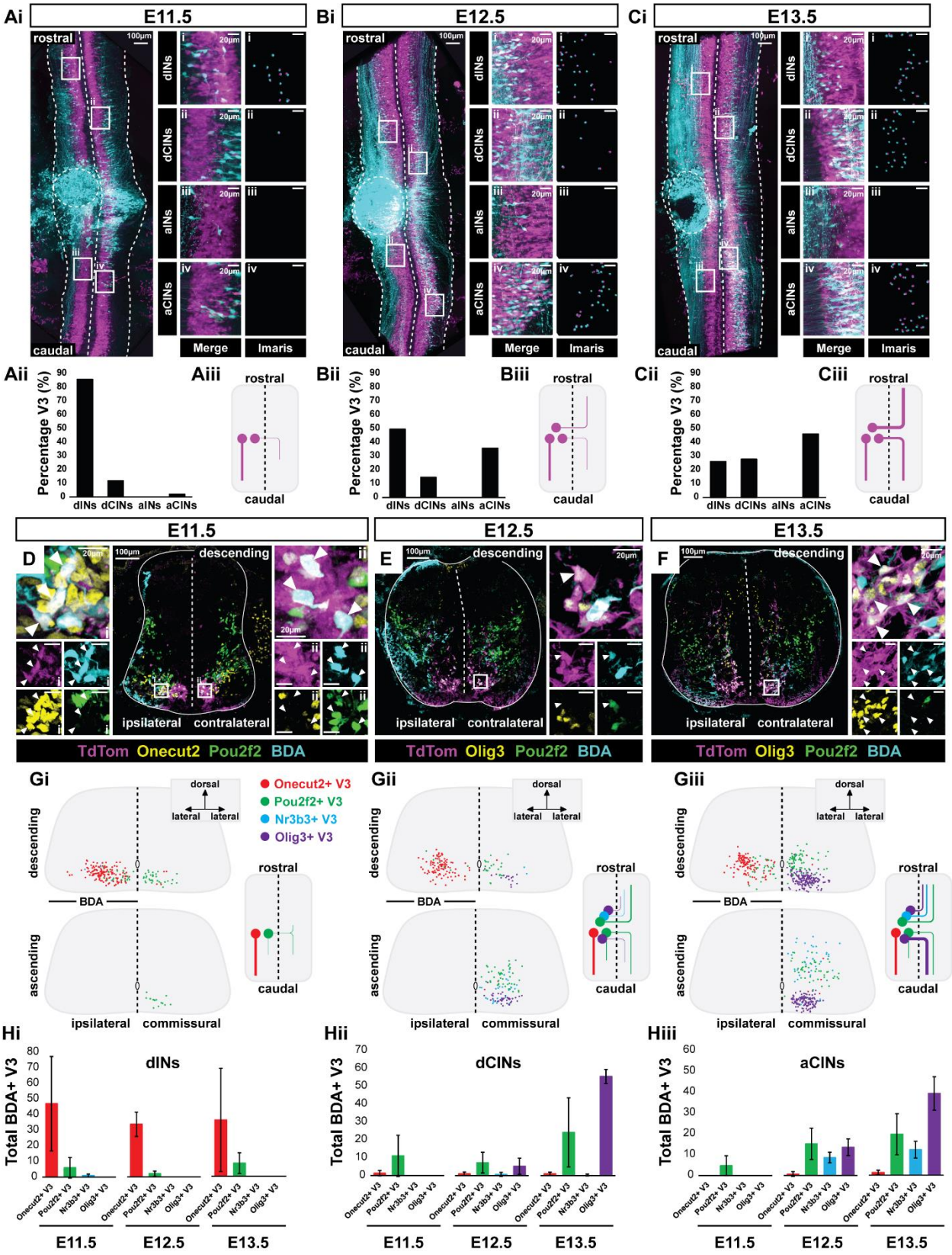

Figure 4.4 V3 axon projection diversity emerges across successive embryonic time points

(Ai-Ci) $Sim1^{Cre}$;Rosa.lsl.tdTom spinal cords injected with Biotin Dextran Amine (BDA) retrograde tract tracer and cleared with Cubic-1 solution at E11.5 (Ai), E12.5 (Bi), and E13.5 (Ci). (Aii-Cii) Percentage of BDA^+ V3 INs that are descending ipsilateral (dINs), descending commissural (dCINs), ascending ipsilateral (aINs), and ascending commissural (aCINs) at E11.5 (Aii), E12.5 (Bii), and E13.5 (Cii). (Aiii-Ciii) Summary schematics V3 IN axon projection phenotypes detected at E11.5 (Aiii), E12.5 (Biii), and E13.5 (Ciii). (D-F) Representative images of coronal sections from $Sim1^{Cre}$;Rosa.lsl.tdTom spinal cords injected with BDA and immunostained post-hoc for V3 specific transcription factors at E11.5 (D), E12.5 (E), and E13.5 (F). (G) Cell distribution plots of $Onecut2^+/BDA^+$, $Pou2f2^+/BDA^+$, $Nr3b3^+/BDA^+$, and $Olig3^+/BDA^+$ V3 INs rostral (descending), caudal (ascending), ipsilateral, and contralateral to the BDA injection site (n=3 animals for each V3 IN subset). (H) Total number of molecularly and anatomically distinct V3 INs retrogradely labeled with BDA across E11.5-E13.5 time points (Hi, descending ipsilateral V3 INs; Hii, descending commissural V3 INs; Hiii, ascending commissural V3 INs; n=3 animals for each V3 IN subset and embryonic timepoint).

Figure 4.5 V3 IN axon projection subtypes differentially assemble across spinal axes by E14.5

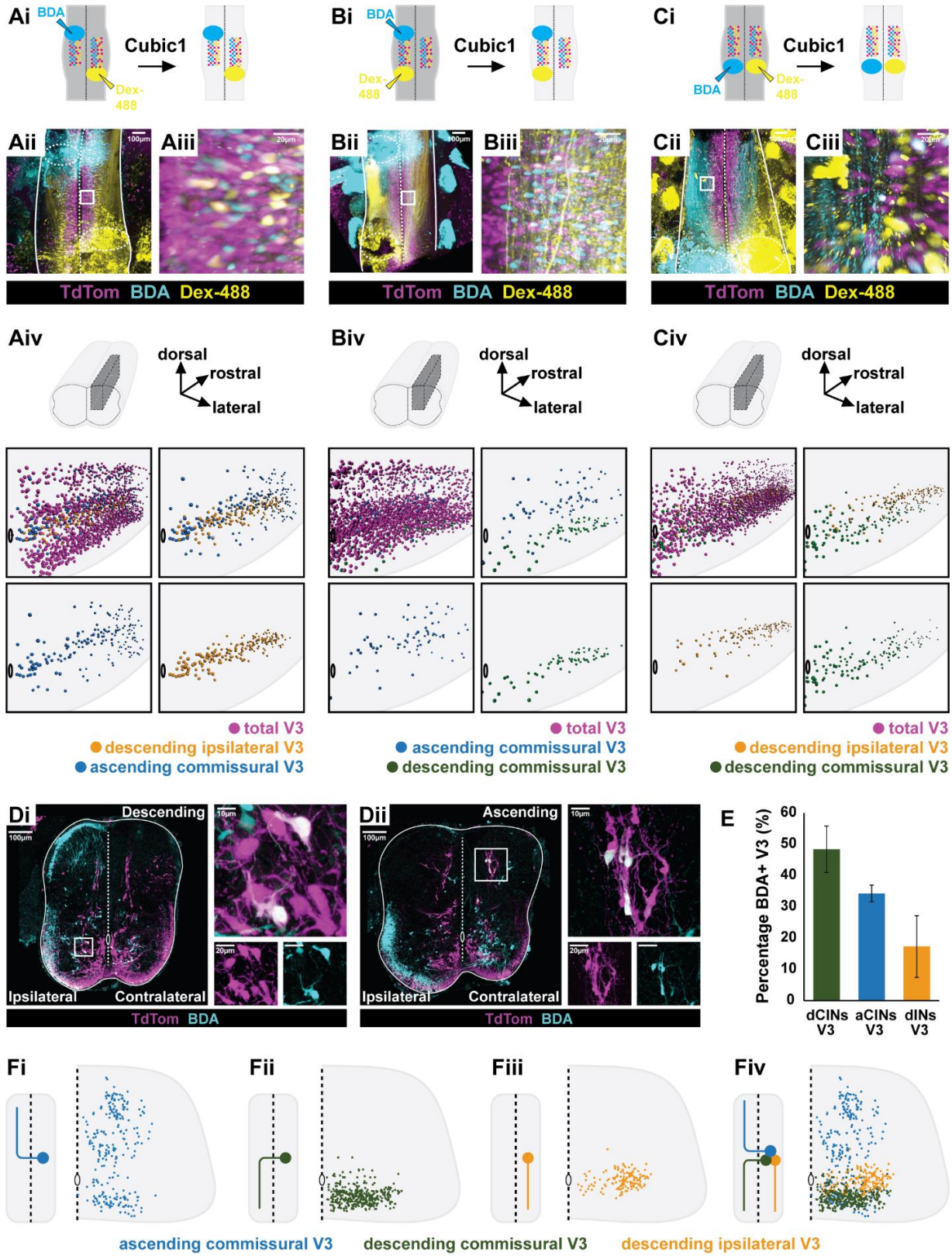

Figure 4.5 V3 IN axon projection subtypes differentially assemble across spinal axes by E14.5

(A-C) Dual retrograde tract tracing combinations (Ai-Ci) of $Sim1^{Cre}$;Rosa.lsl.tdTom spinal cords at E14.5. (Aii,iii-Cii,iii) $Sim1^{Cre}$;Rosa.lsl.tdTom spinal cords cleared with Cubic-1 solution following injections with Biotin Dextran Amine (BDA) and Dextran-488 retrograde tract tracers. (Aiv-Civ) Imaris reconstructed volumes of the relative spatial distributions of distinct V3 axon projection types. (D) Representative images of coronal sections from $Sim1^{Cre}$;Rosa.lsl.tdTom spinal cords injected with BDA at E14.5 [Di, rostral to injection site (descending); Dii, caudal to injection site (ascending)]. (E) Total percentages of V3 axon projection types at E14.5 (n=3). (F) Cell distribution plots of ascending commissural projecting V3 INs (Fi), descending commissural projecting V3 INs (Fii), descending ipsilateral projecting V3 INs (Fiii), and combined V3 projection types (Fiv) [n=3].

Figure 4.6 V3 IN subsets display molecular, spatial, and axon projection specificities by E14.5

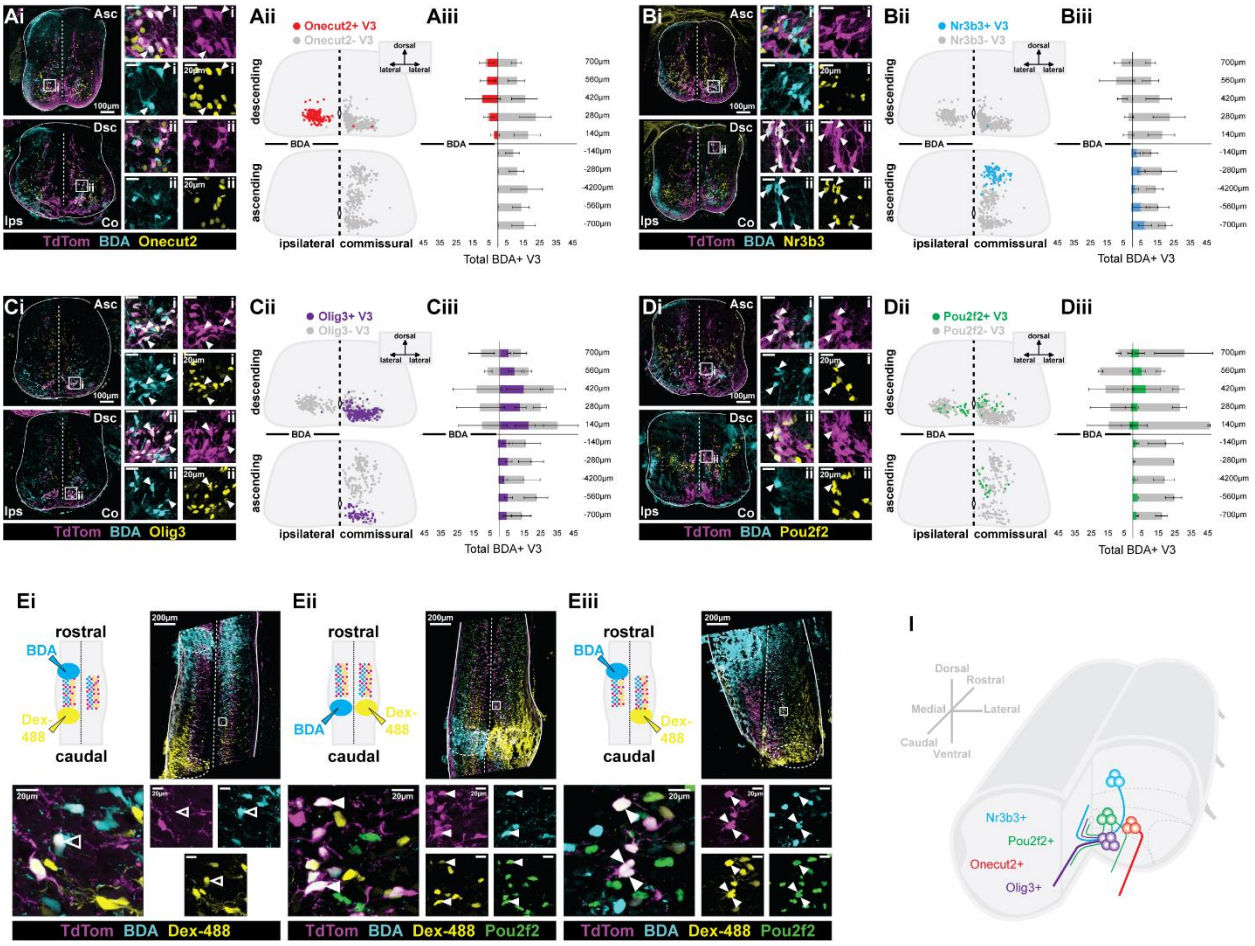

Figure 4.6 V3 IN subsets display molecular, spatial, and axon projection specificities by E14.5

(Ai-Di) Representative images of coronal sections from $Sim1^{Cre}$;Rosa.lsl.tdTom spinal cords injected with BDA and immunolabeled for Onecut2 (Ai), Nr3b3 (Bi), Olig3 (Ci) and Pou2f2 (Di) at E14.5. (Aii-Dii) Cell distribution plots of BDA^+ and $Onecut2^+$ (Aii), $Nr3b3^+$ (Bii), $Olig3^+$ (Cii) and $Pou2f2^+$ (Dii) V3 INs rostral (descending), caudal (ascending), ipsilateral, and contralateral to the BDA injection site (n=3 animals for each V3 IN subset). (Aiii-Diii) Total BDA^+ and $Onecut2^+$ (Aiii), $Nr3b3^+$ (Biii), $Olig3^+$ (Ciii) and $Pou2f2^+$ (Diii) V3 INs rostral (descending), caudal (ascending), ipsilateral, and contralateral to the BDA injection site (n=3 animals for each V3 IN subset). (E) Representative images of longitudinal sections from dual retrograde tract tracing and immunoreactivity of $Sim1^{Cre}$;Rosa.lsl.tdTom spinal cords at E14.5. (I) Summary schematic V3 IN molecular, spatial and axon projection organization in the higher lumbar spinal cord at E14.5.

Figure 4.7 Combined electrophysiological and morphological properties separate V3 IN subpopulations into discrete clusters

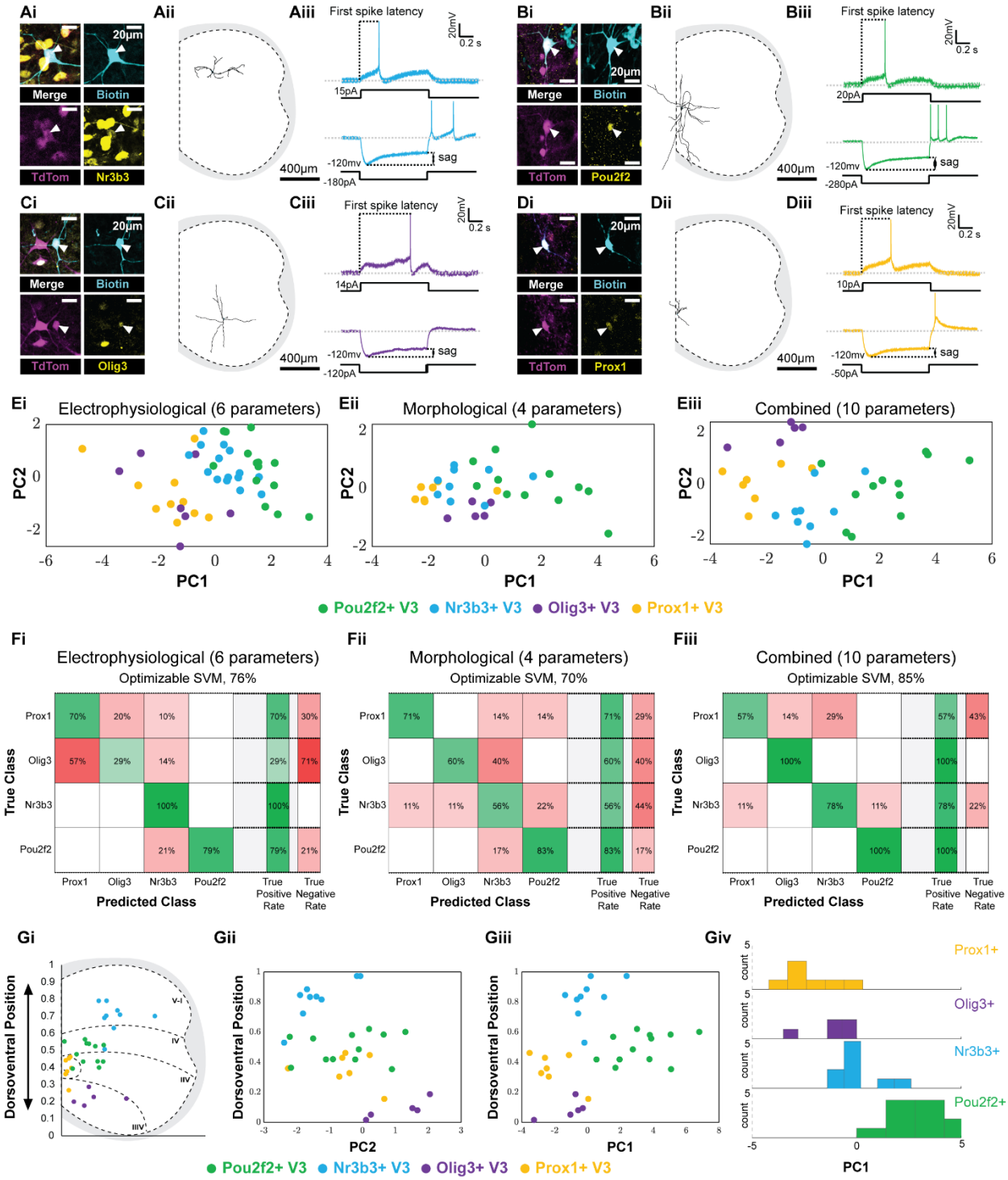

Figure 4.7 Combined electrophysiological and morphological properties separate V3 IN subpopulations into discrete clusters

(Ai-Di) Representative images of patch-clamped and biotin-filled V3 INs immunoreactive for Nr3b3 (Ai), Pou2f2 (Bi), Olig3 (Ci), and Prox1 (Di) between P7 and P12 of $Sim1^{Cre}$;Rosa.lsl.tdTom higher lumbar (L1-L3) spinal cord slices. (Aii-Dii) Example morphology reconstructions of $Nr3b3^{+}$ (Aii), $Pou2f2^{+}$ (Bii), $Olig3^{+}$ (Cii), and $Prox1^{+}$ (Dii) V3 INs. (Aiii-Diii) Representative current-clamp traces of $Nr3b3^{+}$ (Aiii), $Pou2f2^{+}$ (Biii), $Olig3^{+}$ (Ciii), and $Prox1^{+}$ (Diii) V3 INs responding to 1s suprathreshold (top) and subthreshold (bottom) current injections. (E) First (PC1) and second (PC2) principal component plots from electrophysiological (Ei), morphological (Eii), and combined (electrophysiological + morphological, Eiii) principal component analyses of molecularly distinct V3 INs. (Fi) V3 subset prediction accuracies from a support vector machine (SVM) learner. Presented as confusion matrices of electrophysiological (Fi), morphological (Fii), and combined (electrophysiological + morphological, Fiii) predictors. (Gi) Laminar distributions of recorded $Nr3b3^{+}$, $Pou2f2^{+}$, $Olig3^{+}$, and $Prox1^{+}$ V3 INs. (Gii-iii) Molecularly distinct V3 PC2 (Gii) and PC1 (Gi) scores plotted against their dorsoventral positions. (Giv) Histogram distributions of $Prox1^{+}$, $Olig3^{+}$, $Pou2f2^{+}$, and $Nr3b3^{+}$ V3 IN PC1 scores.

Figure 4.8 Neurogenesis timing separates V3 IN intrinsic properties into early-born or late-born identities

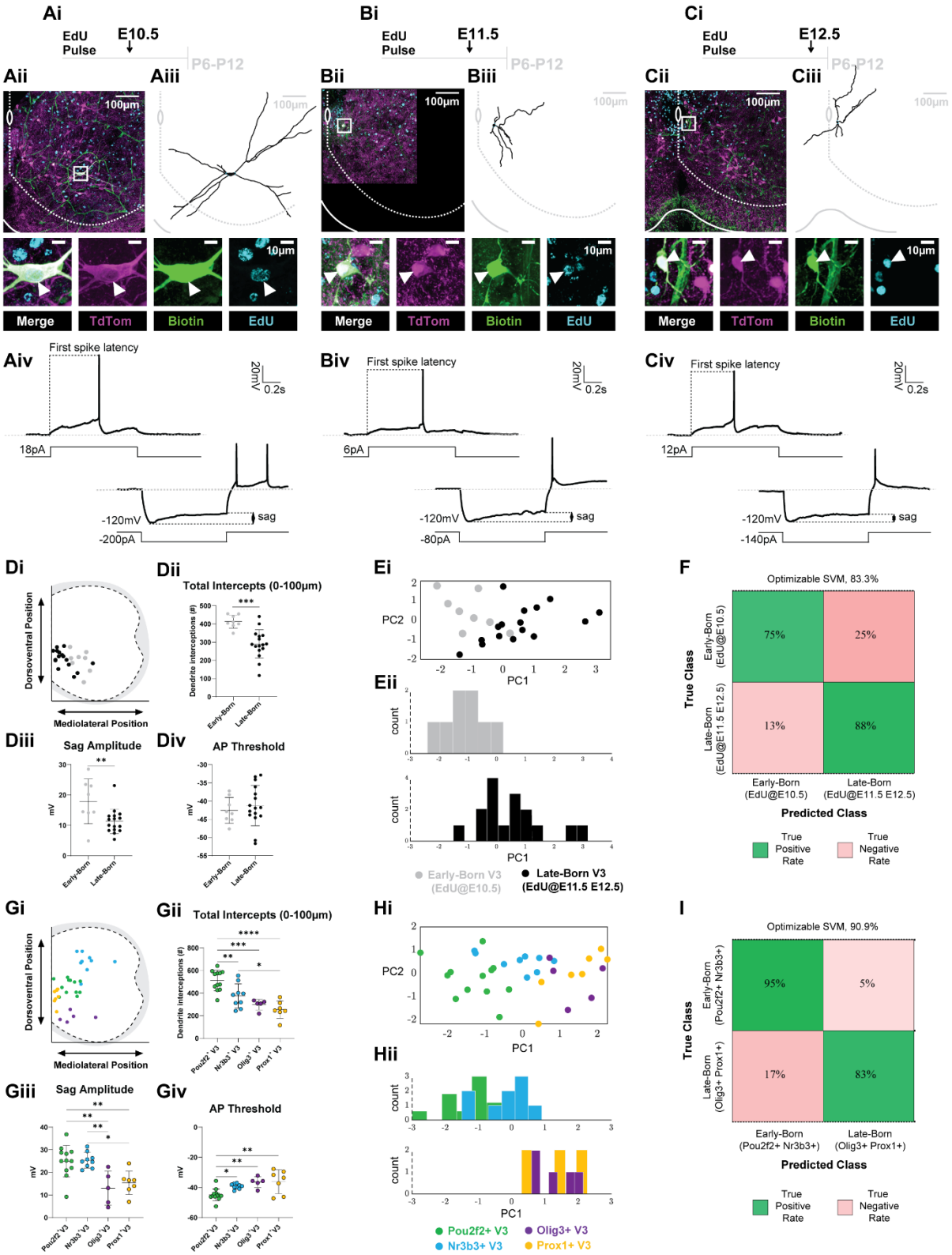

Figure 4.8 Neurogenesis timing separates V3 IN intrinsic properties into early-born or late-born identities

(Ai-Ci) Experimental schematics of EdU injection and postnatal recording times (Ai, EdU@E10.5; Bi, EdU@11.5; Ci, EdU@E12.5) (Aii-Cii) Representative images of patch-clamped and biotin-filled V3 INs immunoreactive for E10.5 EdU^+ V3 (Aii), E11.5 EdU^+ V3 (Bii), E12.5 EdU^+ V3 (Cii) between P6 and P12 of $Sim1^{Cre}$;Rosa.lsl.tdTom higher lumbar (L1-L3) spinal cord slices. (Aiii-Ciii) Example morphology reconstructions of E10.5 EdU^+ V3 (Aiii), E11.5 EdU^+ V3 (Biii), E12.5 EdU^+ V3 (Ciii). (Aiv-Civ) Representative current-clamp traces of E10.5 EdU^+ V3 (Aiv), E11.5 EdU^+ V3 (Biv), E12.5 EdU^+ V3 (Civ) responding to 1s suprathreshold (top) and subthreshold (bottom) current injections. (Di) Laminar distributions of recorded early-born (EdU@E10.5, grey) and late-born (EdU@E11.5 & E12.5, black). (Dii-iv) Comparison of early-born (EdU@E10.5) versus late-born (EdU@E11.5 & E12.5) total intercepts (0-100µm) (Dii), sag amplitude (@-120mV) (Diii), and action potential (AP) threshold (Div) [early-born, n=8 cells; late-born, n=16 cells; * p-value < 0.05, ** p-value < 0.01, *** p-value < 0.001, unpaired t-test]. (Ei) First (PC1) and second (PC2) principal component plots of early-born (EdU@E10.5, grey) and late-born (EdU@E11.5 & E12.5, black) V3 INs using total intercepts (0-100µm), sag amplitude (@-120mV) (Diii), and action potential (AP) threshold. (Eii) Histogram distributions of early-born (EdU@E10.5, grey) and late-born (EdU@E11.5 & E12.5, black) V3 PC1 scores. (F) Early-born (EdU@E10.5) and late-born (EdU@E11.5 & E12.5) V3 IN prediction accuracies from a support vector machine (SVM) learner. Presented as confusion a matrix. (Gi) Laminar distributions of recorded $Nr3b3^+$, $Pou2f2^+$, $Olig3^+$, and $Prox1^+$ V3 INs. (Gii-iv) Comparison of $Nr3b3^+$, $Pou2f2^+$, $Olig3^+$, and $Prox1^+$ V3 IN total intercepts (0-100µm) (Gii), sag amplitude (@-120mV) (Giii), and action potential (AP)

threshold (Giv) [Pou2f2$^+$ V3, n=12 cells; Nr3b3$^+$ V3, n=9 cells; Olig3$^+$ V3, n=5 cells; Prox1$^+$ V3, n=7 cells; * p-value < 0.05, ** p-value < 0.01, *** p-value < 0.001, **** p-value < 0.0001, one-way ANOVA & Tukey's multiple comparisons test]. (Hi) First (PC1) and second (PC2) principal component plots of Nr3b3$^+$, Pou2f2$^+$, Olig3$^+$, and Prox1$^+$ V3 INs using total intercepts (0-100µm), sag amplitude (@-120mV), and action potential (AP) threshold. (Hii) Histogram distributions of Nr3b3$^+$, Pou2f2$^+$, Olig3$^+$, and Prox1$^+$ V3 IN histogram scores. (I) Early-born (Pou2f2$^+$ & Nr3b3$^+$ V3) and late-born (Olig3$^+$ & Prox1$^+$ V3) V3 IN prediction accuracies from a support vector machine (SVM) learner. Presented as a confusion matrix.

Figure 4.9 V3 IN subpopulations diversify across hierarchical temporal and spatial developmental pathways

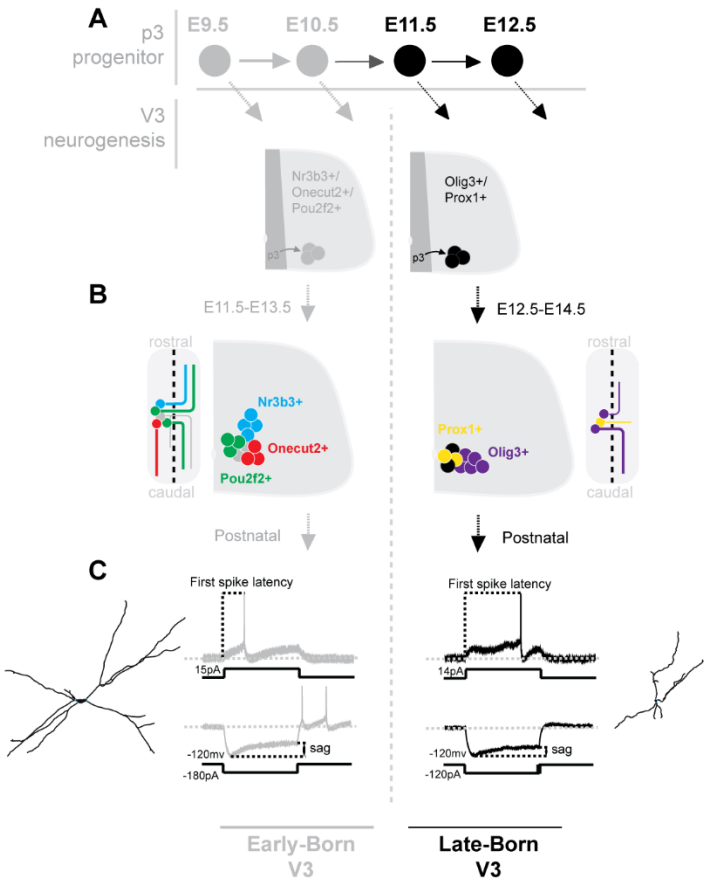

Figure 4.9 V3 IN subpopulations diversify across hierarchical temporal and spatial developmental pathways

(A) Differential neurogenesis timing separates V3 INs into early-born (E9.5-E10.5; Pou2f2/Nr3b3/Onecut2 expression) or late-born (E11.5-E12.5; Olig3/Prox1 expression) temporal subclasses. (B) Early post-mitotic (E11.5-E14.5) spatial mechanisms separate V3 INs within temporal subclasses into molecularly and anatomically distinct subpopulations. (C) By postnatal stages, early-born and late-born V3 temporal subclasses display electrophysiologically and morphologically distinct identities.

7. Supplemental Figures

Supplemental Figure 4.1 Transcription factor expressions in V3 INs at P0

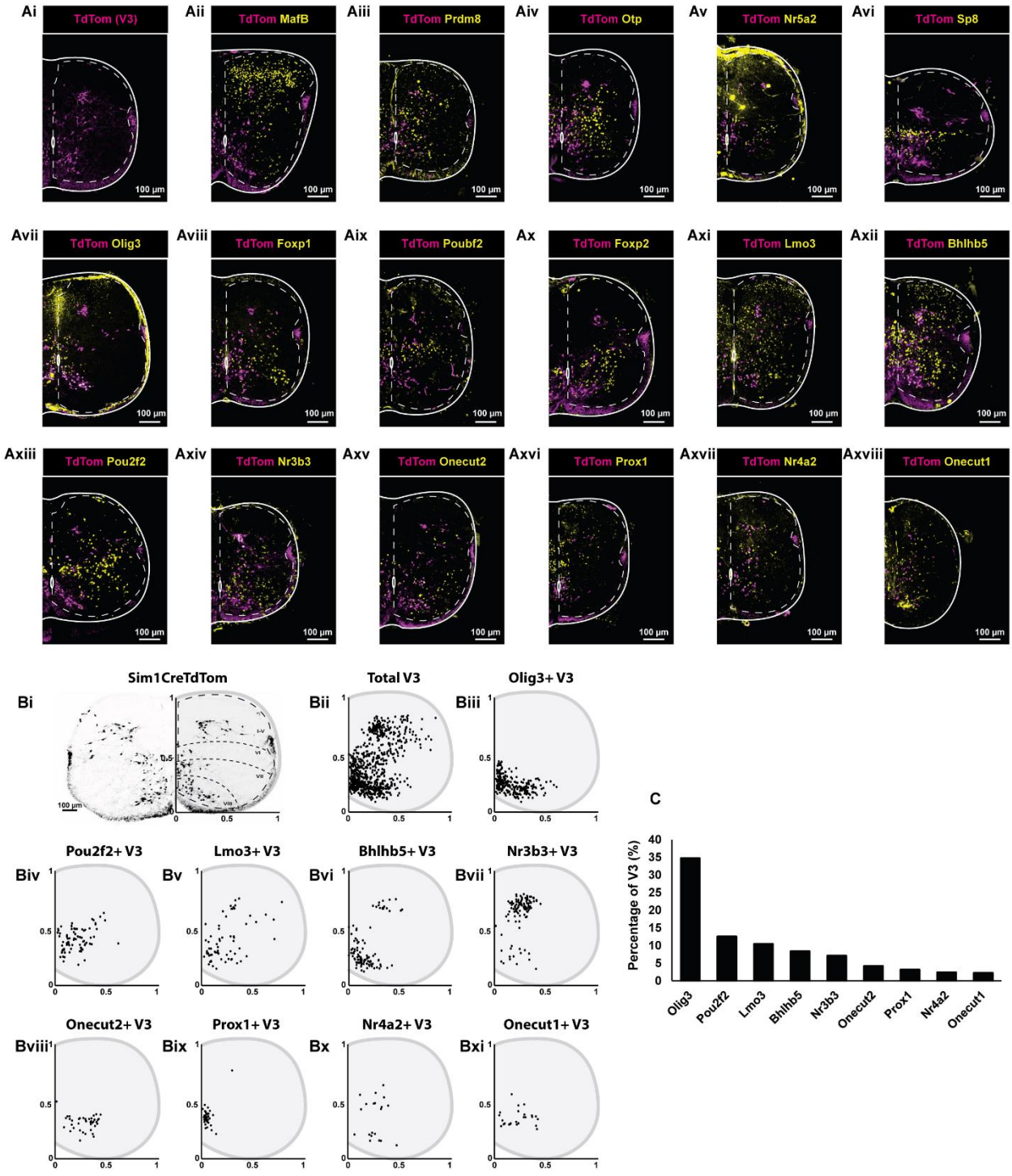

Supplemental Figure 4.1 Transcription factor expressions in V3 INs at P0

(Ai-Axviii) Representative images of transcription factor immunoreactivities in V3 INs (TdTom) in higher lumbar (L1-L3) spinal cord sections from Sim1Cre;Rosa.lsl.tdTom P0 mice. (Bi-Bxi) V3 laminar distribution plots of transcription factor expressing V3 INs (n=1). (C) Percentage of total V3 INs expressing transcription factor (n=1)

Supplemental Figure 4.2 Dual transcription factor expressions in V3 INs at P0

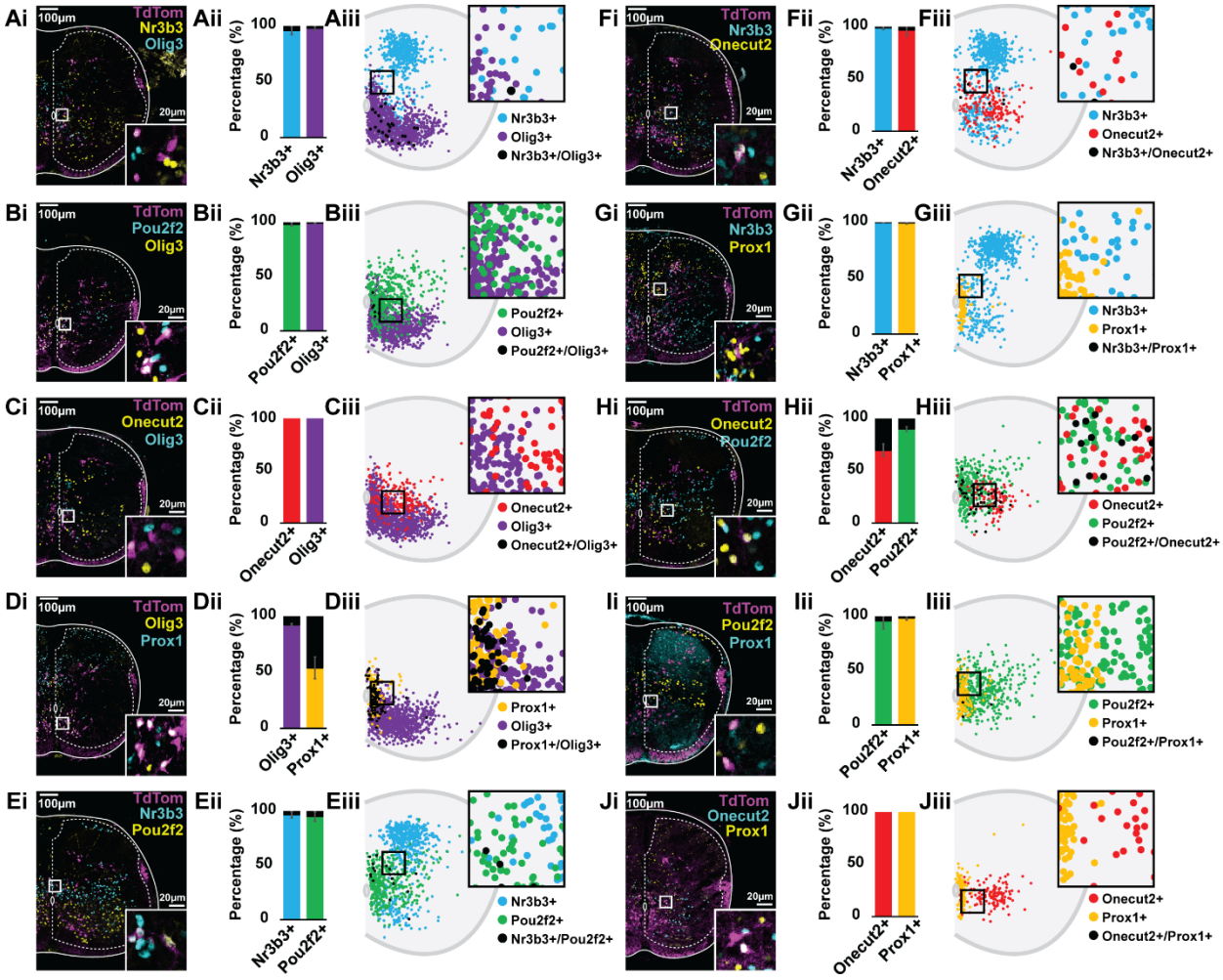

Supplemental Figure 4.2 Dual transcription factor expressions in V3 INs at P0

(Ai-Ji) Representative images of dual transcription factor immunoreactivities in V3 INs (TdTom) in higher lumbar (L1-L3) spinal cord sections from Sim1Cre;Rosa.lsl.tdTom P0 mice. (Aii-Jii) Co-expression percentages of transcription factors in V3 IN subsets. (Aiii-Jiii) V3 laminar distribution plots of single expression and co-expression V3 INs (n=4 animals per combination)

Supplemental Figure 4.3 V3 IN spatial distributions during early embryogenesis

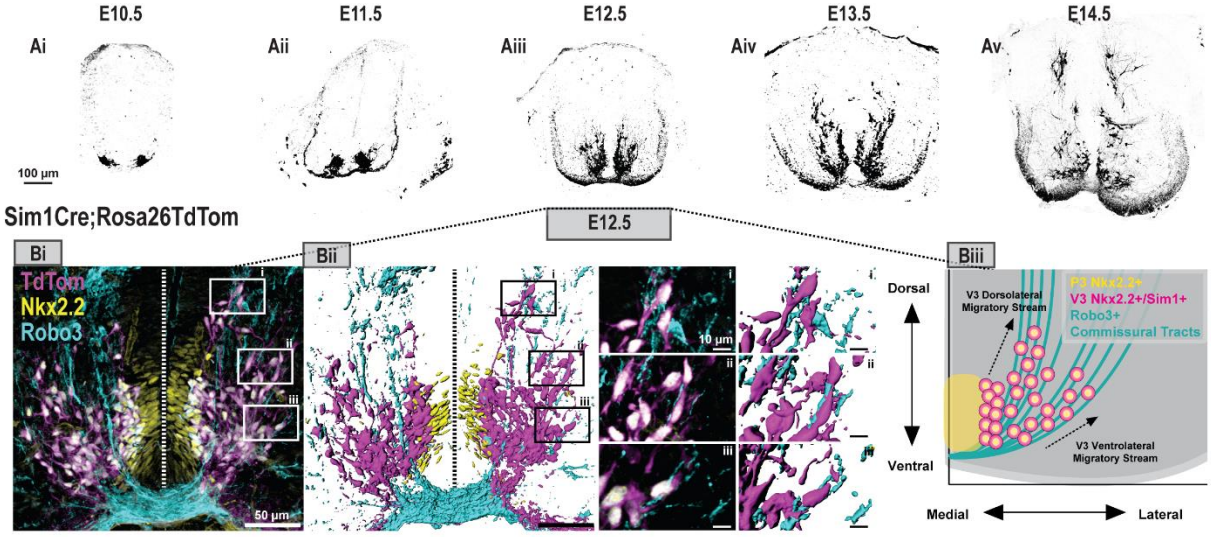

Supplemental Figure 4.3 V3 IN spatial distributions during early embryogenesis

(Ai-Ji) Representative images of V3 INs (TdTom) across E10.5-E14.5 stages from higher lumbar Sim1Cre;Rosa.lsl.tdTom spinal cords. (B) Representative image at E12.5 of V3 INs (TdTom) exiting from the p3 progenitor domain (Nkx2.2) and migrating along the Robo3^{+} commissural processes of dorsal spinal INs (Laumonnerie et al., 2015). (Bi, three-dimensional confocal image take with a 40x objective; Bii, Imaris reconstruction of confocal images; Biii, summary schematic of V3 INs at E12.5).

Supplemental Figure 4.4 V3 axon projections at E11.5

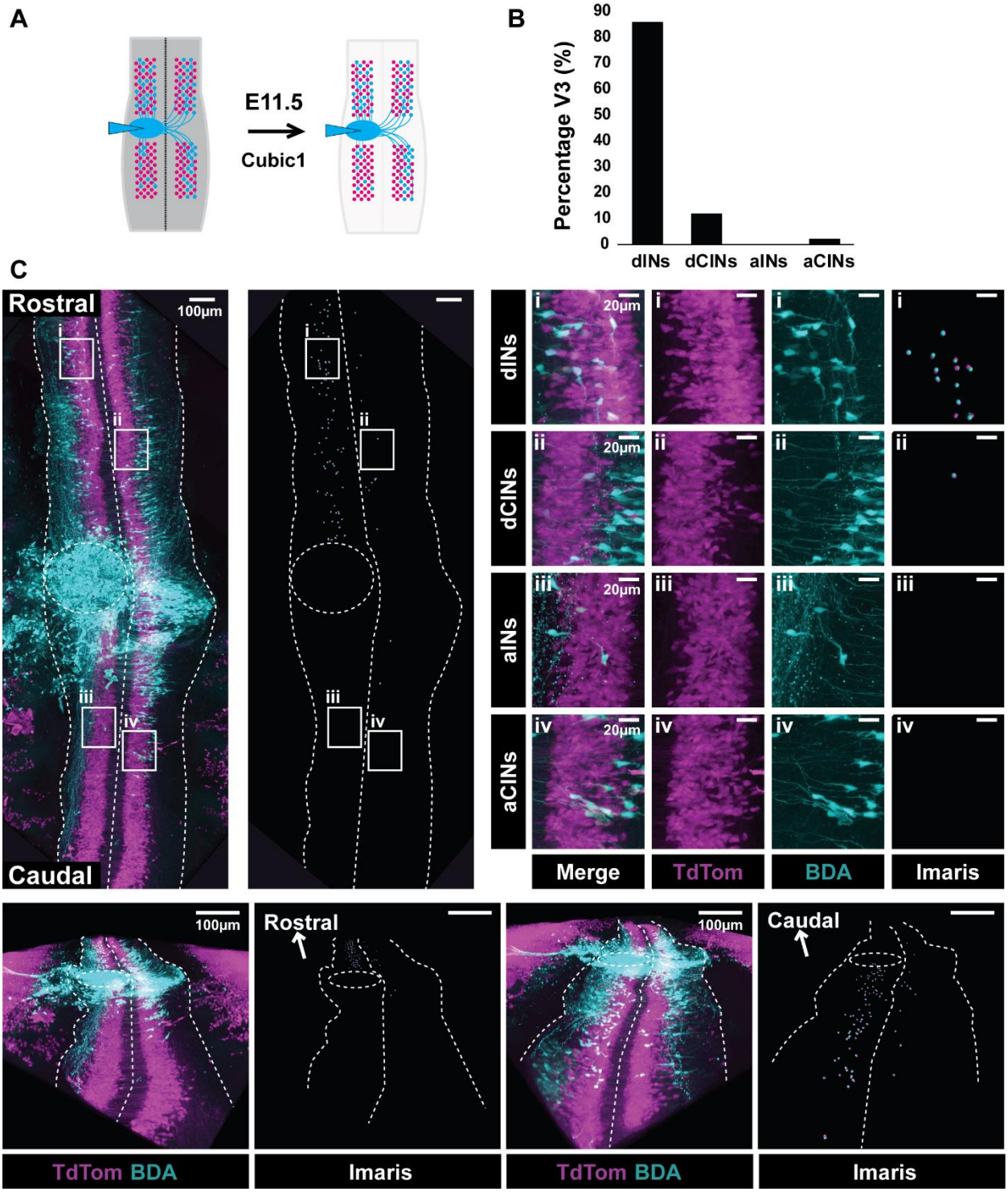

Supplemental Figure 4.4 V3 axon projections at E11.5

(A) Experimental schematic of retrograde biotin-dextran-amine (BDA) tract tracing in a Sim1Cre;Rosa.lsl.tdTom spinal cord followed by tissue clearing with Cubic-1 solution at E11.5. (B) Percentage of total projecting V3 INs that are descending ipsilateral INs (dINs), descending commissural INs (dCINs), ascending ipsilateral (aINs) and ascending commissural INs (aCINs) at E11.5 (n=1). (C) Representative images of BDA^{+} and V3 INs in a cleared Sim1Cre;Rosa.lsl.tdTom spinal cord at E11.5.

Supplemental Figure 4.5 V3 axon projections at E12.5

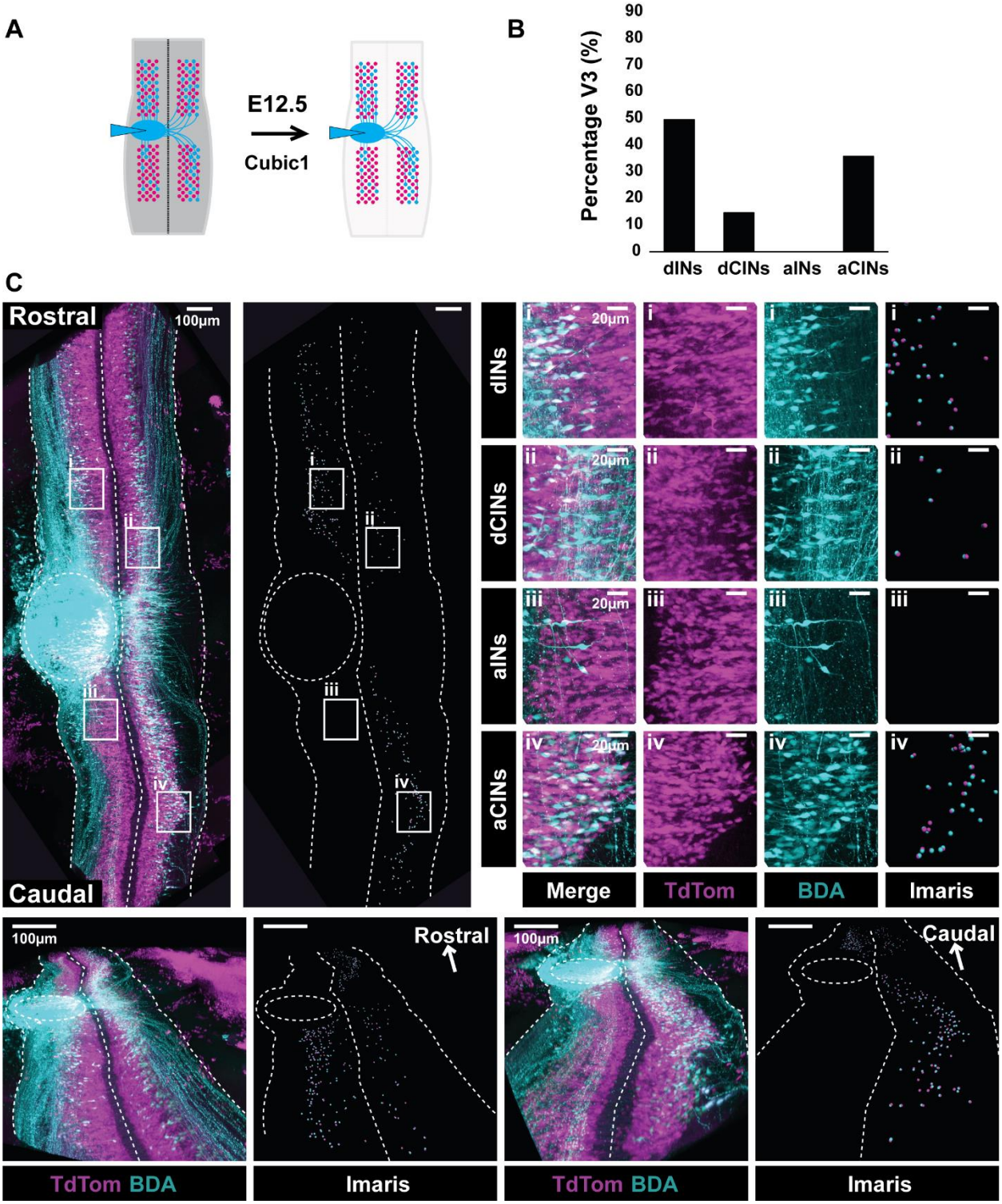

Supplemental Figure 4.5 V3 axon projections at E12.5

(A) Experimental schematic of retrograde biotin-dextran-amine (BDA) tract tracing in a Sim1Cre;Rosa.lsl.tdTom spinal cord followed by tissue clearing with Cubic-1 solution at E12.5. (B) Percentage of total projecting V3 INs that are descending ipsilateral INs (dINs), descending commissural INs (dCINs), ascending ipsilateral (aINs) and ascending commissural INs (aCINs) at E12.5 (n=1). (C) Representative images of BDA^{+} and V3 INs in a cleared Sim1Cre;Rosa.lsl.tdTom spinal cord at E12.5.

Supplemental Figure 4.6 V3 axon projections at E13.5

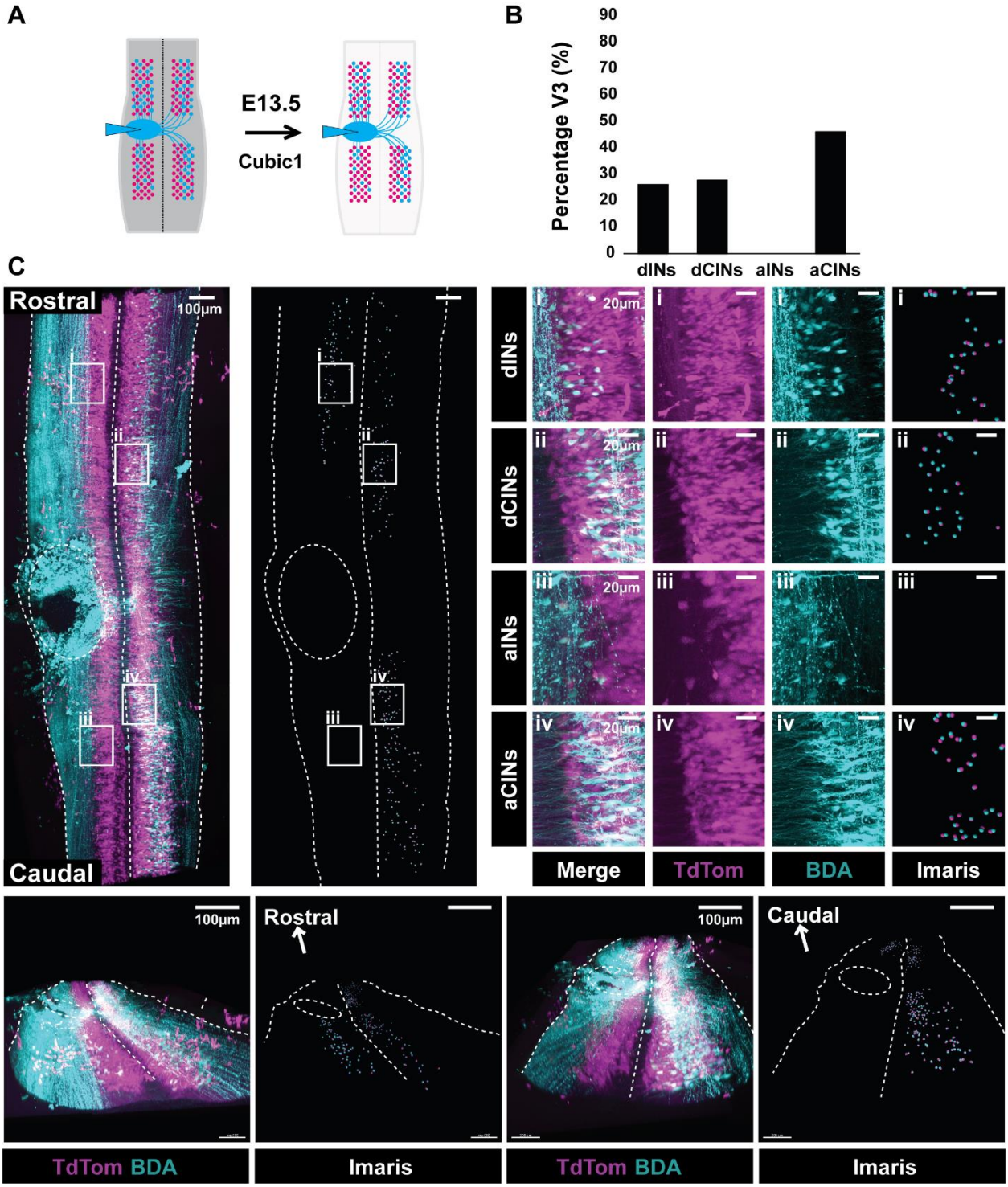

Supplemental Figure 4.6 V3 axon projections at E13.5

(A) Experimental schematic of retrograde biotin-dextran-amine (BDA) tract tracing in a Sim1Cre;Rosa.lsl.tdTom spinal cord followed by tissue clearing with Cubic-1 solution at E13.5. (B) Percentage of total projecting V3 INs that are descending ipsilateral INs (dINs), descending commissural INs (dCINs), ascending ipsilateral (aINs) and ascending commissural INs (aCINs) at E13.5 (n=1). (C) Representative images of BDA^{+} and V3 INs in a cleared Sim1Cre;Rosa.lsl.tdTom spinal cord at E13.5.

Supplemental Figure 4.7 Dual retrograde tract tracing of V3 INs at E14.5: commissural ascending and ipsilateral descending

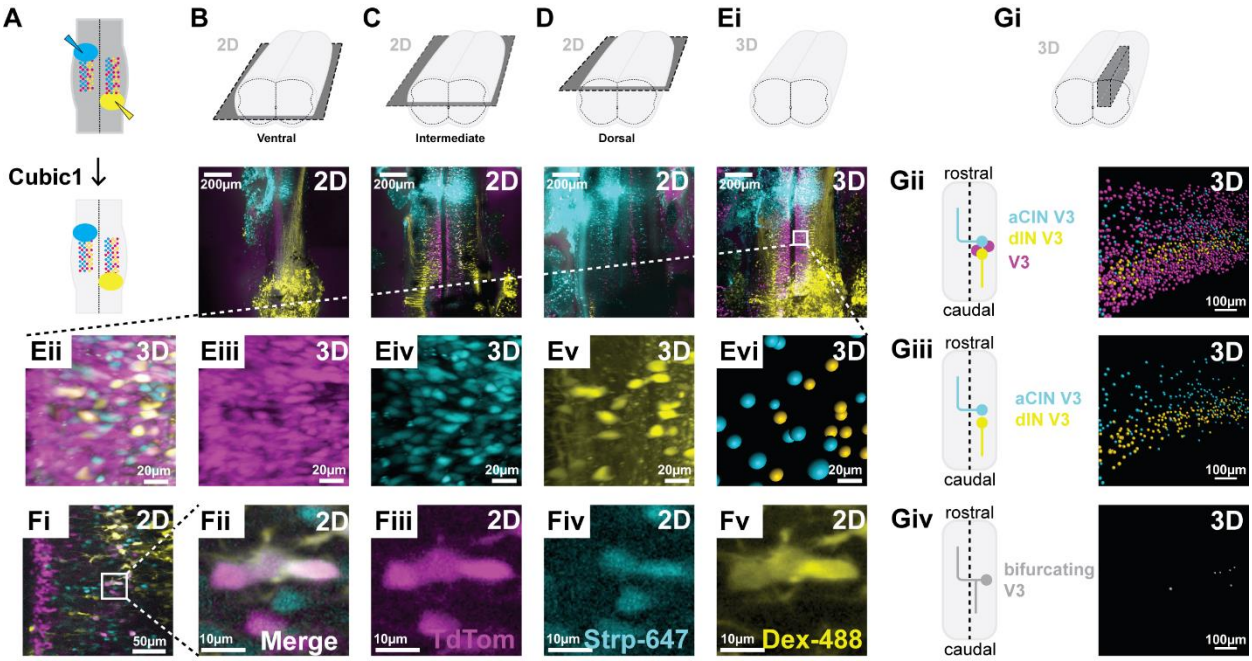

Supplemental Figure 4.7 Dual retrograde tract tracing of V3 INs at E14.5: commissural ascending and ipsilateral descending

(A) Experimental schematic of dual retrograde biotin-dextran-amine (BDA) and Dextran-488 tract tracing in a Sim1Cre;Rosa.lsl.tdTom spinal cord followed by tissue clearing with Cubic-1 solution at E14.5. (B-C) Two-dimensional optical sections at a ventral location (B), intermediate location (C), and dorsal location (D). (E) Three dimension confocal images (Ei-v) and imaris reconstruction (teal spots, ascending commissural V3 INs; yellow spots, descending ipsilateral V3 INs) in cleared spinal cord. (F) Example two-dimensional optical section of bifurcating V3 IN. (G) Imaris reconstructed volumes of the relative spatial distributions of total V3 INs (magenta spots), ascending commissural V3 INs (teal spots), descending ipsilateral V3 INs (yellow spots), and bifurcating V3 INs (grey spots).

Supplemental Figure 4.8 Dual retrograde tract tracing of V3 INs at E14.5: commissural ascending and commissural descending

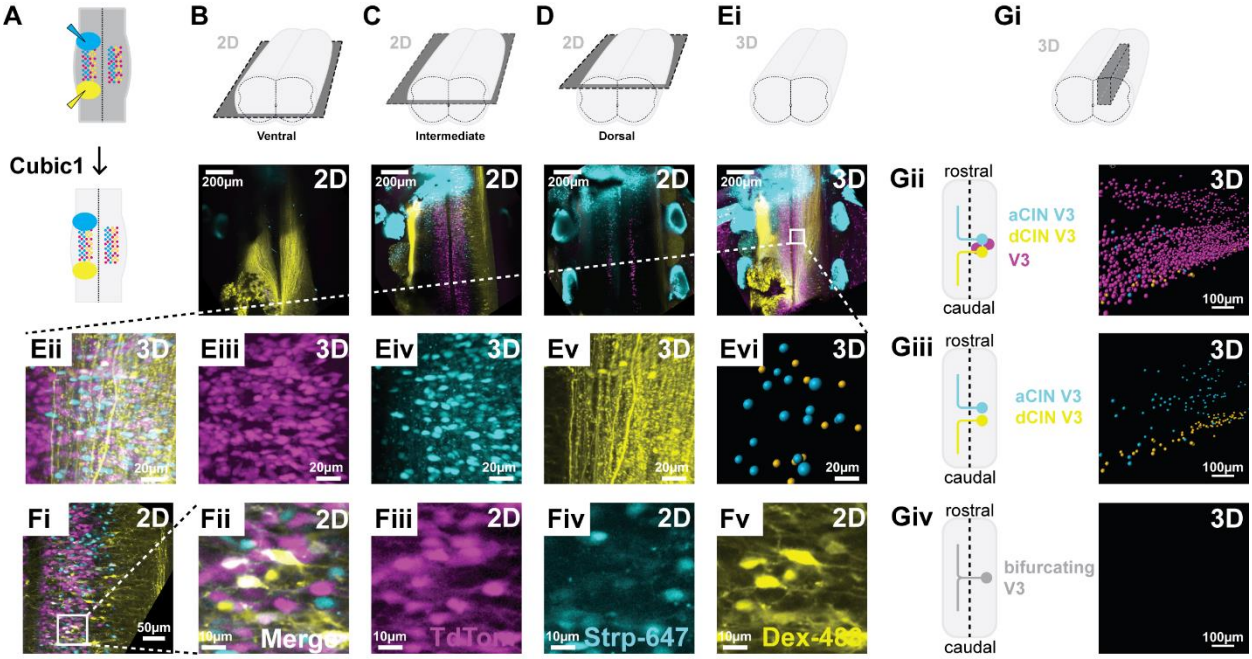

Supplemental Figure 4.8 Dual retrograde tract tracing of V3 INs at E14.5: commissural ascending and commissural descending

(A) Experimental schematic of dual retrograde biotin-dextran-amine (BDA) and Dextran-488 tract tracing in a Sim1Cre;Rosa.lsl.tdTom spinal cord followed by tissue clearing with Cubic-1 solution at E14.5. (B-C) Two-dimensional optical sections at a ventral location (B), intermediate location (C), and dorsal location (D). (E) Three-dimension confocal images (Ei-v) and imaris reconstruction (teal spots, ascending commissural V3 INs; yellow spots, descending commissural V3 INs) in cleared spinal cord. (F) Example two-dimensional optical section of ascending and descending commissural V3 INs. (G) Imaris reconstructed volumes of the relative spatial distributions of total V3 INs (magenta spots), ascending commissural V3 INs (teal spots), descending commissural V3 INs (yellow spots), and bifurcating V3 INs (grey spots).

Supplemental Figure 4.9 Dual retrograde tract tracing of V3 INs at E14.5: commissural descending and ipsilateral descending

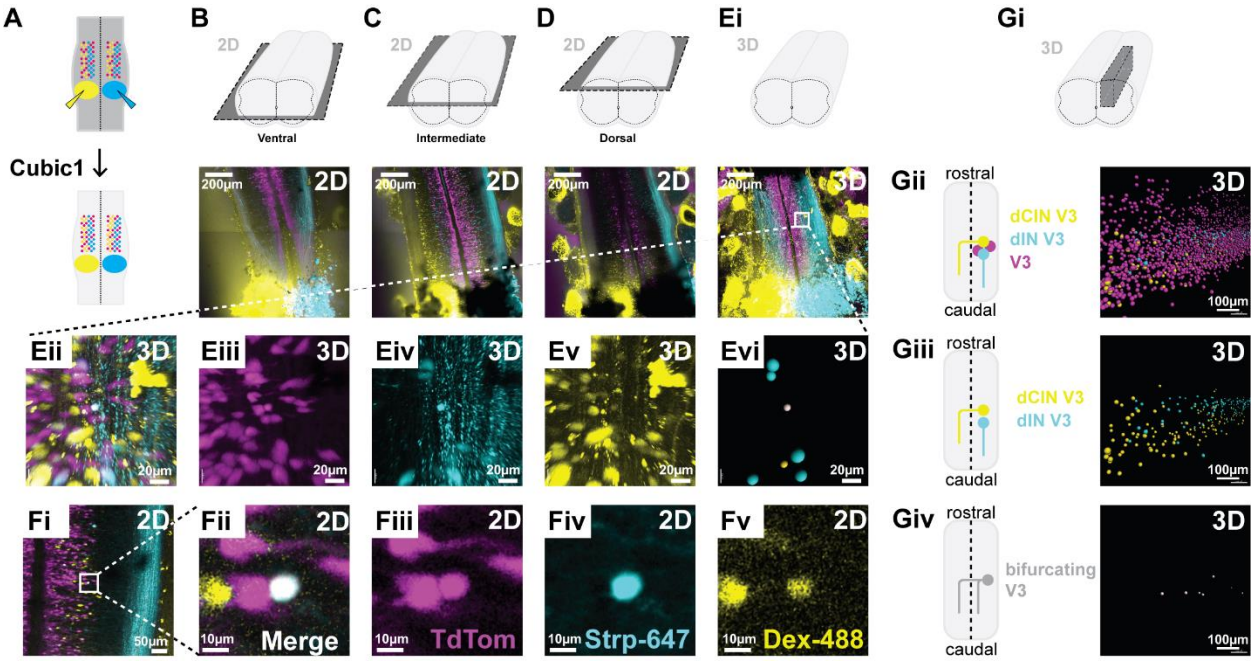

Supplemental Figure 4.9 Dual retrograde tract tracing of V3 INs at E14.5: commissural descending and ipsilateral descending

(A) Experimental schematic of dual retrograde biotin-dextran-amine (BDA) and Dextran-488 tract tracing in a Sim1Cre;Rosa.lsl.tdTom spinal cord followed by tissue clearing with Cubic-1 solution at E14.5. (B-C) Two-dimensional optical sections at a ventral location (B), intermediate location (C), and dorsal location (D). (E) Three-dimension confocal images (Ei-v) and imaris reconstruction (teal spots, descending ipsilateral V3 INs; yellow spots, descending commissural V3 INs; grey spots, bifurcating V3 INs) in cleared spinal cord. (F) Example two-dimensional optical section of bifurcating V3 IN. (G) Imaris reconstructed volumes of the relative spatial distributions of total V3 INs (magenta spots), descending commissural V3 INs (yellow spots), descending ipsilateral V3 INs (teal spots), and bifurcating V3 INs (grey spots).

Supplemental Figure 4.10 Example sholl analyses of molecularly distinct V3 IN subpopulations

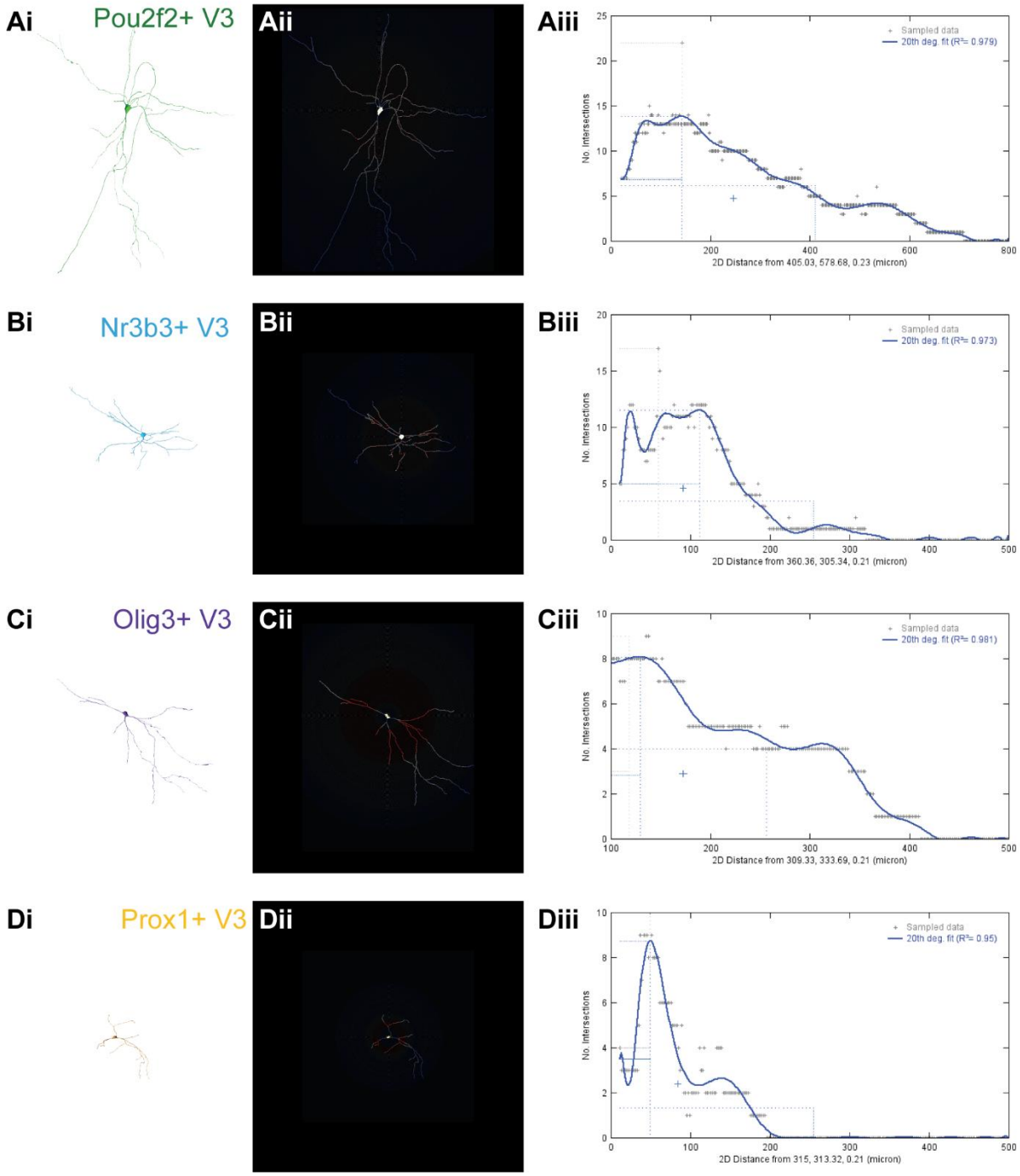

Supplemental Figure 4.10 Example sholl analyses of molecularly distinct V3 IN subpopulations

(A-Di) 3D morphological reconstruction with Imaris software. (A-Dii) Concentric circles (2micron increments) from sholl analysis with FIJI (Red, higher density dendritic intercepts on concentric circle; Blue, lower density dendritic intercepts on concentric circle). (A-Diii) Number of dendritic intercepts with increasing distance from soma.

Supplemental Figure 4.11 Significant electrophysiological and morphological V3 IN properties

A

	Prox1+ V3	Olig3+ V3	Nr3b3+ V3	Pou2f2+ V3	ANOVA (p-value)
Capacitance	33.2 +/- 1.056	37.71 +/- 1.315	67.93 +/- 2.455	104 +/- 5.299	3.88E-09
Input Resistance	0.83 +/- 0.058	0.43 +/- 0.039	0.27 +/- 0.014	0.21 +/- 0.014	1.45E-07
Resting Potential	70.06 +/- 1.132	80.1 +/- 0.534	86.33 +/- 1.526	93.49 +/- 1.042	1.96E-07
Sag Amplitude (120mV)	14.01 +/- 0.769	13.59 +/- 1.15	26.2 +/- 0.75	25.97 +/- 1.016	1.59E-06
Sag Slope (linear)	0.63 +/- 0.059	0.43 +/- 0.035	0.14 +/- 0.007	0.2 +/- 0.014	5.99E-06
Rheobase	0.64 +/- 0.061	0.43 +/- 0.04	0.14 +/- 0.007	0.19 +/- 0.014	9.33E-06
Rheobase Spike Latency	17.09 +/- 1.187	20.97 +/- 0.826	25.48 +/- 1.252	34.27 +/- 0.913	9.44E-06
AP Threshold (first spike)	(-)34.67 +/- 1.035	(-)38.54 +/- 0.67	(-)40.1 +/- 0.33	(-)44.98 +/- 0.535	1.61E-05
First Spike Latency	0.89 +/- 0.065	0.46 +/- 0.04	0.32 +/- 0.026	0.39 +/- 0.031	5.57E-05
First Spike Frequency	0.42 +/- 0.049	0.24 +/- 0.033	0.09 +/- 0.003	0.07 +/- 0.004	5.59E-05
Frequency Adaptation	18.3 +/- 0.338	20.6 +/- 0.456	20.75 +/- 0.587	14.24 +/- 0.583	6.84E-05
Afterhyperpolarization	0.43 +/- 0.051	0.24 +/- 0.035	0.09 +/- 0.003	0.07 +/- 0.004	1.02E-04
AP Threshold (10Hz)	(-)33.94 +/- 0.996	(-)38.71 +/- 0.692	(-)38.47 +/- 0.493	(-)43.19 +/- 0.414	1.16E-04

B

	Prox1+ V3	Olig3+ V3	Nr3b3+ V3	Pou2f2+ V3	ANOVA (p-value)
Total Intercepts (0-100µm)	254.14 +/- 13.383	298.2 +/- 8.06	375.67 +/- 18.568	511.83 +/- 15.789	4.30E-06
Max Intercepts	9.43 +/- 0.511	9.2 +/- 0.335	13 +/- 0.628	18.58 +/- 0.702	6.38E-06
Total Intercepts (100-200µm)	88.29 +/- 14.516	278.2 +/- 18.996	200.78 +/- 19.3	428.67 +/- 25.679	1.42E-05
Mean Intercepts	1.56 +/- 0.163	3.39 +/- 0.167	2.75 +/- 0.224	4.98 +/- 0.253	2.45E-05
Cell Body Volume	693.93 +/- 33.835	1240.79 +/- 28.948	1582.05 +/- 101.887	3791.57 +/- 362.679	8.74E-05
Sum Intercepts	383.14 +/- 39.977	829.8 +/- 40.949	666.56 +/- 52.879	1502.33 +/- 127.694	2.27E-04
Total Primary Dendrites	3.86 +/- 0.234	4 +/- 0.123	5.56 +/- 0.215	6.5 +/- 0.252	4.12E-04

Ci

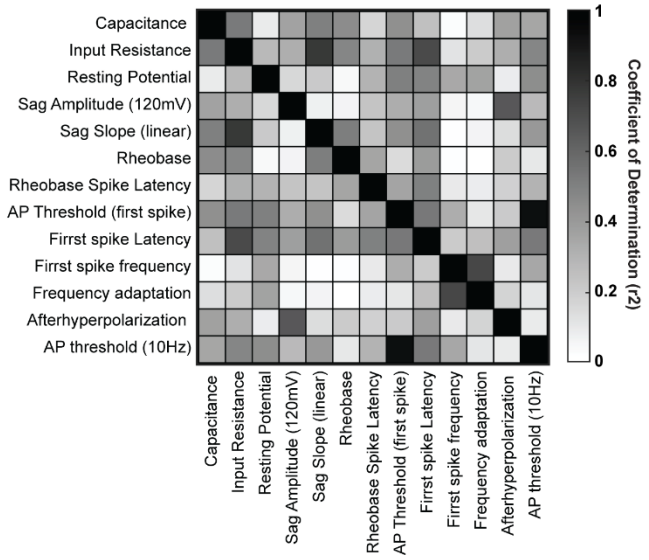

Cii

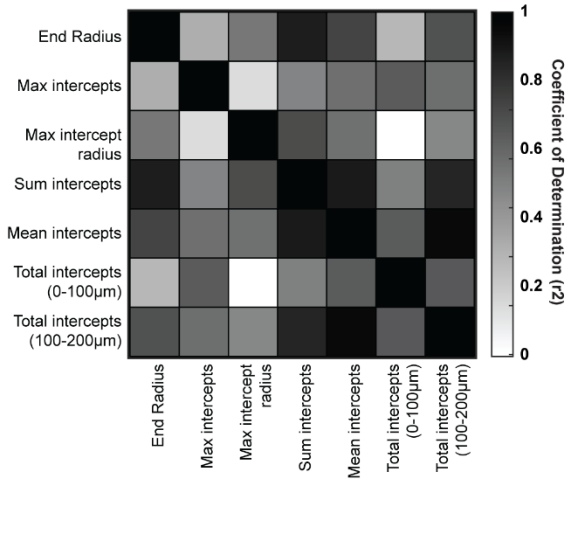

Supplemental Figure 4.11 Significant electrophysiological and morphological V3 IN properties

(A-B) Significant electrophysiological properties (A) and morphological properties (B) between Prox1^{+}, Olig3^{+}, Nr3b3^{+} and Pou2f2^{+} V3 INs. (C) Correlation matrixes between significant electrophysiological properties (Ci) and morphological properties (Cii) across all recorded V3 INs.

Supplemental Figure 4.12 V3 IN electrophysiological and morphological Principle Component Analyses

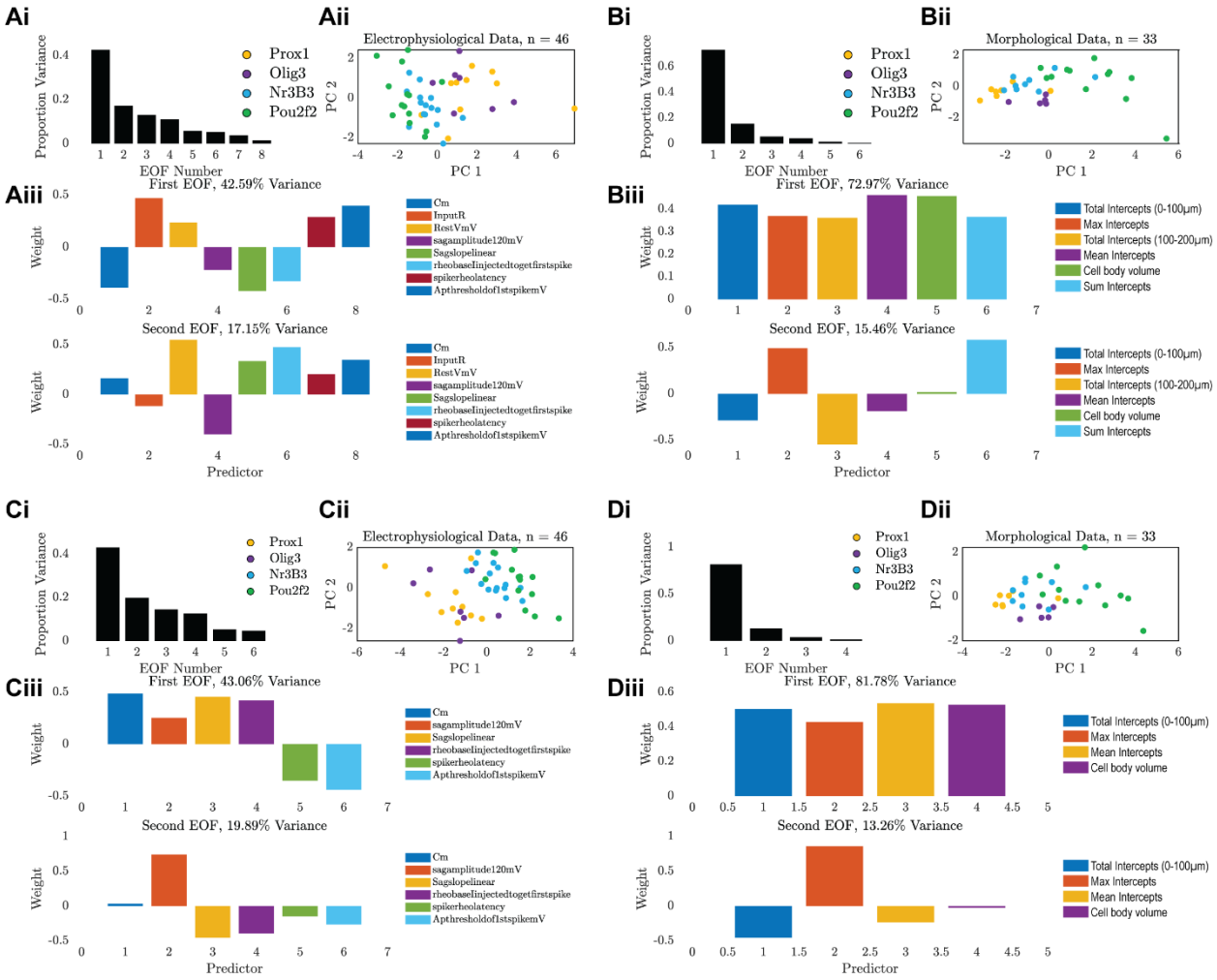

Supplemental Figure 4.12 V3 IN electrophysiological and morphological Principle Component Analyses

Principle component analyses of top eight most significant electrophysiological properties (A), top six most significant morphological properties (B), top six most significant electrophysiological properties (C), top four most significant morphological properties (D) [A-Di, total variance accounted for by independent EOFs; A-Dii, scatter plots of PC1 vs PC2 scores of $Prox1^{+}$, $Olig3^{+}$, $Nr3b3^{+}$, and $Pou2f2^{+}$ V3 INs; Aiii-Diii, weight of specific variables in top two EOFs (PCs)].

Supplemental Figure 4.13 Combined factors for V3 subpopulations separation

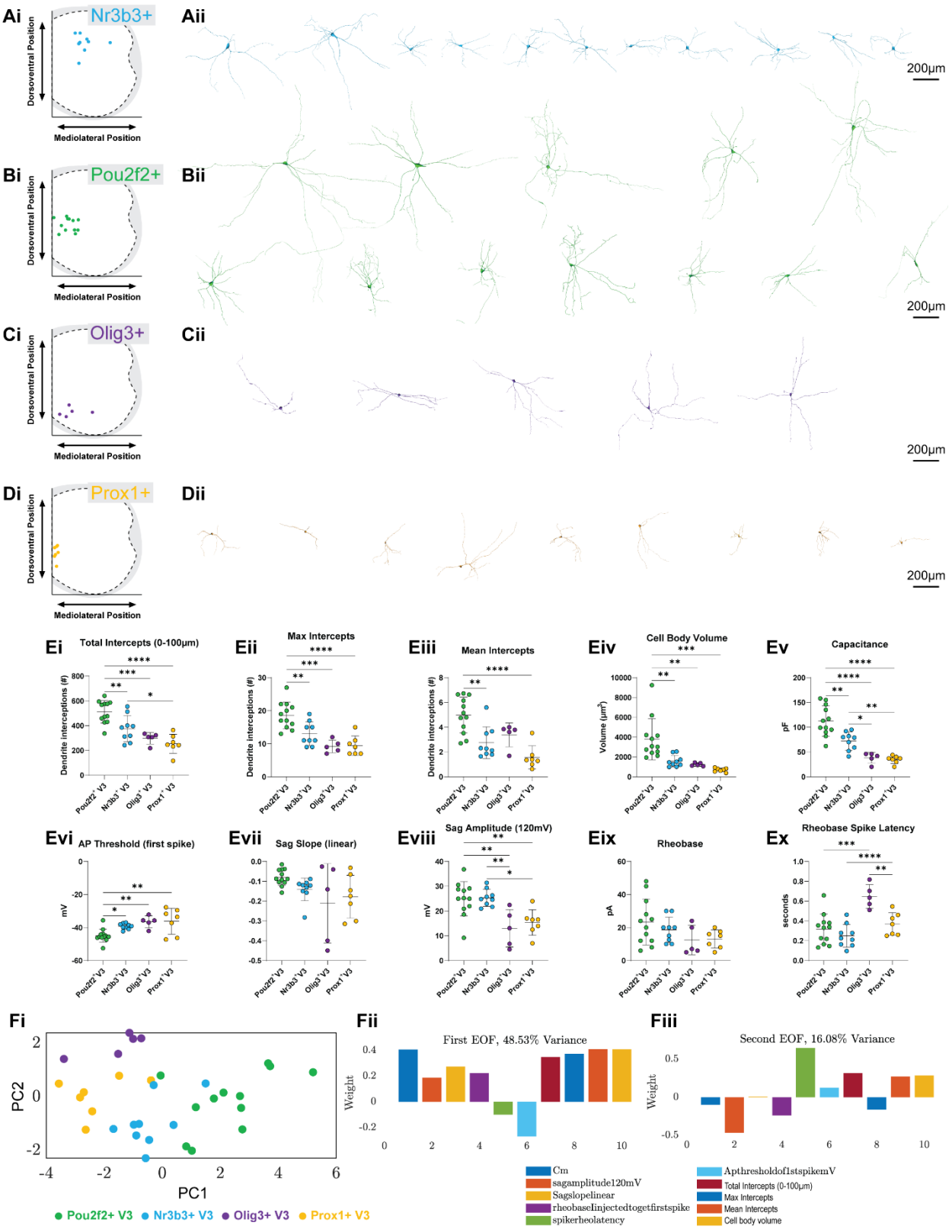

Supplemental Figure 4.13 Combined factors for V3 subpopulations separation

(Ai-Di) Laminar distributions of recorded Nr3b3$^+$ (Ai), Pou2f2$^+$ (Bi), Olig3$^+$ (Ci), and Prox1$^+$ (Di) V3 INs. (Aii-Dii) Morphological reconstructions of biotin-filled Nr3b3$^+$ (Aii), Pou2f2$^+$ (Bii), Olig3$^+$ (Cii), and Prox1$^+$ (Dii) V3 INs. (Ei-x) Comparisons of Pou2f2$^+$ (green), Nr3b3$^+$ (blue), Olig3$^+$ (purple), and Prox1$^+$ (orange) V3 IN properties [Pou2f2$^+$ V3, n=12 cells; Nr3b3$^+$ V3, n=9 cells; Olig3$^+$ V3, n=5 cells; Prox1$^+$ V3, n=7 cells; * p-value < 0.05, ** p-value < 0.01, *** p-value < 0.001, **** p-value < 0.0001, one-way ANOVA & Tukey's multiple comparisons test]. (F) Principal component analyses of combined six electrophysiological properties (Ev-Ex) and four morphological properties (Ei-ix) [Fi, scatter plot of PC1 versus PC2 scores of Prox1$^+$, Olig3$^+$, Nr3b3$^+$, and Pou2f2$^+$ V3 INs; Fii-iii weight of variables in top two EOFs (PCs)].

Supplemental Figure 4.14 Combined factors for V3 neurogenesis time separation

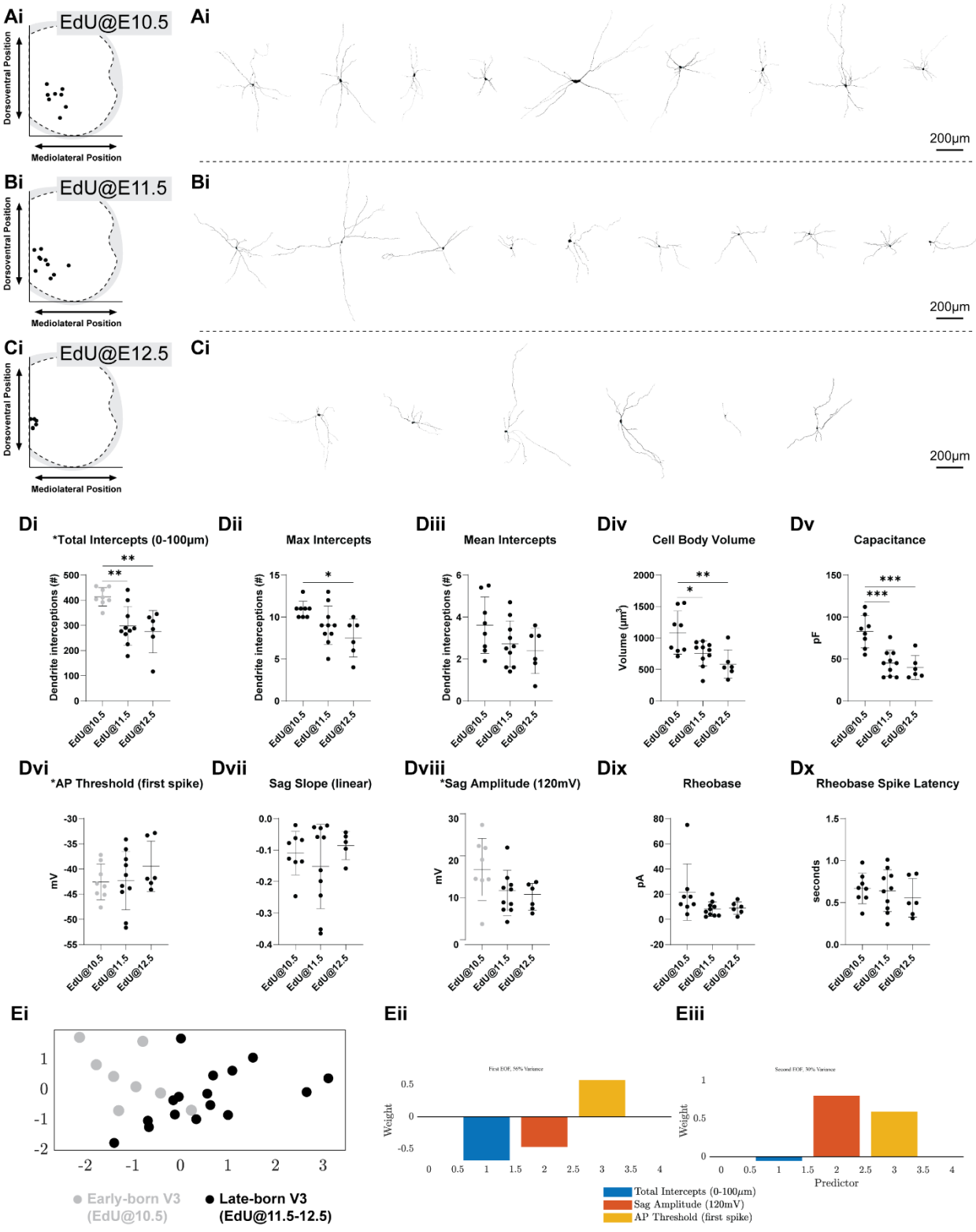

Supplemental Figure 4.14 Combined factors for V3 neurogenesis time separation

(Ai-Ci) Laminar distributions of recorded E10.5 EdU^+ (Ai), E11.5 EdU^+ (Bi), and E12.5 EdU^+ (Ci) V3 INs. (Aii-Cii) Morphological reconstructions of biotin-filled E10.5 EdU^+ (Aii), E11.5 EdU^+ (Bii), and E12.5 EdU^+ (Cii) V3 INs. (Di-x) Comparisons of E10.5 EdU^+, E11.5 EdU^+, and E12.5 EdU^+ V3 INs [E10.5 EdU^+ V3, n=8 cells; E11.5 EdU^+ V3, n=10 cells; E12.5 EdU^+ V3, n=6 cells; * p-value < 0.05, ** p-value < 0.01, *** p-value < 0.001, **** p-value < 0.0001, one-way ANOVA & Tukey's multiple comparisons test]. (E) Principal component analyses of total intercepts (0-100μm, Di), sag amplitude (@-120mV, Dvii), and action potential (AP) threshold (Dvi) of early-born (EdU@E10.5, grey) and late-born (EdU@E11.5 & E12.5, black) V3 INs [Ei, scatter plot of PC1 versus PC2 scores of early-born (EdU@E10.5, grey) and late-born (EdU@E11.5 & E12.5, black) V3 INs; Eii-iii weight of variables in top two EOFs (PCs)].

8. Tables

Table 5.1 Antibody information

Primary AB	Host Species	Source	Catalog#	Working Dilution
Nr3B3 (ERRy)	Mouse	R&D Systems	PP-H6812-00	1:100
Olig3	Guinea Pig	Birchmeier-Kohler Lab		1:10000
Pou2f2 (Oct-2)	Rabbit	abcam	ab178679	1:1000
Prox1	Rabbit	Millipore	AB5475	1:1000
Prox1	Mouse	abcam	ab92825	1:1000
Bhlhb5	Goat	Santa Cruz	sc-6045	1:2000
Onecut1	Rabbit	Santa Cruz	sc-13050	1:200
Onecut2	Sheep	R&D	AF6294	1:1000
Lmo3	Goat	Santa Cruz	sc-82647	1:500
Nr4a2 (Nurr1)	Rabbit	Santa Cruz	sc-5568	1:500
MafB	Rabbit	Sigma	HPA005653	1:2000
Prdm8	Guinea Pig	Jessel Lab, CU1791		1:2000
Otp	Guinea Pig	Jessel Lab, CU1497		1:16000
Nr5a2 (C-17)	Goat	Sanata Cruz	sc-21132	1:100
Sp8 (C18)	Goat	Sanata Cruz	sc-104661	1:2000
Foxp1	Guinea Pig	Jessel Lab, CU1492		1:2000
Poubf2	Rat	Jessel Lab, CU1796		1:2000
Foxp2 (N-16)	Goat	Sanata Cruz	sc-21069	1:500
DsRed	Rabbit	Clontech	632496	1:2000
TdTomato	Goat	Sicgenantibodies	AB8181-200	1:100
RFP	Rat	Chromotek	5F8	1:1000
Robo3	Goat	R&D Systems	AF3155	1:50
Nkx2.2	Mouse	DSHB	74.5A5	1:100
Secondary AB	**Host Species**	**Source**	**Catalog#**	**Working Dilution**
Alexa Fluor 488 anti-Mouse IgG	Donkey	Jackson ImmunoResearch	715-545-150	1:500
Alexa Fluor 488 anti-Rat IgG	Donkey	Jackson ImmunoResearch	712-487-003	1:500
Alexa Fluor 488 anti-Guinea Pig Ig	Donkey	Jackson ImmunoResearch	706-485-148	1:500
Alexa Fluor 488 anti-Sheep IgG	Donkey	Jackson ImmunoResearch	713-545-147	1:500
Alexa Fluor 488 anti-Goat IgG	Donkey	Invitrogen	A11055	1:500
Alexa Fluor 488 anti-Rabbit IgG	Donkey	Jackson ImmunoResearch	711-545-152	1:500
Alexa Fluor 594 anti-Rat IgG	Donkey	Jackson ImmunoResearch	712-585-153	1:500
Alexa Fluor 594 anti-Rabbit IgG	Donkey	Jackson ImmunoResearch	711-585-152	1:500
Alexa Fluor 594 anti-Goat IgG	Donkey	Jackson ImmunoResearch	705-585-147	1:500
Alexa Fluor 647 anti-Mouse IgG	Donkey	Jackson ImmunoResearch	715-605-151	1:500
Alexa Fluor 647 anti-Rabbit IgG	Donkey	Jackson ImmunoResearch	711-605-152	1:500
Cy5 (647) anti-Guinea Pig IgG	Donkey	Jackson ImmunoResearch	706-175-148	1:500
Cy5 (647) anti-Sheep IgG	Donkey	Jackson ImmunoResearch	713-175-147	1:500
Alexa Fluor 647 anti-Mouse IgG	Donkey	Jackson ImmunoResearch	715-605-151	1:500

9. References

Abraira, V., Kuehn, E., Chirila, A., Springel, M., Toliver, A., Zimmerman, A., . . . Ginty, D. (2017). The cellular and synaptic architecture of the mechanosensory dorsal horn. *Cell, 168*(1-2), 295-310.e19. doi:10.1016/j.cell.2016.12.010

Arber, S. (2012). Motor circuits in action: Specification, connectivity, and function. *Neuron, 74*(6), 975-989. doi:10.1016/j.neuron.2012.05.011

Benito Gonzalez, A., & Alvarez, F. (2012). Renshaw cells and ia inhibitory interneurons are generated at different times from p1 progenitors and differentiate shortly after exiting the cell cycle. *The Journal of Neuroscience, 32*(4), 1156-1170. doi:10.1523/JNEUROSCI.3630-12.2012

Bikoff, J., Gabitto, M., Rivard, A., Drobac, E., Machado, T., Miri, A., . . . Jessell, T. (2016). Spinal inhibitory interneuron diversity delineates variant motor microcircuits. *Cell, 165*(1), 207-219. doi:10.1016/j.cell.2016.01.027

Blacklaws, J., Deska Gauthier, D., Jones, C., Petracca, Y., Liu, M., Zhang, H., . . . Zhang, Y. (2015). Sim1 is required for the migration and axonal projections of V3 interneurons in the developing mouse spinal cord. *Developmental Neurobiology, 75*(9), 1003-1017. doi:10.1002/dneu.22266

Borowska, J., Jones, C. T., Deska Gauthier, D., & Zhang, Y. (2015). V3 interneuron subpopulations in the mouse spinal cord undergo distinctive postnatal maturation processes. *Neuroscience, 295*, 221-228. doi:10.1016/j.neuroscience.2015.03.024

Borowska, J., Jones, C., Zhang, H., Blacklaws, J., Goulding, M., & Zhang, Y. (2013). Functional subpopulations of V3 interneurons in the mature mouse spinal cord. *The Journal of Neuroscience, 33*(47), 18553-18565. doi:10.1523/JNEUROSCI.2005-13.2013

Cheng, L., Arata, A., Mizuguchi, R., Qian, Y., Karunaratne, A., Gray, P., . . . Ma, Q. (2004). Tlx3 and Tlx1 are post-mitotic selector genes determining glutamatergic over GABAergic cell fates. *Nature Neuroscience, 7*(5), 510-517. doi:10.1038/nn1221

Chopek, J., Nascimento, F., Beato, M., Brownstone, R., & Zhang, Y. (2018). Sub-populations of spinal V3 interneurons form focal modules of layered pre-motor microcircuits. *Cell Reports, 25*(1), 146-156.e3. doi:10.1016/j.celrep.2018.08.095

Christensen, A., Iyer, S., François, A., Vyas, S., Ramakrishnan, C., Vesuna, S., . . . Delp, S. (2016). In vivo interrogation of spinal mechanosensory circuits. *Cell Reports, 17*(6), 1699-1710. doi:10.1016/j.celrep.2016.10.010

Danner, S., Zhang, H., Shevtsova, N., Borowska Fielding, J., Deska Gauthier, D., Rybak, I., & Zhang, Y. (2019). Spinal V3 interneurons and left-right coordination in mammalian locomotion. *Frontiers in Cellular Neuroscience, 13*, 516-516. doi:10.3389/fncel.2019.00516

Del Barrio, M., Taveira Marques, R., Muroyama, Y., Yuk, D., Li, S., Wines Samuelson, M., . . . Richardson, W. (2007). A regulatory network involving Foxn4, Mash1 and delta-like 4/Notch1 generates V2a and V2b spinal interneurons from a common progenitor pool. *Development, 134*(19), 3427-3436. doi:10.1242/dev.005868

Delile, J., Rayon, T., Melchionda, M., Edwards, A., Briscoe, J., & Sagner, A. (2019). Single cell transcriptomics reveals spatial and temporal dynamics of gene expression in the developing mouse spinal cord. *Development, 146*(12) doi:10.1242/dev.173807

Deska Gauthier, D., Borowska Fielding, J., Jones, C., & Zhang, Y. (2020). The temporal neurogenesis patterning of spinal p3-V3 interneurons into divergent subpopulation assemblies. *The Journal of Neuroscience, 40*(7), 1440-1452. doi:10.1523/JNEUROSCI.1518-19.2019

Deska-Gauthier, D., & Zhang, Y. (2019). The functional diversity of spinal interneurons and locomotor control. *Current Opinion in Physiology, 8*, 99-108. doi:https://doi.org/10.1016/j.cophys.2019.01.005

Duan, B., Cheng, L., Bourane, S., Britz, O., Padilla, C., Garcia Campmany, L., . . . Ma, Q. (2014). Identification of spinal circuits transmitting and gating mechanical pain. *Cell, 159*(6), 1417-1432. doi:10.1016/j.cell.2014.11.003

Francius, C., Harris, A., Rucchin, V., Hendricks, T., Stam, F., Barber, M., . . . Clotman, F. (2013). Identification of multiple subsets of ventral interneurons and differential distribution along

the rostrocaudal axis of the developing spinal cord. *PLoS One, 8*(8), e70325-e70325. doi:10.1371/journal.pone.0070325

Gabitto, M., Pakman, A., Bikoff, J., Abbott, L. F., Jessell, T., & Paninski, L. (2016). Bayesian sparse regression analysis documents the diversity of spinal inhibitory interneurons. *Cell, 165*(1), 220-233. doi:10.1016/j.cell.2016.01.026

Glasgow, S., Henke, R. M., Macdonald, R., Wright, C. V. E., & Johnson, J. (2005). Ptf1a determines GABAergic over glutamatergic neuronal cell fate in the spinal cord dorsal horn. *Development, 132*(24), 5461-5469. doi:10.1242/dev.02167

Gosgnach, S., Bikoff, J., Dougherty, K., El Manira, A., Lanuza, G., & Zhang, Y. (2017). Delineating the diversity of spinal interneurons in locomotor circuits. *The Journal of Neuroscience, 37*(45), 10835-10841. doi:10.1523/JNEUROSCI.1829-17.2017

Goulding, M. (2009). Circuits controlling vertebrate locomotion: Moving in a new direction. *Nature Reviews.Neuroscience, 10*(7), 507-518. doi:10.1038/nrn2608

Häring, M., Zeisel, A., Hochgerner, H., Rinwa, P., Jakobsson, J. E. T., Lönnerberg, P., . . . Ernfors, P. (2018). Neuronal atlas of the dorsal horn defines its architecture and links sensory input to transcriptional cell types. *Nature Neuroscience, 21*(6), 869-880. doi:10.1038/s41593-018-0141-1

Hayashi, M., Hinckley, C., Driscoll, S., Moore, N., Levine, A., Hilde, K., . . . Pfaff, S. (2018). Graded arrays of spinal and supraspinal V2a interneuron subtypes underlie forelimb and hindlimb motor control. *Neuron, 97*(4), 869-884.e5. doi:10.1016/j.neuron.2018.01.023

Hobert, O., Carrera, I., & Stefanakis, N. (2010). The molecular and gene regulatory signature of a neuron. *Trends in Neurosciences (Regular Ed.), 33*(10), 435-445. doi:10.1016/j.tins.2010.05.006

Jessell, T. M. (2000). Neuronal specification in the spinal cord: Inductive signals and transcriptional codes. *Nature Reviews Genetics, 1*(1), 20-29. doi:10.1038/35049541

John, A., Wildner, H., & Britsch, S. (2005). The homeodomain transcription factor Gbx1 identifies a subpopulation of late-born GABAergic interneurons in the developing dorsal spinal cord. *Developmental Dynamics, 234*(3), 767-771. doi:10.1002/dvdy.20568

Kiehn, O. (2016). Decoding the organization of spinal circuits that control locomotion. *Nature Reviews.Neuroscience, 17*(4), 224-238. doi:10.1038/nrn.2016.9

Kimura, Y., Satou, C., & Higashijima, S. (2008). V2a and V2b neurons are generated by the final divisions of pair-producing progenitors in the zebrafish spinal cord. *Development, 135*(18), 3001-3005. doi:10.1242/dev.024802

Laumonnerie, C., Tong, Y., Alstermark, H., & Wilson, S. (2015). Commissural axonal corridors instruct neuronal migration in the mouse spinal cord. *Nature Communications, 6*, 7028-7028. doi:10.1038/ncomms8028

Lim, J., & Choi, H. (2015). Estrogen-related receptor gamma regulates dopaminergic neuronal phenotype by activating GSK3ß/NFAT signaling in SH-SY5Y cells. *Journal of Neurochemistry, 133*(4), 544-557. doi:10.1111/jnc.13085

Lu, D., Niu, T., & Alaynick, W. (2015). Molecular and cellular development of spinal cord locomotor circuitry. *Frontiers in Molecular Neuroscience, 8*, 25-25. doi:10.3389/fnmol.2015.00025

Mizuguchi, R., Kriks, S., Cordes, R., Gossler, A., Ma, Q., & Goulding, M. (2006). Ascl1 and Gsh1/2 control inhibitory and excitatory cell fate in spinal sensory interneurons. *Nature Neuroscience, 9*(6), 770-778. doi:10.1038/nn1706

Okigawa, S., Mizoguchi, T., Okano, M., Tanaka, H., Isoda, M., Jiang, Y., . . . Itoh, M. (2014). Different combinations of notch ligands and receptors regulate V2 interneuron progenitor proliferation and V2a/V2b cell fate determination. *Developmental Biology, 391*(2), 196-206. doi:10.1016/j.ydbio.2014.04.011

Petracca, Y., Sartoretti, M., Di Bella, D., Marin Burgin, A., Carcagno, A., Schinder, A., & Lanuza, G. (2016). The late and dual origin of cerebrospinal fluid-contacting neurons in the mouse spinal cord. *Development, 143*(5), 880-891. doi:10.1242/dev.129254

Sathyamurthy, A., Johnson, K., Matson, K. J. E., Dobrott, C., Li, L., Ryba, A., . . . Levine, A. (2018). Massively parallel single nucleus transcriptional profiling defines spinal cord neurons and their activity during behavior. *Cell Reports, 22*(8), 2216-2225. doi:10.1016/j.celrep.2018.02.003

Satou, C., Kimura, Y., & Higashijima, S. (2012). Generation of multiple classes of V0 neurons in zebrafish spinal cord: Progenitor heterogeneity and temporal control of neuronal diversity. *The Journal of Neuroscience, 32*(5), 1771-1783. doi:10.1523/JNEUROSCI.5500-11.2012

Sockanathan, S., & Jessell, T. M. (1998). Motor neuron-derived retinoid signaling specifies the subtype identity of spinal motor neurons. *Cell, 94*(4), 503-514. doi:10.1016/S0092-8674(00)81591-3

Stam, F., Hendricks, T., Zhang, J., Geiman, E., Francius, C., Labosky, P., . . . Goulding, M. (2012). Renshaw cell interneuron specialization is controlled by a temporally restricted transcription factor program. *Development, 139*(1), 179-190. doi:10.1242/dev.071134

Sweeney, L., Bikoff, J., Gabitto, M., Brenner Morton, S., Baek, M., Yang, J., . . . Jessell, T. (2018). Origin and segmental diversity of spinal inhibitory interneurons. *Neuron, 97*(2), 341-355.e3. doi:10.1016/j.neuron.2017.12.029

Zeisel, A., Hochgerner, H., Lönnerberg, P., Johnsson, A., Memic, F., van der Zwan, J., . . . Linnarsson, S. (2018). Molecular architecture of the mouse nervous system. *Cell, 174*(4), 999-1014.e22. doi:10.1016/j.cell.2018.06.021

Zhang, Y., Narayan, S., Geiman, E., Lanuza, G., Velasquez, T., Shanks, B., . . . Goulding, M. (2008). V3 spinal neurons establish a robust and balanced locomotor rhythm during walking. *Neuron, 60*(1), 84-96. doi:10.1016/j.neuron.2008.09.027

CHAPTER 5. CONCLUSSION

Understanding how the central nervous system controls movement requires an identification and detailed investigation of interneurons in the spinal cord. At the turn of the millennia several pioneering works revealed early embryonic morphogen gradients that pattern discrete progenitor domains across the dorsoventral spinal axis. Each respective progenitor domain then gives rise to molecularly distinct post-mitotic interneuron classes, which assemble with one another into the core rhythm generating and pattern forming motor networks of the spinal cord. While each cardinal interneuron class possesses general molecular, anatomical, and physiological properties, extensive heterogeneity further exists within each class. This heterogeneity has obscured efforts to understand how specific circuit logics translate into specific functional outputs. Furthermore, how early embryonic mechanisms diversify cardinal interneuron classes into divergent subpopulations remains largely unknown.

For my Ph.D. studies, I utilized the cardinal V3 interneuron class as a model system to study the fundamental principals guiding interneuron diversity in the mouse spinal cord. V3 interneurons serve as an ideal model system as they uniquely distribute across dorsal to ventral spinal laminae, form discernable cell density clustering patterns, display mixed axon projections, have heterogeneous intrinsic membrane properties, and display a wide range of functional roles across varied sensorimotor behaviours. Specifically, I aimed to answer two fundamental questions of V3 interneuron diversity: 1) Does V3 interneuron diversity underlie behavioural sensorimotor diversity? and 2) How do V3 interneuron subpopulations diversify during early embryogenesis?

First, I investigated the task-specific recruitment patterns of both cardinal V3 and V2a interneurons. I revealed that excitatory V3 and V2a interneurons are functionally organized into topographically clustered and task-specific recruitment modules. Interestingly, V3 and V2a interneurons with overlapping spatial distributions displayed distinct task-specific recruitment patterns. This suggests functional divergence and independence between excitatory spinal IN classes, regardless of spatial position. Additionally, topographically clustered subsets within each cardinal class displayed distinct recruitment patterns. This suggests task-specific functional divergence of spatially discrete clusters within excitatory V3 and V2a interneuron classes, respectively.

Next, I asked how circuit connections may translate to task-specific recruitments. I focused on sensory information entering the spinal cord from the periphery. Topographically separate V3 interneuron clusters received distinct modality and nerve-specific sensory innervations. Thus, I have provided evidence for sensory specific connectivity as key recruitment logic for heterogeneous V3 interneurons through identifying V3 anatomical clusters, the task-specific recruitment patterns of those clusters, and their sensory specific innervations.

While my recruitment studies suggest functional divergence between V3 anatomical clusters, to truly address how V3 interneuron diversity translates to functional diversity I needed to reveal the subpopulation identities of differentially clustered V3 interneurons. To that end, I screened for the expression of several candidate transcriptions factors in V3 interneuron subsets. I identified five molecularly distinct V3 interneuron subpopulations that each displayed unique axon projection profiles, morphologies, and intrinsic membrane properties. Perhaps most

intriguingly, each V3 interneuron subpopulation differentially clustered within each of the distinct topographical recruitment domains.

Nr3b3^{+} V3 interneurons clustered within the dorsomedial V3 domain, which displayed a hind paw cutaneous-dependent recruitment pattern. On the other hand, Pou2f2^{+}, Prox1^{+}, Olig3^{+} and Onecut2^{+} all displayed varying degrees of clustering within ventral laminae at P0, which would become defined as a ventral V3 recruitment domain in the adult. This ventral recruitment domain displayed ubiquitous recruitment across almost all sensorimotor tasks performed (speed-, to hindlimb load-, to balance-, to hind paw cutaneous-dependent tasks). This raised the possibility that the non-task-specific recruitment patterns we observed in the ventral V3 domains were a result of a mixture of developmentally and molecularly distinct V3 interneuron subpopulations. Thus, further task-specific recruitment organization may exist between molecularly distinct V3 interneuron subpopulations clustered within the ventral spinal cord. However, we were not able to test this hypothesis directly as the transcription factor expression profiles we identified in V3 interneurons neonatally were not reliably detected in adult stages (data not show). Thus, we will need an alternative approach to identify and target V3 interneuron subpopulations from embryonic, to neonatal, to adult stages.

The second questions I aimed to answer was how do V3 interneuron subpopulations diversify during early embryogenesis? Interestingly, I discovered neurogenesis timing as a key development principal separating V3 interneurons into molecularly, anatomically, morphologically, and electrophysiologically distinct interneuron subclasses. These finds not only shed new light on the importance of temporal mechanisms guiding spinal interneuron

diversification, but they also present an exciting opportunity to target V3 interneuron subpopulations from embryonic to adult stages.

We have begun to develop novel transgenic mouse approaches to target V3 temporal subclasses at adult ages. This will allow us to more completely understand how early embryonic diversification of V3 INs translates into circuit connectivities, and ultimately functional divergence in the adult. Specifically, we have developed an intersectional and inducible genetic approach that will allow us to specifically target late-born V3 INs for molecular, anatomical and functional analysis in the adult (Figure5.1).

Taken together, my current work has provided an entry point into defining and targeting excitatory interneuron subpopulations in the spinal cord. Going forward, we will expand our developmental subpopulation findings to functional experiments at adult stages. Together, this work offers new insights into the spinal cord circuit logic, which may lend to our understanding of certain spinal disease pathologies and injury states.

1. Figures

Figure 5.1 Targeting late-born V3 IN subclass

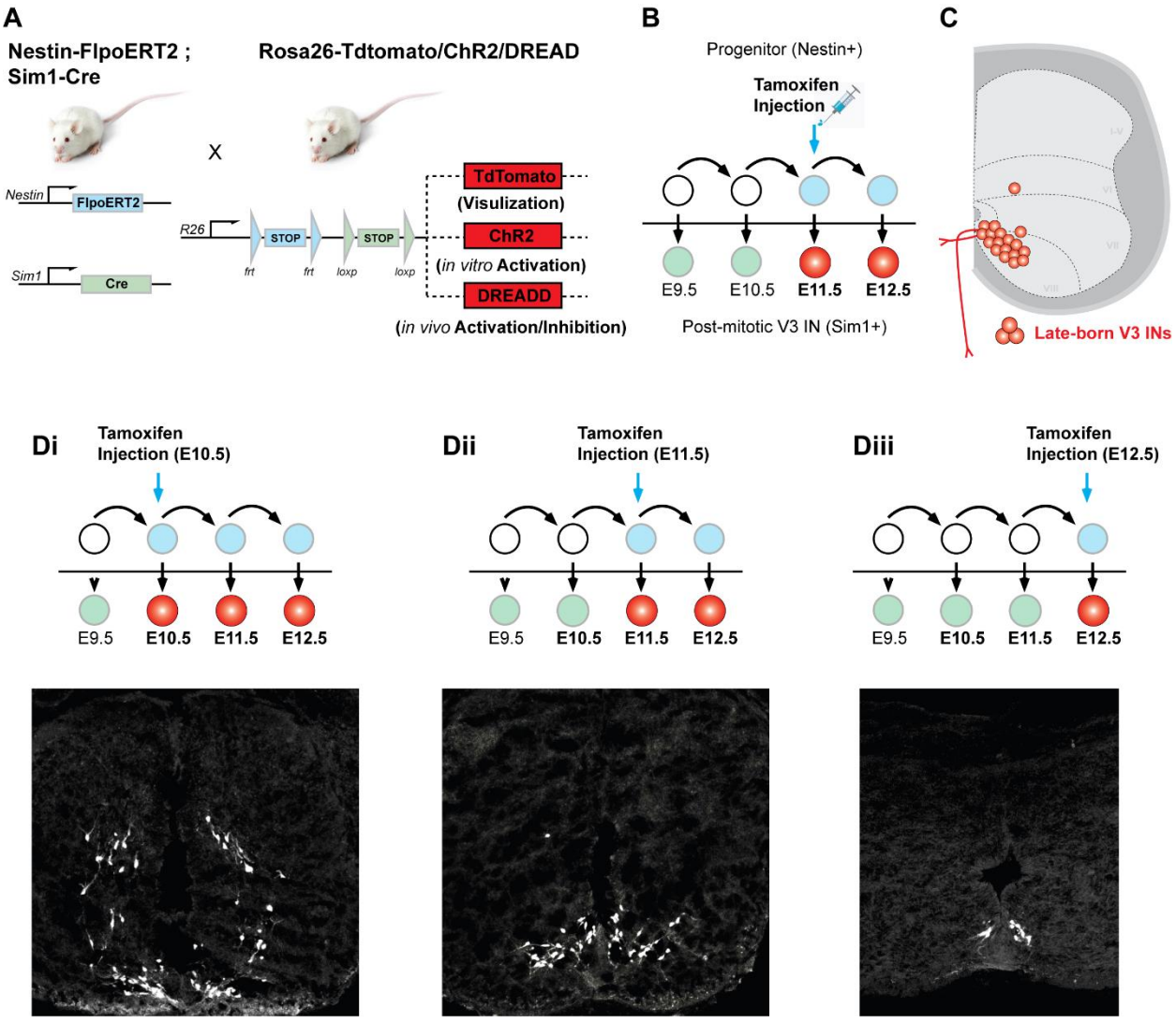

Figure 5.1 Targeting late-born V3 IN subclass

(A) Second generation $Sim1^{Cre}$;$Nestin^{FlpoER}$ mice crossed with mice harbouring reporter or functional protein genes downstream of a frt-flanked STOP cassette and a loxP-flanked STOP cassette. (B) Tamoxifen injection will induce Flpo entry into the nucleus and frt excision. Cells that express both Sim1 (V3 INs) and Nestin (progenitor cells) at time of or after tamoxifen injection will expresses reporter (TdTomato) or functional (ChR2, DREADD) proteins. This will allow for the targeting of the late-born V3 temporal subclass with tamoxifen injection at E11.5. (C) Illustration of anatomically restricted late-born V3 INs. (D) Example images of TdTomato expression at E14.5 in higher lumbar spinal cords following tamoxifen injection at E10.5 (Di), E11.5 (Dii), and E12.5 (Diii).

REFERENCE

Abraira, V., Kuehn, E., Chirila, A., Springel, M., Toliver, A., Zimmerman, A., . . . Ginty, D. (2017). The cellular and synaptic architecture of the mechanosensory dorsal horn. *Cell, 168*(1-2), 295-310.e19. doi:10.1016/j.cell.2016.12.010

Akay, T., Tourtellotte, W., Arber, S., & Jessell, T. (2014). Degradation of mouse locomotor pattern in the absence of proprioceptive sensory feedback. *Proceedings of the National Academy of Sciences of the United States of America, 111*(47), 16877-16882. doi:10.1073/pnas.1419045111

Akay, T., & Murray, A. (2021). Relative contribution of proprioceptive and vestibular sensory systems to locomotion: Opportunities for discovery in the age of molecular science. *International Journal of Molecular Sciences, 22*(3) doi:10.3390/ijms22031467

Al Mosawie, A., Wilson, J. M., & Brownstone, R. M. (2007). Heterogeneity of V2-derived interneurons in the adult mouse spinal cord. *European Journal of Neuroscience, 26*(11), 3003-3015. doi:10.1111/j.1460-9568.2007.05907.x

Allan, D., & Thor, S. (2015). Transcriptional selectors, masters, and combinatorial codes: Regulatory principles of neural subtype specification. *Wiley Interdisciplinary Reviews: Developmental Biology, 4*(5), 505-528. doi:10.1002/wdev.191

Alvarez, F., Jonas, P., Sapir, T., Hartley, R., Berrocal, M., Geiman, E., . . . Goulding, M. (2005). Postnatal phenotype and localization of spinal cord V1 derived interneurons. *Journal of Comparative Neurology, 493*(2), 177-192. doi:10.1002/cne.20711

Alvarez, F., Villalba, R., Zerda, R., & Schneider, S. (2004). Vesicular glutamate transporters in the spinal cord, with special reference to sensory primary afferent synapses. *Journal of Comparative Neurology, 472*(3), 257-280. doi:10.1002/cne.20012

Ampatzis, K., Song, J., Ausborn, J., & El Manira, A. (2014). Separate microcircuit modules of distinct v2a interneurons and motoneurons control the speed of locomotion. *Neuron, 83*(4), 934-943. doi:10.1016/j.neuron.2014.07.018

Andersson, L., Larhammar, M., Memic, F., Wootz, H., Schwochow, D., Rubin, C., . . . Kullander, K. (2012). Mutations in DMRT3 affect locomotion in horses and spinal circuit function in mice. *Nature, 488*(7413), 642-646. doi:10.1038/nature11399

Arber, S., Ladle, D. R., Lin, J. H., Frank, E., & Jessell, T. M. (2000). ETS gene Er81 controls the formation of functional connections between group ia sensory afferents and motor neurons. *Cell, 101*(5), 485-498. doi:10.1016/S0092-8674(00)80859-4

Arber, S. (2012). Motor circuits in action: Specification, connectivity, and function. *Neuron, 74*(6), 975-989. doi:10.1016/j.neuron.2012.05.011

Ausborn, J., Mahmood, R., & El Manira, A. (2012). Decoding the rules of recruitment of excitatory interneurons in the adult zebrafish locomotor network. *Proceedings of the*

National Academy of Sciences of the United States of America, 109(52), E3631-E3639. doi:10.1073/pnas.1216256110

Bagnall, M., & McLean, D. (2014). Modular organization of axial microcircuits in zebrafish. *Science, 343*(6167), 197-200. doi:10.1126/science.1245629

Bailey, C. S., Kitchell, R. L., Guinan, M. J., & Sharp, J. W. (1992). Dorsal nerve root origins of the cutaneous nerves of the feline pelvic limb. *Anatomia, Histologia, Embryologia, 21*(1), 23-31. doi:10.1111/j.1439-0264.1992.tb00315.x

Bailey, C. S., & Kitchell, R. L. (1987). Cutaneous sensory testing in the dog. *Journal of Veterinary Internal Medicine, 1*(3), 128-135. doi:10.1111/j.1939-1676.1987.tb02000.x

Bassett, E., & Wallace, V. (2012). Cell fate determination in the vertebrate retina. *Trends in Neurosciences (Regular Ed.), 35*(9), 565-573. doi:10.1016/j.tins.2012.05.004

Bellardita, C., & Kiehn, O. (2015). Phenotypic characterization of speed-associated gait changes in mice reveals modular organization of locomotor networks. *Current Biology, 25*(11), 1426-1436. doi:10.1016/j.cub.2015.04.005

Benito Gonzalez, A., & Alvarez, F. (2012). Renshaw cells and ia inhibitory interneurons are generated at different times from p1 progenitors and differentiate shortly after exiting the cell cycle. *The Journal of Neuroscience, 32*(4), 1156-1170. doi:10.1523/JNEUROSCI.3630-12.2012

Berg, E., Björnfors, E. R., Pallucchi, I., Picton, L., & El Manira, A. (2018). Principles governing locomotion in vertebrates: Lessons from zebrafish. *Frontiers in Neural Circuits, 12*, 73-73. doi:10.3389/fncir.2018.00073

Bertuzzi, M., & Ampatzis, K. (2018). Spinal cholinergic interneurons differentially control motoneuron excitability and alter the locomotor network operational range. *Scientific Reports, 8*(1), 1988-1988. doi:10.1038/s41598-018-20493-z

Bhumbra, G., Bannatyne, B. A., Watanabe, M., Todd, A., Maxwell, D., & Beato, M. (2014). The recurrent case for the renshaw cell. *The Journal of Neuroscience, 34*(38), 12919-12932. doi:10.1523/JNEUROSCI.0199-14.2014

Bikoff, J., Gabitto, M., Rivard, A., Drobac, E., Machado, T., Miri, A., . . . Jessell, T. (2016). Spinal inhibitory interneuron diversity delineates variant motor microcircuits. *Cell, 165*(1), 207-219. doi:10.1016/j.cell.2016.01.027

Bikoff, J. B. (2019). Interneuron diversity and function in the spinal motor system. *Current Opinion in Physiology, 8*, 36-43. doi:https://doi.org/10.1016/j.cophys.2018.12.013

Bizzi, E., Cheung, V. C. K., d'Avella, A., Saltiel, P., & Tresch, M. (2008). Combining modules for movement. *Brain Research Reviews, 57*(1), 125-133. doi:10.1016/j.brainresrev.2007.08.004

Bizzi, E., Giszter, S. F., Loeb, E., Mussa Ivaldi, F. A., & Saltiel, P. (1995). Modular organization of motor behavior in the frog's spinal cord. *Trends in Neurosciences (Regular Ed.), 18*(10), 442-446. doi:10.1016/0166-2236(95)94494-P

Björnfors, E. R., & El Manira, A. (2016). Functional diversity of excitatory commissural interneurons in adult zebrafish. *Elife, 5* doi:10.7554/eLife.18579

Blacklaws, J., Deska Gauthier, D., Jones, C., Petracca, Y., Liu, M., Zhang, H., . . . Zhang, Y. (2015). Sim1 is required for the migration and axonal projections of V3 interneurons in the developing mouse spinal cord. *Developmental Neurobiology, 75*(9), 1003-1017. doi:10.1002/dneu.22266

Blankenship, A., & Feller, M. (2010). Mechanisms underlying spontaneous patterned activity in developing neural circuits. *Nature Reviews Neuroscience, 11*(1), 18-29. doi:10.1038/nrn2759

Boeri, J., Le Corronc, H., Lejeune, F., Le Bras, B., Mouffle, C., Angelim, Monara Kaelle S C, . . . Czarnecki, A. (2018). Persistent sodium current drives excitability of immature renshaw cells in early embryonic spinal networks. *The Journal of Neuroscience, 38*(35), 7667-7682. doi:10.1523/JNEUROSCI.3203-17.2018

Böhm, U., Prendergast, A., Djenoune, L., Nunes Figueiredo, S., Gomez, J., Stokes, C., . . . Wyart, C. (2016). CSF-contacting neurons regulate locomotion by relaying mechanical stimuli to spinal circuits. *Nature Communications, 7*, 10866-10866. doi:10.1038/ncomms10866

Borowska, J., Jones, C. T., Deska Gauthier, D., & Zhang, Y. (2015). V3 interneuron subpopulations in the mouse spinal cord undergo distinctive postnatal maturation processes. *Neuroscience, 295*, 221-228. doi:10.1016/j.neuroscience.2015.03.024

Borowska, J., Jones, C., Zhang, H., Blacklaws, J., Goulding, M., & Zhang, Y. (2013). Functional subpopulations of V3 interneurons in the mature mouse spinal cord. *The Journal of Neuroscience, 33*(47), 18553-18565. doi:10.1523/JNEUROSCI.2005-13.2013

Bourane, S., Grossmann, K., Britz, O., Dalet, A., Del Barrio, M., Stam, F., . . . Goulding, M. (2015). Identification of a spinal circuit for light touch and fine motor control. *Cell, 160*(3), 503-515. doi:10.1016/j.cell.2015.01.011

Briscoe, J., Sussel, L., Serup, P., Hartigan O'Connor, D., Jessell, T. M., Rubenstein, J. L., & Ericson, J. (1999). Homeobox gene Nkx2.2 and specification of neuronal identity by graded sonic hedgehog signalling. *Nature, 398*(6728), 622-627. doi:10.1038/19315

Britz, O., Zhang, J., Grossmann, K., Dyck, J., Kim, J., Dymecki, S., . . . Goulding, M. (2015). A genetically defined asymmetry underlies the inhibitory control of flexor-extensor locomotor movements. *Elife, 4* doi:10.7554/eLife.04718

Buckley, D., Burroughs Garcia, J., Kriks, S., Lewandoski, M., & Waters, S. (2020). Gbx1 and Gbx2 are essential for normal patterning and development of interneurons and motor neurons in the embryonic spinal cord. *Journal of Developmental Biology, 8*(2) doi:10.3390/jdb8020009

Buckley, D., Burroughs Garcia, J., Lewandoski, M., & Waters, S. (2013). Characterization of the Gbx1-/- mouse mutant: A requirement for Gbx1 in normal locomotion and sensorimotor circuit development. *Plos One, 8*(2), e56214-e56214. doi:10.1371/journal.pone.0056214

Bui, T., Akay, T., Loubani, O., Hnasko, T., Jessell, T., & Brownstone, R. (2013). Circuits for grasping: Spinal dI3 interneurons mediate cutaneous control of motor behavior. *Neuron, 78*(1), 191-204. doi:10.1016/j.neuron.2013.02.007

Bui, T., Stifani, N., Akay, T., & Brownstone, R. (2016). Spinal microcircuits comprising dI3 interneurons are necessary for motor functional recovery following spinal cord transection. *Elife, 5* doi:10.7554/eLife.21715

Buss, R. R., & Drapeau, P. (2001). Synaptic drive to motoneurons during fictive swimming in the developing zebrafish. *Journal of Neurophysiology, 86*(1), 197-210. doi:10.1152/jn.2001.86.1.197

Caldeira, V., Dougherty, K., Borgius, L., & Kiehn, O. (2017). Spinal Hb9::Cre-derived excitatory interneurons contribute to rhythm generation in the mouse. *Scientific Reports, 7*, 41369-41369. doi:10.1038/srep41369

Caqueret, A., Coumailleau, P., & Michaud, J. (2005). Regionalization of the anterior hypothalamus in the chick embryo. *Developmental Dynamics, 233*(2), 652-658. doi:10.1002/dvdy.20372

Cheng, L., Arata, A., Mizuguchi, R., Qian, Y., Karunaratne, A., Gray, P., . . . Ma, Q. (2004). Tlx3 and Tlx1 are post-mitotic selector genes determining glutamatergic over GABAergic cell fates. *Nature Neuroscience, 7*(5), 510-517. doi:10.1038/nn1221

Chopek, J., Nascimento, F., Beato, M., Brownstone, R., & Zhang, Y. (2018). Sub-populations of spinal V3 interneurons form focal modules of layered pre-motor microcircuits. *Cell Reports, 25*(1), 146-156.e3. doi:10.1016/j.celrep.2018.08.095

Christensen, A., Iyer, S., François, A., Vyas, S., Ramakrishnan, C., Vesuna, S., . . . Delp, S. (2016). In vivo interrogation of spinal mechanosensory circuits. *Cell Reports, 17*(6), 1699-1710. doi:10.1016/j.celrep.2016.10.010

Clark, B., Stein O'Brien, G., Shiau, F., Cannon, G., Davis Marcisak, E., Sherman, T., . . . Blackshaw, S. (2019). Single-cell RNA-seq analysis of retinal development identifies NFI factors as regulating mitotic exit and late-born cell specification. *Neuron,* doi:10.1016/j.neuron.2019.04.010

Crone, S., Quinlan, K., Zagoraiou, L., Droho, S., Restrepo, C., Lundfald, L., . . . Sharma, K. (2008). Genetic ablation of V2a ipsilateral interneurons disrupts left-right locomotor coordination in mammalian spinal cord. *Neuron, 60*(1), 70-83. doi:10.1016/j.neuron.2008.08.009

Crone, S., Zhong, G., Harris Warrick, R., & Sharma, K. (2009). In mice lacking V2a interneurons, gait depends on speed of locomotion. *The Journal of Neuroscience, 29*(21), 7098-7109. doi:10.1523/JNEUROSCI.1206-09.2009

Danner, S., Shevtsova, N., Frigon, A., & Rybak, I. (2017). Computational modeling of spinal circuits controlling limb coordination and gaits in quadrupeds. *Elife, 6* doi:10.7554/eLife.31050

Danner, S., Zhang, H., Shevtsova, N., Borowska Fielding, J., Deska Gauthier, D., Rybak, I., & Zhang, Y. (2019). Spinal V3 interneurons and left-right coordination in mammalian locomotion. *Frontiers in Cellular Neuroscience, 13*, 516-516. doi:10.3389/fncel.2019.00516

de Leon, R., Hodgson, J. A., Roy, R. R., & Edgerton, V. R. (1994). Extensor- and flexor-like modulation within motor pools of the rat hindlimb during treadmill locomotion and swimming. *Brain Research, 654*(2), 241-250. doi:10.1016/0006-8993(94)90485-5

Del Barrio, M., Taveira Marques, R., Muroyama, Y., Yuk, D., Li, S., Wines Samuelson, M., . . . Richardson, W. (2007). A regulatory network involving Foxn4, Mash1 and delta-like 4/Notch1 generates V2a and V2b spinal interneurons from a common progenitor pool. *Development, 134*(19), 3427-3436. doi:10.1242/dev.005868

Delile, J., Rayon, T., Melchionda, M., Edwards, A., Briscoe, J., & Sagner, A. (2019). Single cell transcriptomics reveals spatial and temporal dynamics of gene expression in the developing mouse spinal cord. *Development, 146*(12) doi:10.1242/dev.173807

Deplancke, B., Alpern, D., & Gardeux, V. (2016). The genetics of transcription factor DNA binding variation. Cell, 166(3), 538-554. 10.1016/j.cell.2016.07.012

Deska Gauthier, D., Borowska Fielding, J., Jones, C., & Zhang, Y. (2020). The temporal neurogenesis patterning of spinal p3-V3 interneurons into divergent subpopulation assemblies. *The Journal of Neuroscience, 40*(7), 1440-1452. doi:10.1523/JNEUROSCI.1518-19.2019

Deska-Gauthier, D., & Zhang, Y. (2019). The functional diversity of spinal interneurons and locomotor control. *Current Opinion in Physiology, 8*, 99-108. doi:https://doi.org/10.1016/j.cophys.2019.01.005

Dewitz, C., Pimpinella, S., Hackel, P., Akalin, A., Jessell, T., & Zampieri, N. (2018). Nuclear organization in the spinal cord depends on motor neuron lamination orchestrated by catenin and afadin function. *Cell Reports, 22*(7), 1681-1694.

Doe, C. (2017). Temporal patterning in the drosophila CNS. *Annual Review of Cell and Developmental Biology, 33*, 219-240. doi:10.1146/annurev-cellbio-111315-125210

Donelan, J. M., & Pearson, K. (2004). Contribution of sensory feedback to ongoing ankle extensor activity during the stance phase of walking. *Canadian Journal of Physiology and Pharmacology, 82*(8-9), 589-598. doi:10.1139/y04-043

Dougherty, K., Zagoraiou, L., Satoh, D., Rozani, I., Doobar, S., Arber, S., . . . Kiehn, O. (2013). Locomotor rhythm generation linked to the output of spinal shox2 excitatory interneurons. *Neuron, 80*(4), 920-933. doi:10.1016/j.neuron.2013.08.015

Dougherty, K., & Kiehn, O. (2010). Functional organization of V2a-related locomotor circuits in the rodent spinal cord. *Annals of the New York Academy of Sciences, 1198*, 85-93. doi:10.1111/j.1749-6632.2010.05502.x

Duan, B., Cheng, L., Bourane, S., Britz, O., Padilla, C., Garcia Campmany, L., . . . Ma, Q. (2014). Identification of spinal circuits transmitting and gating mechanical pain. *Cell, 159*(6), 1417-1432. doi:10.1016/j.cell.2014.11.003

Duysens, J. (1977). Fluctuations in sensitivity to rhythm resetting effects during the cat's step cycle. *Brain Research, 133*(1), 190-195. doi:10.1016/0006-8993(77)90063-4

Dyck, J., Lanuza, G., & Gosgnach, S. (2012). Functional characterization of dI6 interneurons in the neonatal mouse spinal cord. *Journal of Neurophysiology, 107*(12), 3256-3266. doi:10.1152/jn.01132.2011

Ellaway, P., Taylor, A., & Durbaba, R. (2015). Muscle spindle and fusimotor activity in locomotion. *Journal of Anatomy, 227*(2), 157-166. doi:10.1111/joa.12299

Engberg, I., & Lundberg, A. (1969). An electromyographic analysis of muscular activity in the hindlimb of the cat during unrestrained locomotion. *Acta Physiologica Scandinavica, 75*(4), 614-630. doi:10.1111/j.1748-1716.1969.tb04415.x

Ericson, J., Rashbass, P., Schedl, A., Brenner Morton, S., Kawakami, A., van Heyningen, V., . . . Briscoe, J. (1997). Pax6 controls progenitor cell identity and neuronal fate in response to graded shh signaling. *Cell, 90*(1), 169-180. doi:10.1016/s0092-8674(00)80323-2

Falgairolle, M., Puhl, J., Pujala, A., Liu, W., & O'Donovan, M. (2017). Motoneurons regulate the central pattern generator during drug-induced locomotor-like activity in the neonatal mouse. *Elife, 6* doi:10.7554/eLife.26622

Ferreira Pinto, M., Ruder, L., Capelli, P., & Arber, S. (2018). Connecting circuits for supraspinal control of locomotion. *Neuron, 100*(2), 361-374. doi:10.1016/j.neuron.2018.09.015

Fidelin, K., Djenoune, L., Stokes, C., Prendergast, A., Gomez, J., Baradel, A., . . . Wyart, C. (2015). State-dependent modulation of locomotion by GABAergic spinal sensory neurons. *Current Biology, 25*(23), 3035-3047. doi:10.1016/j.cub.2015.09.070

Fink, A. J. P., Croce, K., Huang, Z. J., Abbott, L. F., Jessell, T., & Azim, E. (2014). Presynaptic inhibition of spinal sensory feedback ensures smooth movement. *Nature, 509*(7498), 43-48. doi:10.1038/nature13276

Francius, C., Harris, A., Rucchin, V., Hendricks, T., Stam, F., Barber, M., . . . Clotman, F. (2013). Identification of multiple subsets of ventral interneurons and differential distribution along the rostrocaudal axis of the developing spinal cord. *PLoS One, 8*(8), e70325-e70325. doi:10.1371/journal.pone.0070325

Gabitto, M., Pakman, A., Bikoff, J., Abbott, L. F., Jessell, T., & Paninski, L. (2016). Bayesian sparse regression analysis documents the diversity of spinal inhibitory interneurons. *Cell, 165*(1), 220-233. doi:10.1016/j.cell.2016.01.026

Glasgow, S., Henke, R. M., Macdonald, R., Wright, C. V. E., & Johnson, J. (2005). Ptf1a determines GABAergic over glutamatergic neuronal cell fate in the spinal cord dorsal horn. *Development, 132*(24), 5461-5469. doi:10.1242/dev.02167

Gosgnach, S., Bikoff, J., Dougherty, K., El Manira, A., Lanuza, G., & Zhang, Y. (2017). Delineating the diversity of spinal interneurons in locomotor circuits. *The Journal of Neuroscience, 37*(45), 10835-10841. doi:10.1523/JNEUROSCI.1829-17.2017

Gosgnach, S., Lanuza, G., Butt, S. J. B., Saueressig, H., Zhang, Y., Velasquez, T., . . . Goulding, M. (2006). V1 spinal neurons regulate the speed of vertebrate locomotor outputs. *Nature, 440*(7081), 215-219. doi:10.1038/nature04545

Goulding, M., Lanuza, G., Sapir, T., & Narayan, S. (2002). The formation of sensorimotor circuits. *Current Opinion in Neurobiology, 12*(5), 508-515. doi:10.1016/s0959-4388(02)00371-9

Goulding, M. (2009). Circuits controlling vertebrate locomotion: Moving in a new direction. *Nature Reviews.Neuroscience, 10*(7), 507-518. doi:10.1038/nrn2608

Griener, A., Zhang, W., Kao, H., Haque, F., & Gosgnach, S. (2017). Anatomical and electrophysiological characterization of a population of dI6 interneurons in the neonatal mouse spinal cord. *Neuroscience, 362*, 47-59. doi:10.1016/j.neuroscience.2017.08.031

Grillner, S., & Zangger, P. (1979). On the central generation of locomotion in the low spinal cat. *Experimental Brain Research, 34*(2), 241-261. doi:10.1007/BF00235671

Grillner, S., & Zangger, P. (1984). The effect of dorsal root transection on the efferent motor pattern in the cat's hindlimb during locomotion. *Acta Physiologica Scandinavica, 120*(3), 393-405. doi:10.1111/j.1748-1716.1984.tb07400.x

Grillner, S. (2003). The motor infrastructure: From ion channels to neuronal networks. *Nature Reviews Neuroscience, 4*(7), 573-586. doi:10.1038/nrn1137

Grillner, S., & El Manira, A. (2020). Current principles of motor control, with special reference to vertebrate locomotion. *Physiological Reviews, 100*(1), 271-320. doi:10.1152/physrev.00015.2019

Gross, M., Dottori, M., & Goulding, M. (2002). Lbx1 specifies somatosensory association interneurons in the dorsal spinal cord. *Neuron, 34*(4), 535-549. doi:10.1016/S0896-6273(02)00690-6

Guertin, P., Angel, M. J., Perreault, M. C., & McCrea, D. A. (1995). Ankle extensor group I afferents excite extensors throughout the hindlimb during fictive locomotion in the cat. *The Journal of Physiology, 487*(1), 197-209. doi:10.1113/jphysiol.1995.sp020871

Hägglund, M., Borgius, L., Dougherty, K., & Kiehn, O. (2010). Activation of groups of excitatory neurons in the mammalian spinal cord or hindbrain evokes locomotion. *Nature Neuroscience, 13*(2), 246-252. doi:10.1038/nn.2482

Hägglund, M., Dougherty, K., Borgius, L., Itohara, S., Iwasato, T., & Kiehn, O. (2013). Optogenetic dissection reveals multiple rhythmogenic modules underlying locomotion. *Proceedings of the National Academy of Sciences of the United States of America, 110*(28), 11589-11594. doi:10.1073/pnas.1304365110

Hägglund, M., Dougherty, K., Borgius, L., Itohara, S., Iwasato, T., & Kiehn, O. (2013). Optogenetic dissection reveals multiple rhythmogenic modules underlying locomotion. *Proceedings of the National Academy of Sciences of the United States of America, 110*(28), 11589-11594. doi:10.1073/pnas.1304365110

Haque, F., Rancic, V., Zhang, W., Clugston, R., Ballanyi, K., & Gosgnach, S. (2018). wt1. *The Journal of Neuroscience, 38*(25), 5666-5676. doi:10.1523/JNEUROSCI.0328-18.2018

Häring, M., Zeisel, A., Hochgerner, H., Rinwa, P., Jakobsson, J. E. T., Lönnerberg, P., . . . Ernfors, P. (2018). Neuronal atlas of the dorsal horn defines its architecture and links sensory input to transcriptional cell types. *Nature Neuroscience, 21*(6), 869-880. doi:10.1038/s41593-018-0141-1

Harris, A., Masgutova, G., Collin, A., Toch, M., Hidalgo Figueroa, M., Jacob, B., . . . Clotman, F. (2019). Onecut factors and Pou2f2 regulate the distribution of V2 interneurons in the mouse developing spinal cord. *Frontiers in Cellular Neuroscience, 13*, 184-184. doi:10.3389/fncel.2019.00184

Harris, K., & Shepherd, G. M. G. (2015). The neocortical circuit: Themes and variations. *Nature Neuroscience, 18*(2), 170-181. doi:10.1038/nn.3917

Hayashi, M., Hinckley, C., Driscoll, S., Moore, N., Levine, A., Hilde, K., . . . Pfaff, S. (2018). Graded arrays of spinal and supraspinal V2a interneuron subtypes underlie forelimb and hindlimb motor control. *Neuron, 97*(4), 869-884.e5. doi:10.1016/j.neuron.2018.01.023

Hilde, K., Levine, A., Hinckley, C., Hayashi, M., Montgomery, J., Gullo, M., . . . Pfaff, S. (2016). Satb2 is required for the development of a spinal exteroceptive microcircuit that modulates limb position. *Neuron, 91*(4), 763-776. doi:10.1016/j.neuron.2016.07.014

Hoang, P., Chalif, J., Bikoff, J., Jessell, T., Mentis, G., & Wichterle, H. (2018). Subtype diversification and synaptic specificity of stem cell-derived spinal interneurons. *Neuron, 100*(1), 135-149.e7. doi:10.1016/j.neuron.2018.09.016

Hobert, O., Carrera, I., & Stefanakis, N. (2010). The molecular and gene regulatory signature of a neuron. *Trends in Neurosciences (Regular Ed.), 33*(10), 435-445. doi:10.1016/j.tins.2010.05.006

Holguera, I., & Desplan, C. (2018). Neuronal specification in space and time. *Science, 362*(6411), 176-180. doi:10.1126/science.aas9435

Honda, C. N. (1995). Differential distribution of calbindin-D28k and parvalbumin in somatic and visceral sensory neurons. *Neuroscience, 68*(3), 883-892. doi:10.1016/0306-4522(95)00180-Q

Huang, Z. J., & Scheiffele, P. (2008). GABA and neuroligin signaling: Linking synaptic activity and adhesion in inhibitory synapse development. *Current Opinion in Neurobiology, 18*(1), 77-83. doi:10.1016/j.conb.2008.05.008

Hubbard, J., Böhm, U., Prendergast, A., Tseng, P., Newman, M., Stokes, C., & Wyart, C. (2016). Intraspinal sensory neurons provide powerful inhibition to motor circuits ensuring postural

control during locomotion. *Current Biology, 26*(21), 2841-2853. doi:10.1016/j.cub.2016.08.026

Hurteau, M., Thibaudier, Y., Dambreville, C., Chraibi, A., Desrochers, E., Telonio, A., & Frigon, A. (2017). Nonlinear modulation of cutaneous reflexes with increasing speed of locomotion in spinal cats. *The Journal of Neuroscience, 37*(14), 3896-3912. doi:10.1523/JNEUROSCI.3042-16.2017

Hutchison, D. L., Roy, R. R., Hodgson, J. A., & Edgerton, V. R. (1989). EMG amplitude relationships between the rat soleus and medial gastrocnemius during various motor tasks. *Brain Research, 502*(2), 233-244. doi:10.1016/0006-8993(89)90618-5

Jessell, T. M. (2000). Neuronal specification in the spinal cord: Inductive signals and transcriptional codes. *Nature Reviews Genetics, 1*(1), 20-29. doi:10.1038/35049541

John, A., Wildner, H., & Britsch, S. (2005). The homeodomain transcription factor Gbx1 identifies a subpopulation of late-born GABAergic interneurons in the developing dorsal spinal cord. *Developmental Dynamics, 234*(3), 767-771. doi:10.1002/dvdy.20568

Kabayiza, K., Masgutova, G., Harris, A., Rucchin, V., Jacob, B., & Clotman, F. (2017). The onecut transcription factors regulate differentiation and distribution of dorsal interneurons during spinal cord development. *Frontiers in Molecular Neuroscience, 10*, 157-157. doi:10.3389/fnmol.2017.00157

Kambiz, S., Baas, M., Duraku, L. S., Kerver, A. L., Koning, A. H. J., Walbeehm, E. T., & Ruigrok, T. J. H. (2014). Innervation mapping of the hind paw of the rat using evans blue extravasation, optical surface mapping and CASAM. *Journal of Neuroscience Methods, 229*, 15-27. doi:10.1016/j.jneumeth.2014.03.015

Kawaguchi, A. (2019). Temporal patterning of neocortical progenitor cells: How do they know the right time? *Neuroscience Research, 138*, 3-11. doi:10.1016/j.neures.2018.09.004

Kiehn, O., & Butt, S. J. B. (2003). Physiological, anatomical and genetic identification of CPG neurons in the developing mammalian spinal cord. *Progress in Neurobiology, 70*(4), 347-361. doi:10.1016/S0301-0082(03)00091-1

Kiehn, O. (2006). Locomotor circuits in the mammalian spinal cord. *Annual Review of Neuroscience, 29*, 279-306. doi:10.1146/annurev.neuro.29.051605.112910

Kiehn, O. (2016). Decoding the organization of spinal circuits that control locomotion. *Nature Reviews.Neuroscience, 17*(4), 224-238. doi:10.1038/nrn.2016.9

Kimura, Y., Okamura, Y., & Higashijima, S. (2006). Alx, a zebrafish homolog of Chx10, marks ipsilateral descending excitatory interneurons that participate in the regulation of spinal locomotor circuits. *The Journal of Neuroscience, 26*(21), 5684-5697. doi:10.1523/JNEUROSCI.4993-05.2006

Kimura, Y., Satou, C., & Higashijima, S. (2008). V2a and V2b neurons are generated by the final divisions of pair-producing progenitors in the zebrafish spinal cord. *Development, 135*(18), 3001-3005. doi:10.1242/dev.024802

Kimura, Y., & Higashijima, S. (2019). Regulation of locomotor speed and selection of active sets of neurons by V1 neurons. *Nature Communications, 10*(1), 2268-2268. doi:10.1038/s41467-019-09871-x

Kishore, S., Cadoff, E., Agha, M., & McLean, D. (2020). Orderly compartmental mapping of premotor inhibition in the developing zebrafish spinal cord. *Science, 370*(6515), 431-436. doi:10.1126/science.abb4608

Kishore, S., & Fetcho, J. (2013). Homeostatic regulation of dendritic dynamics in a motor map in vivo. *Nature Communications, 4*, 2086-2086. doi:10.1038/ncomms3086

Knogler, L., Ryan, J., Saint Amant, L., & Drapeau, P. (2014). A hybrid electrical/chemical circuit in the spinal cord generates a transient embryonic motor behavior. *The Journal of Neuroscience, 34*(29), 9644-9655. doi:10.1523/JNEUROSCI.1225-14.2014

Koch, S., Del Barrio, M., Dalet, A., Gatto, G., Günther, T., Zhang, J., . . . Goulding, M. (2017). RORß spinal interneurons gate sensory transmission during locomotion to secure a fluid walking gait. *Neuron, 96*(6), 1419-1431.e5. doi:10.1016/j.neuron.2017.11.011

Kruspe, M., Thieme, H., Guntinas Lichius, O., & Irintchev, A. (2014). Motoneuron regeneration accuracy and recovery of gait after femoral nerve injuries in rats. *Neuroscience, 280*, 73-87. doi:10.1016/j.neuroscience.2014.08.051

Lafreniere Roula, M., & McCrea, D. (2005). Deletions of rhythmic motoneuron activity during fictive locomotion and scratch provide clues to the organization of the mammalian central pattern generator. *Journal of Neurophysiology, 94*(2), 1120-1132. doi:10.1152/jn.00216.2005

Lai, H., Seal, R., & Johnson, J. (2016). Making sense out of spinal cord somatosensory development. *Development, 143*(19), 3434-3448. doi:10.1242/dev.139592

Lallemend, F., & Ernfors, P. (2012). Molecular interactions underlying the specification of sensory neurons. *Trends in Neurosciences, 35*(6), 373-381. doi:10.1016/j.tins.2012.03.006

Lamotte d'Incamps, B., Bhumbra, G., Foster, J., Beato, M., & Ascher, P. (2017). Segregation of glutamatergic and cholinergic transmission at the mixed motoneuron renshaw cell synapse. *Scientific Reports, 7*(1), 4037-4037. doi:10.1038/s41598-017-04266-8

Lanuza, G., Gosgnach, S., Pierani, A., Jessell, T., & Goulding, M. (2004). Genetic identification of spinal interneurons that coordinate left-right locomotor activity necessary for walking movements. *Neuron, 42*(3), 375-386. doi:10.1016/S0896-6273(04)00249-1

Laumonnerie, C., Tong, Y., Alstermark, H., & Wilson, S. (2015). Commissural axonal corridors instruct neuronal migration in the mouse spinal cord. *Nature Communications, 6*, 7028-7028. doi:10.1038/ncomms8028

Lemieux, M., Josset, N., Roussel, M., Couraud, S., & Bretzner, F. (2016). Speed-dependent modulation of the locomotor behavior in adult mice reveals attractor and transitional gaits. *Frontiers in Neuroscience, 10*, 42-42. doi:10.3389/fnins.2016.00042

Lim, J., & Choi, H. (2015). Estrogen-related receptor gamma regulates dopaminergic neuronal phenotype by activating GSK3ß/NFAT signaling in SH-SY5Y cells. *Journal of Neurochemistry, 133*(4), 544-557. doi:10.1111/jnc.13085

Lu, D., Niu, T., & Alaynick, W. (2015). Molecular and cellular development of spinal cord locomotor circuitry. *Frontiers in Molecular Neuroscience, 8*, 25-25. doi:10.3389/fnmol.2015.00025

Lundfald, L., Restrepo, C. E., Butt, S. J. B., Peng, C., Droho, S., Endo, T., . . . Kiehn, O. (2007). Phenotype of V2-derived interneurons and their relationship to the axon guidance molecule EphA4 in the developing mouse spinal cord. *European Journal of Neuroscience, 26*(11), 2989-3002. doi:10.1111/j.1460-9568.2007.05906.x

Marion, J., Yang, C., Caqueret, A., Boucher, F., & Michaud, J. (2005). Sim1 and Sim2 are required for the correct targeting of mammillary body axons. Development, 132(24), 5527-5537. 10.1242/dev.02142

Masgutova, G., Harris, A., Jacob, B., Corcoran, L., & Clotman, F. (2019). Pou2f2 regulates the distribution of dorsal interneurons in the mouse developing spinal cord. *Frontiers in Molecular Neuroscience, 12*, 263-263. doi:10.3389/fnmol.2019.00263

Matsushima, T., & Grillner, S. (1992). Neural mechanisms of intersegmental coordination in lamprey: Local excitability changes modify the phase coupling along the spinal cord. *Journal of Neurophysiology, 67*(2), 373-388. doi:10.1152/jn.1992.67.2.373

Mayer, C., Hafemeister, C., Bandler, R., Machold, R., Batista Brito, R., Jaglin, X., . . . Satija, R. (2018). Developmental diversification of cortical inhibitory interneurons. Nature, 555(7697), 457-462. doi:10.1038/nature25999

Mayer, W., Murray, A., Brenner Morton, S., Jessell, T., Tourtellotte, W., & Akay, T. (2018). Role of muscle spindle feedback in regulating muscle activity strength during walking at different speed in mice. *Journal of Neurophysiology,* doi:10.1152/jn.00250.2018

McCrea, D., & Rybak, I. (2007). Modeling the mammalian locomotor CPG: Insights from mistakes and perturbations. *Prog Brain Res, 165*, 235-253. doi:10.1016/S0079-6123(06)65015-2

McCrea, D., & Rybak, I. (2008). Organization of mammalian locomotor rhythm and pattern generation. *Brain Research Reviews, 57*(1), 134-146. doi:10.1016/j.brainresrev.2007.08.006

McHanwell, S., & Biscoe, T. J. (1981). The localization of motoneurons supplying the hindlimb muscles of the mouse. Philosophical Transactions - Royal Society.Biological Sciences, 293(1069), 477-508. doi:10.1098/rstb.1981.0082

McLean, D., Fan, J., Higashijima, S., Hale, M., & Fetcho, J. (2007). A topographic map of recruitment in spinal cord. *Nature, 446*(7131), 71-75. doi:10.1038/nature05588

McLean, D., Masino, M., Koh, I. Y. Y., Lindquist, W. B., & Fetcho, J. (2008). Continuous shifts in the active set of spinal interneurons during changes in locomotor speed. *Nature Neuroscience, 11*(12), 1419-1429. doi:10.1038/nn.2225

McLean, D., & Fetcho, J. (2009). Spinal interneurons differentiate sequentially from those driving the fastest swimming movements in larval zebrafish to those driving the slowest ones. *The Journal of Neuroscience, 29*(43), 13566-13577. doi:10.1523/JNEUROSCI.3277-09.2009

Merkulyeva, N., Veshchitskii, A., Gorsky, O., Pavlova, N., Zelenin, P., Gerasimenko, Y., . . . Musienko, P. (2018). Distribution of spinal neuronal networks controlling forward and backward locomotion. *The Journal of Neuroscience, 38*(20), 4695-4707. doi:10.1523/JNEUROSCI.2951-17.2018

Meziane, H., Fraulob, V., Riet, F., Krezel, W., Selloum, M., Geffarth, M., . . . Rhinn, M. (2013). The homeodomain factor Gbx1 is required for locomotion and cell specification in the dorsal spinal cord. *Peerj, 1*, e142-e142. doi:10.7717/peerj.142

Michaud, J. L., Rosenquist, T., May, N. R., & Fan, C. M. (1998). Development of neuroendocrine lineages requires the bHLH-PAS transcription factor SIM1. Genes & Development, 12(20), 3264-3275. 10.1101/gad.12.20.3264

Miles, G., Hartley, R., Todd, A., & Brownstone, R. (2007). Spinal cholinergic interneurons regulate the excitability of motoneurons during locomotion. *Proceedings of the National Academy of Sciences of the United States of America, 104*(7), 2448-2453. doi:10.1073/pnas.0611134104

Mizuguchi, R., Kriks, S., Cordes, R., Gossler, A., Ma, Q., & Goulding, M. (2006). Ascl1 and Gsh1/2 control inhibitory and excitatory cell fate in spinal sensory interneurons. *Nature Neuroscience, 9*(6), 770-778. doi:10.1038/nn1706

Moran Rivard, L., Kagawa, T., Saueressig, H., Gross, M. K., Burrill, J., & Goulding, M. (2001). Evx1 is a postmitotic determinant of v0 interneuron identity in the spinal cord. *Neuron, 29*(2), 385-399. doi:10.1016/S0896-6273(01)00213-6

Müller, T., Brohmann, H., Pierani, A., Heppenstall, P., Lewin, G., Jessell, T., & Birchmeier, C. (2002). The homeodomain factor lbx1 distinguishes two major programs of neuronal differentiation in the dorsal spinal cord. *Neuron, 34*(4), 551-562. doi:10.1016/s0896-6273(02)00689-x

Myers, C., Lewcock, J., Hanson, M. G., Gosgnach, S., Aimone, J., Gage, F., . . . Pfaff, S. (2005). Cholinergic input is required during embryonic development to mediate proper assembly of spinal locomotor circuits. *Neuron, 46*(1), 37-49. doi:10.1016/j.neuron.2005.02.022

Myers, P. Z., Eisen, J. S., & Westerfield, M. (1986). Development and axonal outgrowth of identified motoneurons in the zebrafish. *The Journal of Neuroscience, 6*(8), 2278-2289. doi:10.1523/JNEUROSCI.06-08-02278.1986

Myers, P. Z. (1985). Spinal motoneurons of the larval zebrafish. *Journal of Comparative Neurology, 236*(4), 555-561. doi:10.1002/cne.902360411

Nissen, U., Mochida, H., & Glover, J. (2005). Development of projection-specific interneurons and projection neurons in the embryonic mouse and rat spinal cord. Journal of Comparative Neurology, 483(1), 30-47.

Oberst, P., Agirman, G., & Jabaudon, D. (2019). Principles of progenitor temporal patterning in the developing invertebrate and vertebrate nervous system. *Current Opinion in Neurobiology, 56*, 185-193. doi:https://doi.org/10.1016/j.conb.2019.03.004

Okigawa, S., Mizoguchi, T., Okano, M., Tanaka, H., Isoda, M., Jiang, Y., . . . Itoh, M. (2014). Different combinations of notch ligands and receptors regulate V2 interneuron progenitor proliferation and V2a/V2b cell fate determination. *Developmental Biology, 391*(2), 196-206. doi:10.1016/j.ydbio.2014.04.011

Osterberg, N., Wiehle, M., Oehlke, O., Heidrich, S., Xu, C., Fan, C., . . . Roussa, E. (2011). Sim1 is a novel regulator in the differentiation of mouse dorsal raphe serotonergic neurons. PLoS One, 6(4), e19239-e19239. 10.1371/journal.pone.0019239

Petracca, Y., Sartoretti, M., Di Bella, D., Marin Burgin, A., Carcagno, A., Schinder, A., & Lanuza, G. (2016). The late and dual origin of cerebrospinal fluid-contacting neurons in the mouse spinal cord. *Development, 143*(5), 880-891. doi:10.1242/dev.129254

Pierani, A., Moran Rivard, L., Sunshine, M. J., Littman, D. R., Goulding, M., & Jessell, T. M. (2001). Control of interneuron fate in the developing spinal cord by the progenitor homeodomain protein Dbx1. *Neuron, 29*(2), 367-384. doi:10.1016/S0896-6273(01)00212-4

Pierotti, D. J., Roy, R. R., Gregor, R. J., & Edgerton, V. R. (1989). Electromyographic activity of cat hindlimb flexors and extensors during locomotion at varying speeds and inclines. *Brain Research, 481*(1), 57-66. doi:10.1016/0006-8993(89)90485-X

Pocratsky, A., Burke, D., Morehouse, J., Beare, J., Riegler, A., Tsoulfas, P., . . . Magnuson, D. S. K. (2017). Reversible silencing of lumbar spinal interneurons unmasks a task-specific network for securing hindlimb alternation. *Nature Communications, 8*(1), 1963-1963. doi:10.1038/s41467-017-02033-x

Pujala, A., & Koyama, M. (2019). Chronology-based architecture of descending circuits that underlie the development of locomotor repertoire after birth. *Elife, 8* doi:10.7554/eLife.42135

Ray, R., Corcoran, A., Brust, R., Kim, J., Richerson, G., Nattie, E., & Dymecki, S. (2011). Impaired respiratory and body temperature control upon acute serotonergic neuron inhibition. *Science, 333*(6042), 637-642. doi:10.1126/science.1205295

Rekling, J. C., Funk, G. D., Bayliss, D. A., Dong, X. W., & Feldman, J. L. (2000). Synaptic control of motoneuronal excitability. *Physiological Reviews, 80*(2), 767-852. doi:10.1152/physrev.2000.80.2.767

RENSHAW, B. (1946). Central effects of centripetal impulses in axons of spinal ventral roots. *Journal of Neurophysiology, 9*, 191-204. doi:10.1152/jn.1946.9.3.191

Roussel, Y., Paradis, M., Gaudreau, S., Lindsey, B., & Bui, T. (2020). Spatiotemporal transition in the role of synaptic inhibition to the tail beat rhythm of developing larval zebrafish. *Eneuro, 7*(1) doi:10.1523/ENEURO.0508-18.2020

Roy, R. R., Hutchison, D. L., Pierotti, D. J., Hodgson, J. A., & Edgerton, V. R. (1991). EMG patterns of rat ankle extensors and flexors during treadmill locomotion and swimming. *Journal of Applied Physiology, 70*(6), 2522-2529. doi:10.1152/jappl.1991.70.6.2522

Roy, R. R., Hutchison, D. L., Pierotti, D. J., Hodgson, J. A., & Edgerton, V. R. (1991). EMG patterns of rat ankle extensors and flexors during treadmill locomotion and swimming. *Journal of Applied Physiology, 70*(6), 2522-2529. doi:10.1152/jappl.1991.70.6.2522

Sagar, S. M., Sharp, F. R., & Curran, T. (1988). Expression of c-fos protein in brain: Metabolic mapping at the cellular level. *Science, 240*(4857), 1328-1331. doi:10.1126/science.3131879

Saint Amant, L. (2010). Development of motor rhythms in zebrafish embryos. *Progress in Brain Research, 187*, 47-61. doi:10.1016/B978-0-444-53613-6.00004-6

Sathyamurthy, A., Johnson, K., Matson, K. J. E., Dobrott, C., Li, L., Ryba, A., . . . Levine, A. (2018). Massively parallel single nucleus transcriptional profiling defines spinal cord neurons and their activity during behavior. *Cell Reports, 22*(8), 2216-2225. doi:10.1016/j.celrep.2018.02.003

Satou, C., Kimura, Y., & Higashijima, S. (2012). Generation of multiple classes of V0 neurons in zebrafish spinal cord: Progenitor heterogeneity and temporal control of neuronal diversity. *The Journal of Neuroscience, 32*(5), 1771-1783. doi:10.1523/JNEUROSCI.5500-11.2012

Schweitzer, J., Löhr, H., Bonkowsky, J., Hübscher, K., & Driever, W. (2013). Sim1a and Arnt2 contribute to hypothalamo-spinal axon guidance by regulating Robo2 activity via a Robo3-dependent mechanism. Development, 140(1), 93-106. 10.1242/dev.087825

Shevtsova, N., Talpalar, A., Markin, S., Harris Warrick, R., Kiehn, O., & Rybak, I. (2015). Organization of left-right coordination of neuronal activity in the mammalian spinal cord: Insights from computational modelling. *The Journal of Physiology, 593*(11), 2403-2426. doi:10.1113/JP270121

Sockanathan, S., & Jessell, T. M. (1998). Motor neuron-derived retinoid signaling specifies the subtype identity of spinal motor neurons. *Cell, 94*(4), 503-514. doi:10.1016/S0092-8674(00)81591-3

Song, J., Ampatzis, K., Björnfors, E. R., & El Manira, A. (2016). Motor neurons control locomotor circuit function retrogradely via gap junctions. *Nature, 529*(7586), 399-402. doi:10.1038/nature16497

Stam, F., Hendricks, T., Zhang, J., Geiman, E., Francius, C., Labosky, P., . . . Goulding, M. (2012). Renshaw cell interneuron specialization is controlled by a temporally restricted transcription factor program. *Development, 139*(1), 179-190. doi:10.1242/dev.071134

Stein, P. S. G. (2008). Motor pattern deletions and modular organization of turtle spinal cord. *Brain Research Reviews, 57*(1), 118-124. doi:10.1016/j.brainresrev.2007.07.008

Stepien, A., Tripodi, M., & Arber, S. (2010). Monosynaptic rabies virus reveals premotor network organization and synaptic specificity of cholinergic partition cells. *Neuron, 68*(3), 456-472. doi:10.1016/j.neuron.2010.10.019

Sultan, K., & Shi, S. (2018). Generation of diverse cortical inhibitory interneurons. Wiley Interdisciplinary Reviews: Developmental Biology, 7(2) doi:10.1002/wdev.306

Sürmeli, G., Akay, T., Ippolito, G., Tucker, P., & Jessell, T. (2011). Patterns of spinal sensory-motor connectivity prescribed by a dorsoventral positional template. Cell, 147(3), 653-665. doi:10.1016/j.cell.2011.10.012

Sweeney, L., Bikoff, J., Gabitto, M., Brenner Morton, S., Baek, M., Yang, J., . . . Jessell, T. (2018). Origin and segmental diversity of spinal inhibitory interneurons. *Neuron, 97*(2), 341-355.e3. doi:10.1016/j.neuron.2017.12.029

Swett, J. E., & Woolf, C. J. (1985). The somatotopic organization of primary afferent terminals in the superficial laminae of the dorsal horn of the rat spinal cord. *Journal of Comparative Neurology, 231*(1), 66-77. doi:10.1002/cne.902310106

Syed, M., Mark, B., & Doe, C. (2017). Playing well with others: Extrinsic cues regulate neural progenitor temporal identity to generate neuronal diversity. Trends in Genetics (Regular Ed.), 33(12), 933-942. doi:10.1016/j.tig.2017.08.005

Talpalar, A., Bouvier, J., Borgius, L., Fortin, G., Pierani, A., & Kiehn, O. (2013). Dual-mode operation of neuronal networks involved in left-right alternation. *Nature, 500*(7460), 85-88. doi:10.1038/nature12286

Tripodi, M., Stepien, A., & Arber, S. (2011). Motor antagonism exposed by spatial segregation and timing of neurogenesis. *Nature, 479*(7371), 61-66. doi:10.1038/nature10538

Vanderhorst, V. G., & Holstege, G. (1997). Organization of lumbosacral motoneuronal cell groups innervating hindlimb, pelvic floor, and axial muscles in the cat. Journal of Comparative Neurology, 382(1), 46-76. doi:10.1002/(SICI)1096-9861(19970526)382:1<46::AID-CNE4>3.0.CO;2-K

Wen, H., Eckenstein, K., Weihrauch, V., Stigloher, C., & Brehm, P. (2020). Primary and secondary motoneurons use different calcium channel types to control escape and swimming behaviors in zebrafish. *Proceedings of the National Academy of Sciences of the United States of America, 117*(42), 26429-26437. doi:10.1073/pnas.2015866117

Wiggin, T., Anderson, T., Eian, J., Peck, J., & Masino, M. (2012). Episodic swimming in the larval zebrafish is generated by a spatially distributed spinal network with modular functional organization. *Journal of Neurophysiology, 108*(3), 925-934. doi:10.1152/jn.00233.2012

Xu, C., & Fan, C. (2007). Allocation of paraventricular and supraoptic neurons requires Sim1 function: A role for a Sim1 downstream gene PlexinC1. Molecular Endocrinology, 21(5), 1234-1245. 10.1210/me.2007-0034

Yakovenko, S., Mushahwar, V., VanderHorst, V., Holstege, G., & Prochazka, A. (2002). Spatiotemporal activation of lumbosacral motoneurons in the locomotor step cycle. Journal of Neurophysiology, 87(3), 1542-1553. doi:10.1152/jn.00479.2001

Zagoraiou, L., Akay, T., Martin, J., Brownstone, R., Jessell, T., & Miles, G. (2009). A cluster of cholinergic premotor interneurons modulates mouse locomotor activity. *Neuron, 64*(5), 645-662. doi:10.1016/j.neuron.2009.10.017

Zeisel, A., Hochgerner, H., Lönnerberg, P., Johnsson, A., Memic, F., van der Zwan, J., . . . Linnarsson, S. (2018). Molecular architecture of the mouse nervous system. *Cell, 174*(4), 999-1014.e22. doi:10.1016/j.cell.2018.06.021

Zhang, J., Lanuza, G., Britz, O., Wang, Z., Siembab, V., Zhang, Y., . . . Goulding, M. (2014). V1 and v2b interneurons secure the alternating flexor-extensor motor activity mice require for limbed locomotion. *Neuron, 82*(1), 138-150. doi:10.1016/j.neuron.2014.02.013

Zhang, Y., Narayan, S., Geiman, E., Lanuza, G., Velasquez, T., Shanks, B., . . . Goulding, M. (2008). V3 spinal neurons establish a robust and balanced locomotor rhythm during walking. *Neuron, 60*(1), 84-96. doi:10.1016/j.neuron.2008.09.027

Zhong, G., Droho, S., Crone, S., Dietz, S., Kwan, A., Webb, W., . . . Harris Warrick, R. (2010). Electrophysiological characterization of V2a interneurons and their locomotor-related activity in the neonatal mouse spinal cord. *The Journal of Neuroscience, 30*(1), 170-182. doi:10.1523/JNEUROSCI.4849-09.2010

Zhong, S., Zhang, S., Fan, X., Wu, Q., Yan, L., Dong, J., . . . Wang, X. (2018). A single-cell RNA-seq survey of the developmental landscape of the human prefrontal cortex. *Nature, 555*(7697), 524-528. doi:10.1038/nature25980

Ziskind Conhaim, L., & Hochman, S. (2017). Diversity of molecularly defined spinal interneurons engaged in mammalian locomotor pattern generation. *Journal of Neurophysiology, 118*(6), 2956-2974. doi:10.1152/jn.00322.2017